PB 181582
Price $5.00

UNITED STATES
DEPARTMENT OF THE INTERIOR

THIN FILM VAPOR COMPRESSION SALINE WATER CONVERSION SYSTEM

OFFICE OF SALINE WATER

RESEARCH AND DEVELOPMENT PROGRESS REPORT NO. 85

For sale by the U.S. Department of Commerce, Office of Technical Services,
Washington, D.C., 20230

Created in 1849, the Department of the Interior--America's Department of Natural Resources--is concerned with the management, conservation, and development of the Nation's water, wildlife, mineral, forest, and park and recreational resources. It also has major responsibilities for Indian and Territorial affairs.

As the Nation's principal conservation agency, the Department of the Interior works to assure that nonrenewable resources are developed and used wisely, that park and recreational resources are conserved for the future, and that renewable resources make their full contribution to the progress, prosperity, and security of the United States--now and in the future.

U N I T E D S T A T E S

D E P A R T M E N T O F T H E I N T E R I O R

Stewart L. Udall, Secretary

Kenneth Holum, Assistant Secretary
for Water and Power Development

SALINE WATER RESEARCH AND DEVELOPMENT PROGRESS REPORT NO. 85

THIN FILM VAPOR COMPRESSION SALINE WATER CONVERSION SYSTEM

by

A. Willenbrock, Jr., R. M. Chamberlin, D. R. Fraser,
G. E. McGinnis, J. A. Cyphers and J. Wisnicki
Westinghouse Electric Corporation
Research and Development Center
Beulah Road, Churchill Boro
Pittsburgh 35, Pennsylvania

for

OFFICE OF SALINE WATER

Charles F. MacGowan, Director

Joseph J. Strobel, Chief, Division of Processes Development

Charles L. Gransee, Chief, Branch of Heat Transfer

February 1964

FOREWORD

This is the eightyfifth of a series of reports designed to present accounts of progress on saline water conversion with the expectation that the exchange of such data will contribute to the long-range development of economical processes applicable to large-scale, low-cost demineralization of sea and other saline waters.

Except for minor editing, the data herein are as contained in a report submitted by the Westinghouse Electric Corporation under Contract No. 14-01-0001-273, which has been accepted as fulfilling the provisions of that contract. The data and conclusions given in this report are essentially those of the Contractor and are not necessarily endorsed by the Department of the Interior.

TABLE OF CONTENTS

(Cont'd) TABLE OF CONTENTS

INTRODUCTION

This report is the final report on the research and development program carried out by the Westinghouse Electric Corporation on the Westinghouse Thin Film Vapor Compression Saline Water Conversion System. The work accomplished during this program was performed in accordance with the requirements of Contract 14-01-001-273 and amendment No. 1 to that contract. The term of the original contract was for 15 months beginning on March 21, 1962. Amendment No. 1 constituted an extension of time and funds thus extending the contract completion date to August 15, 1963.

The objectives of this contract were to:

1. Establish experimental proof of the basic assumptions made in the Westinghouse proposal for the Thin Film Vapor Compression Saline Water Conversion System.

2. Develop the technology of the components of the system to a point where a pilot plant could be designed.

The Westinghouse Thin Film Vapor Compression System as delineated in the Westinghouse proposal dated October 1961 and described in the Office of Saline Water 1962 Saline Water Conversion Report is briefly described in the Task I portion of this report. A schematic of the system is shown in Figure I-1.

The pre-contract Westinghouse Engineering Study showed that for the economic and technical assumptions made that a near optimum cost/k-gal could be achieved by the system with an evaporator temperature of 120°F. The following values of the system parameters define the cycle operating point:

Sea Water Temperature, Tso	65°F
Evaporator Sea Water Feed Temperature, Tsea =	120°F
Condenser Temperature, Tc =	122°F
Sea Water Feed Flow Rate, W_s =	4.6 lb/hr-ft
Product Water Production Rate, W_f =	1.84 lb/hr-ft
Mean Condensing Film Thickness, Ycm =	0.0015 in

The Thin Film Vapor Compression System attempts to achieve low cost potable water by combining components having low capital costs with a cycle requiring low energy input. Basically, the system consists of a low temperature difference (2°F), thin falling film evaporator-condenser module integrated into a vapor compression cycle. The module is constructed by accordian folding a thin (0.030 inch) sheet of carbon steel or aluminum, and installing the module in a shell designed to contain a vacuum.

The cycle operating conditions, the mechanism for transfering the required heat and the geometry of the surface were all aimed at minimizing the cost of producing potable water. The relatively high heat transfer coefficients associated with thin, falling evaporating and condensing films minimized the temperature difference required across the heat transfer surface. The small temperature difference and, therefore, the small difference in pressure between the evaporator and condenser plus the low evaporating temperature permitted the use of thin inexpensive heat transfer surface materials and minimized the energy input requirements. The surface geometry was designed to permit low cost mass production techniques in the fabrication of the heat transfer modules.

The research and development program reported on here was designed to examine and evaluate the more critical areas of the proposed system. These critical areas are summarized below:

1. Determination of the characteristics of a satisfactory saline water (Evaporating) film flowing on a vertical or nearly vertical flat surface.

2. Development of the technology to create and maintain this satisfactory film.

3. Determination of minimum cost materials consistent with environment, life and manufacturing requirements.

4. Development of improvements in heat transfer by specially formed surfaces.

5. Evaluation of manufacturing techniques to fabricate the heat transfer surface.

This report is divided into five sections, each section covers the work performed under a specific task covering one of the critical areas of the system. The task designations I thru IV are in the same order as the listing of critical areas above, i.e., Task I covers Item 1, Task II - Item 2 etc. Task V, which was the

special responsibility of the principle investigator, had as its goal system analysis and surveillance. The manufacturing studies were performed under Task V and would normally have been reported on under the Task V designation; however, the length of the report covering these studies was such that it was more convenient to incorporate it in Appendices B, C, D, E and F.

The references, nomenclature, derivations of analytical expressions and theory sample calculations for each task are given in Appendix A. The designations A-1, A-II, etc., means Appendix A, Task I, Appendix A Task II, etc. A-I & II signifies Appendix A Task I & II.

SUMMARY

The goals of the research and development program for the Thin Film Vapor Compression System have been achieved. The technical assumptions have been verified experimentally; the required developments have been accomplished; the economic assumptions have been studied and re-evaluated; and the technology required to design a pilot plant has been attained. The conclusion to be reached here, as a result of this program, is that at the conclusion of a pilot plant development program a one million GPD Thin Film Vapor Compression Sea Water Conversion System could be built which would produce water at a cost comparable to current multistage flash plants.

TASK I - To Determine the Characteristics of a Satisfactory Saline Water Film

Task Description

A thin film vapor compression sea water conversion system is shown schematically in Figure I-1. The incoming sea water is filtered and given whatever pretreatment is required, such as chlorination and acid addition. The flow is then divided into two streams - the first passing through a conventional liquid-liquid tube-in-shell multipass exchanger heated by the product water, and the second passing through a similar concentrated brine heat exchanger. These two streams are then recombined and deaerated to an oxygen concentration of 0.1 ppm. After deaeration, the feed water is heated to the design inlet temperature by a fired or steam heater.

Feed water is then delivered to the heat transfer module at the prescribed chemical, thermal, and deaerated condition. The conditioned sea water is distributed over the top portion of the vertical heat transfer surfaces by a spray system. As this water flows down the surface in a thin, gravity driven, film, approximately one-half of the water is evaporated. The residual concentrated brine flow at the base of the surfaces is pumped through the brine heat exchang preheated, and dumped. The pressure in the evaporating side of the module is equal to the saturation pressure of the evaporating saline film.

The product water in vapor form is removed from the evaporating saline film by the compressor, compressed, and ducted into the condensing section of the module where it condenses on the back side of the evaporator surface. The resultant condensate (product), driven by gravity, flows down the surface in a thin film. The product is then collected and pumped through the fresh water heat exchanger after which it is ready for use as potable water.

The heart of this system is the heat transfer module which when reduced to its simplest form consists of a multiplicity of parallel thin vertical or nearly vertical sheet metal plates. Each plate having an evaporating saline film on one side and a condensing fresh water film on the other. The heat required to evaporate the fresh water from the sea water is furnished by the condensing vapor and flows through the condensing film, through the plate and into the evaporating saline film. The energy to drive this heat is supplied by the compressor which raises the energy level of the evaporated vapor just enough to allow the flow of heat.

Each film then, is a resistance through which the heat must flow and, therefore, knowledge of the thermal and flow characteristics of these films, particularly the saline film, is of prime importance. The desired mean film thicknesses of these two films for this application is 0.0025 inches for the evaporating film and 0.0015 inches for the condensing film. Once it had been established that gravity driven water films 0.0015 inches thick could be obtained, it seemed reasonable to assume that the Nusselt equations for condensing films would describe and predict the heat transfer coefficients on the condensing side. The primary problem that remained was to determine experimentally if a modified form of the Nusselt equation could be used to describe and predict the heat transfer coefficient of evaporating thin films; and, if the system composed of the two films separated by a thin plate would have the overall heat transfer coefficient required to yield the predicted performance of the system. The required overall heat transfer coefficient assuming a 0.030 inch thick steel plate and fouling factor of 0.004 was 700 Btu/hr-ft^2 - °F. Even if the modified form of the Nusselt equation was found to hold, there remained the secondary problem of determining the effect, if any, on the heat transfer coefficient of a non-uniform flow. Since the proposed system utilized a spray distribution system, it was recognized that the saline film would not necessarily be uniform in either the horizontal or vertical direction or both.

The first problem is dealt with in Task I and the second in Task II.

The design and performance of the Thin Film Vapor Compression Saline Water Conversion System is dependent on the flow and heat transfer characteristics of a falling film of saline water. A system-oriented approach was felt to be most applicable to the task of defining a satisfactory thin film. Since the medium desired for the effective transfer of heat is a uniform thin sea water film, this task was directed toward obtaining this film in such a situation that the thermodynamic characteristics could be determined and used as an unqualified measure of the satisfactory or unsatisfactory nature of the film.

Summary

A satisfactory thermodynamic determination of the characteristic of saline water films has been accomplished under Task I. The film is inherently stable as predicted and the value of the experimentally determined overall heat transfer coefficient is 95 per cent of the theoretical coefficient.

Technical Approach

The design oriented approach constituted a measure of the effects of the properties as a whole and resulted in data which in the final analysis is most directly applicable to thin film vapor compression system design. Thus, the problem of determining the accuracy with which each of the properties is known is resolved into the single task of determining the accuracy with which the overall transfer of heat can be predicted.

There were some problems to be solved in order to approach the problem on an overall performance basis. First, the system had to be free of any effects such as pulsed feed flows; that is, the base line heat transfer data should come from the most idealized geometry possible. Toward this end the films were created at the top of a heat exchanger surface by a multiplicity of small notched weirs in parallel. Stability and uniformity of flow through weirs had to be established and was accomplished through cold flow checks using dye to evaluate film uniformity.

In order to initially wet the plate, the feed flow had to be increased many times its design flow. Provisions for this type of local flooding have been found necessary in all circumstances.

Since it was thought possible that the dissolved air in the feed water could affect the heat transfer a packed column deaerator was designed to deliver water at an oxygen concentration of 0.1 ppm which is the level set for the elimination of serious corrosion. The inerts proved significant enough to justify a quantitative determination of their effect.

Measurement of flow of a fluid with variable properties, particularly the concentrated brine, can only be done accurately by collecting the flow.

Temperature differences of the order of 2°F are difficult to measure satisfactorily through the use of thermocouples; therefore, the differential pressure between the condenser and evaporator, corrected for vapor pressure lowering at the average salinity, was used to find the actual temperature difference.[1] The system performance can be further described without a dependence on the vapor pressure lowering data simply by comparing the differential pressure with the production which is, after all, the design parameter of economic significance since it determines the compressor work. This is in keeping with the objective or design oriented approach mentioned previously.

In order to obtain a more comprehensive picture of the system performance, provisions were included to vary temperature level, feed water subcooling, feedwater flow, production rate, and inert removal.

Each of the above problems being attacked in the manner described resulted in the successful completion of Task I.

Description of Experimental Apparatus

Figures I-2 and I-3 are the corresponding schematic and photograph respectively of the Task I thin film vapor compression rig. The feedwater portion of the system consists of a constant temperature bath, deaerator, feedwater pump and module inlet flow meter delivering 120°F deaerated saltwater to the module. The level in the constant temperature bath is maintained by preheated make-up water.

The module (Figure I-4) consists of two 1' x 1.5' x .030 inch monel heat transfer surfaces mounted back to back and joined at the top by a pair of matched weir plates which are capable of producing identical saline films on the two plates. The total active area of these two plates is three square feet.

Since plate wetting, film uniformity, and stability were of particular concern, the design of the Task I rig included maximum visual access. The major material of construction was acrylic plastic which yields not only good visibility, but because of its low thermal conductivity, affords good insulation. In order to thermally shield the test section from the surroundings, a blanketing hot air system was designed and fabricated. Air at a temperature slightly greater than the temperature of the product vapor is directed over the faces of the module at a velocity of 700 fpm. The overall heat transfer coefficient for the above conditions was calculated to be 0.15 BTU/hr-ft^2 F° making any heat leak into the module negligible but still enough to prevent condensation from forming on the face plates. This assured good visual access.

The space between the two plates constitutes the condenser into the bottom of which the compressed water vapor from the evaporating saline film is introduced. This vapor being at a higher pressure and therefore having a higher saturation temperature than the evaporating film will condense on the back of the heat transfer surface, the latent heat passes through the plate and evaporates a like amount of water from the saline film.

In this rig, the compressor is a positive displacement sliding vane pump with a variable speed drive. Excess superheat resulting from friction in the compressor is removed satisfactorily from the module inlet manifold. Inert removal is accomplished through a tap at the top of the condenser and through the condensate drain at the bottom.

Metering of the condensate and concentrated brine flow was accomplished by collecting the flows and then correcting the density for temperature and salinity. These flows can be metered to within one per cent of the true flow using this method. The product flow along with the pressure differential from condenser to evaporator gives the most accurate description of system performance. The pressure differential is measured in inches of water and can be read to within two per cent. The estimation of the active area and boiling point elevation (vapor pressure lowering) can also contribute errors of the same order of magnitude.

For overall system monitoring, calibrated copper constantan thermocouples were used. Thermocouple outputs were measured with a potentiometer which could detect changes in output voltage equivalent to .2°F in the 120-122°F range.

Absolute pressure levels were measured using closed end mercury manometers with a readability to the nearest .05 cm Hg.

Oxygen concentration of the module feed water could be determined by drawing a sample of the feed flow out through a cooler and into a standard collection bottle and then running the Winkler oxygen concentration determination on the sample.

Inlet salinity was fixed at 3.50 per cent NaCl solution by premixing the feedwater in this concentration. The outlet salinity was determined by evaporation of samples. Since there is a relationship between the inlet and outlet salinities and the ratio of the mass flows, it was possible to obtain a cross check on the mass balance. The salinity of any sodium chloride solution can be measured to within one per cent by evaporation and weighing.

Surface tension measurements were made using a manual tensiometer which had a repeatability of around $\pm$ 5 per cent. This scatter makes detection of the predicted small changes in the concentrated brine surface tension impossible to detect; however any gross changes resulting from contaminants can be detected.

Results

The objective of Task I was to determine the characteristics of a satisfactory saline water film. This was accomplished through the successful operation of the thin film heat transfer configuration coupled with a vapor compressor. All items of both technological and quantitive significance gained during the work on this phase will be reported in this section. The nomenclature and sample design and performance calculations are shown in Appendix A-I & II.

A singular difficulty was encountered during start up of the Task I system. With feed water at design temperature and with the evaporator pressure equal to the saturation pressure of the feed water it was difficult to remove any vapor from the evaporator, with the compressor, without lowering the evaporator pressure below the feed water saturation pressure. This condition resulted in vigorous flashing in the weir reservoir which destroyed the continuity of the film on the plate. In order to remove vapor from the evaporator without flashing, heat must be supplied through the plate to produce the vapor. This condition exists automatically under equilibrium conditions, but must be induced during start up. This was accomplished by supplying auxiliary steam from an external source to the condenser.

The starting difficulty is aggravated by the presence of inerts in the system after initial pump down. These inerts build up in the condenser faster than they can be removed with the provisions for steady state operation and resist the transfer of heat through the plates. The auxiliary steam helps to purge the condenser of these inerts.

A successful starting procedure of the Task I rig consisted of the following steps:

1. Initiate the evaporating side film while the system is still at atmospheric pressure.

2. Pump the system down close to the saturation pressure of the feed water.

3. Introduce steam into the condenser in order to purge inerts and provide the compressor with its start up flow.

4. Open inert extraction valve and increase compressor speed to operating point.

The significant parameters used in determining the heat transfer coefficient of the system consisting of a falling evaporating saline film and a falling condensing pure water film separated by a thin heat transfer surface were:

1. Effluent brine and product flows

2. Pressure difference between the condenser and evaporator

These values could be determined with accuracy and repeatability.

Verification of the theory[2] of thin film heat transfer was made within engineering accuracy. There is, however, another effect on the overall heat transfer that could not be determined from these tests. That is, the effect of fouling on the heat transfer coefficients.

Some of the factors which do affect the heat transfer coefficient, U_o, and which were investigated with the Task I rig are:

1. Circulation ratio "R", feed flow/product flow

2. Temperature level "Tsea", feed water saturation temperature

3. Influent flow "W_s", lbs/hr-ft

4. Noncondensables

5. Transients in the evaporating film

All of the Task I tests were run with a 3.5 per cent NaCl solution.

Figures I-5, I-6, and I-7 show the change in overall coefficient of heat transfer, U_o, with a change in the circulation ratio, R, for several flows at some nominal temperature level. The range of R over which U_o could be determined was limited in some cases by compressor capacity.

Figure I-8 is intended to demonstrate the effect of the temperature level on the overall coefficient. This figure is a composite of the curves from Figures I-5, I-6 and I-7 corresponding to the

nominal design flow. Figure I-8 justifies the acceptance of a characteristic shape to the experimental U_o versus R curve for Task I heat transfer. The theoretical heat transfer is shown in Figure I-9. The experimental data is 6.2 per cent low at the design circulation ratio. (Fig. I-10)

The variation of the ratio, $\frac{\Delta P}{Pe}$, (the pressure rise to the absolute pressure level in the evaporator) with the production per foot width of heat transfer surface for the Task I runs with design influent flow is shown in Figure 10. This is the curve which must be considered in the last analysis since it represents the amount of compressor work required to produce the desired amount of product. The relationship between $\frac{\Delta P}{Pe}$ and compressor pressure ratio is shown in Appendix A-I & II-5. Included on Figure I-11 is the predicted system performance and here the experimental results are 6.7 per cent lower than theory at the design point.

Since the geometry of the thin film system tends to resist the natural removal of inerts from the condenser a check was made to determine if reduction in heat transfer would occur at very low contamination levels. Any air in the product vapor will tend to pack up against the condensing film as the vapor condenses. Under the action of gravity these inerts tend to fall. however, the incoming vapor is traveling upwards and tends to carry the inerts back to the top but since the vapor velocity at the top of the condenser is zero the the inerts will again try to fall. Thus the geometry tends to entrain noncondensables.

The procedure for determining the leak rate of air into the system was to measure inlet and outlet oxygen concentration with the module at operating temperature and pressure, but not producing water. The increase in oxygen concentration of the flow through the module with no air bubbles in either the inlet or outlet was used to establish the steady state leak. In addition to this leak, controlled leaks were introduced to find the relationship between per cent inerts by volume in the product vapor flow and the overall heat transfer coefficient.

The necessity for removal of inerts at the top of the condenser at the minimum leak rate was demonstrated by an increase in differential pressure when inert removal was attempted using the bottom tap only. A return to the lower differential pressure occurs when inerts are removed from the top.

How the overall heat transfer coefficient is affected by the volume ratio of inerts entering the system to the vapor flowing through the system, Qi/Qv, both evaluated at condenser pressure and temperature is shown in Figure I-12 and Table 1. Note that the per cent inerts by volume is in the range of 0 to .01 per cent (0 - 100 ppm by volume). Conservative extrapolation of this data indicates that 95 per cent of theoretical heat transfer can be attained with the total exclusion of inerts. Although this could never be achieved practically, the amount of leakage into a conversion system two orders of magnitude larger would not have to be any greater than that into the Task I rig. This is because the number of seals, particularly the compressor shaft seals, necessary in each case would be the same. Thus, it is safe to assume that the result obtained by extrapolation of Figure I-12 is attainable.

An alternative way of presenting this same information is shown in Figure I-13. This curve eliminates the dependence of the experimental data on the boiling point elevation and therefore, can be used for an overall quantitative evaluation of the theoretical data. Again a conservative extrapolation places the maximum expected differential pressure at less than 4 per cent above that predicted.

Since the film will be created by periodic application of sea water from a traversing spray, the effect of a sudden wave passing over the plate with subsequent cessation of flow was of interest. The average feed rate over the period investigated remained constant at the design level as would be the case with spray distribution. The effect on the differential pressure could readily be measured as a function of time starting when the steady film feed was interrupted by a wave. (See Figure I-14). At point "A" the evaporating film was suddenly made thicker with a resultant increase in ΔP to point "B" at which point the wave passed far enough down the plate to leave behind a thinner than normal film. The average salinity of this residual film is less than that of a steady state film. This effect is due to the wiping action of the wave. This resulted in increased heat transfer rates to the point "C" at which the boiling point elevation of the rapidly evaporating film starts to overcome the effect of decreased thickness. The boiling point elevation becomes the predominant factor until the steady state film starts to reform at point "D". The higher than normal ΔP in this case was a result of the high operating temperature - approximately 125°F.

It might be noted that on the composite Figure I-15 that 94 per cent of all data points regardless of feed flow (Ws), circulation ratio (R) or inlet temperature (Tsea) fall within the $\pm$ 4 per cent range included between the two dotted lines. The effect on the overall heat transfer of the variables Ws, R and Tsea in the range covered was so small as to be almost undetectable within the experimental accuracy of the Task I rig.

There are several more points of information that were derived from the experience with Task I. The first was the method for the creation of the film. This can be accomplished through local flooding of the plates or by adding wetting agents to the feed flow for a short time providing the wetting agents don't react with the feed water. It was also found that when fresh water was used to flood the plates with saline water flowing over them, portions of the plates previously wet with a uniform film would cease to maintain that uniform film. There was an instability in the film on the weir plate which was apparently associated with this same effect.

During the initial shake down runs of the Task III corrosion rig, the sea water film just down stream of the weir notches on the feed plate was observed to separate into discrete streams. Although the film flow could be restarted by flooding with sea water the film would break down again after a short period of time. Previous observations of the effect of fresh water coming in contact with a saline water film led to the belief that this film separation was due to product vapor condensing on a subcooled weir film.

It was decided to try to duplicate this phenomena on the Task I rig where observation and control were more convenient. After design running conditions had been stabilized, the feed water was cooled until the film down stream of the weir notches separated into discrete streams. This occurred when the feed flow was subcooled some 10-15 F°. It should be noted that in both cases, the first in the Task III rig with sea water and the second in the Task I rig with a 3.5 per cent NaCl solution, that the separation started on the weir plate where the film receives no heat from the condenser. Apparently the condensing vapor sets up concentration gradients in the film causing the thinner portions of the film to flow into the thicker portions and gradually causing the film to break down. During the Task I test the film could not be re-established by simply raising the feed water temperature back to its design value. The theory concerned with this instability problem is discussed in detail in Task IV.

Surface tension lowering contaminants should have an unstabilizing effect on an evaporating brine film since the increase in contamination parallels the increase in salinity and can overcome the increase in surface tension associated with an increase in salinity. This would result in the thin portions of the film having a lower surface tension and flowing into the thicker portions. Although the instability was noted during several runs of the Task I rig, no attack on the problem was made until Task II.

Carry-over was measured by checking the product purity in ppm by weight of NaCl. The product purity was consistently below 0.4 ppm indicating no carry-over which was expected in this case of ideal feedwater distribution.

Acid treated sea water was run through the Task I rig on one occasion and indicated that the performance fell within the $\pm$ 4 per cent range on Figure 14.

The agreement between the circulation ratio as determined from the measured flows, and the salinities has been generally within 2 per cent indicating the degree of reliability of the associated measurements.

Conclusions and Recommendations

1. 95 per cent of the theoretical performance was attainable in this the ideal or base line thin film vapor compression saline water conversion rig.

2. Wetting of the surfaces will not occur naturally and must be induced. Initial wetting can be accomplished by flooding nozzles.

3. From the damaging effect that fresh water was observed to have on a saline film, it would be advisable to design the shell so that condensation could not fall onto the heat transfer surface.

4. Start up requires either a compressor by-pass or variable speed drive. The latter choice would favor a turbine drive.

5. Continuous removal of inerts from the dead ended condenser is necessary to achieve the level of performance reported.

6. A particularly tight vacuum system will be required because the heat transfer can be reduced significantly by very small quantities of inerts - in the range of 0 - .01 per cent by volume of the total flow. The effect of inerts is probably amplified by the tendency of the geometry of the system to trap them.

7. Feedwater temperature must be kept subcooled 2 F° to prevent flashing in the weir reservoir, but must not exceed 10 F° or channeling on the weir plates will occur.

8. Work on Task I has determined the characteristics of a satisfactory thin film and has demonstrated within its capabilities the feasibility of the Thin Film Vapor Compression System as a saline water conversion process.

TABLE I - SUMMARY OF THE EFFECT OF INERTS ON THE OVERALL HEAT TRANSFER COEFFICIENT

Date		1-22	1-22	1-31	1-31	1-31	1-31	2-1
Run		1	2	2	3	4	5	2
Base leak	(sccm)	2.75	2.75	.30	.30	.30	.30	.21
Controlled leak	(sccm)	6.0	9.6	0.	3.00	.65	1.40	0.
Gross leak	(sccm)	8.75	12.15	.30	3.30	.95	1.70	.21
T_c	°F	123.7	124.5	127.8	129.6	128.6	129.2	124.3
P_c	cm Hg abs.	9.86	10.08	10.38	10.71	10.50	10.71	9.80
Q_i	cfm x 10^4	21.4	29.1	.70	7.51	2.20	3.86	.52
w_f	lbm/hr	4.28	3.82	4.61	4.87	4.85	4.93	4.45
v_G	ft^3/lbm	181.7	178.0	173.1	167.6	171.5	167.6	182.7
Q_v	cfm	12.95	11.34	13.31	13.60	13.87	13.78	13.55
Q_i/Q_v	x 10^4	1.652	2.56	.053	.552	.159	.280	.038
U_o	Btu/hr-ft^2F°	430.	395.	813.	755.	810.	755.	791.
$U_{theo.}$	But/hr-ft^2F°	840.	840.	840.	840.	840.	840.	840.
$U_o/U_{theo.}$		.512	.470	.968	.899	.964	.899	.942
ΔP	in H_2O	4.7	5.1	4.4	5.1	4.75	5.1	3.95
P_e	in H_2O	47.9	48.7	51.0	52.1	51.3	52.1	48.3
$\Delta P/P_e$		.0981	.1048	.0853	.0979	.0926	.0979	.0818
$\Delta P_{exp.}/\Delta P_{theo.}$		1.29	1.61	1.041	1.13	1.07	1.11	1.033

TABLE I - (Continued)

Date		2-1	2-1	2-1	2-18	2-18	2-18
Run		3	4	5	6	7	8
Base leak	sccm	.21	.21	.21	.24	.24	.24
Controlled leak	sccm	1.46	3.10	5.89	0.	.98	2.70
Gross leak	sccm	1.67	3.31	6.10	.24	1.22	2.94
T_c	°F	123.9	124.9	125.6	126.9	128.2	127.6
P_c	cm Hg abs.	9.75	9.95	10.10	10.55	10.93	10.75
Q_i	cfm x 10^4	4.13	8.03	14.61	.66	3.26	8.00
w_f	lbm/hr	4.45	4.56	4.50	4.42	4.55	4.68
v_G @ P_c	ft^3/lbm	183.6	180.2	177.7	170.2	164.5	167.2
Q_v	cfm	13.61	13.71	13.31	12.58	12.49	13.05
Q_i/Q_v	x 10^4	.303	.585	1.098	.058	.261	.613
U_o	Btu/hr-ft^2F°	752.	720.	655.	759.	737.	692.
$U_{theo.}$	Btu/hr-ft^2F°	840.	840.	840.	840.	840.	840.
$U_c/U_{theo.}$		.895	.857	.780	.904	.878	.824
ΔP	in H_2O	4.10	4.35	4.70	4.35	4.69	4.95
P_e	in H_2O	47.9	48.8	49.2	52.0	52.3	52.1
$\Delta P/P_e$		.0856	.0892	.0955	.0836	.0897	.0950
$\Delta P_{exp.}/\Delta P_{theo.}$		1.081	1.099	1.191	1.063	1.105	1.138

DWG. 626A734

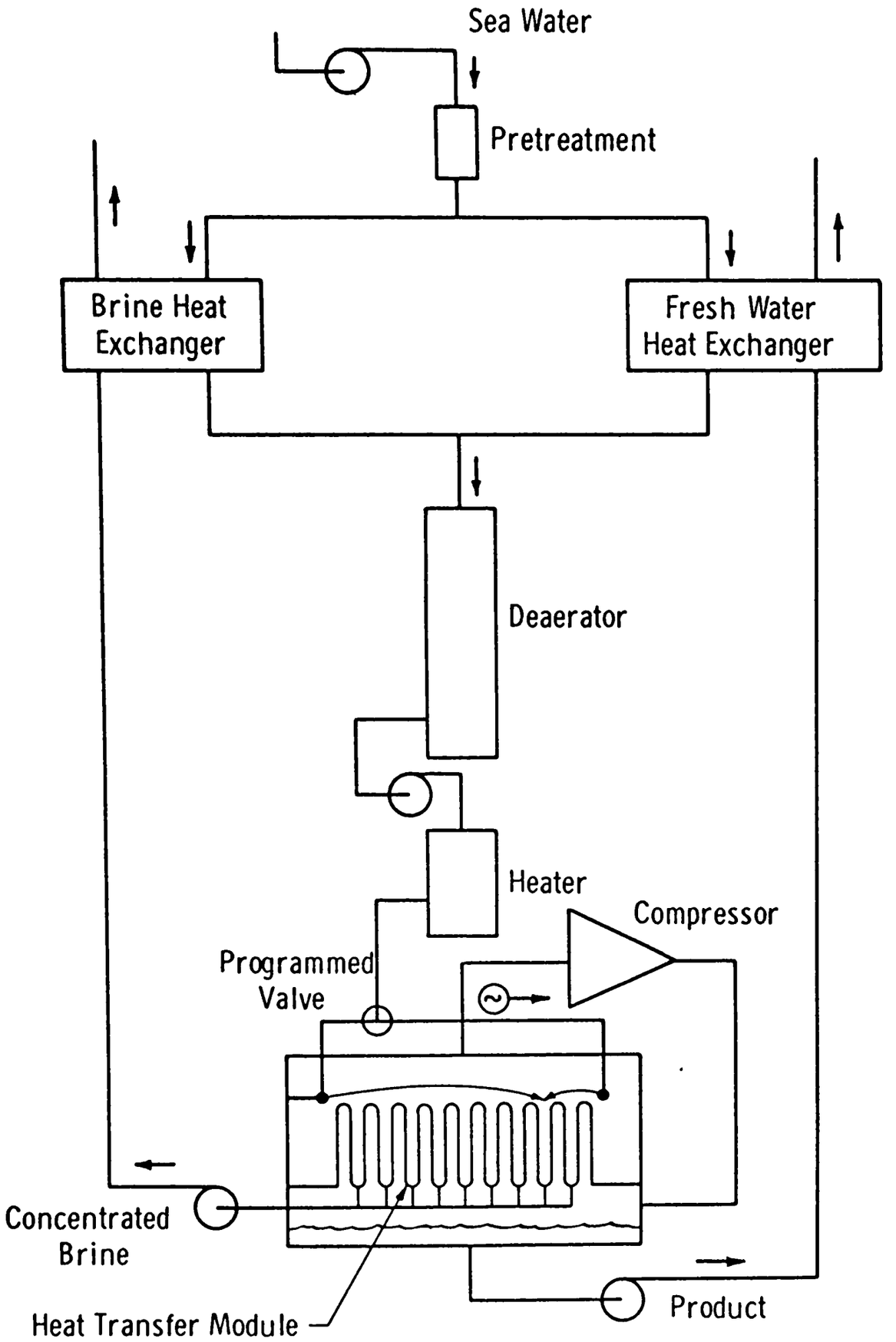

Thin film vapor compression system schematic

Figure I-1

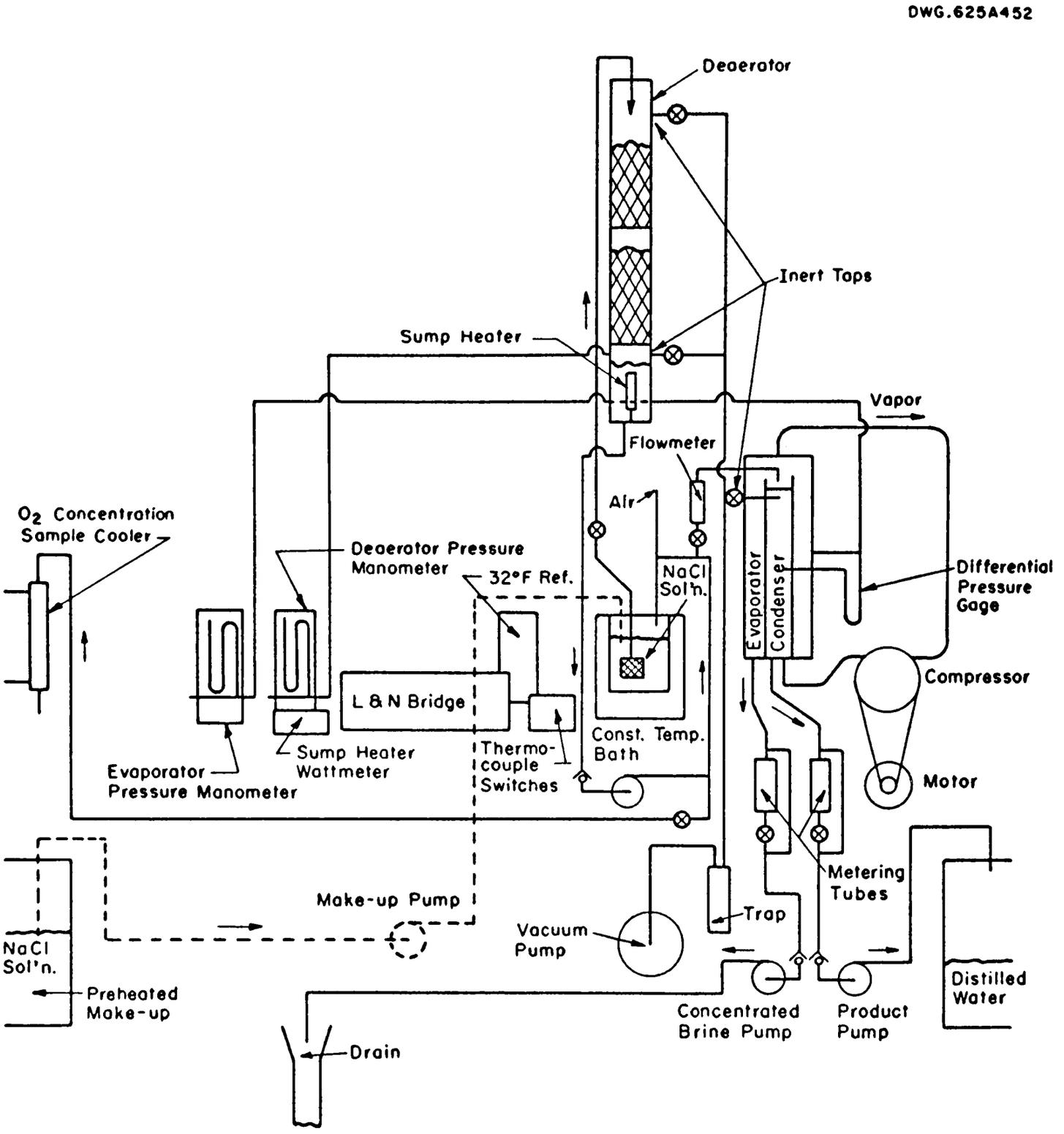

Task I Test Rig Schematic

Figure I-2

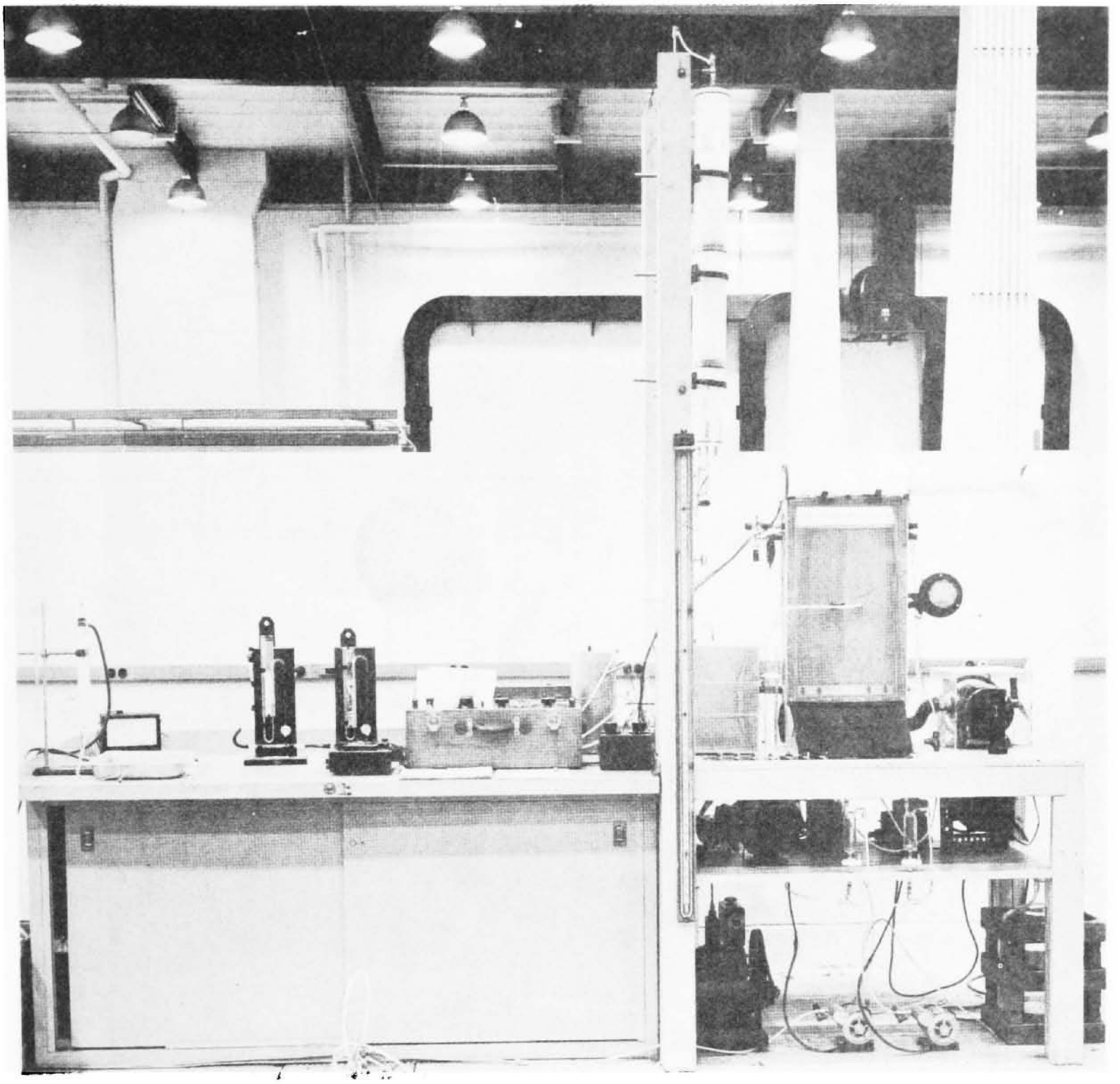

Figure I-3 Task I Thin Film Vapor Compression System

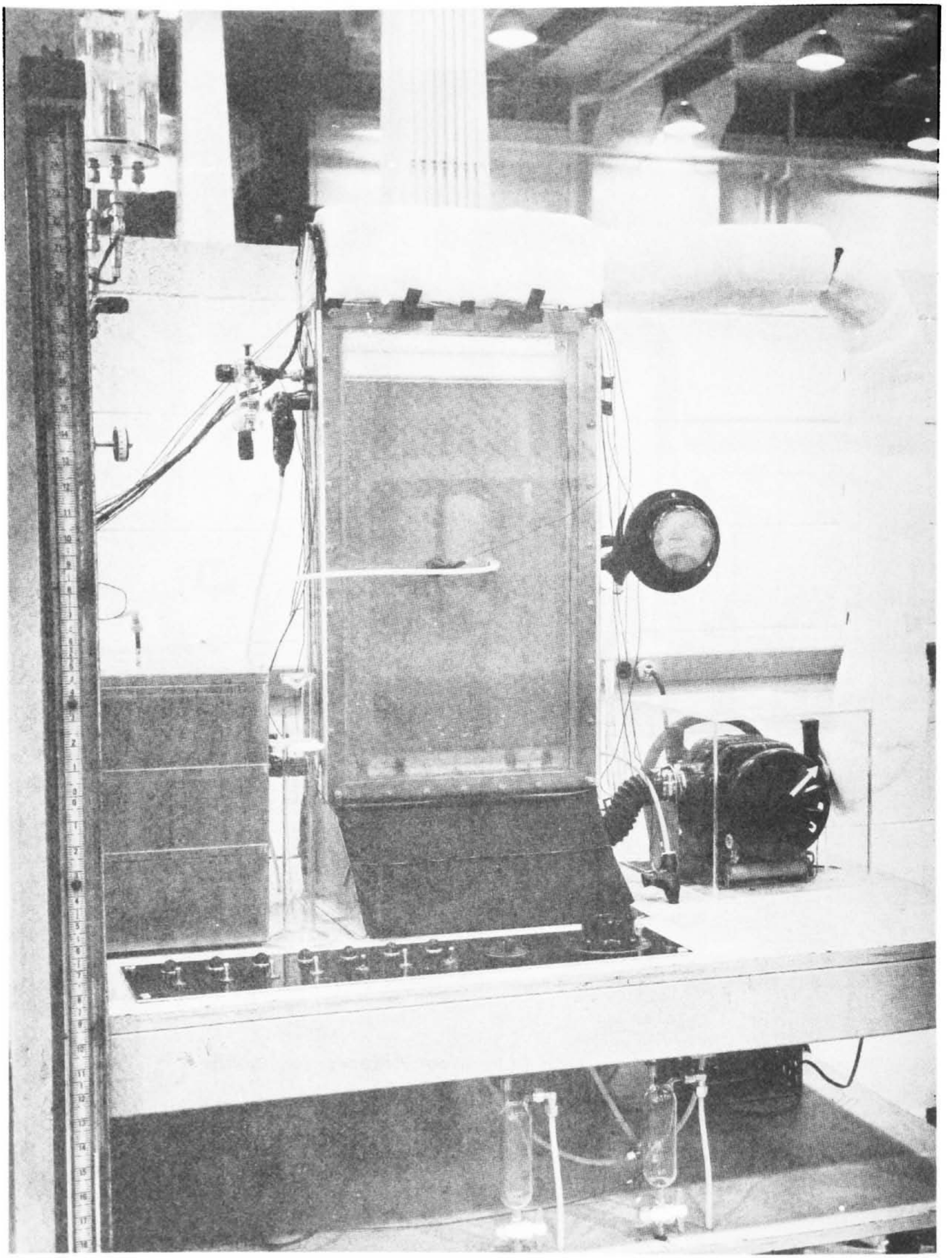

Figure I-4 Task I Base Line Heat Transfer Module

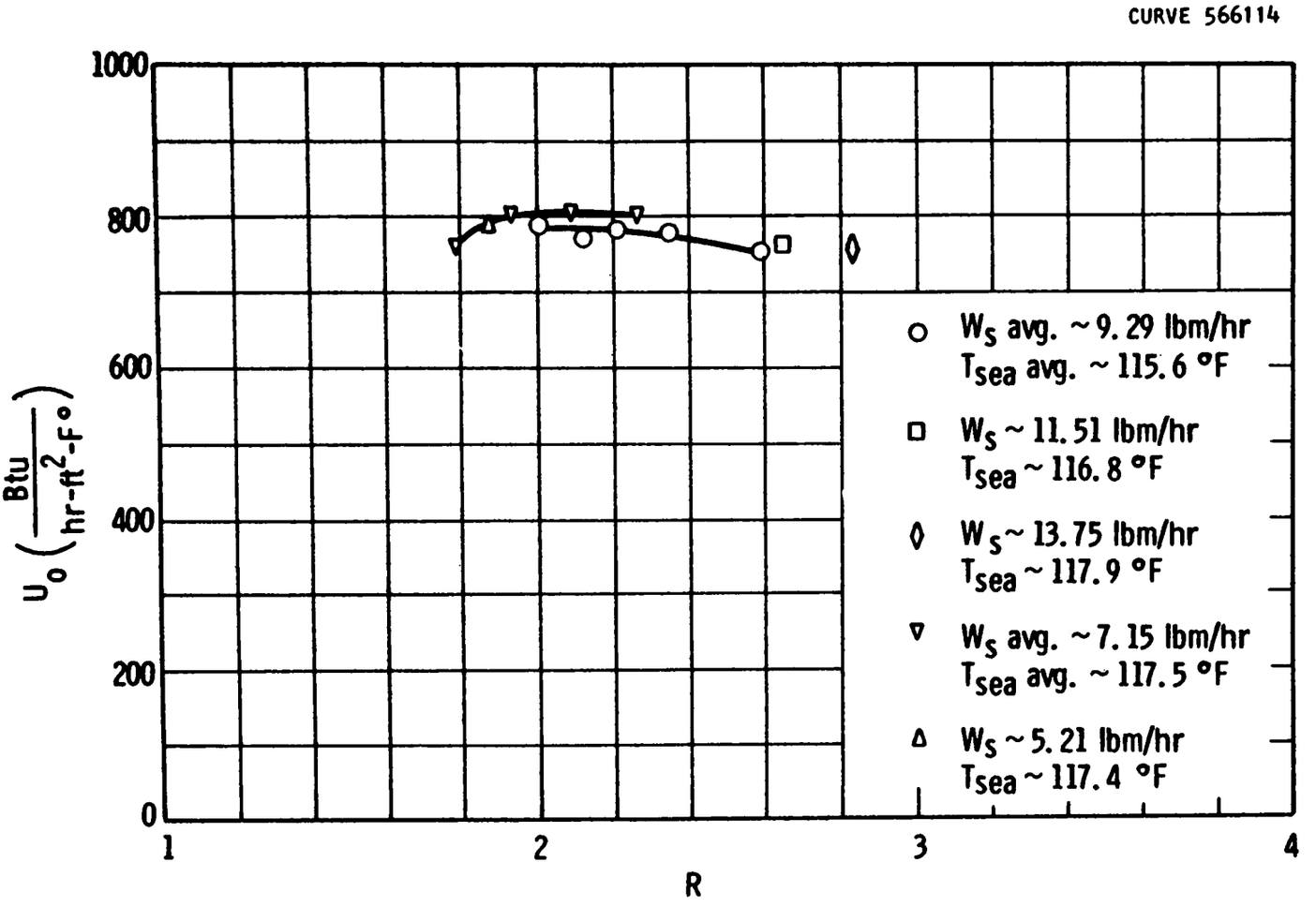

Fig. I-5—Overall heat transfer coefficient vs. circulation ratio

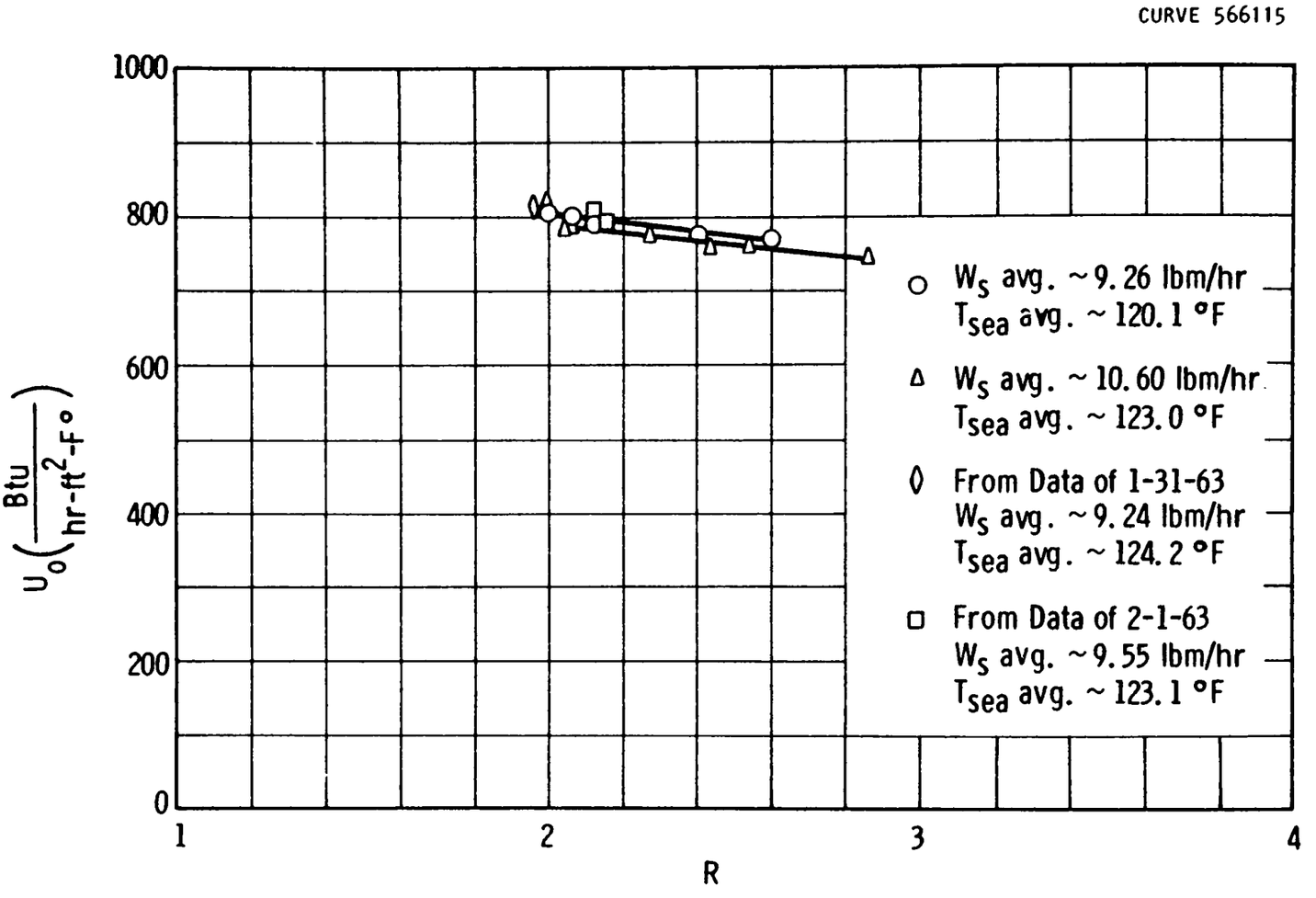

Fig. I-6-Overall heat transfer coefficient vs. circulation ratio

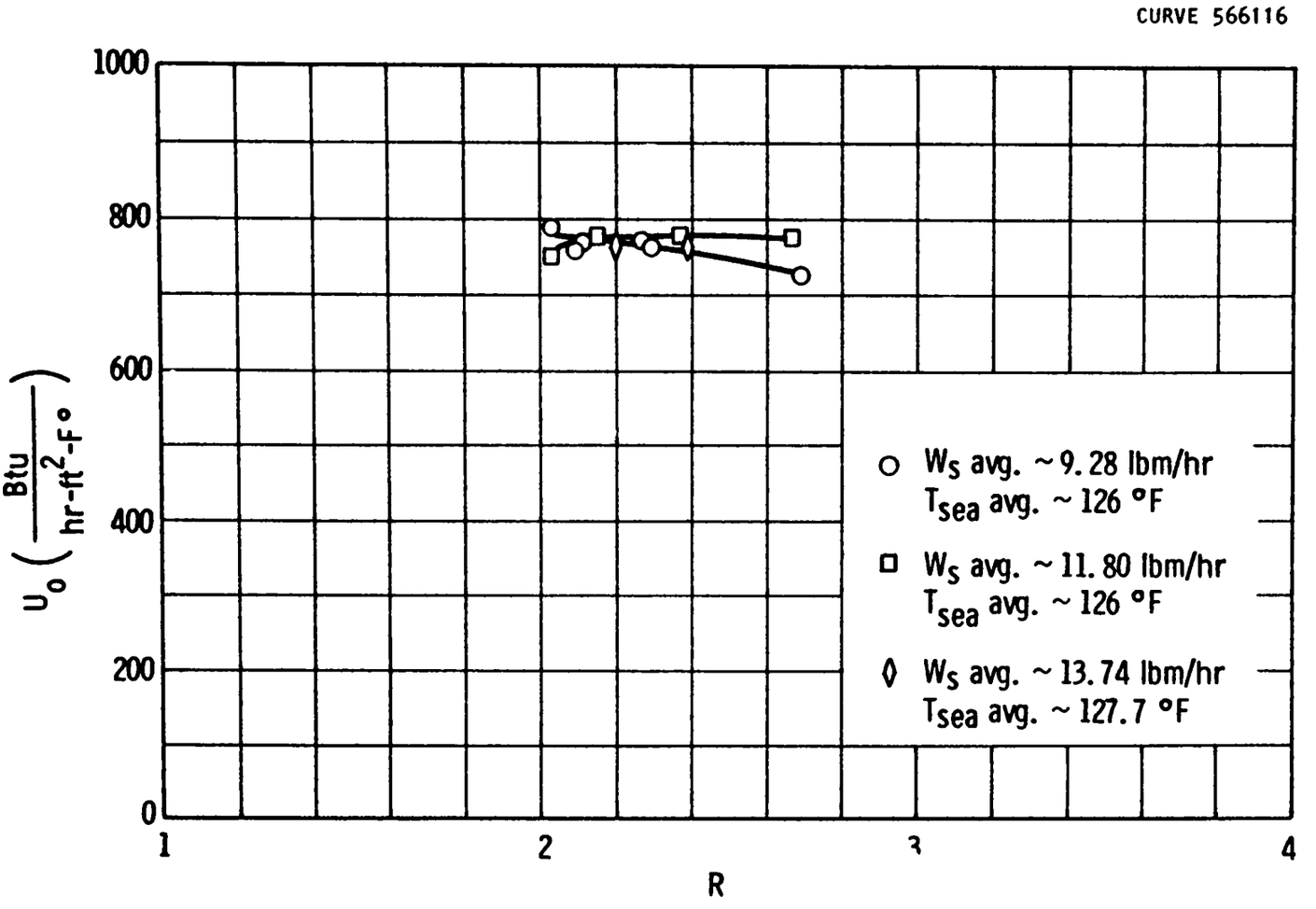

Fig.I-7 —Overall heat transfer coefficient vs. circulation ratio

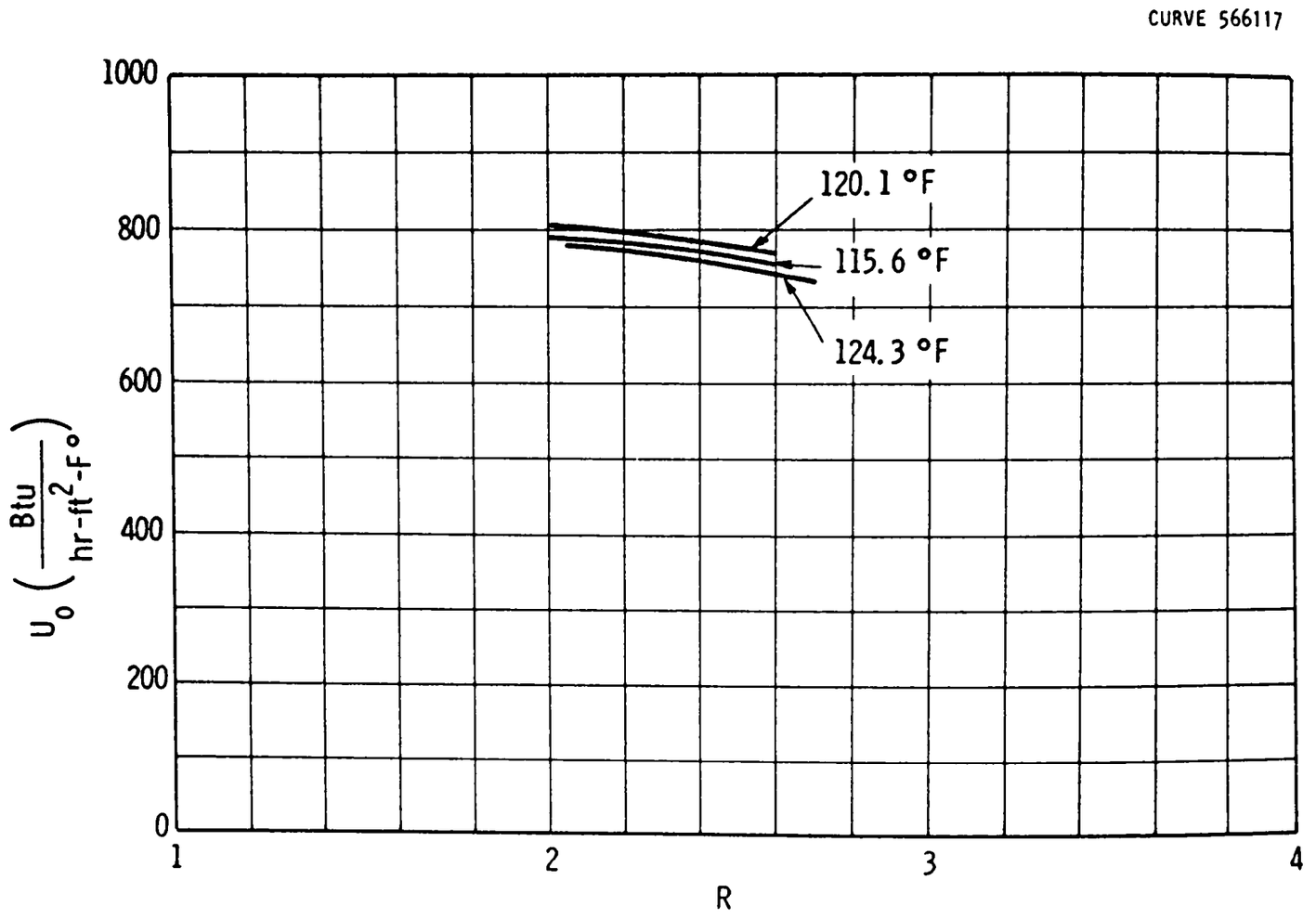

Fig. 3 —Composite of experimental data for design flow at the indicated T_{sea} temperatures — Taken from figures 1, 2 and 3

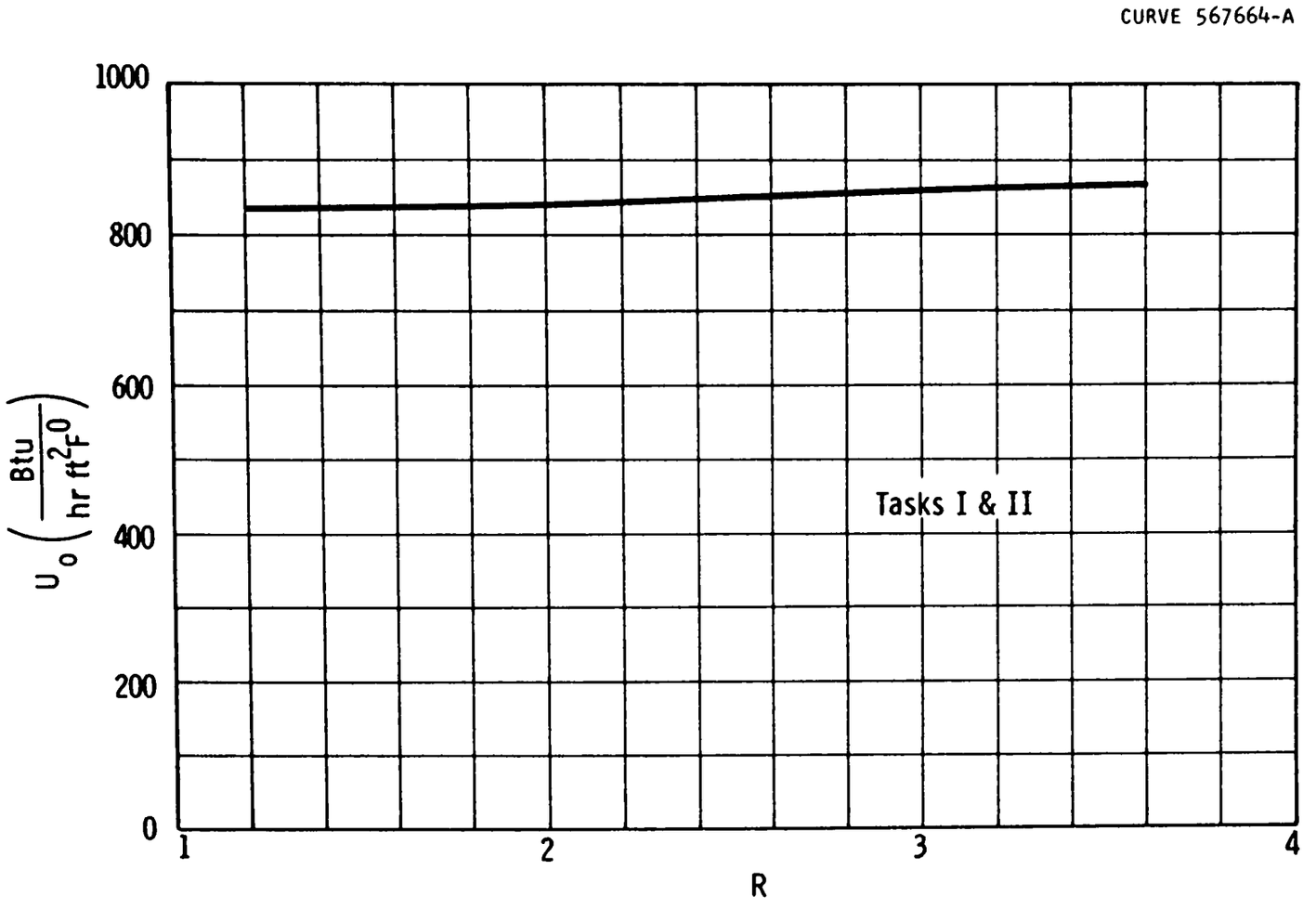

Fig. I-9 — Theoretical heat transfer for 3.40% sea water - neglecting B.P.E. limitation at low circulation ratios

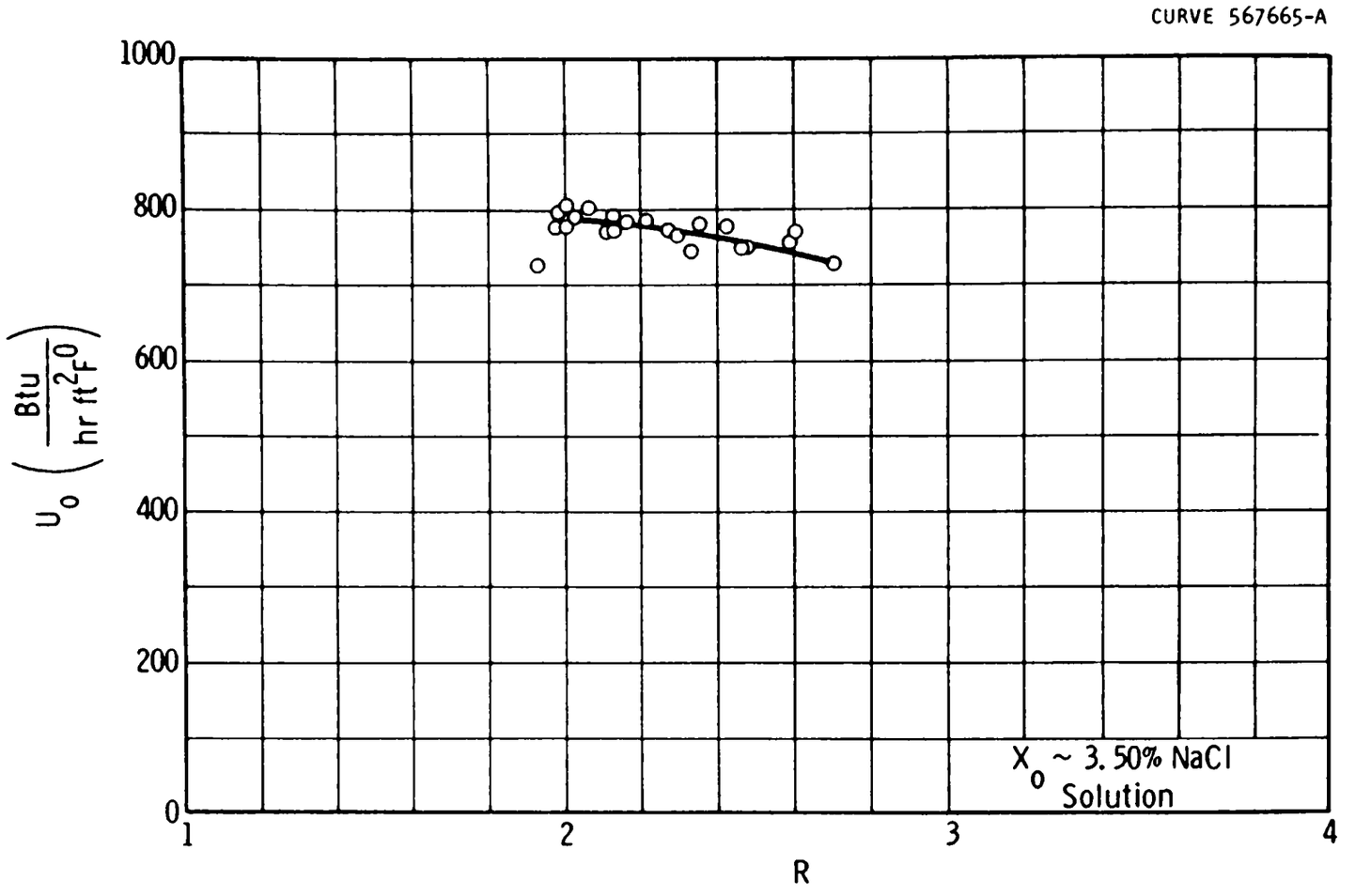

Fig. I-10—All Task I data with design inlet flow

CURVE 567666-A

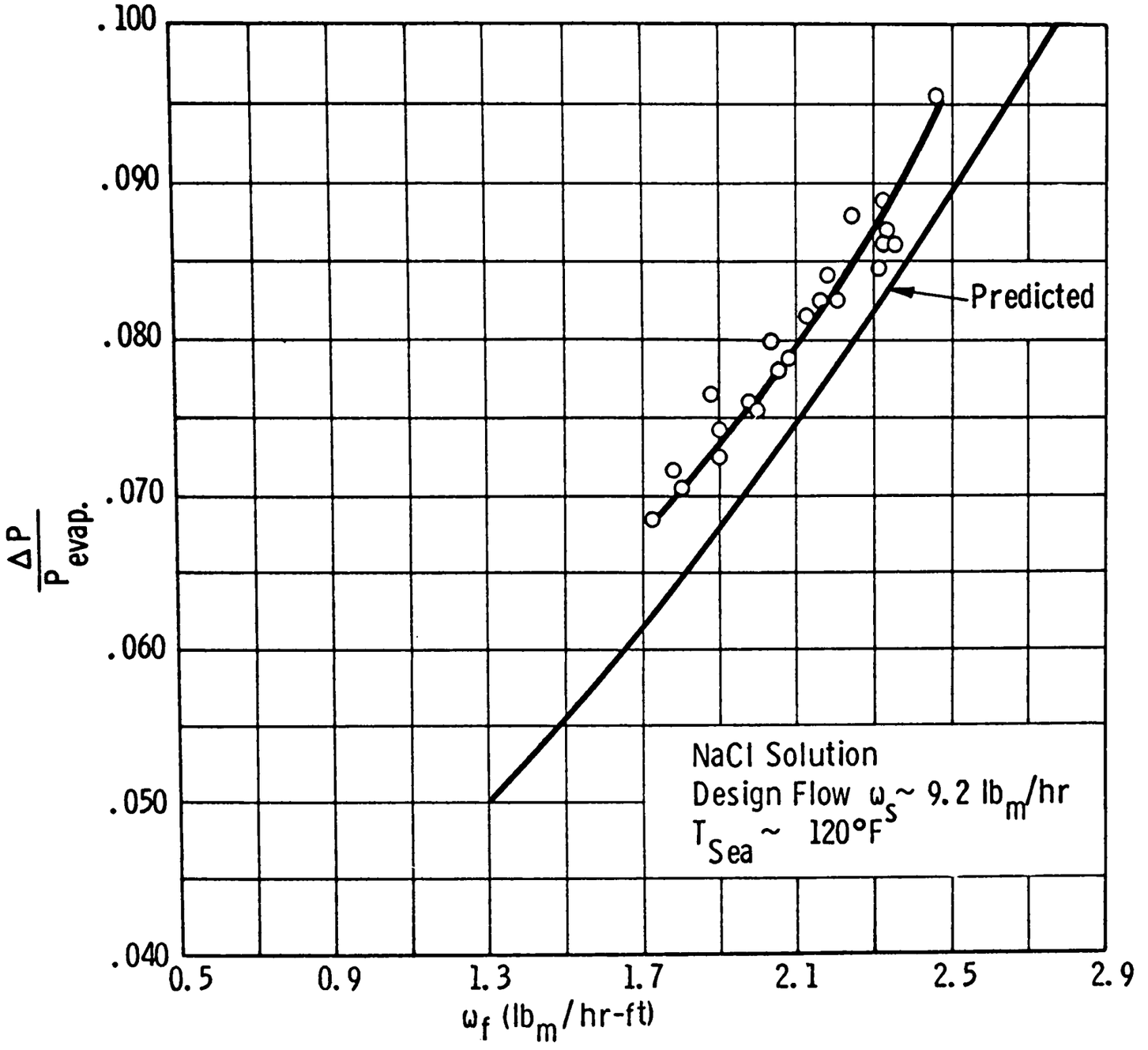

Fig. I-11—Task I heat transfer

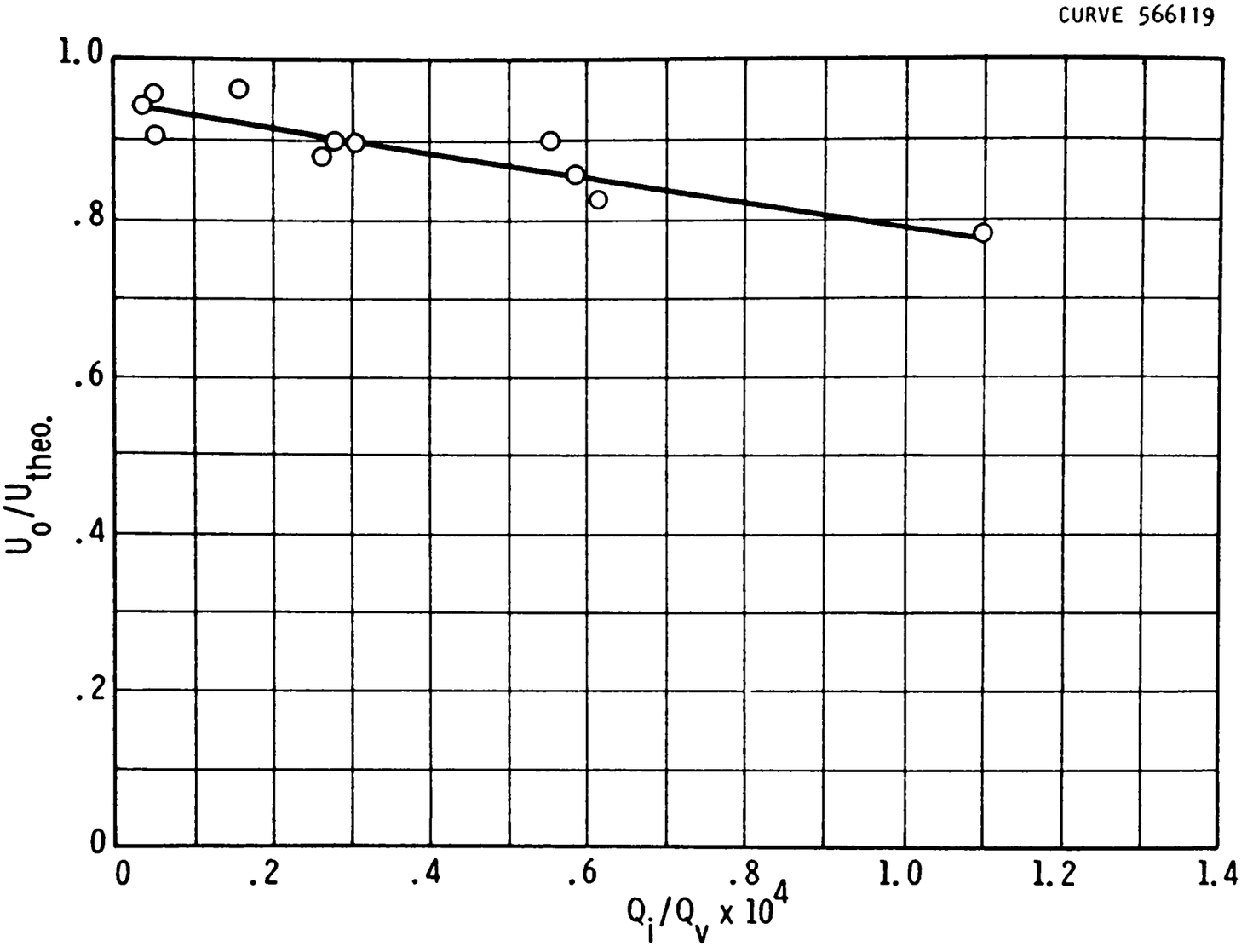

Fig. I-12—Experimental determination of the effects of inerts

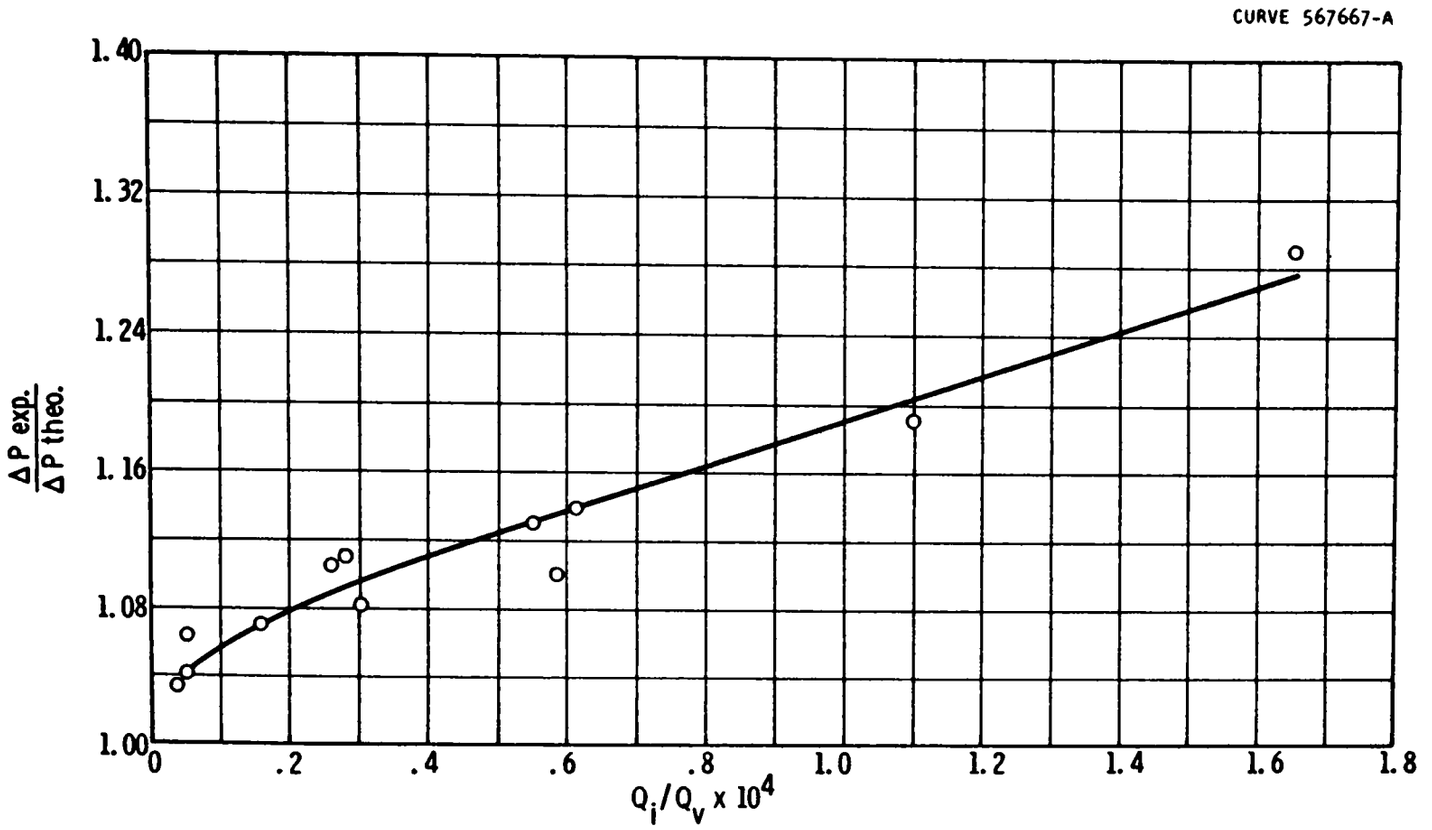

Fig. I-13 Experimental determination of inert effects on differential pressure required to obtain theoretical production rate.

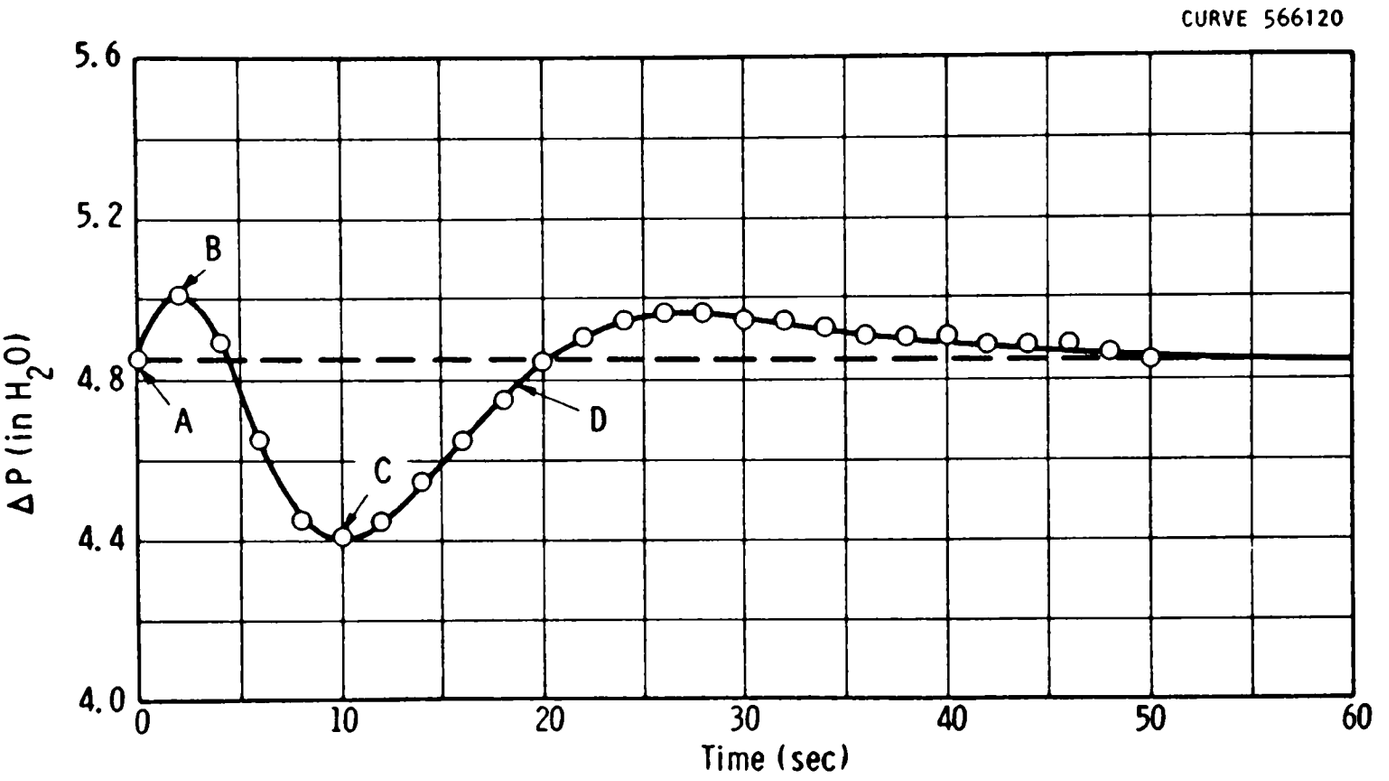

Fig. I-14 —Effect on ΔP of transient flow

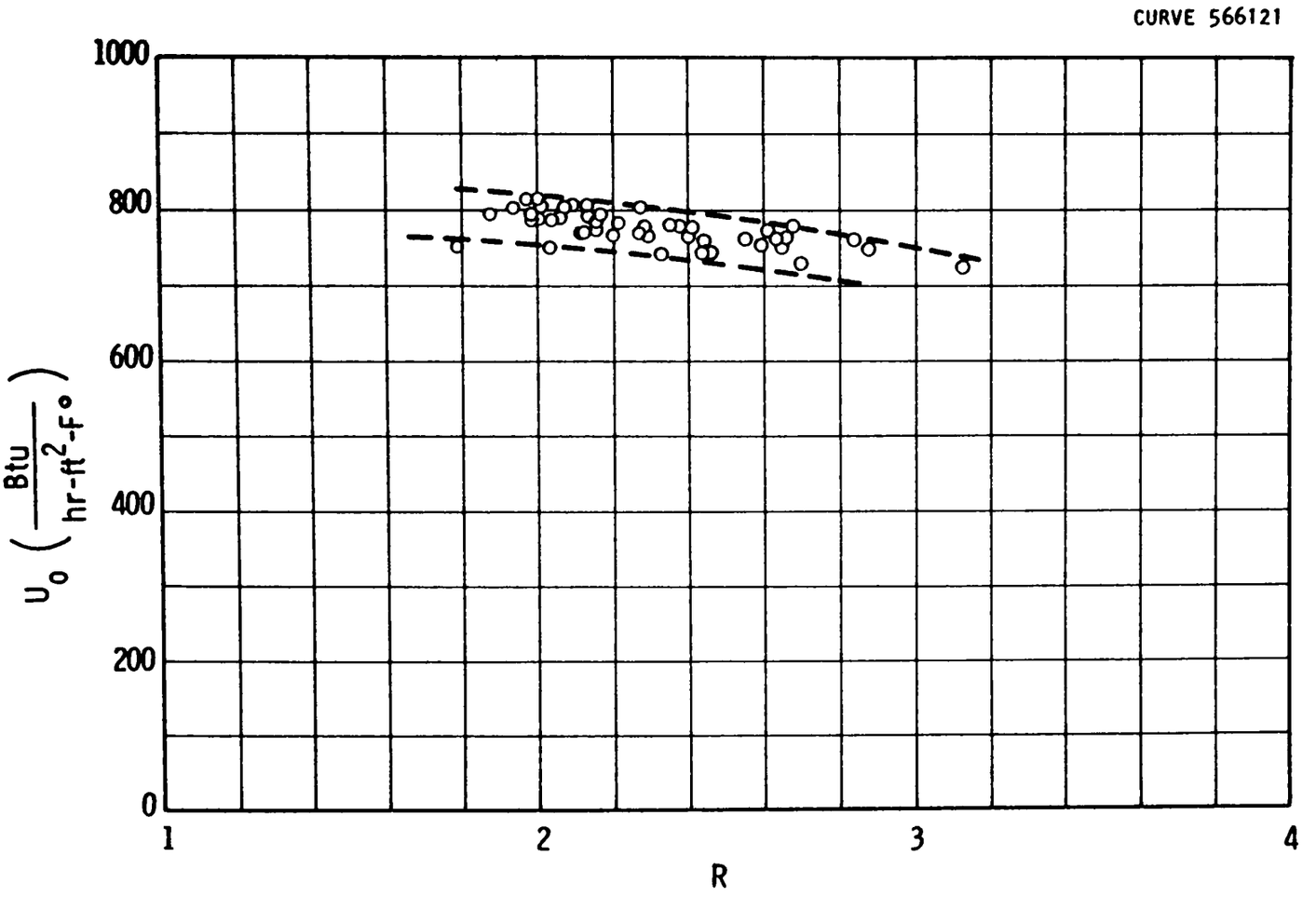

Fig. I-15—Composite of all Task I data

TASK II - The Development of the Technology of Creating and Maintaining a Satisfactory Film

Task Description

This task is concerned with the problem of designing and developing a sea water distribution system capable of supplying the required quantity of water to a heat transfer module. The heat transfer module consists of 120 vertical sheet metal plates 1-3 feet in width, 1.5 feet high and spaced 0.5 inches apart. (See Fig. I-1) The system requirements are such that:

1. Equal quantities of sea water must be supplied to each plate.
2. The resulting saline film must exhibit flow characteristics which will yield the required heat transfer performance.

The distribution system was designed to distribute a relatively large quantity of sea water with a minimum amount of hardware. The components of the system consist of two stationary spray bars, one at each end of the module, and a valve to program the pressure driving the water. The programmed pressure causes the sea water to travel varying distances by changing the efflux velocity from the spray bars. The pressure is programmed in a manner causing the spray to travel back and forth across the top of the module.

The characteristics of a saline film capable of yielding the required heat transfer performance were determined in Task I. The primary goal of Task II was to design and develop the distribution system to a point where it would create and maintain this satisfactory film. The degree of success with which the goal of Task II was met can be determined by comparing the experimental heat transfer data obtained on the Task II rig with that obtained in Task I.

Other goals of Task II were:

1. To determine the thermodynamic performance of the heat transfer module over a range of circulation ratios.
2. To compare the performance of the system using sodium chloride aqueous solutions and actual sea water.
3. To acquire experience in operating the conceptual Thin Film Vapor Compression system and thereby gain insight into the problems and peculiarities of the system as a whole.

Except for the effects of fouling, the data obtained during the experiments with the Task II rig were intended to verify all the assumptions necessary for the design and evaluations of the Thin Film Vapor Compression system.

Summary

The goals of Task II were met. The conceptual spray distribution system was developed to a satisfactory degree of performance and the theoretical performance of the Thin Film Vapor Compression system was verified experimentally. Adequate Technology was acquired to permit the design of a pilot plant; and the experimental results of Task II indicate that physical and thermodynamic properties of sodium chloride solutions can be used to design and predict the performance of the Thin Film Vapor Compression system for the conversion of sea water. This conclusion should be qualified to the extent that it has been shown to hold in the temperature range 115°F to 130°F.

Technical Approach

Determination of what variables must be known to describe the Task II rig operation satisfactorily can be simplified by stating that all the information pertinent to the thermodynamic character of the Task I rig is equally applicable in this case. In fact, one of the objectives of Task II is to obtain technical data, equivalent to that of Task I. There is in addition the variables of flow, temperature level, and pressures, the consideration of the hydraulics of the Task II distribution system. Here the flow through,and pressure drop across the components of the variable velocity spray distribution system as well as the degree of uniformity of the sprayed pattern must be known and controlled to evaluate the effectiveness of the distribution. Because any design assumes a fixed feed flow, a particular solution is applicable to only one geometry. Any modifications in the distribution system operation must be compensated for in the programmed disc of the value. This mechanical versatility must be incorporated into the programmed valve.

In order to verify the assumption that sea water and sodium chloride solutions can be described as having nearly the same physical and thermodynamic properties, the Task II distribution and distillation sections were run over the same range of fresh water production with both a sodium chloride solution and sea water.

The problem of non-wetting was anticipated through the installation of an overhead flooding nozzle.

Because of the low pressures at which the system operates, the shell design was of mechanical significance. Also of importance in considering the shell design is the physical and visual access which can be provided without compounding sealing problems. Severe corrosive attack of the tank material would not normally occur if the pressure and oxygen concentration at design conditions were maintained. The experimental nature of this work required frequent access to the shell at atmospheric pressure and therefore the shell interior was given a corrosion resistant coating. Ducting of the product vapor required a geometry which would minimize carryover and pressure drop.

Deaeration of the feed water was necessary both for reduction of corrosion and to keep inerts at the lowest possible level. A packed column deaerator was designed to accomplish this.

Description of Experimental Apparatus

A schematic and the corresponding photographs of the Task II spray tank are shown in Figures II-1, II-2, and II-3. This system utilizes recirculation of the feed water brine to reduce flow and heat requirements. The feed water is heated initially in the storage bath, filtered and sprayed, superheated, through a hard rubber nozzle into the top of the deaerator. After deaeration, a feed water pump delivers the water to the programmed valve (Figure II-4) at a pressure controlled by a bypass on the feed water pump and determined by the required pressure drop from the programmed valve to the spray tank. After the cyclic proportioning of the flow to the spray bars (Figure II-5), the water is sprayed into the tank and distributed uniformly over the area equivalent to the top of a module five feet long and one foot wide with 120 plates each one and a half feet high. The sprayed water falls to the tank sump from which it is pumped back to the storage bath to complete the closed loop of the Task II distribution system.

Tests were run to verify the design of the distribution system, including the programmed valve and spray bars. This was accomplished using a one-by-five-foot sampling tray divided into five equal compartments. The tray was positioned in the tank so that it lay in the same plane as the top of a 120 plate module. Figure II-6 shows this test arrangement schematically. The flow from any one of the compartments could be collected separately as well as the flow into the other four compartments and the flow not caught by the tray.

A representative heat transfer module consisting of a single fold (two plates) comparable in capacity and theoretical performance to the module in Task I was located in the tank so that it would receive its design flow from the distribution system. This flow then passes down the plate in the form of an evaporating thin film. The vapor over this film is pulled off by a compressor and delivered to the space between the plates at a higher pressure where it condenses. This product water and the concentrated brine runoff at the bottom of the evaporator plate are then collected and pumped up to atmospheric pressure.

The module is formed by folding a one-by-three-foot plate 30 mils thick in half so that two 1-by-1.5-foot plates are formed, joined at their common edge by a 1/4" radius and sealed on both sides and the bottom so that the condenser is separated from the tank or evaporator (Figure II-7). Two additional dummy modules or baffle plates were used to protect the falling film from the effect of extraneous feed and to produce a counterflow of the product vapor over the evaporating film. Additional folds were simulated by 1/2" diameter rods to create the correct splash pattern at the top of the active fold.

All flows were controlled using needle valves which needed no adjustment after the system reached equilibrium. Flow rates were again determined by collecting the flows and correcting for density, a method accurate to within one percent. The temperature in the tank was controlled by a tank sump heater which made up for any heat losses through the insulation. Because of the larger thermal mass of the tank, random changes in temperature were kept below 1°F. The thermal profile was obtained using calibrated copper-constantan thermocouples.

Salinities of the sodium chloride solutions were determined by evaporation and showed satisfactory agreement with the measured circulation ratio. Since titration of sea water is the only valid way of measuring its salinity, several spot checks were made, and when they were shown to be in good agreement with the circulation ratio the concentrated brine salinities were subsequently determined from the circulation ratio and the known inlet salinity.

Absolute pressures were measured with closed end mercury manometers accurate to within .05 centimeters of mercury. The differential pressure was measured in inches of water and could be found accurately to within two percent.

Because of the brine recirculation feature of the Task II rig, significant changes in surface tension were encountered. Enough in fact to result in erratic and unstable saline films with a resultant 30 percent decrease in heat transfer during the initial test runs. Flushing of the system did not completely remove the surface tension lowering contaminants but did result in stable films.

Two inert taps were included; one at the top of the condenser and another in the bottom of the tank.

Results

The objective of Task II was to establish and maintain the satisfactory thin film as defined by the results of Task I. This section includes the information obtained from the effort in this direction.

Of preliminary importance was the determination of the ability of the distribution system to establish a constant unit flow through the area defined by the top of a 120 plate module. Using the five compartment collecting tray and the flow arrangement shown in Figure II-6, the efficiency of the distribution system as shown in Table II was measured. The overall efficiency of distribution was 93.9 percent, that is 93.9 percent of the water passing through the spray bars was collected in the tray. This would require a feed flow 6.5 percent greater than design. The uniformity of distribution is shown by the variations in the flow onto each of the unit areas remaining within 5 percent of the mean unit area flow.

The distribution system checks were run at the programmed valve frequency which resulted in the best apparent heat transfer (Figure II-8). The programmed disc profile was modified during the distribution system checks to achieve the results reported. The original theoretical design was different from the final programmed valve shape (Figure II-9), particularly in the higher flow positions. Since pressure drop in the lines between the valve and spray bars would tend to have this effect, line loss should be included in future design work.

Construction of the spray bar jets by the simple drilling of tubing was not enough to damp out the velocity effect of the flow in the tubing on the flow through the jets. By making the jets from short tubes with a length to inside diameter ratio of 5, the erratic action of the spray was overcome satisfactorily.

The relative vertical position of the programmed valve and spray bars is important because the pressure reduction of a negative head of water behind any valve carrying water near its saturation temperature can result in flashing behind the valve and erratic flow.

The appearance of the sea water spray at atmospheric conditions is shown in Figure II-10. With the increased drag of the air on the sprayed water, the pattern was slightly more dispersed than at the design operating temperature and pressure. The appearance of the spray in this photograph is, however, representative of that under a vacuum. The deviation of the individual sprays from solid streams helps to explain the necessity for some overflow as measured in the distribution system check. Obviously it would be impossible to distribute the design feed flow to the ends of the heat transfer module without spraying some water beyond the ends.

A possible improvement in the thin film distribution system that was indicated by observation of the Task II rig is the elimination of one of the spray bars. With the heat transfer surface folded over a diameter equal to the plate spacing, it is possible that either spray bar could maintain a flowing film on both evaporating sides of any fold. Before implementing this scheme more development work would be required.

There was no natural tendency for the plates to wet and the film to form uniformly either under atmospheric or operating conditions. Attempts to induce the film by stopping the spray on the surface under consideration and passing about six times the nominal design flow over the plate failed to wet the plate. This was the maximum flow possible with the design distribution system. An auxiliary flooding nozzle was then installed to direct approximately 15 times the design flow over the plate. This successfully wet the plate which was then maintained wet by the distribution system.

Start up of the Task II rig proved much simpler than in Task I because slight superheating of the feed water did not destroy the brine film. As in the case of Task I, the level of inerts must be very low before vapor compression can be started.

In order to keep the vapor velocity over the evaporating film at the design level, the vapor was baffled into the same volume as would be available on a full sized module. Although all of the heat transfer data reported under Task II was obtained with these baffles in place, several early runs without the baffles did have slightly better performance.

The spray frequency of 40 cycles/minute which was used in all tests resulted in water being applied to each plate every 3/4 of a second, and referring to Figure I-14 it can be seen that this is much less than the period of fluctuation found for a pulsed flow.

Operation of the Task II rig with a 3.5 percent sodium chloride solution can be described in terms of the same parameters as in Task I.

Overall transfer of heat as determined from the rate of fresh water production and the pressure differential required to get that production versus the circulation ratio is shown in Figure II-11. This data is on the same coordinates as Figure I-10, the equivalent Task I data, and a comparison of the two curves shows close agreement at the design circulation ratio of 2.2. The spread between the two curves at the lower circulation ratios may be due to the increasing effect of surface tension lowering contaminates in Task II. Surface tensions were checked and the conditions for film instability did exist in that the surface tension of the concentrated brine was lower than the inlet brine. Figure I-9 shows the theoretical heat transfer.

The other convenient presentation of these results is in Figure II-12 where $\Delta P/P_e$ versus W_f is plotted. Again, comparing this to the comparable Task I data in Figure I-11, good agreement between Task II data and the base line heat transfer data is found.

After finalizing the distribution system design and demonstrating the reproducibility of the base line heat transfer data using a spray created film of sodium chloride solution, there came problems of justifying the assumption that the properties of sea water and sodium chloride solutions were similar.

Operation of the Task II system with sea water was chosen to check this assumption and although this proves nothing about a particular property, it does indicate the degree of success with which these properties can be used to predict a result. Sea water delivered by truck from Wrightsville Beach having a salinity of 3.40 percent and no pretreatment other than filtering and chlorination was used for these runs.

The distribution system was found to operate satisfactorily with sea water as was indicated by observation. The system was operated over as large a range of production as possible with the results shown in Figure II-13, including the overall coefficients for operation of the module both in the

center and close to the end of the tank. The average curve for these results shows that sea water will perform as well as the theory predicts using the properties of sodium chloride aqueous solutions.

There is a small difference in the performance of the module depending on whether it is in the front or center location. This difference is shown in Figures II-14 and II-15 and can be attributed to the poorer distribution occurring in the spray pattern at the point of maximum travel.

Performance of the system based on the differential pressure is also in close agreement with the theory and above that of the sodium chloride solution (Figure II-16).

Product purity was not as good as was reported for Task I (0.4 ppm); instead it ran around 5.0 ppm. This might be expected since the spray distribution can generate small droplets of sea water which could be picked up by the compressor.

Another observation concerning the maintenance of a thin film which should be considered in design is the unreliable nature of the film in the 1/4 inch wide strip along the fixed sides of the plate. Portions of this area were frequently inactive or intermittently wet. This area amounts to about four percent in the one foot wide test module and on a full size (three foot wide) module would occupy about 1.4 percent of the total area.

The effect of introducing subcooled water through the spray bars was not the same as was noted on the weir fed plates in Task I. The reason for this probably being the absence of the definite boundary between the unwet portions of the weir plate and the flowing film on the weir plate that existed in the Task I rig. This boundary is subject to instabilizing concentration gradients resulting from vapor condensation on the inactive subcooled saline film.

The measure of the outlet surface tension is not a good method of predicting instability since the surface tension of the concentrated brine was always less than the inlet brine even in the case where film stability could be visually ascertained. Since this could be due to contamination of the small flow in the brine pumping loop, the increase in surface tension accompanying the increase salinity could not be detected. Significant feed water surface tension lowering was found necessary to generate instability. Slight reduction in surface tension was found to be acceptable.

A stable film was found to exist with an inlet surface tension of 73 dynes/cm and outlet brine surface tension of 69 dynes/cm. Instability occurred with surface tensions of 61 and 58 for the feed water and concentrated brine respectively, with reduction in the overall coefficient from 30 to 40 percent. In a single pass conversion system contaminants would be washed out and not trapped in a closed loop.

Conclusions and Recommendations

Thin film vapor compression distillation of sea water can be accomplished as effectively as predicted by Nusselt's theory. The satisfactory system utilizes, as a means for maintaining the thin saline film on the heat transfer surface, the varying velocity spray bars. The vapor formed by the evaporation of the saline film is then compressed and directed into the condenser where the product water is condensed on the back of the heat transfer surface with the latent heat passing through the plate into the evaporating film.

Establishment and maintenance of a thin film of water using a spray distribution system has been shown feasible and the necessary information for design of such a system is available. In addition, the effect of such a method of film maintenance on the ideal or base line heat transfer was shown to actually favor the spray distribution. Design of the system on the basis of the theory and properties of sodium chloride solutions will yield satisfactory results.

Wetting of the plates by local flooding proved to be the only way to establish the films. Concentrating the feed water spray on any one plate resulted in an insufficient flow to wet the plate so auxiliary flooding nozzles are necessary for satisfactory film creation.

Compressor start-up is not hampered by the lack of initial vapor flow since the feed water can flash several degrees without disrupting the evaporating film. Because of the possible presence of inerts initially and the eventual change in a system performance, it will be necessary to incorporate enough flexibility in the compression system to accommodate these changes. A steam turbine is the most logical compressor drive since it is capable of adjusting to changes in compressor duty.

Task II has established experimental verification of the basic heat transfer assumptions made in the Westinghouse study of the Thin Film Vapor Compression system and developed the technology of the heat transfer surface and distribution system to the point where a pilot plant can be designed.

TASK II - DISTRIBUTION SYSTEM CHECK

Compartment #	1	2	3	4	5	Nominal Temperature 115°F
Single Compartment Flow (cc/min)	880	860	850	815	870	3.50% NaCl Solution
Remaining Compartments Flow (cc/min)	3340	3400	3400	3380	3280	Avg. Compartment Flow - 855 cc/min
Total Tray Flow (cc/min)	4220	4260	4250	4195	4150	Max. Deviation from Aug. - 40 cc/min (4.68%)
Overflow (cc/min)	280	300	260	260	252	
						Avg. Total Flow - 4485 cc/min
						Avg. Overflow - 270 cc/min (6.02%)

Compartment #	1	2	3	4	5	Nominal Temperature 119°F
Single Compartment Flow (cc/min)	850	840	840	820	880	3.50% NaCl Solution
Remaining Compartments Flow (cc/min)	3400	3450	3380	3480	3400	Avg. Compartment Flow - 846 cc/min
Total Tray Flow (cc/min)	4250	4290	4220	4300	4280	Max. Deviation from Aug. - 34 cc/min (4.02%)
Overflow	260	274	280	292	284	
						Avg. Total Flow - 4546 cc/min
						Avg. Overflow - 278 cc/min (6.1%)

TABLE II

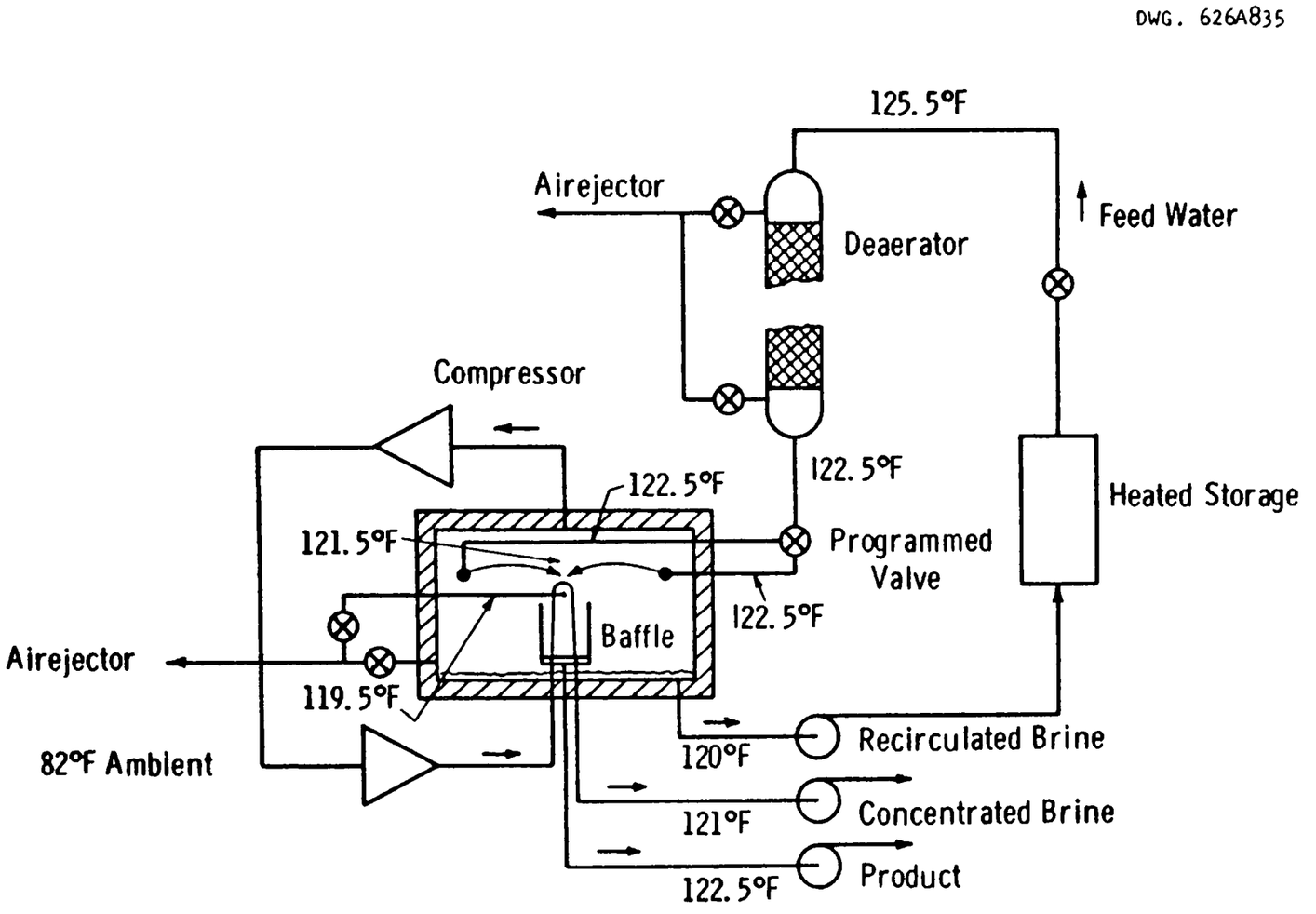

Task II schematic and temperature profile

Figure II-1

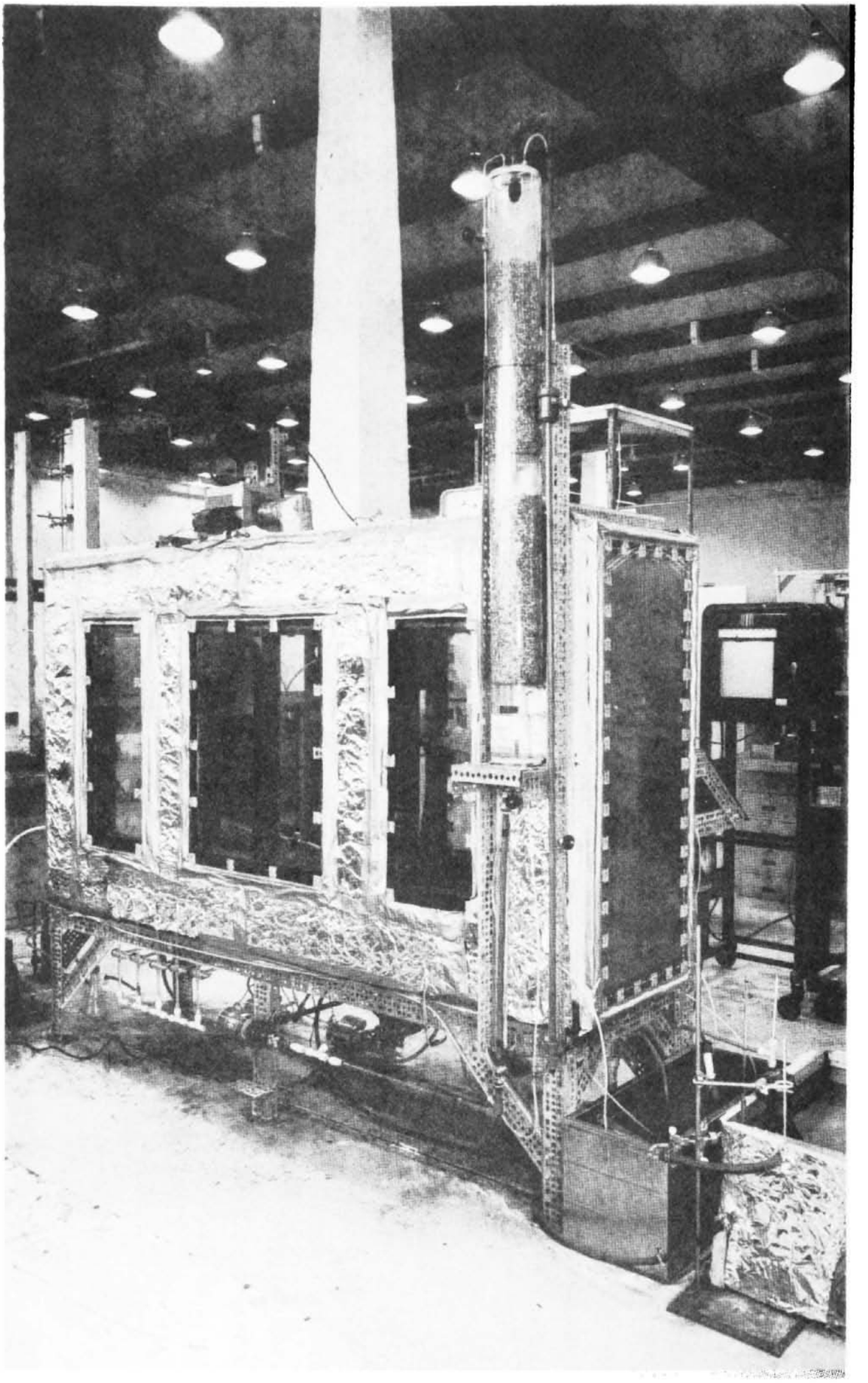

Figure II-2 Task II Spray Tank from Deaerator Side

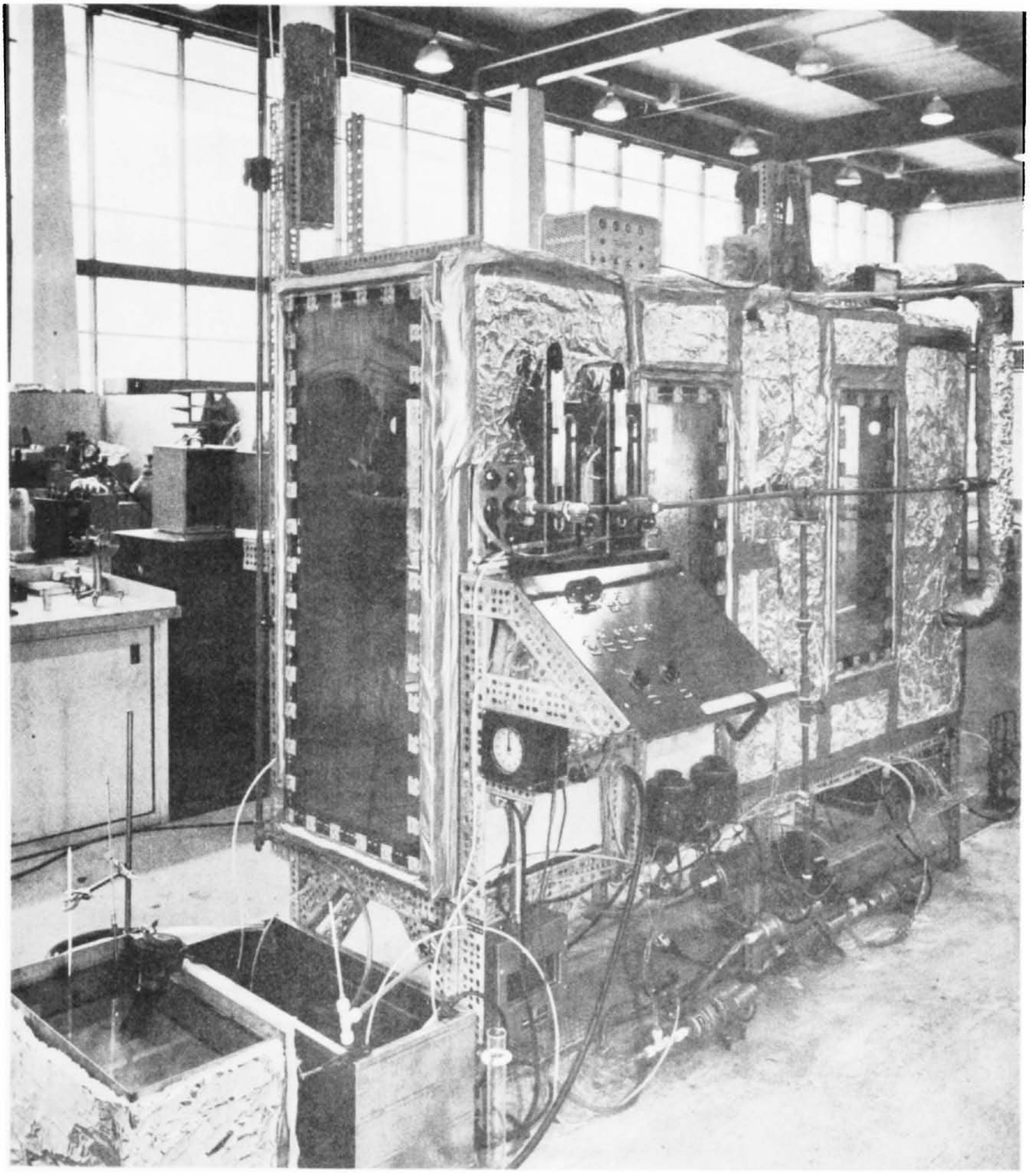

Figure II-3 Task II Spray Tank from Control Side

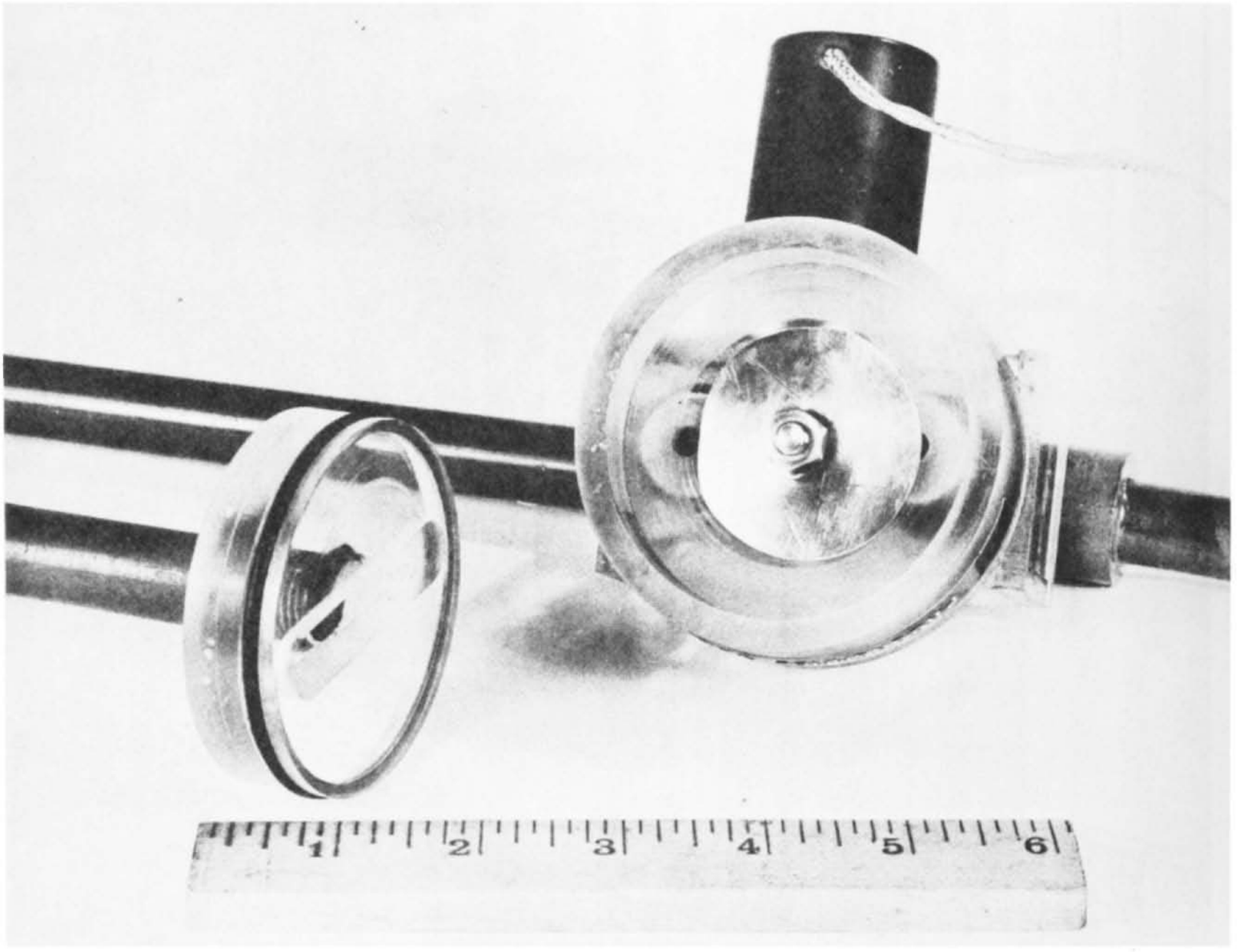

Figure II-4 Task II Programmed Valve Showing Profiled Cam

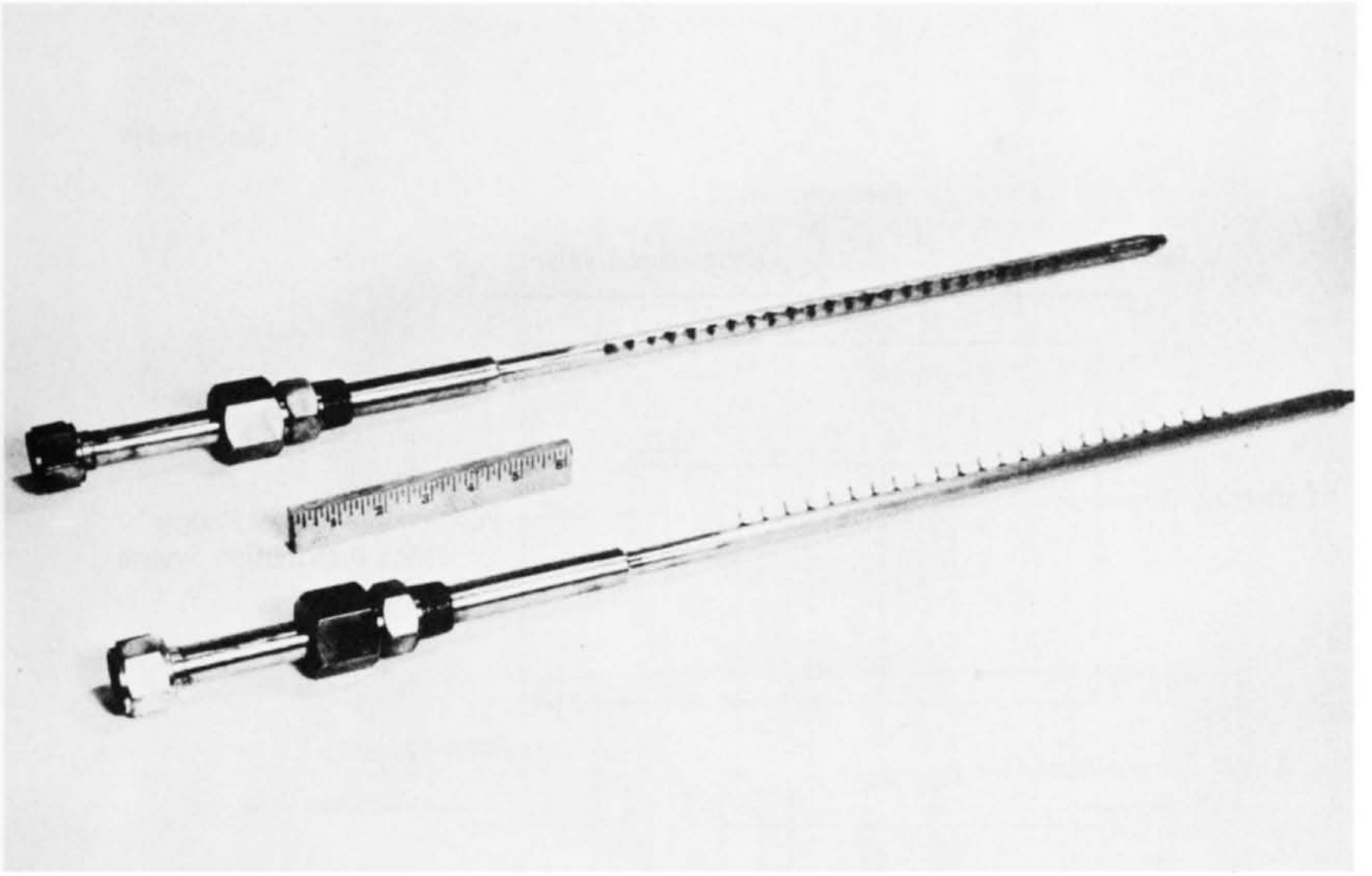

Figure II-5 Task II Distribution System Spray Bars

DWG. 626A836

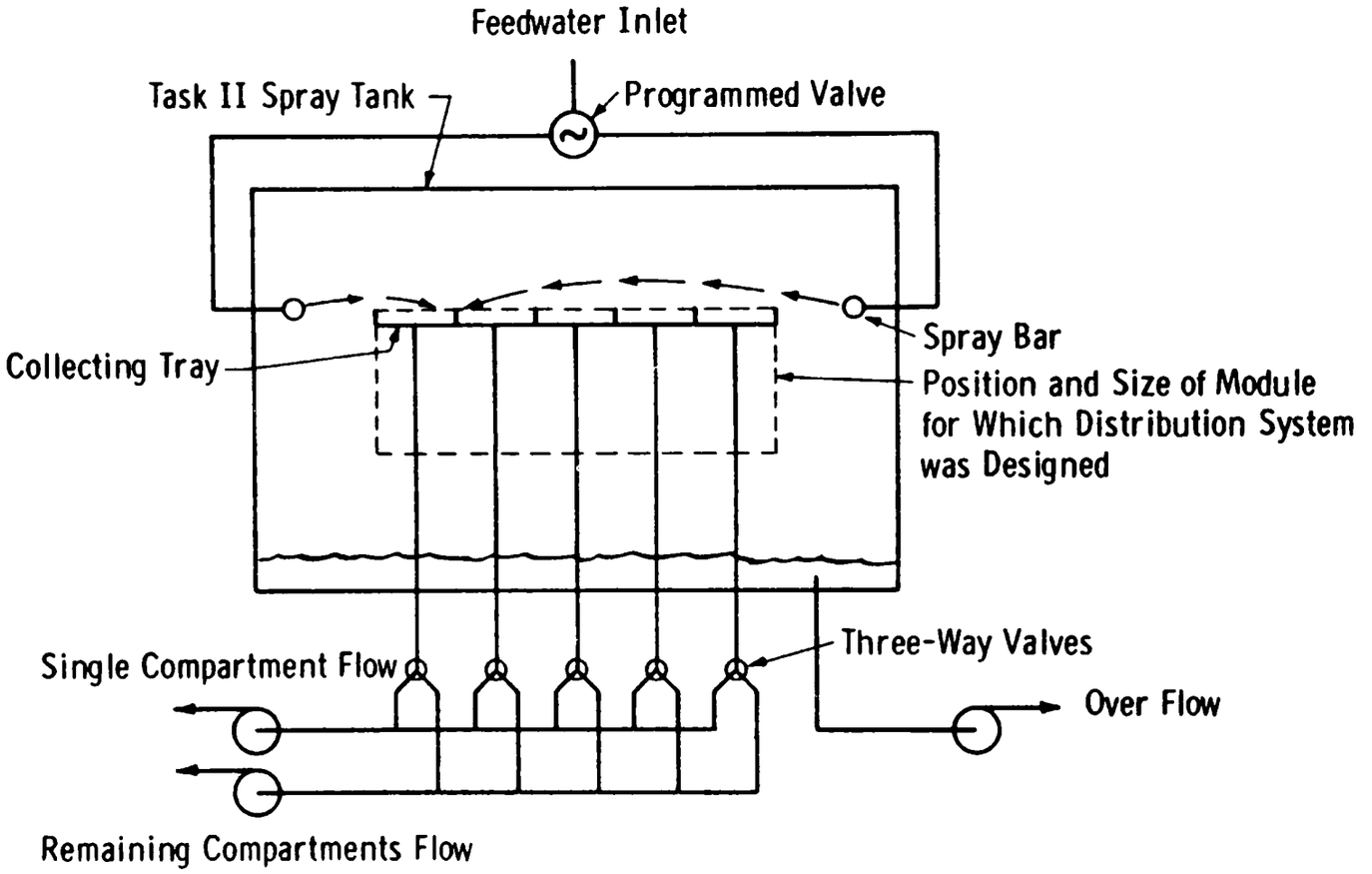

Task II flow distribution checking system schematic

Figure II-6

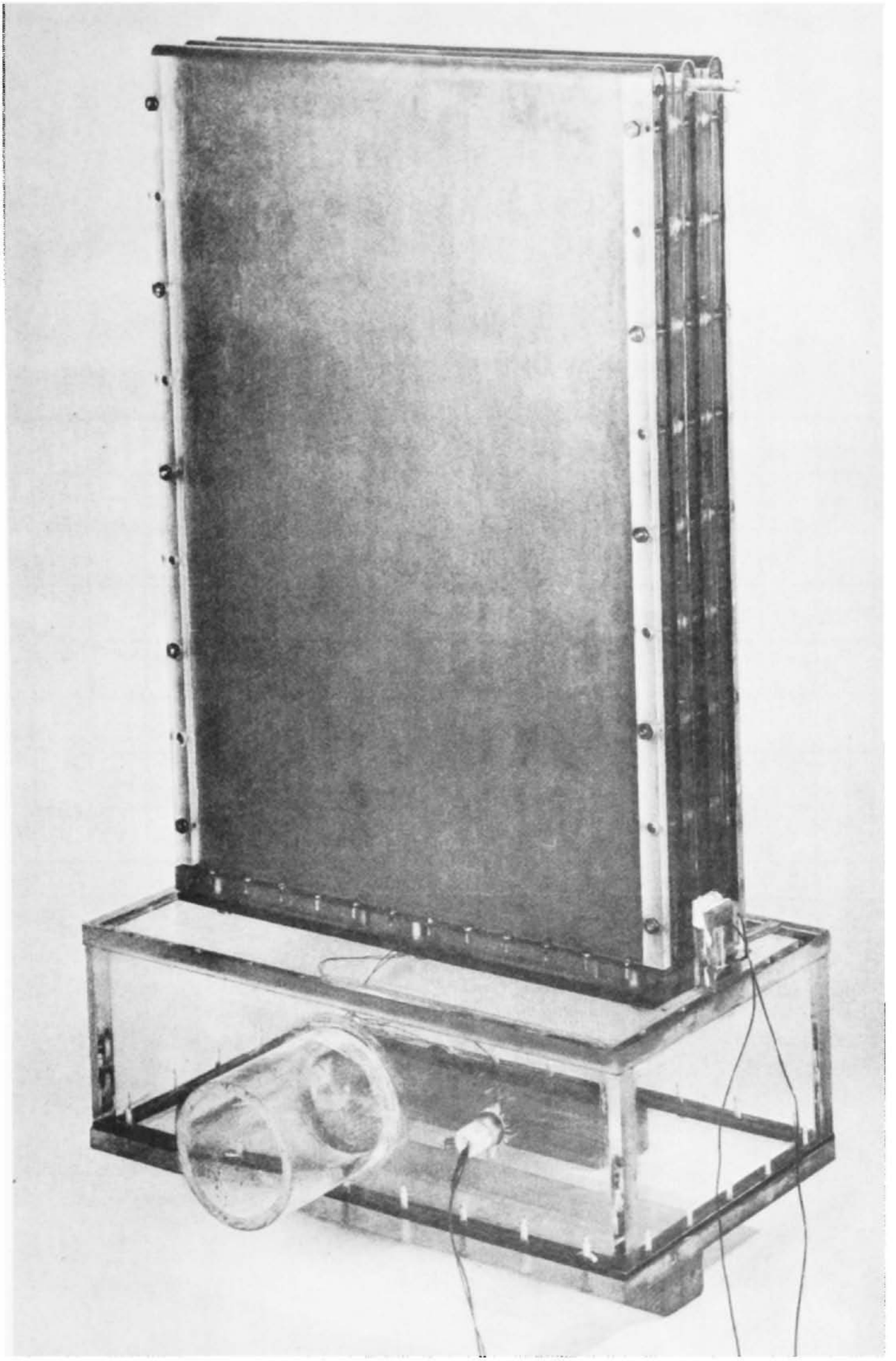

Figure II-7 Task II Heat Transfer Module

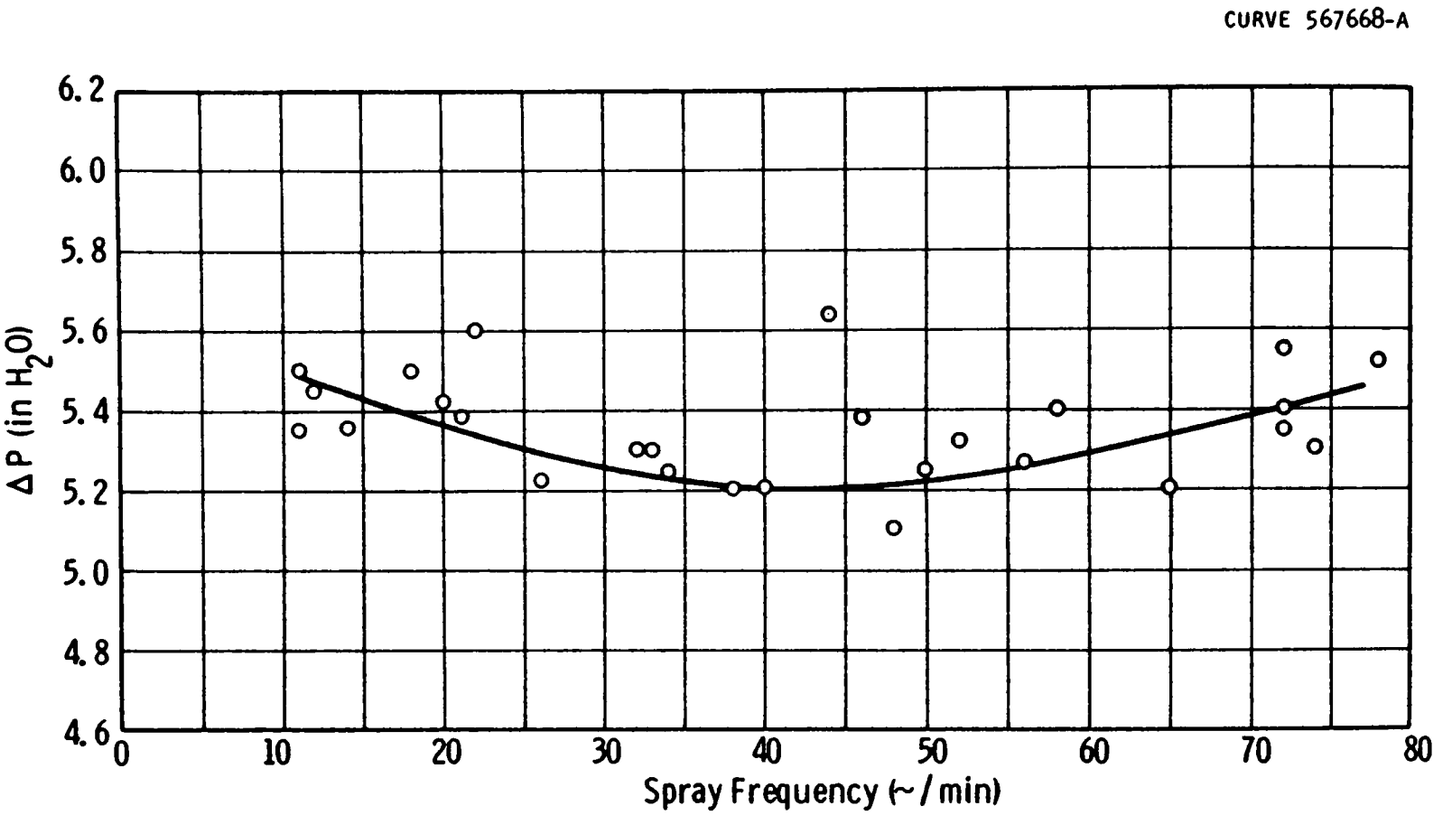

Fig. II-8 —Effect of spray frequency on ΔP in Task II

CURVE 567669-A

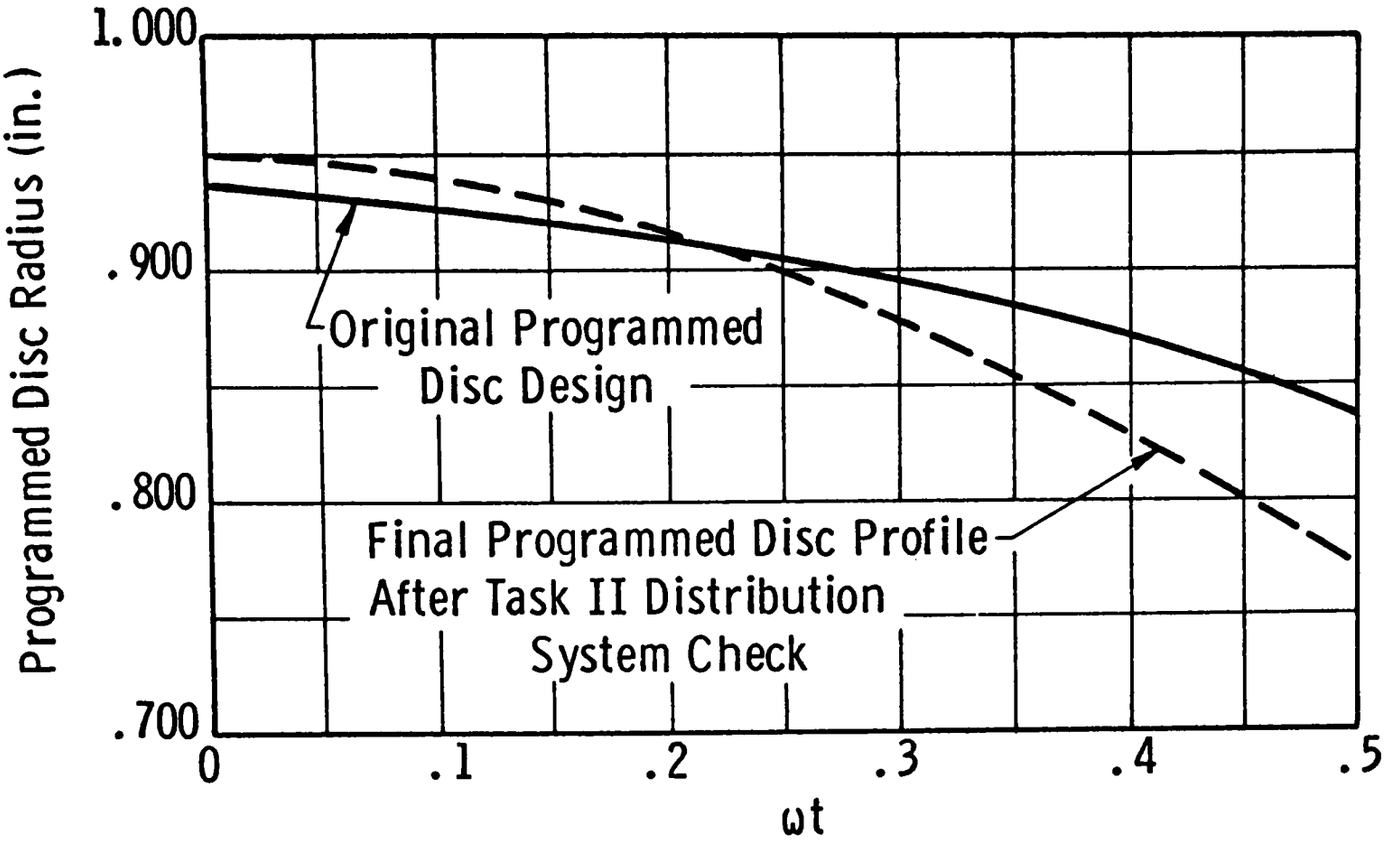

Fig II-9 —Programmed disc profile

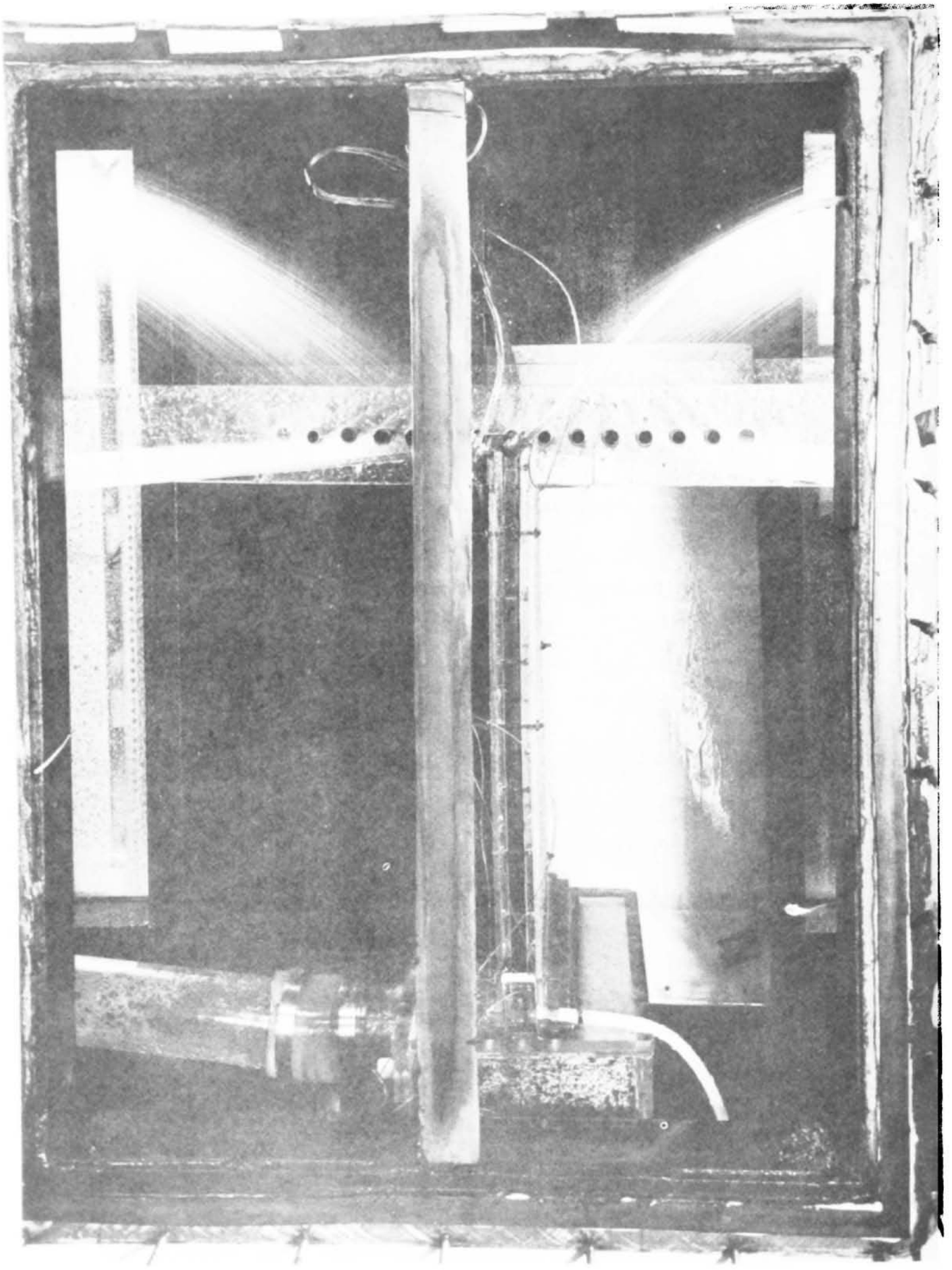

Figure II-10 Task II Heat Transfer Module and Sprayed Feed Water - Center Operating Position

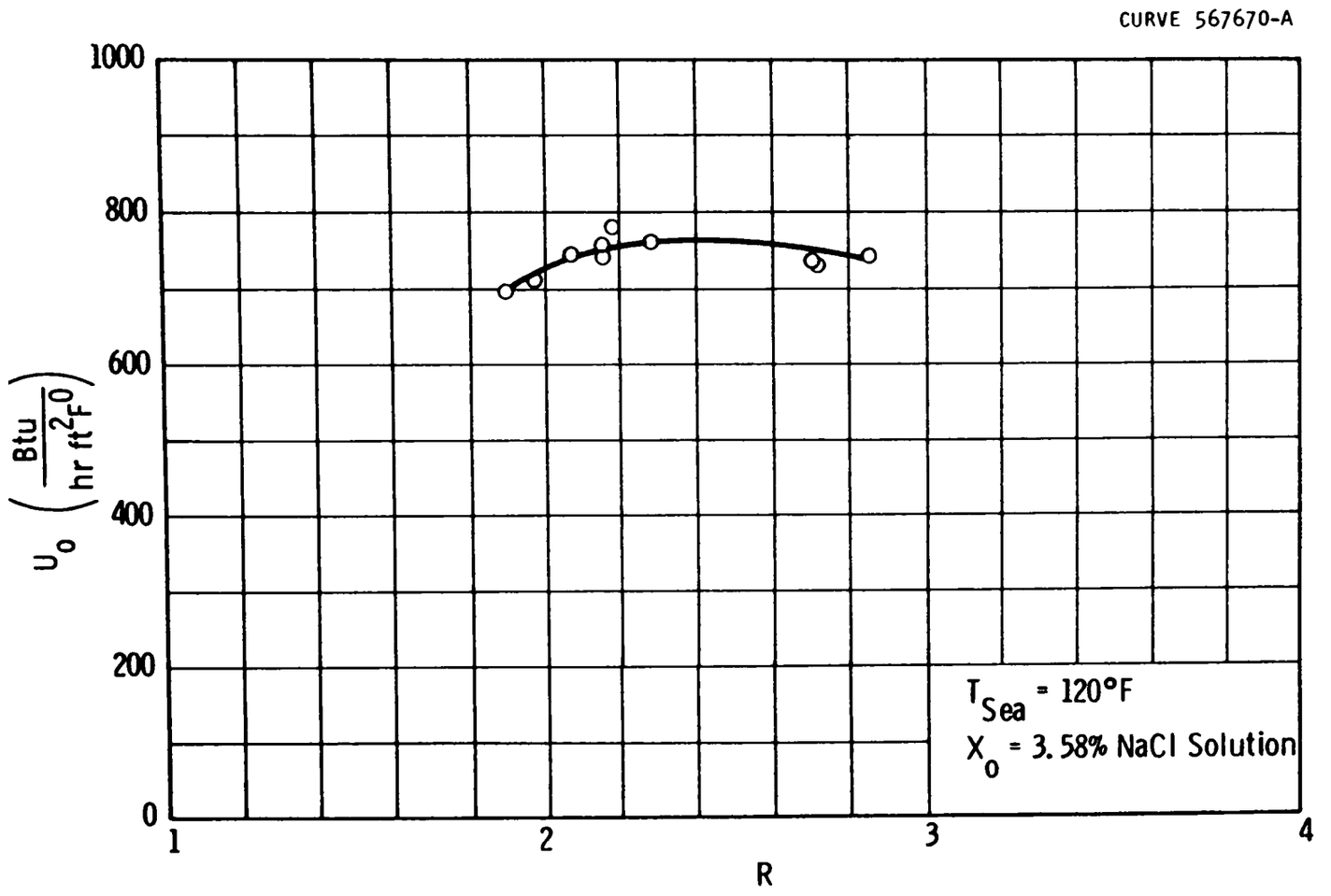

Fig. II-11—Task II heat transfer module with evaporating vapor retaining plates

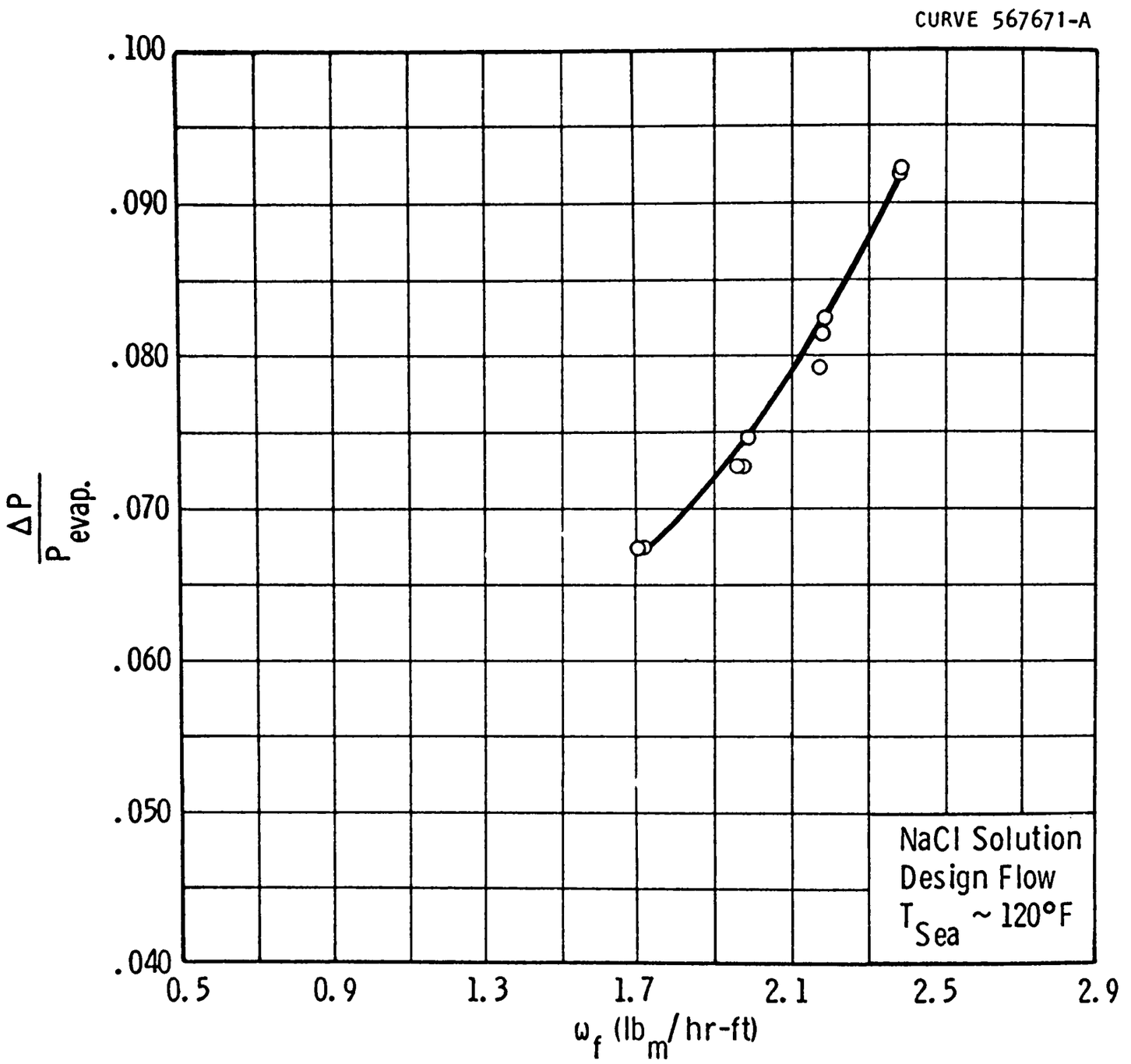

Fig.II-12—Task II heat transfer

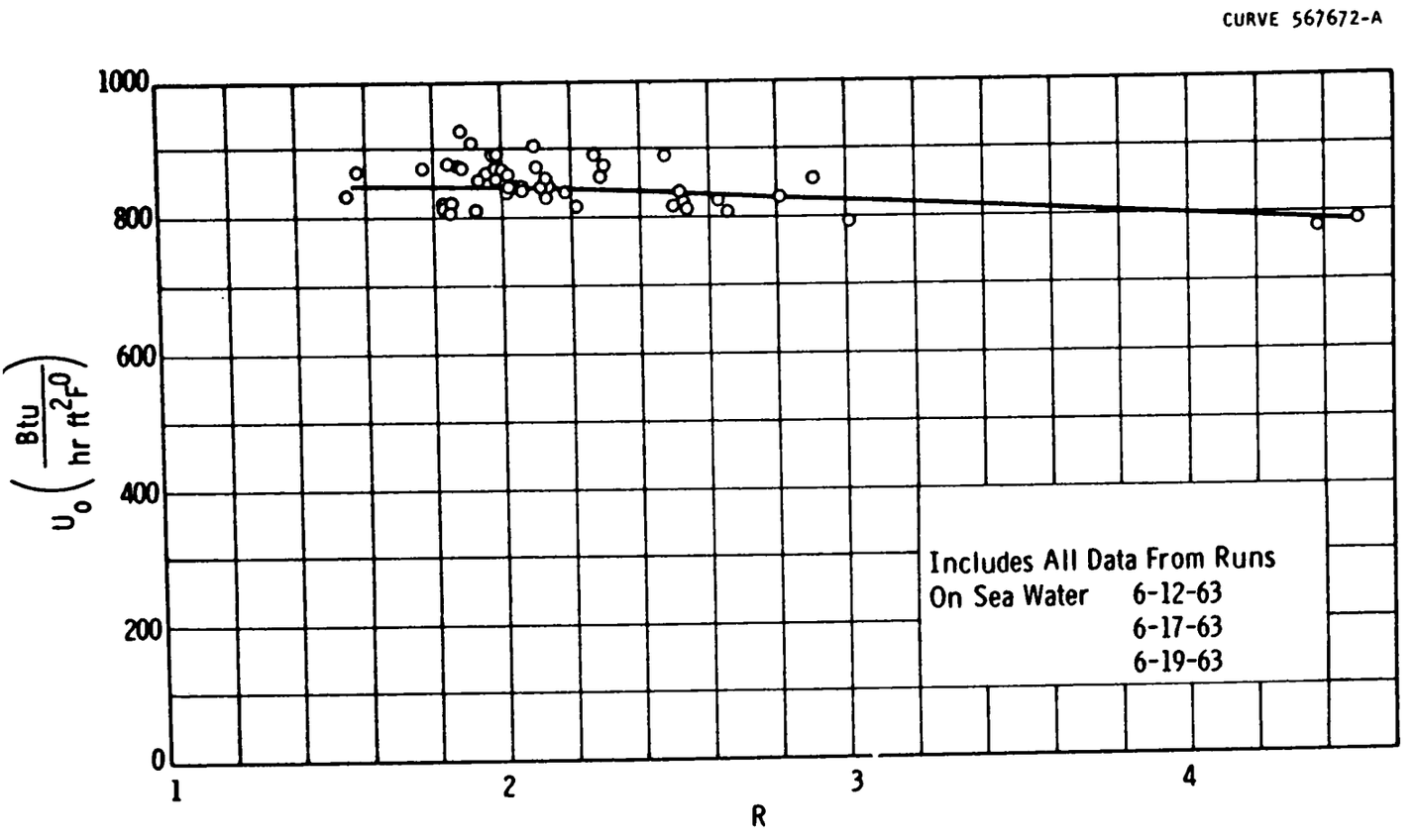

Fig. II - 13 Task II heat transfer

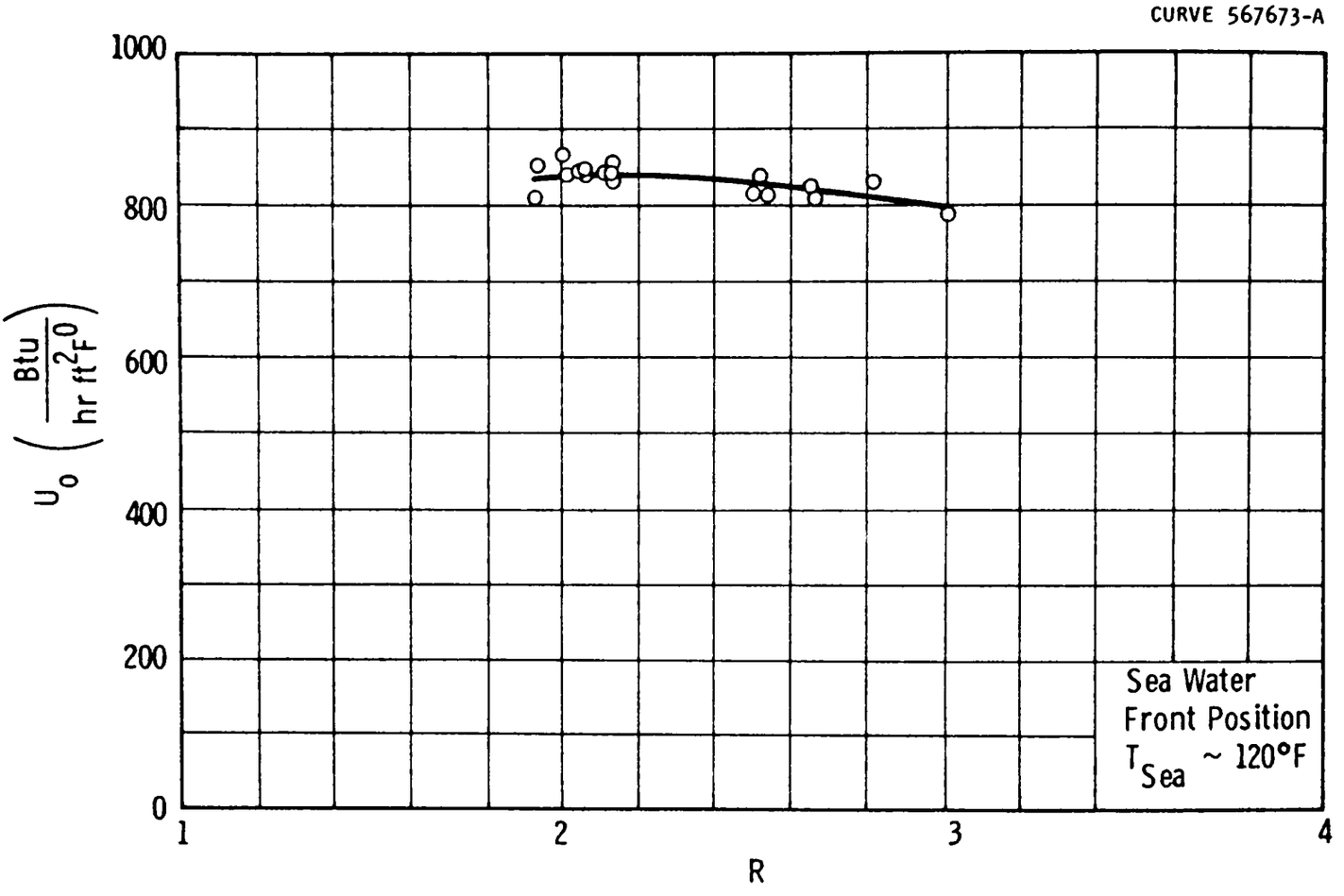

Fig. II-14 — Task II heat transfer

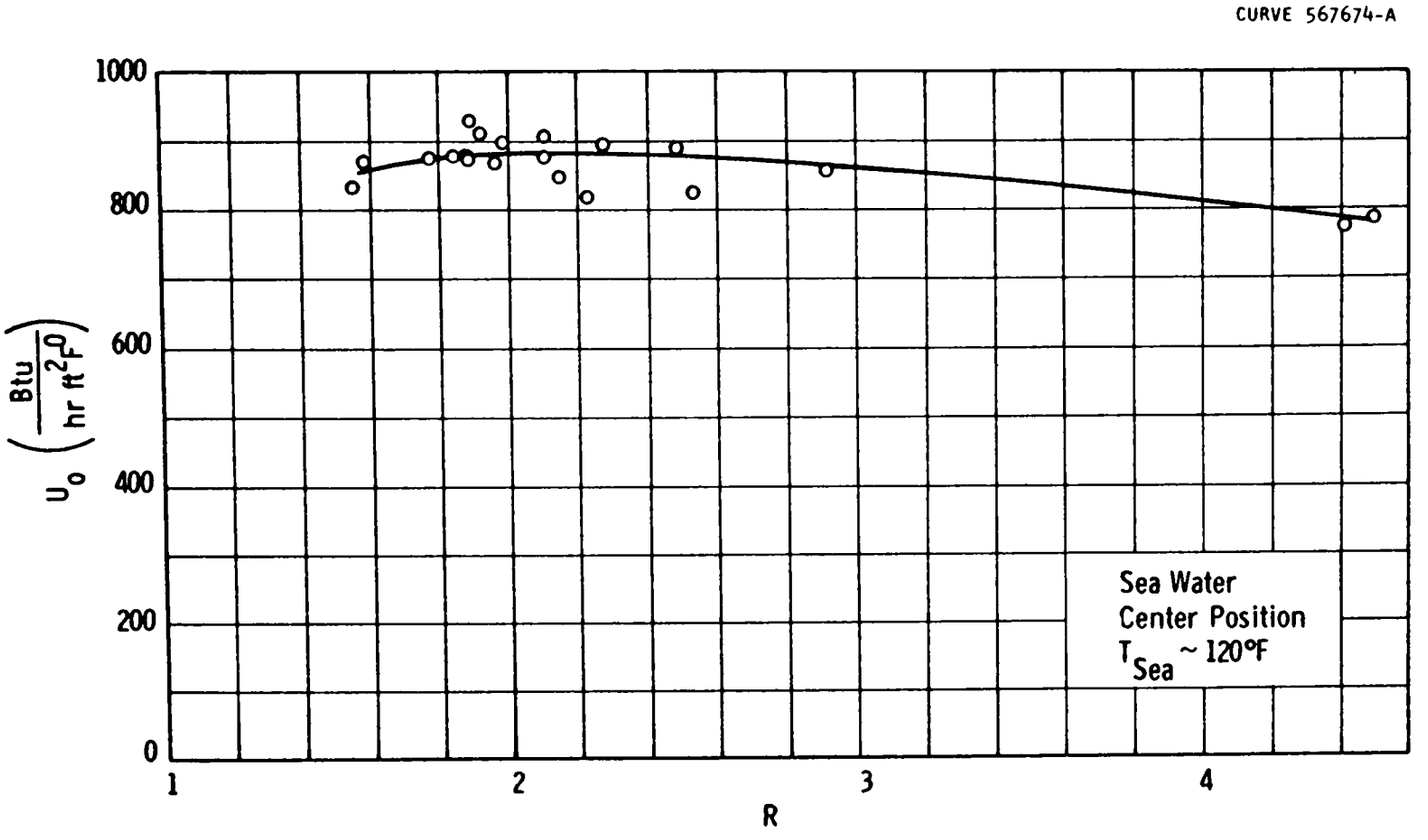

Fig. II-15 - Task II heat transfer

CURVE 567675-A

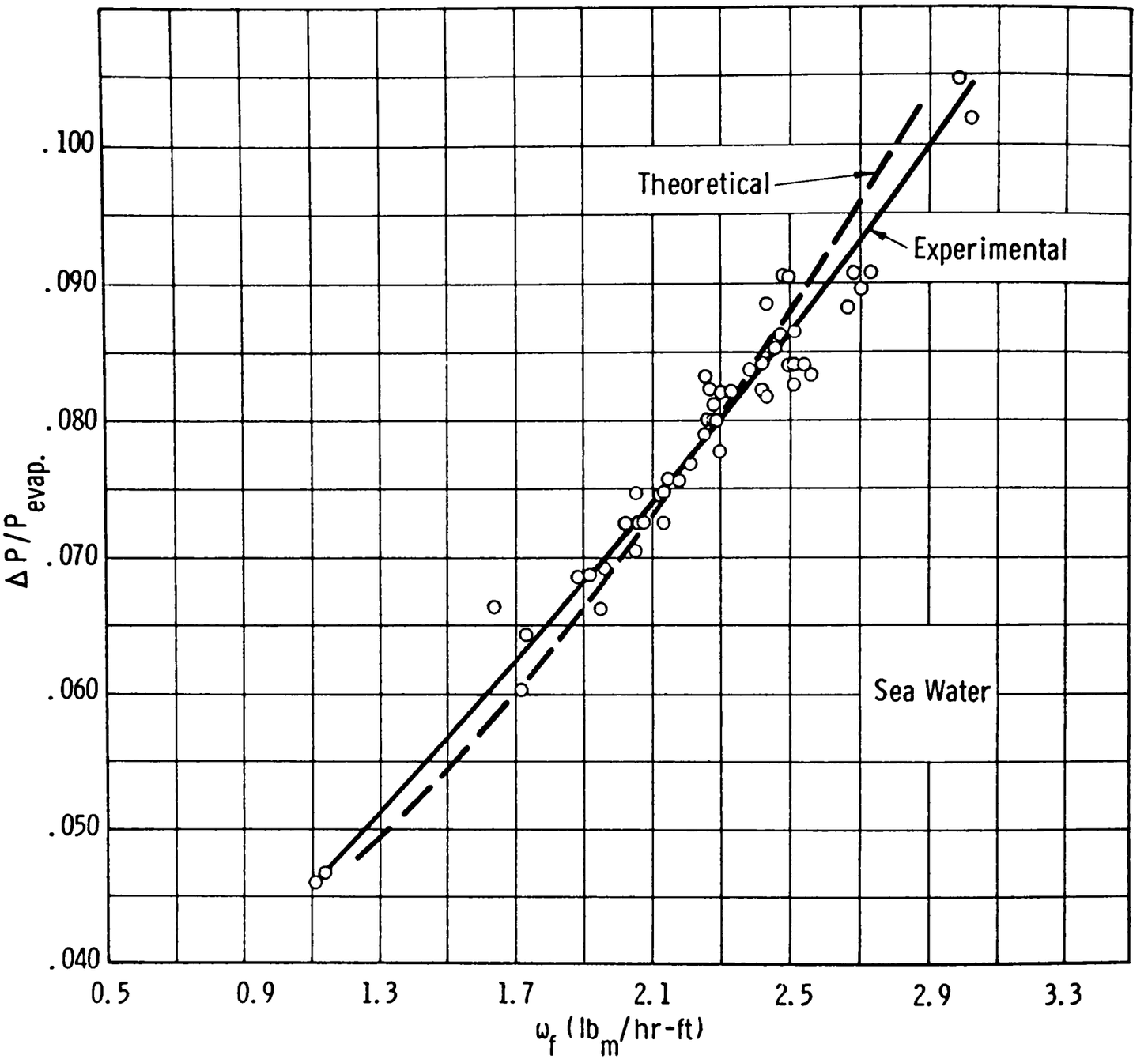

Fig. II-16—Task II heat transfer

Task III - Determine the Minimum Cost Materials Consistent with Environment, Life, and Manufacturing Requirements.

Task Description

The goal of Task III was to determine the minimum cost materials consistent with environment, life and manufacturing requirements.

The environmental requirements are quite severe. The heat transfer surface must exist upward of ten years; covered by a film of sea water with gradations in salinity; with a constant spray of water attempting to erode away the upper plate surface; and, with some degree of acidity added to control scaling. Perhaps as severe an environment will be encountered by the surface before and during fabrication. Certainly the condition of the surface at startup time cannot be that of unprotected iron subject to atmospheric conditions for periods of weeks. Tests must be conducted which will subject materials to the operating environment and at the same time give the materials no more protection during fabrication than would be economically feasible on the ultimate system. It must be recognized that the evaluation of short term tests is difficult, particularly with respect to corrosion; it is hoped that some trends can be indicated. Short term environment tests can have much value in evaluating such requirements as initial wettability, and the ability to remain wet after the initiation of fouling due to scaling and corrosion.

The materials selected must have low initial cost and must be adaptable to manufacturing capabilities. Joining methods must be simple enough and cheap enough to qualify under the low cost surface area requirements. Protective coatings or oxides must stand up to the manufacturing bending, drawing or forming methods that must be used to accomplish low cost mass production.

The general form of the heat transfer surface as visualized at this time is shown in Figures V-1, V-2 and V-3. Task III is intended to examine selected materials in the environmental conditions as set forth in Task I and II sections of this report. The excellence factor for selecting the material will be composed of economic and technical considerations such as the following:

Economic	1.	Base Material Cost
	2.	Manufacturing Costs
	3.	Joining and Closure Costs
	4.	Size, Shape, Storage and Handling Extras
Technical	1.	Pitting, Corrosion, and Erosion Resistance
	2.	Scaling and Fouling Resistance
	3.	Wettability
	4.	Overall Heat Transfer Performance

The important criteria for selection are ultimately the cost, life and effects on heat transfer due to fouling, corrosion and erosion.

Technical Approach

The design philosophy was formed from the following concepts:

I. On Environment Simulation

A. The compressor function can be accomplished more cheaply and with fewer problems by producing steam for the condensing side of the plates with a flash tank; and by condensing the product vapor directly in a water-cooled condenser.

B. Economics limit the erosion study to that of the film flowing down the plate. The erosion problems due to the spray system entail too high an apparatus cost for adequate study. The films will be created by notched weirs. This choice will permit the study of more materials at more pH conditions than would the choice of spray distribution.

C. The environment for successful operation of conversion apparatus of the type under study must be treated to prevent scaling and at the same time provide the least severe corrosive conditions for the heat transfer material being used. For this reason four different sea water conditions will be provided with respect to pH; one, untreated; two, three, and four, treated with sulfuric acid to produce pH levels of 7.5, 7.0, and 6.5. All feed water will be deaerated to .1 ppm O_2 or below.

The first condition should determine the need for scale control by acid addition; the next three should indicate the optimum pH level for each material with respect to corrosion. For example, steel is normally more resistant in higher pH sea water, while aluminum performs best in water of pH between 6.0 - 6.5.

The feed water used throughout Task III testing was natural sea water transported in stainless steel tank trucks from Wrightsville Beach, North Carolina. The sea water remained in the tank truck no longer than thirty hours from time of loading until transfer to a reinforced plastic storage tank.

II. On Isolation of Heat Transfer Surface Fouling

A. Eliminate fouling due to dirt by providing extremely effective filtration equipment.

B. Chlorinate the water in storage to guard against marine fouling.

C. Use non-corrosive materials for all equipment. Let the specimens be the only source of corrosion products.

III. On Material Selection

The following four materials will be submitted to test, their selection based on the requirements discussed under Task Description:

A. Carbon Steel - lowest cost.

B. Tin Plate - should have greater corrosion resistance than steel with only slight increase in cost. Reported to be anodic to steel in water of very low dissolved oxygen content.

C. High Purity Aluminum 1188 - good corrosion resistance, easily fabricated low pitting tendency because of purity. Next lowest cost basic material to steel.

D. Aluminum Alloy 5050 - magnesium addition reported to improve corrosion resistance over other alloys, low pitting tendency, can be brazed and welded, cost still acceptable.

IV. Listing the necessary functions required to fulfill the task goals for the experimental apparatus will derive the flow chart. The following functions are required to simulate the conversion system and to gather the necessary data.

1. Filter all solids from the sea water, chlorinate to .5 ppm residual.

2. Heat sea water to deaeration temperature. This temperature is slightly in excess of the saturation pressure in the deaerator. This temperature head will permit flashing upon entrance. The literature and advice suggest a 3 - 5°F head.

3. Adjust pH level by addition of sulfuric acid.

4. Deaerate.

5. Control flow rate to each plate.

6. Measure runoff from plates, both brine and product. Provide means for sampling brine in order that salinity be measured.

7. Control absolute pressure in the evaporator; control differential pressure across the evaporator and condenser.

Function Number	Technical Approach
1	The sea water will be filtered with a diatomite filter upon removal from the tank truck and sodium hypochlorite added for chlorination as it enters the storage tank. It will be filtered again at time of withdrawl from the storage tank with a cartridge filter.
2	Glass heat exchangers will be used. Two will be provided to be used alternately in the event scaling of the coils results.
3	The flow of sea water will be controlled by the sum of the resistance of two needle valves in series. A standpipe at the top of the rig will provide a constant head above the needle valves. The acid flow will be controlled by controlling the outlet pressure of a resistance tube through which the acid is flowing. The outlet pressure can be controlled using the relative pressure drop across each of the two needle valves. The pressure in the line between the two valves can vary from atmospheric (first valve wide open, second valve throttling) to deaeration pressure (first valve throttling, second valve wide open). A capillary tube can be used for the resistance tube for for acid flow.
4	A glass pipe packed with glass raschig rigs over which the sea water will flow in thin films will be used. A sump will be provided in which a coil will be immersed. Hot water from the slave system flowing through this coil will provide stripping steam which will flow upward through the column.
5	The flow rate to each plate will be controlled using a constant head device (flowbox) to maintain a constant head over a titanium orifice. Four orifices will be placed in each flow box. The specimens will be mounted in groups of four, one of each material, in a framework of cast acrylic. Each bank of four specimens will be fed by a flow box.
6	Measuring tubes will be provided. These tubes will be sized and calibrated to allow one man to make rate measurements on two test banks (eight brine eight product) in a single measuring sequence. A complete set of readings (eight banks) can thus be made in four measuring sequences of approximately 10 minutes each. The tube on the brine side will have a three-way valve so that a sample can be removed with a vacuum bottle.

Function Number	Technical Approach
7	The evaporating side of the plates will feed a glass condenser, a penumatic controller on the cold water flow to the condenser coils will maintain the absolute pressure. The differential pressure will be controlled by controlling the rate at which steam is produced on the condensing side of the plates. A pneumatic controller will monitor the superheated water flow rate to the flash tank.

Summary

The scaling corrosion test rig for completing the requirements stated in Task III Goals was built and operated satisfactorily. The continuous operation was satisfactory although the duration of the test was less than originally desired.

Results proved that carbonate scale will foul heat transfer surfaces if the feed water is not treated for scale control. Results pertaining to corrosion though not permitting an estimate of the life of the heat transfer material did indicate aluminum to be the best choice. Further, considering these two conclusions, results indicated a pH level of 6.5 - 7.0 to be most desirable.

Description of Experimental Apparatus

Figure III-1 shows the flowpath to accomplish functions 1 through 4. The sea water was pumped out of the tank truck, through a diatomaceous earth filter and into the non-metallic storage tank. As shown in Figure III-1, the water was again filtered after the pump and enroute to the standpipe at the very top of the rig. This standpipe was the constant head supply for the control valves downstream. The water was heated in one of the two glass heat exchangers; the outlet temperature was controlled by a pneumatic controller. The water flow was then separated into four equal parts and sulfuric acid was added to three of these to adjust the pH level. The four streams then passed through individual packed columns to remove the dissolved gases and the evolved carbon dioxide. The flow out of each deaerator column was again split and fed equally to two flow boxes. The flow boxes were devices for maintaining a constant head over four orifices, one orifice for each specimen. Figure III-2 shows the split in flow out of the deaerator and the subsequent split into four parts to feed the individual specimens.

Figure III-3 shows the flow to the specimens and the measuring tubes for measuring the runoff of both sides of the plate. Figure III-2 and Figure III-3 have shown the accomplishment of functions 5 and 6 above.

Figure III-4 shows the accomplishment of function 7. The rectangular boxes shown in Figure III-4 represent the flash tank at the top with the condenser beneath it. The eight tubes extending from these boxes are the connections to the eight banks. The flash tank was connected to the condensing side of the bank, and the condenser was connected to the evaporating side. The absolute pressure controller maintained the correct pressure in the evaporator by controlling the cold water flow to the glass condenser coils. The differential pressure was maintained by varying the hot water flow rate to the flash tank.

Figure III-5 shows the hot water system for the heat exchangers and the flash tank.

Figure III-6 shows a cut-away view of an individual specimen. The four specimens were mounted such that each was completely isolated with respect to liquid flows from the others. The four were connected to the same manifold for vapor flow. The troughs for sea water feed, condensate runoff and brine runoff were formed as the frame of the bank was closed. Figure III-7 is a close-up showing two banks. The three small manifolds leading to the central portion of the plates were the feed lines for the flooding nozzles. At startup, it was necessary to completely flood the plates to initiate adequate wetting.

Figure III-8 is a photograph showing the control panel and the pH adjustment apparatus. Figure III-9 is an overall view of the test rig. Figure III-10 shows the pneumatic controllers in the foreground and the pneumatic valves in the background. The rig was automated to the economic limit to permit unattended operation.

Vernier Heaters

Task I contains a description of the film breakdown problem encountered if the plates are fed sea water which is greatly subcooled from system temperature. The flow boxes shown in Fig. III-2 contain a titanium tube intended to serve as a vernier heater. During system operation, product vapor was admitted to the tube. Condensation in this tube would contribute heat in amounts proportional to the amount of subcooling. This vernier heater then contributed greatly to keeping the water in the flowbox at the correct temperature. At startup, however, no product was available for the vernier heater. This situation necessitated the feeding of steam from the flash tank directly to the condenser manifold during startup to help heat the flowbox mass. In fact, the system was permitted to "soak" at temperature maintained by the flash tank steam for a period of twenty-four hours before startup was attempted. During the soak period the sea water feed was shunted around the bank; sea water was in contact with the plates for less than one hour before films were formed.

Non-Condensible Taps

Leaks, dissolved gases and perhaps some outgassing contributed to a non-condensible buildup on the condensing side of the plates. Even small amounts of non-condensibles reduced the saturation pressure (partial pressure) of the condensing steam to greatly reduce production. This problem is magnified in a small temperature difference system. The condensing side of the plates was vented to the vacuum pump from a tap near the bottom of the plate. The valve in this line was adjusted such that some steam flow was evident in the tap line.

Sea Water Flow Control

Upon heating, the sea water gave up appreciable volumes of dissolved gases. These bubbles were a nuisance to the control valves and meters. An arrangement of vents and a small amount of recirculation eliminated the bubbles before they reached the control panel.

Deaeration

The problems encountered in deaeration were partially economic. Best performance is attained using a full-cone type nozzle to spray the water over the packed column. Because of the small flow rates in the rig, standard nozzles could not be obtained. A simple glass orifice was used which gave satisfactory results as long as generous amounts of stripping steam was made available.

The stripping steam was produced with coils in the deaerator sumps. The deaerator inert vent was connected directly to the vacuum pump through a manually set valve. Changes in the vacuum pump inlet conditions or changes in the stripping steam production rates caused minor fluctuations in the deaerator pressure level. A more sophisticated venting arrangement would have provided automatic controls for deaerator pressure. This automatic pressure regulation would have required 15% + more expense for hardware. The fluctuations in deaerator pressure with the manual control did not warrant that expense. The pH control would have been improved slightly with this arrangement.

Measuring Tubes

The measuring tubes used were calibrated from the stopcock upward. This tube remained in the brine/product lines. To take a flow rate measurement, the operator closed the stopcock and let the flow accumulate. This method introduced an error due to the small stream on the tube wall at time zero. This method was used because the error was considered insignificant and because the added expense of insuring a completely empty tube was prohibitive, since there were 64 measuring tubes.

Orifices

The fabrication of thirty-two titanium orifice plates was a major problem. The goal was to obtain groups of four which would deliver flow-rates within a 2% spread at a given liquid head. The orifice size was .024". Minor burrs and irregularities in thickness of the plate made this performance difficult. A great deal of hand work resolved this problem.

An improved mounting configuration would have the individual orifices outside the flow box for accessibility. This would permit more adjustments to be made on a given orifice in the same amount of time.

Flooding Plates

The initial bank design provided one flooding nozzle for each plate. The procedure at startup was to feed weirs at the correct flow rate, at the same time flood the plate until wetting was complete. The flooding nozzles were then turned off, and the weir feed maintained the film. In the final configuration, three nozzles per plate were used. Figure III-7 shows the small manifolds feeding the flooding nozzles in the cover plate at the center of the specimens.

Condensation in Gauges and Control Lines

A problem that was foreseen and adequately provided for was that of condensation in gauges and control lines. The condensation was avoided by wrapping the gauge lines with a strip heater and maintaining the surface of the lines above the saturation temperature of the vapor in the lines. All instruments subject to condensation were mounted in a closed cabinet. The instrument cabinet was heated and maintained at a temperature above the saturation temperature. The magnitude of this problem was evident on one occasion when the heaters were shut down for modification.

pH Adjustment

The pH control problem was underestimated at the design phase. The "two-valve feeder" arrangement as described in Apparatus Description worked quite well; however, the requirements for maintaining pH to $\pm$ .1 unit at the 6.5 and 7.0 levels were too stringent for manually controlled valves. The pH vs. acid addition characteristics of sea water are such that only good automatic control could accomplish $\pm$.1 unit under Task III conditions. Figure III-11 shows this characteristic. The long plateau on curve A (upper left portion) represents the effect of carbonate and

bicarbonate buffering ions contained in sea water. The remainder of Curve A follows quite closely the acid addition vs. pH characteristic of distilled water. Curve B represents the distilled water characteristic assuming complete dissociations of the acid, i.e., all hydrogen ions added result in a direct change in pH according to the logarithmic function $pH = \log 1/[H^+]$.

It can be seen that the allowable % change in acid feed to maintain $\pm$ .1 pH in the 5 to 7 pH range is extremely small with sea water as compared to distilled water. For example, referring to curve A, the allowable % change in acid volume flow to maintain pH = 6.0 $\pm$ .1 is approximately 1/2%, while with distilled water it is approximately 10%. The curves in Figure III-11 are based on an acid concentration of 1% by weight since this was the most dilute acid permitted by the feed system employed. Only a very slight improvement could be realized in any further acid dilution within reason.

Analysis has shown that the sum of errors, i.e., initial acid concentration $\pm$ x_1%, sea water flow control $\pm$ x_2%, and acid flow $\pm$ x_3% must be less than 1%. That is $(x_1 + x_2 + x_3) < 1\%$. It can be seen that pH control to $\pm$ .1 pH unit is a high level control problem. The apparatus shown was able to maintain pH at 6.9 $\pm$ .4, and 7.5 $\pm$ .2 which indicated an overall sum of errors of approximately 1.5 - 2% which is as good performance as can be expected with manual control. Actually the true critical parameter was the ratio of sea water flow to acid flow and not the two independently. In the rig, factors which caused acid flow to increase also caused sea water to increase, although not as a one-to-one functional relationship. In general, the pH control as attained permitted reasonable pH ranges and yielded significant results for the test time period achieved.

Measurements

Liquid flow rates were measured as described with the calibrated measuring tubes. The tubes were calibrated to units of cubic centimeters and could be read accurately to 0.5 cc. A five minute sample time would yield an accuracy of 0.1 cc/min. A representative number for the flow rates was 10 cc/min, consequently the accuracy of the reading was 1%.

Temperatures of liquids were measured to 1°F with copper-constantan thermocouples. The temperature measurements were used only for monitoring purposes.

Pressure measurements were the basis for heat transfer data. Absolute pressure was measured with mercury manometers. The absolute pressure could be read accurately to 0.05 centimeters of Mercury. Differential pressure was measured with U-tube manometers filled with water. The differential pressure could be read accurately to 0.1 inches of water. Differential pressure gauges were provided for monitoring the system. Measurement of pH was made on a glass-calomel electrode pH meter. The accuracy of the readings were 0.1 pH unit.

Salinity measurements were made by determining chloride content and relating salinity using Knudsen's Hydrographical Tables. A standard silver-nitrate titration was used to determine chlorinity. Dissolved oxygen content of the feed water was determined employing the standard Winkler reaction:

$$MnSO_4 + 2KOH \longrightarrow \underline{Mn(OH)_2} + K_2SO_4$$

$$\underline{Mn(OH)_2} + \frac{1}{2} O_2 \longrightarrow \underline{MnO_2} + H_2O$$

$$\underline{MnO_2} + 2KI \longrightarrow MnSO_4 + \underline{I_2} + K_2SO_4 + 2H_2O$$

followed by solvent extraction of the iodine with chloroform. The absorbance of this iodine-chloroform mixture was then measured with a spectrophotometer. Reference to a standard curve of absorbance vs. iodine concentration (or the equivalent oxygen concentration) provided a rapid method of determining dissolved oxygen.

Results

Heat Transfer Data - A summary of these data is represented in Figures III-12 through III-14. A typical data sheet is shown in Table III-1. It will be noted that data readings did not begin until approximately 80 - 100 hours after initial startup. During this period various adjustments and modifications were being made on the test rig to attain specified test conditions and to reach steady state operation.

Data on some test plates in particular the tin, were quite scattered. This scatter was primarily caused by non-uniform wetting of the evaporating side of the plate. Those plates having satisfactory wetting were selected for discussion. The performance of the heat transfer surface, i.e., the effects of fouling, is shown by plotting circulation ratio R vs. elapsed time. R was determined by the ratio (brine flow rate + condensate flow rate)/condensate flow rate.

Discussion of Results

I. Tin Plate

The heat transfer data were extremely scattered and on many plates production was practically nil. The reason for this was explained by the observation that adequate wetting could not be maintained. Data on the few plates which did wet indicated fouling early in the test, the fouling being in most cases of the same degree as that on steel plates. All tin plates revealed red corrosion product during startup and rapid corrosion in certain areas during the period from shutdown to specimen removal. The tin coating in these areas had obviously been lost during test.

II. Carbon Steel

Heat transfer data revealed little difference in the three acid treated environments but did confirm the observance of scale formation in the untreated or raw sea water environment. Considerable red oxide corrosion product was observed during startup, this changing to black oxide as the test progressed. The color change is typical of iron corrosion in atmospheres changing from high to low oxygen content. Rapid formation of red oxide corrosion product occurred from the shutdown point to time of removal (several hours). The circulation ratio on all steel panels was significantly higher than theoretical even early in the test, confirming the rapid corrosion observed during startup.

III. Aluminum

Data indicated aluminum to have the best performance as a heat transfer surface. Circulation ratios were lower than either steel or tin plate, in all four environments. The plot of R vs. elapsed time for the untreated raw sea water environment (Figure III-12) shows an initial R equal to the theoretical with a rapid rise within a subsequent 24 hour period. This is explained by the observance of scale formation during this period. As time progressed, this curve shows very little further degradation for the remainder of the test. The indication here is that scale buildup progressed very slowly after reaching a certain thickness during the first 170 hours of test. This could not be confirmed by visual observation. The scale thickness measured at the end of the test was approximately .001" - .003". Visual examination during the latter stages of test and after specimen removal revealed a pitting tendency in the low pH (4.5 - 6.5) environment which was absent in the others.

Figure III-15 shows the appearance after test, of the evaporating side of aluminum specimens exposed to the four environments. The scale can be readily seen on Specimen No. 1. The dark streaks on the remaining specimens are thin oxide films.

Figure III-16 shows the appearance of the condensing side of aluminum specimens. The oxide film here was thicker, but attack was general and slight, probably occurring during initial stages of testing when the hot water system used as a steam source still contained considerable oxygen.

Figure III-17 shows an area of pitting typical of that observed on the evaporating side of aluminum specimens exposed to the low pH environment.

Photographs of the steel and tin plate specimens were not included since the rapid corrosion occurring after shutdown masked the effects of exposure to deaerated water during operation.

Conclusions

A. Treatment to prevent scaling is mandatory for heat transfer surfaces operating at a sea water inlet temperature of 120°F and a concentration factor of 1.5 to 2.

B. Scale can be prevented using sulfuric acid feed addition to produce a pH of 6.5 - 7.0 after deaeration. A slightly higher pH, up to 7.5 might be allowable, but would not be recommended where aluminum is the heat transfer surface. Although not proven in this test, aluminum is more corrosion resistant to pH 6.0 - 7.0 water than in water of higher pH. The additional cost of acid to go from 7.5 to 6.5 pH is negligible.

C. High Purity Aluminum 1188 or Aluminum Alloy 5050 is recommended for the heat transfer surface of the subject sea water conversion system. Steel presents a major problem of corrosion during manufacture, during startup, and during shutdown. Very elaborate procedures of protection during manufacture, and purging prior to and during any shut down, would be required.

   Tin plate is undesirable for these same reasons and in addition creates an additional problem of non-wetting.

SUMMARY OF HEAT TRANSFER DATA

TASK III

I Date	Time (Hrs)	pH Range	P Cond. (Cm.Hg.)	P Bank (in.H_2O)	pH	O_2 (ppm)	Flow Rate Measurements: Tin Br.	Tin Cnd.	Tin Tot.	Tin R	Steel Br.	Steel Cnd.	Steel Tot.	Steel R	Aluminum Br.	Aluminum Cnd.	Aluminum Tot.	Aluminum R
8-1	0	8.4	-	-	8.4	.110	-	-	-	-	-	-	-	-	-	-	-	-
8-7	148	"	8.60	3.38	-	-	-	-	-	-	10.8	8.80	19.6	2.24	9.0	9.40	18.4	1.96
8-8	175	"	8.60	3.13	8.4	.090	13.2	7.00	20.2	2.89	12.2	7.30	19.5	2.67	10.6	7.90	18.5	2.34
8-9	195	"	8.55	3.13	8.5	-	13.5	6.80	20.3	2.98	12.9	7.20	20.1	2.78	11.0	7.50	18.5	2.47
8-10	221	"	8.55	3.25	8.5	.083	14.0	7.10	21.1	2.96	13.2	7.10	20.3	2.86	11.0	8.00	19.0	2.38
8-11	243	"	8.55	3.13	8.4	-	14.6	7.20	21.8	3.02	14.0	6.90	20.9	3.04	12.0	8.30	20.3	2.44
8-12	268	"	8.60	3.13	8.5	-	14.0	7.00	21.0	3.00	14.0	6.30	20.3	3.22	10.8	8.10	18.9	2.34
8-13	290	"	8.60	3.50	8.5	.095	14.0	6.90	20.9	3.03	14.2	6.40	20.6	3.22	10.8	8.30	19.1	2.30
8-3	0	7.3,7.7	-	-	7.3	.095	-	-	-	-	-	-	-	-	-	-	-	-
8-6	80	"	8.60	3.38	-	-	-	-	-	-	10.0	7.80	17.8	2.28	9.2	8.60	17.8	2.06
8-7	104	"	8.60	3.38	7.4	.083	-	-	-	-	9.70	8.70	18.4	2.11	9.6	9.30	18.9	2.04
8-8	126	"	8.60	3.25	7.7	-	11.5	6.40	17.9	2.80	10.9	7.50	18.4	2.45	10.7	8.30	19.0	2.29
8-9	149	"	8.55	3.25	7.3	-	12.4	6.60	19.0	2.88	11.0	7.60	18.6	2.05	10.4	8.70	19.1	2.20
8-10	171	"	8.60	3.00	7.4	.083	12.4	6.90	19.3	2.80	10.6	7.50	18.1	2.41	10.6	9.00	19.6	2.18
8-10	175	"	8.55	3.38	-	-	12.8	6.60	19.4	2.94	11.0	7.30	18.3	2.50	10.3	8.80	19.1	2.17
8-11	194	"	8.60	3.13	7.6	-	12.7	6.70	19.4	2.90	11.0	7.50	18.5	2.46	10.1	8.60	18.7	2.18
8-12	219	"	8.60	3.13	7.6	-	12.4	6.90	19.3	2.80	10.6	7.80	18.4	2.36	9.7	9.0	18.7	2.07
8-12	224	"	8.60	3.50	-	-	12.0	6.90	18.4	2.74	10.6	7.80	18.4	2.36	9.6	9.2	18.8	2.05
8-13	241	"	8.60	3.50	7.4	.090	11.8	7.30	19.1	2.62	10.6	7.90	18.5	2.34	9.0	9.4	18.4	1.96
8-2	0	4.5,6.5	-	-	5.1	.120	-	-	-	-	-	-	-	-	-	-	-	-
8-6	102	"	8.60	3.25	4.8	-	9.7	7.20	16.9	2.36	11.7	6.60	18.3	2.76	10.2	8.50	18.7	2.20
8-8	147	"	8.60	3.25	5.8	-	10.8	6.80	17.6	2.60	11.5	6.50	18.0	2.77	8.6	9.40	18.0	1.91
8-8	152	"	8.60	3.25	-	-	10.9	6.70	17.6	2.62	11.0	6.80	17.8	2.62	9.0	9.00	18.0	2.00
8-9	168	"	8.55	3.25	6.0	.095	10.2	6.80	17.0	2.49	10.2	6.90	17.1	2.47	9.9	8.50	18.4	2.16
8-9	174	"	8.55	3.50	-	-	10.6	6.90	17.5	2.54	11.0	6.70	17.7	2.64	9.2	8.90	18.1	2.03
8-10	193	"	8.55	3.13	4.5	-	10.6	6.80	17.4	2.56	10.5	6.70	17.2	2.56	9.3	8.90	18.2	2.05
8-10	196	"	8.55	3.25	-	-	10.8	6.80	17.6	2.58	11.0	6.90	17.9	2.60	9.3	9.30	18.6	2.00
8-11	217	"	8.55	3.25	6.5	.083	10.6	7.30	17.9	2.46	10.7	7.40	18.1	2.44	9.0	9.60	18.6	1.94
8-12	241	"	8.60	3.25	5.5	-	11.0	6.80	17.8	2.62	11.6	6.80	18.4	2.71	9.7	9.40	19.1	2.03
8-13	265	"	8.60	3.38	6.0	.083	9.2	7.40	16.6	2.24	9.5	7.40	16.9	2.30	8.7	10.4	19.1	1.84
8-13	270	"	8.60	3.63	-	-	10.6	7.50	18.0	2.44	10.8	7.20	18.0	2.50	9.0	10.2	19.2	1.88

TABLE III-1

DWG. 626A507

Task III corrosion rig flow diagram

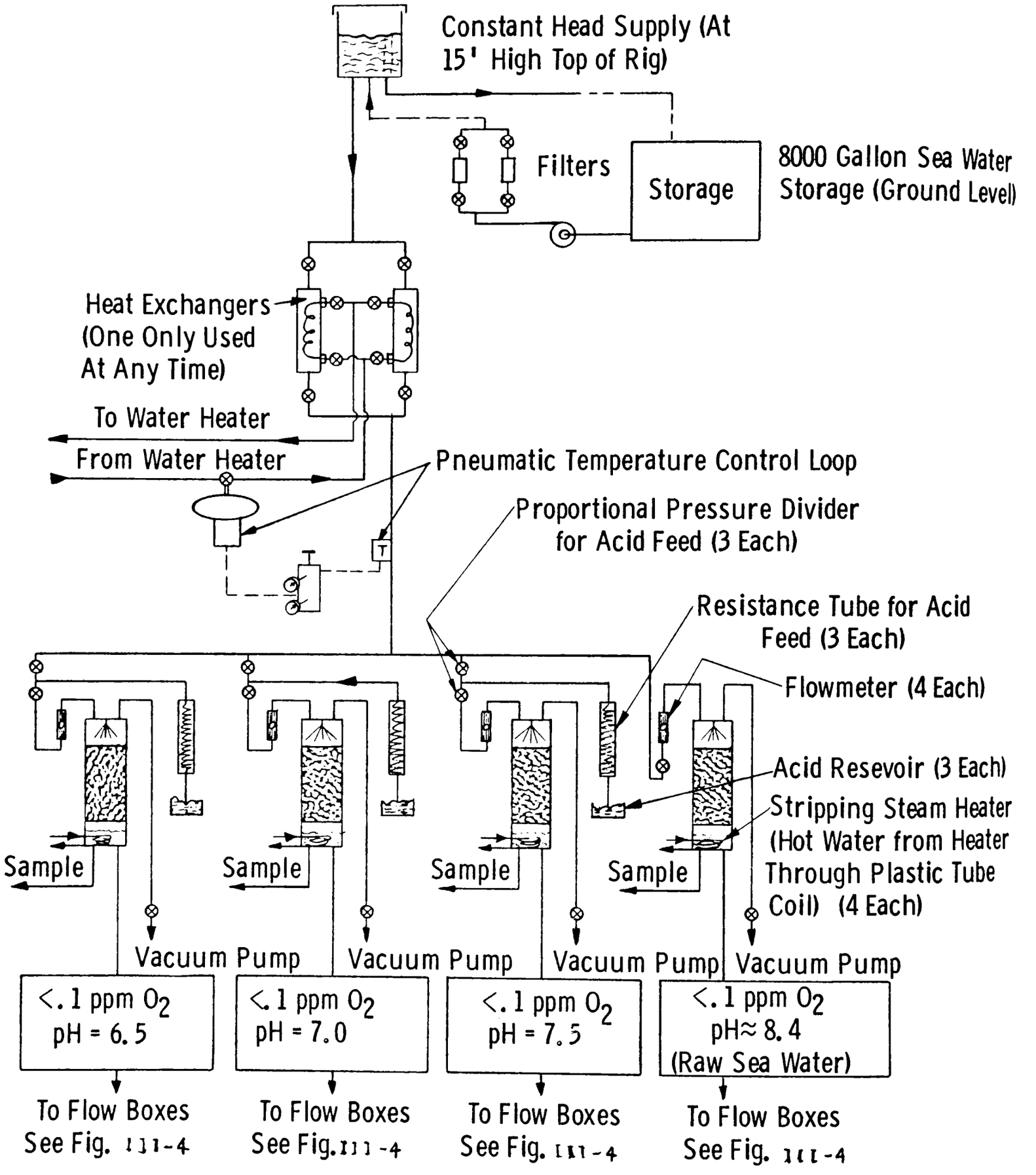

Fig. III-1—Storage, feed, acid treat and deaeration

DWG. 626A471

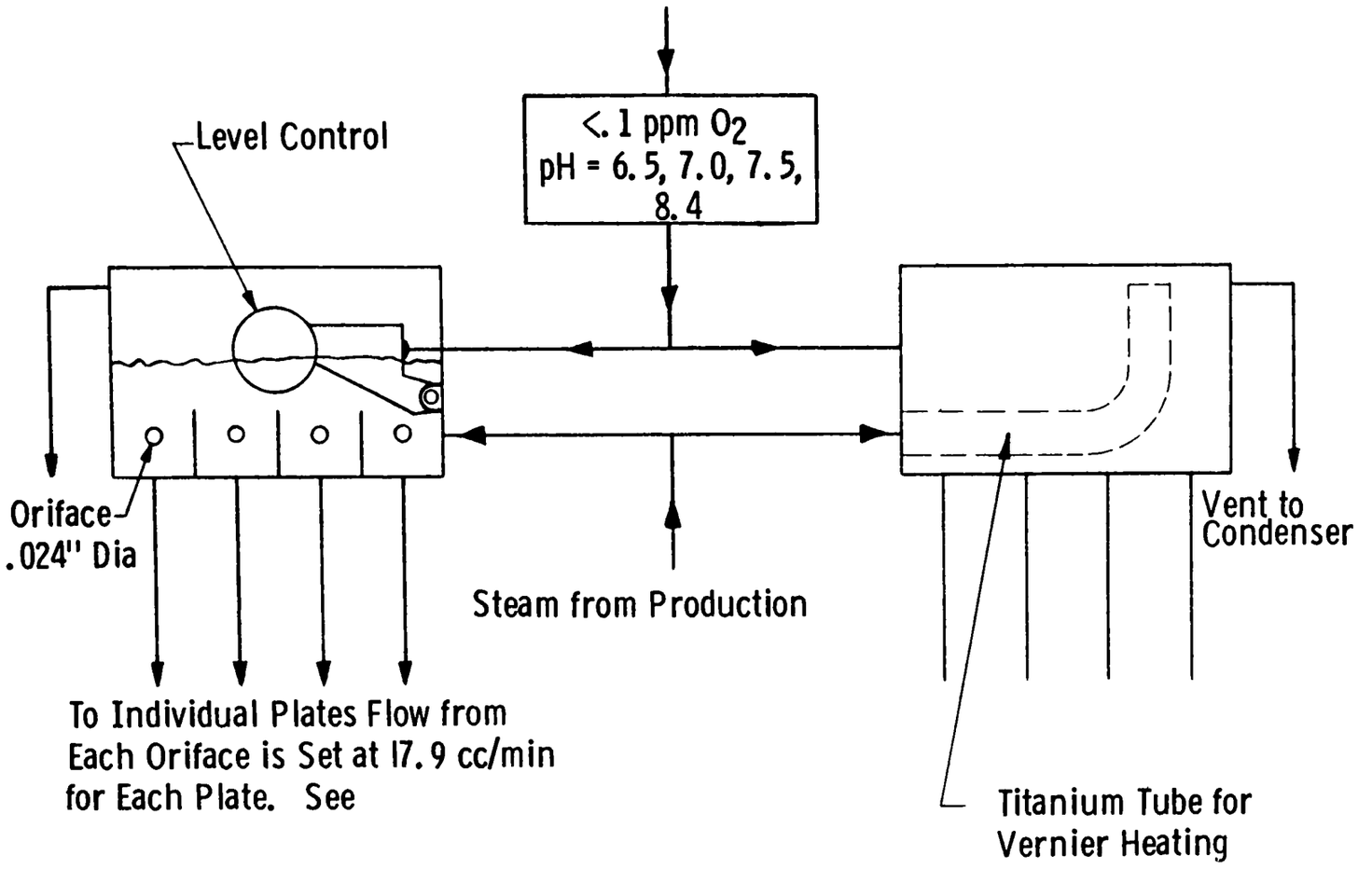

Fig. III-2 —Flow boxes

DWG. 626A472

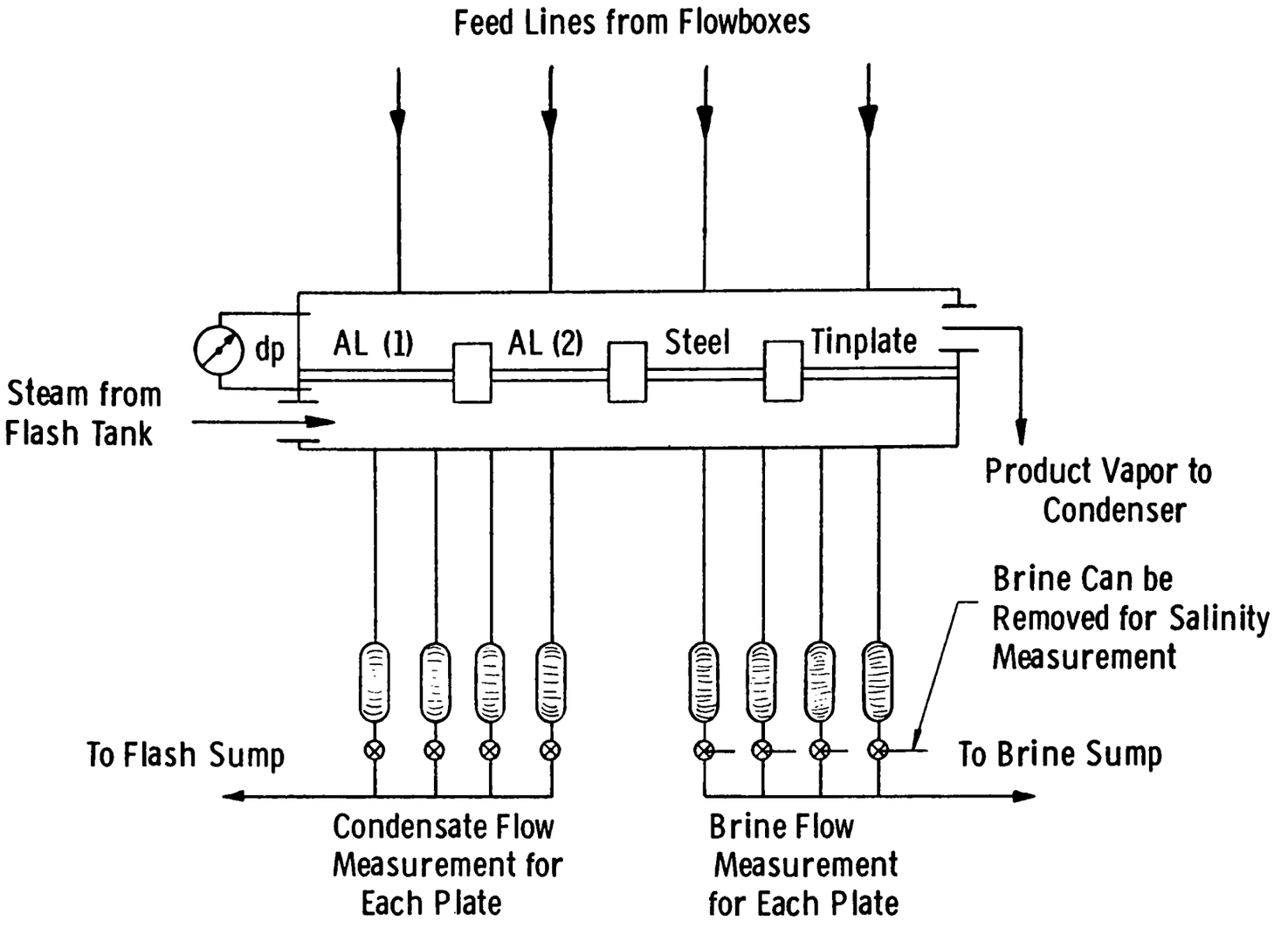

Fig. 111-3 —Schematic of one bank (of 8) containing specimens

DWG. 626A474

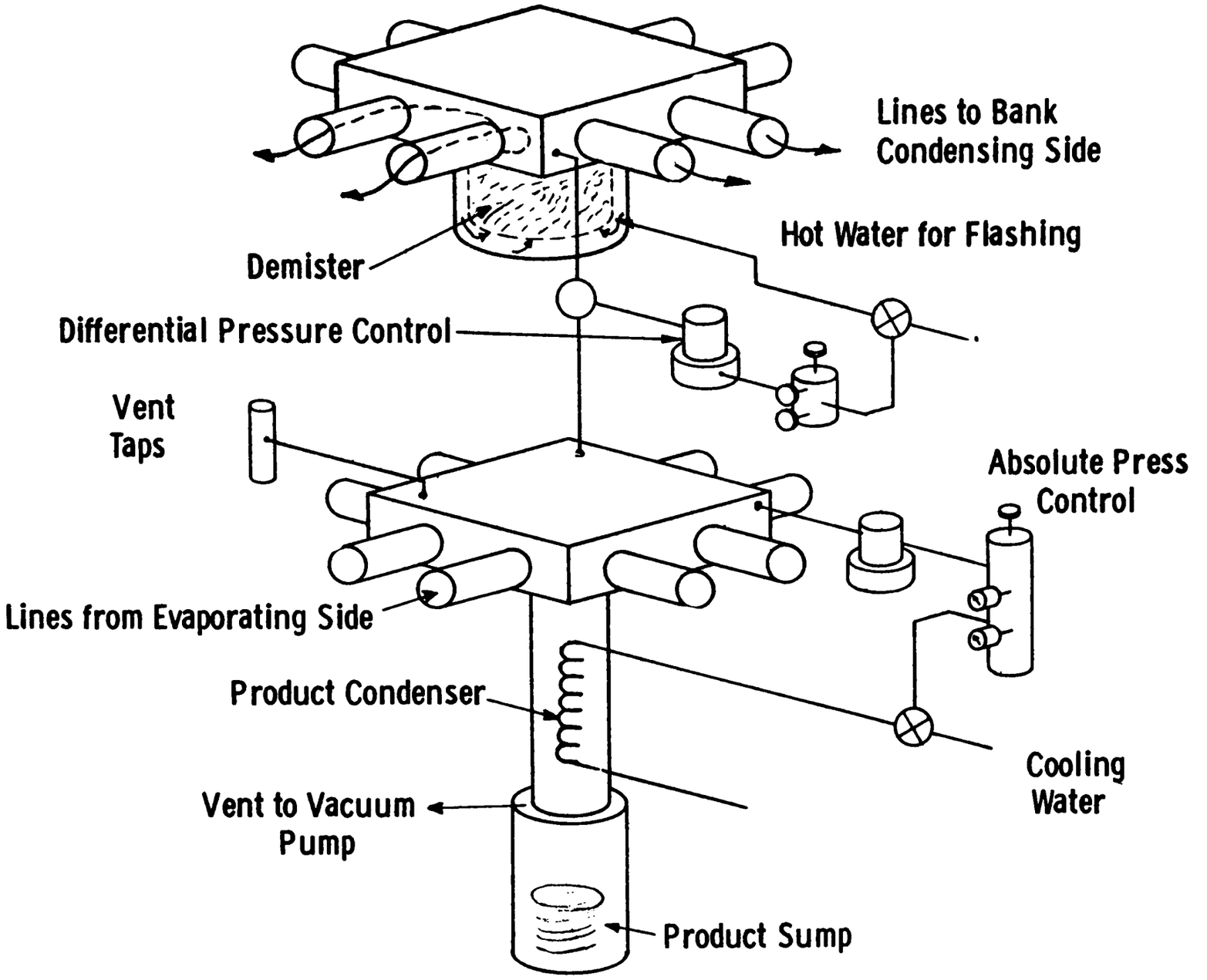

Fig. 111-4 —Flash tank, condenser and pressure control

DWG. 626A475

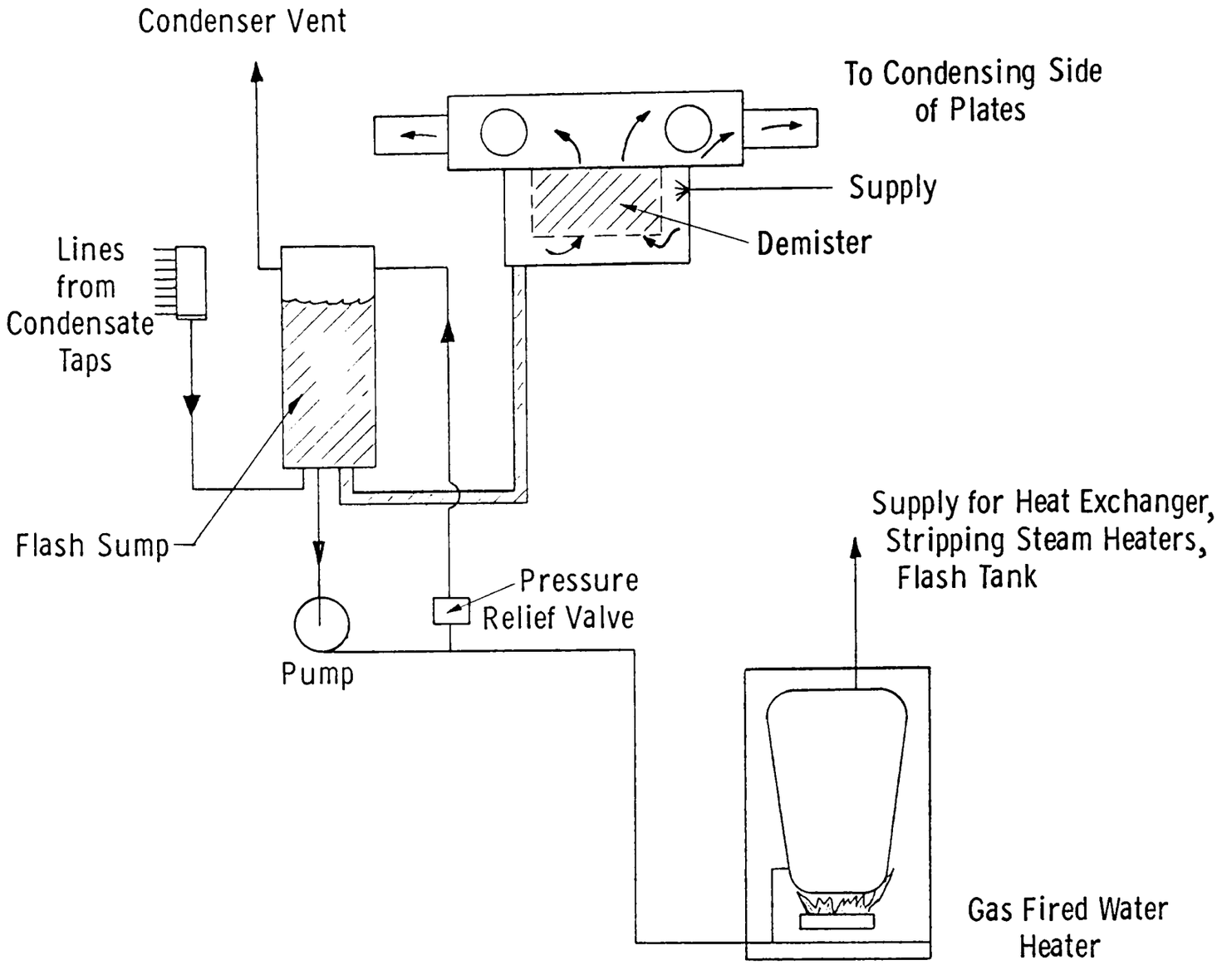

Fig. III-5 —Flash tank, flash sump, and fired heater

DWG. 626A473

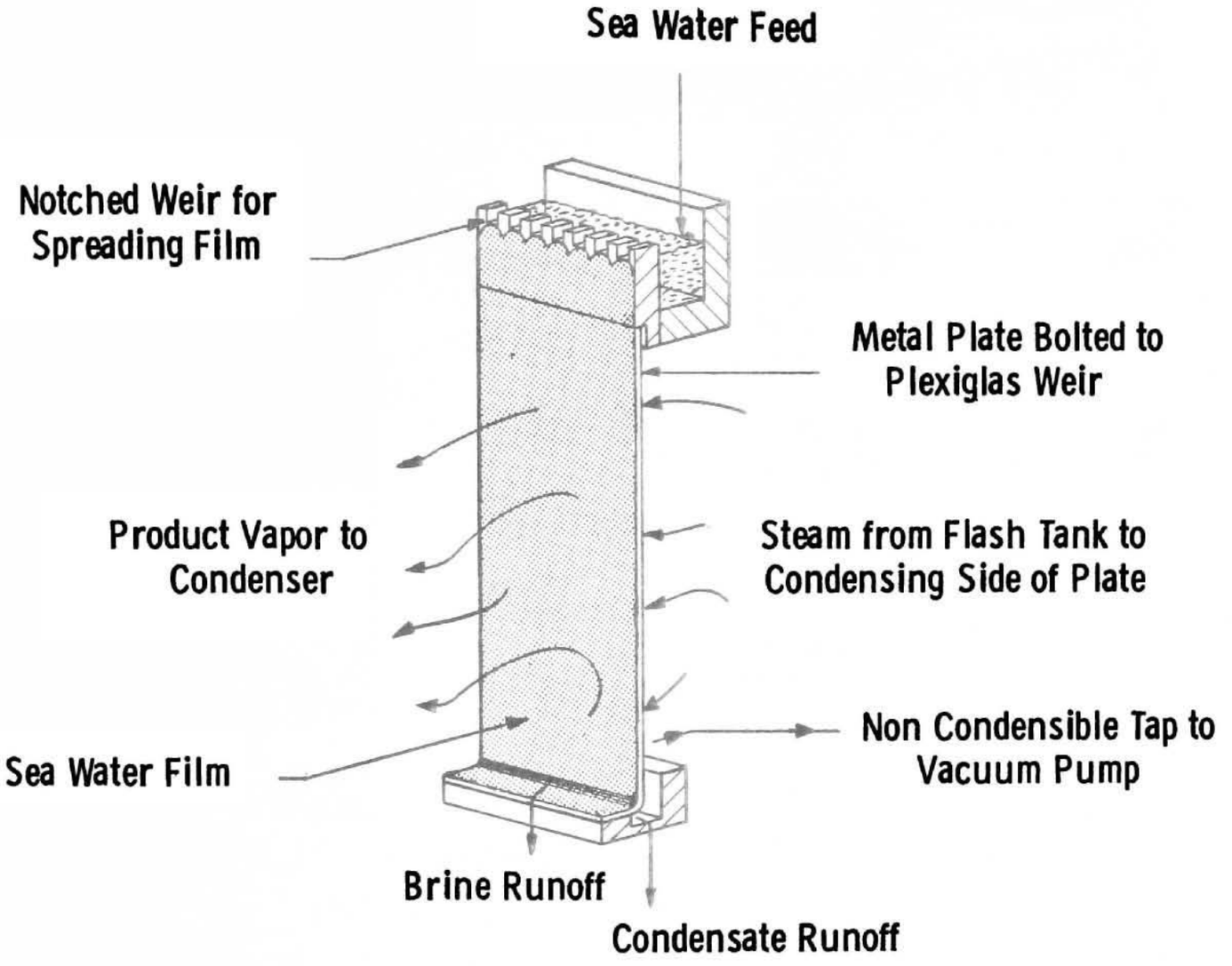

Fig. III-6 —Skeleton view of individual plates

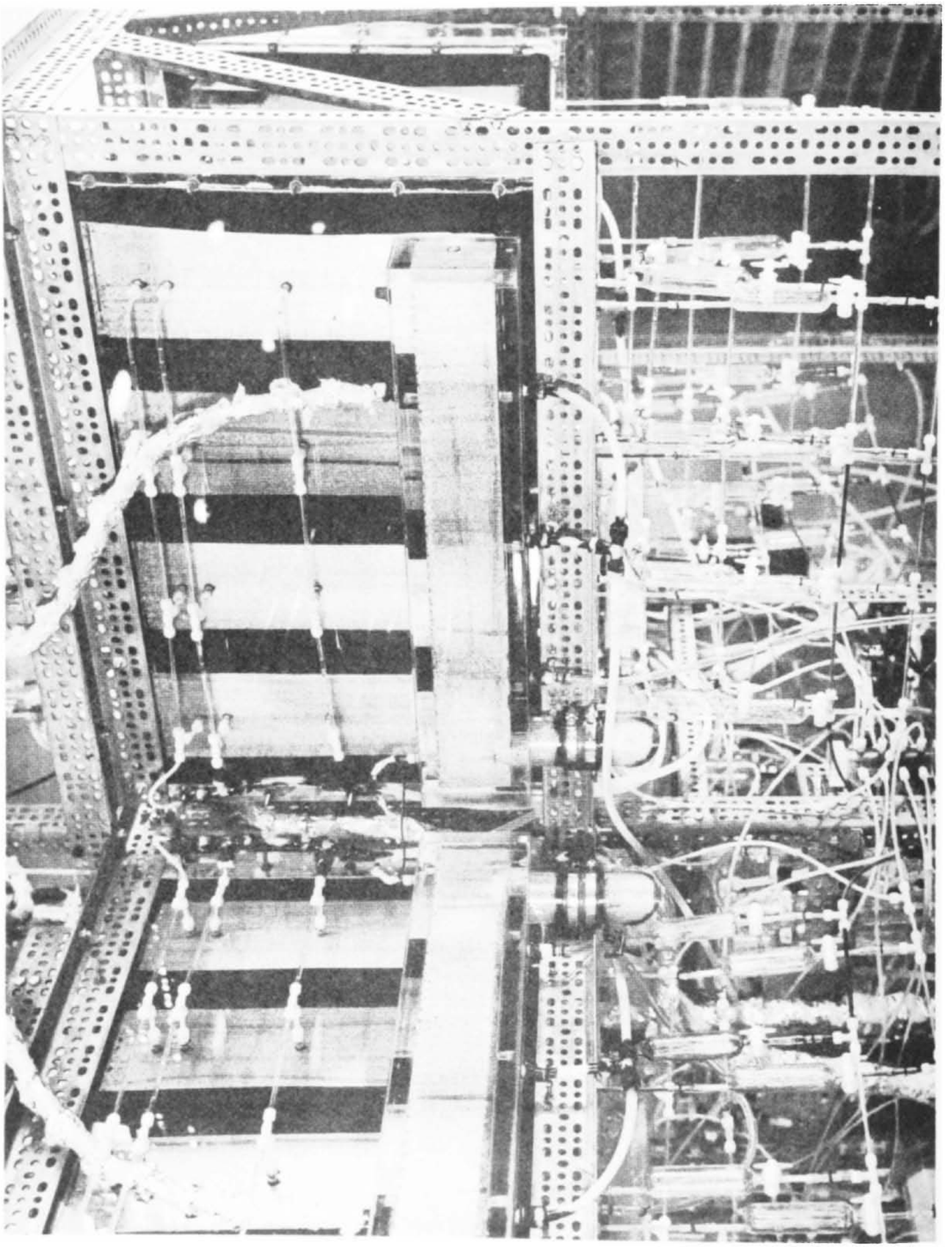

Fig. III-7. Closeup of banks.

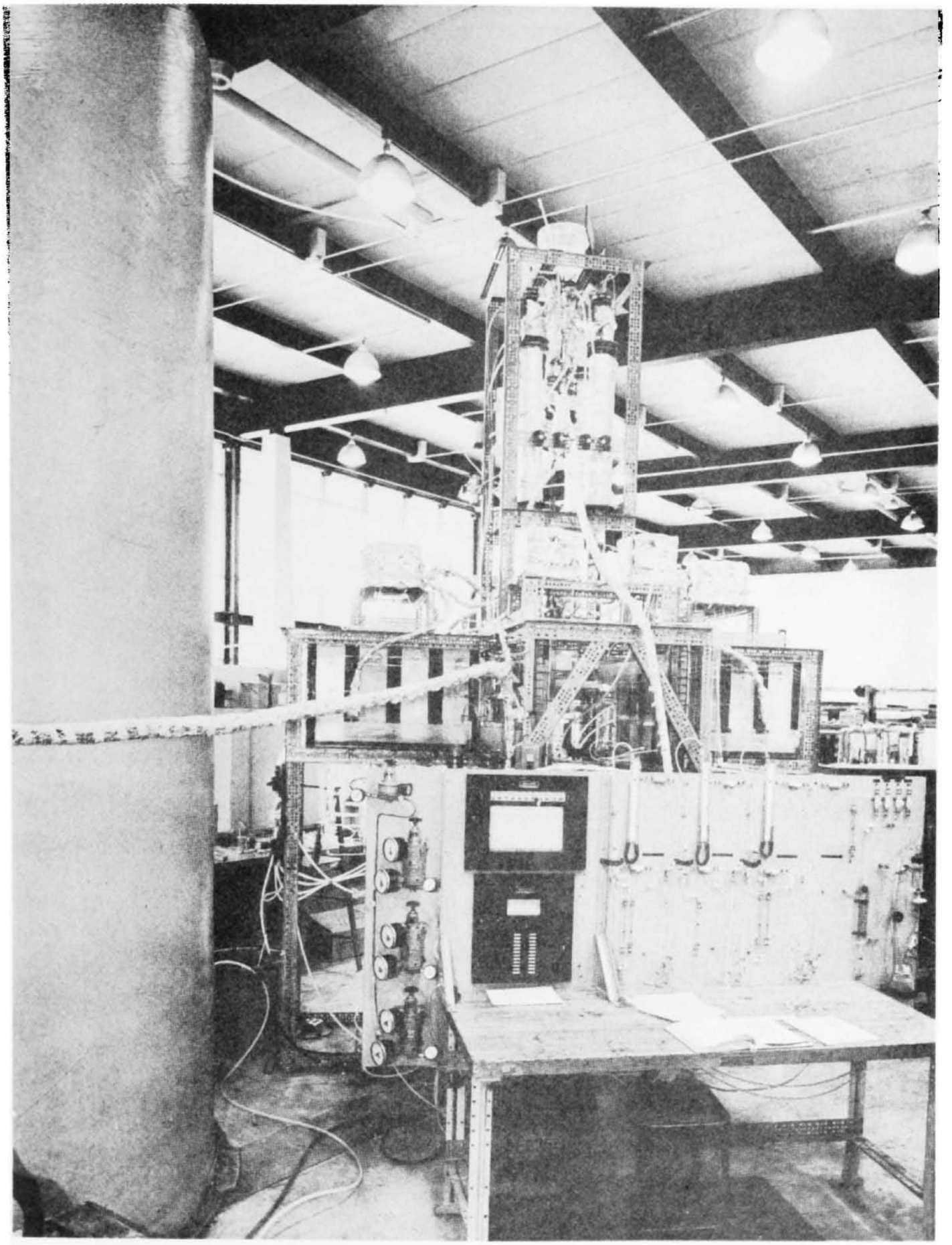

Fig. III-8. Instrument panel; shows monitor system for acid feed and sampling apparatus.

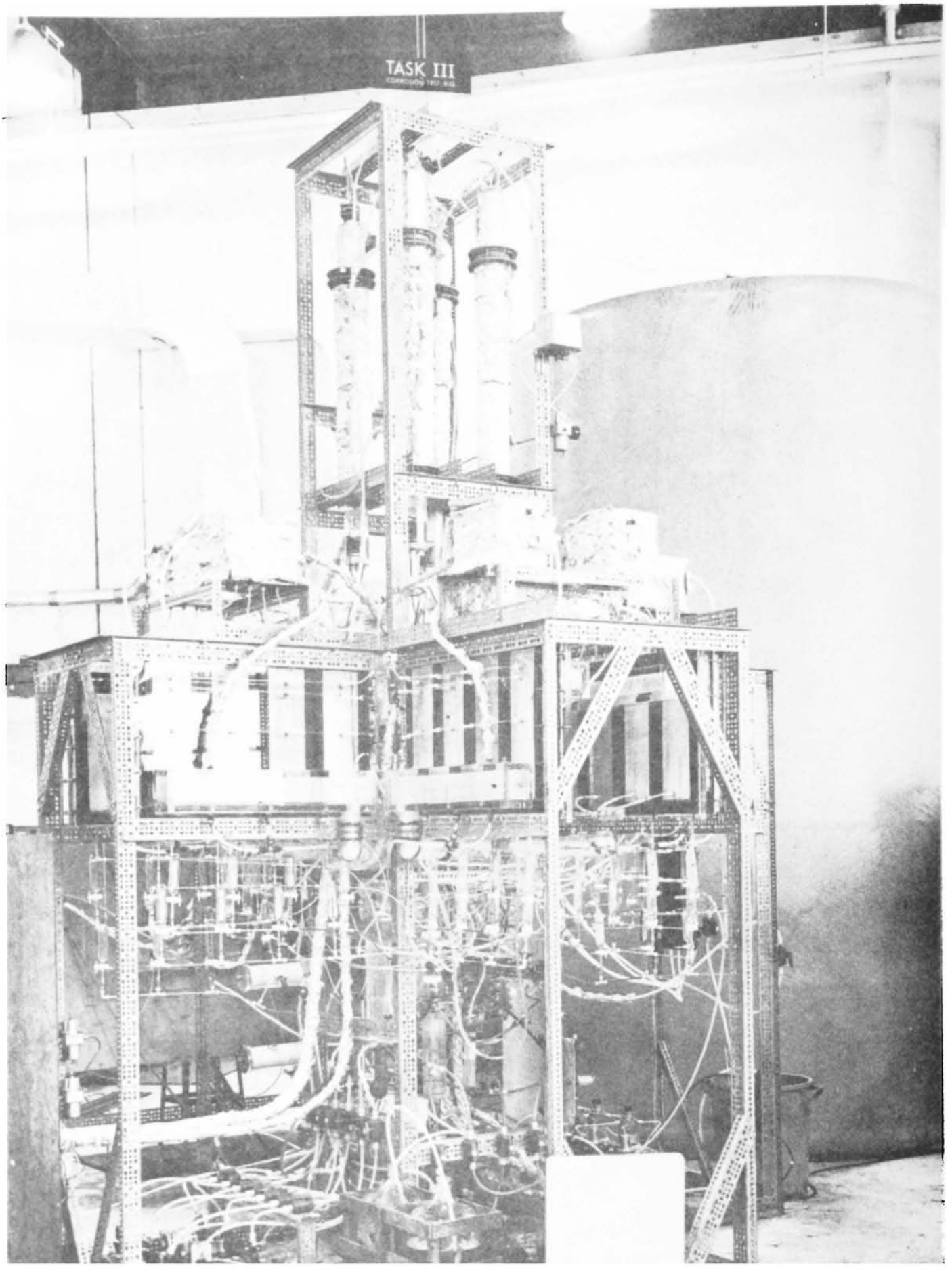

Fig. III-9. Overall view of Task III corrosion rig.

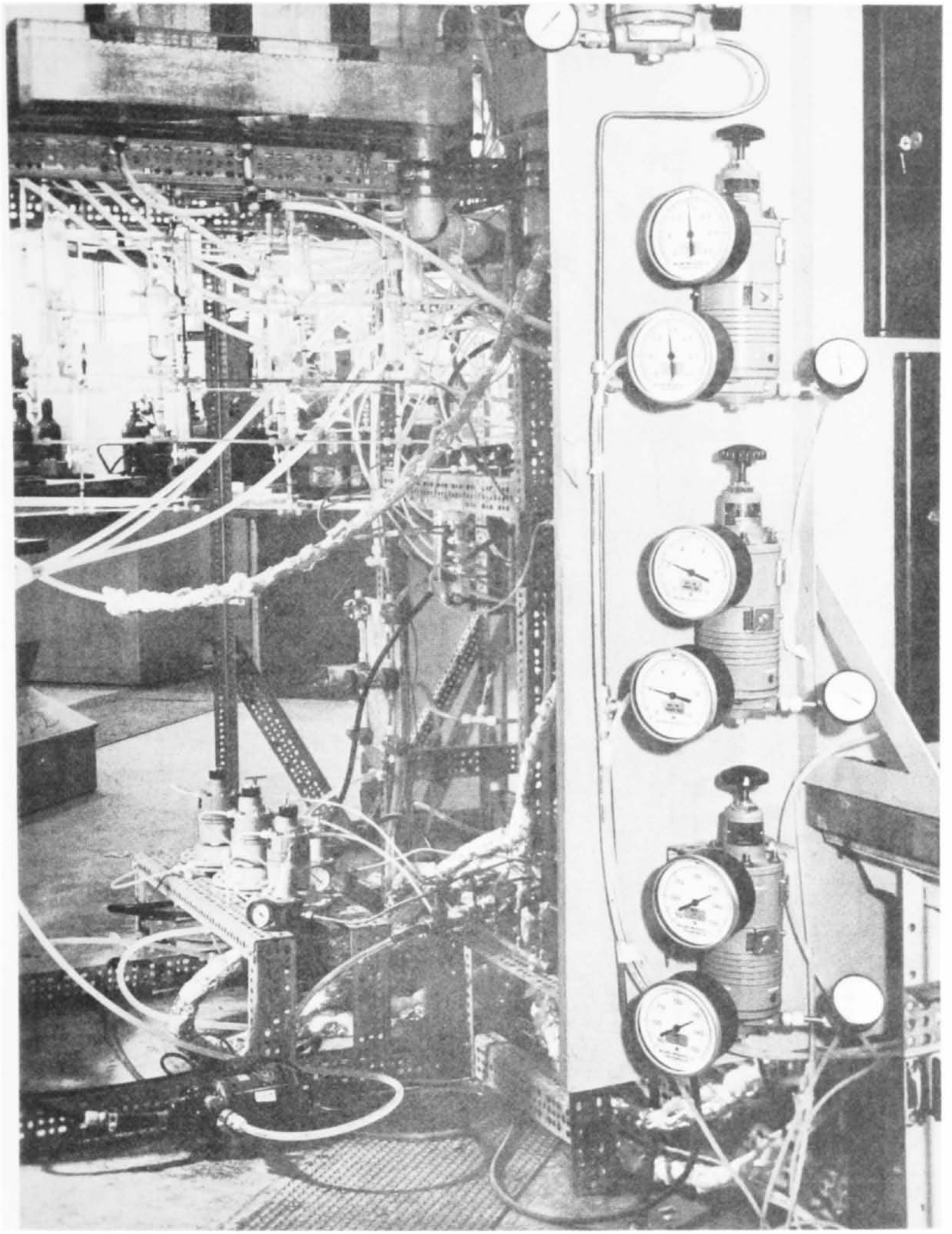

Fig. III-10. Pneumatic controllers and valves for maintaining temperature, absolute pressure and differential pressure.

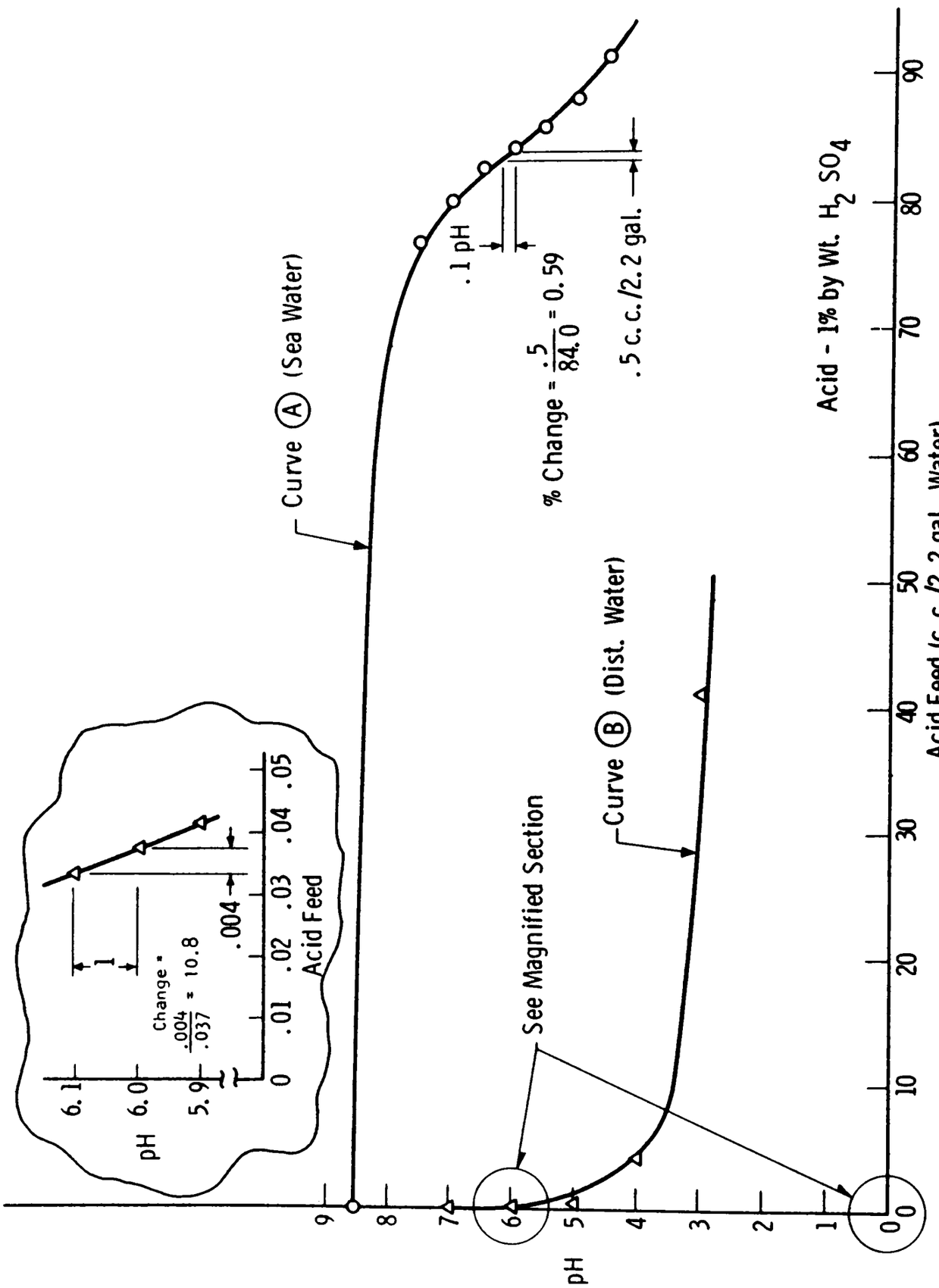

Fig. III-11—Acid feed vs. pH characteristic of sea water

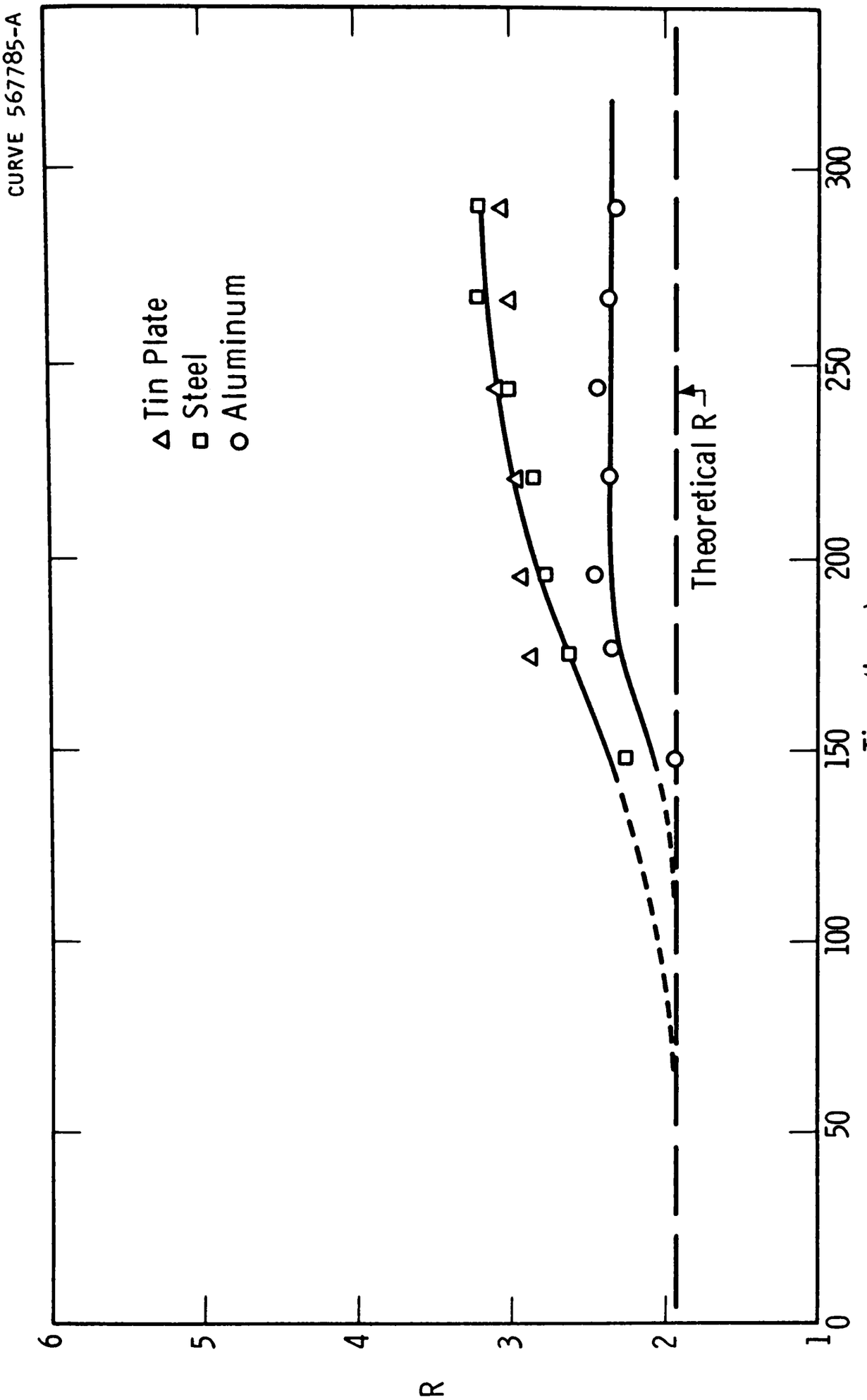

Fig. III-12—Effect of fouling in pH 8.5 feed water

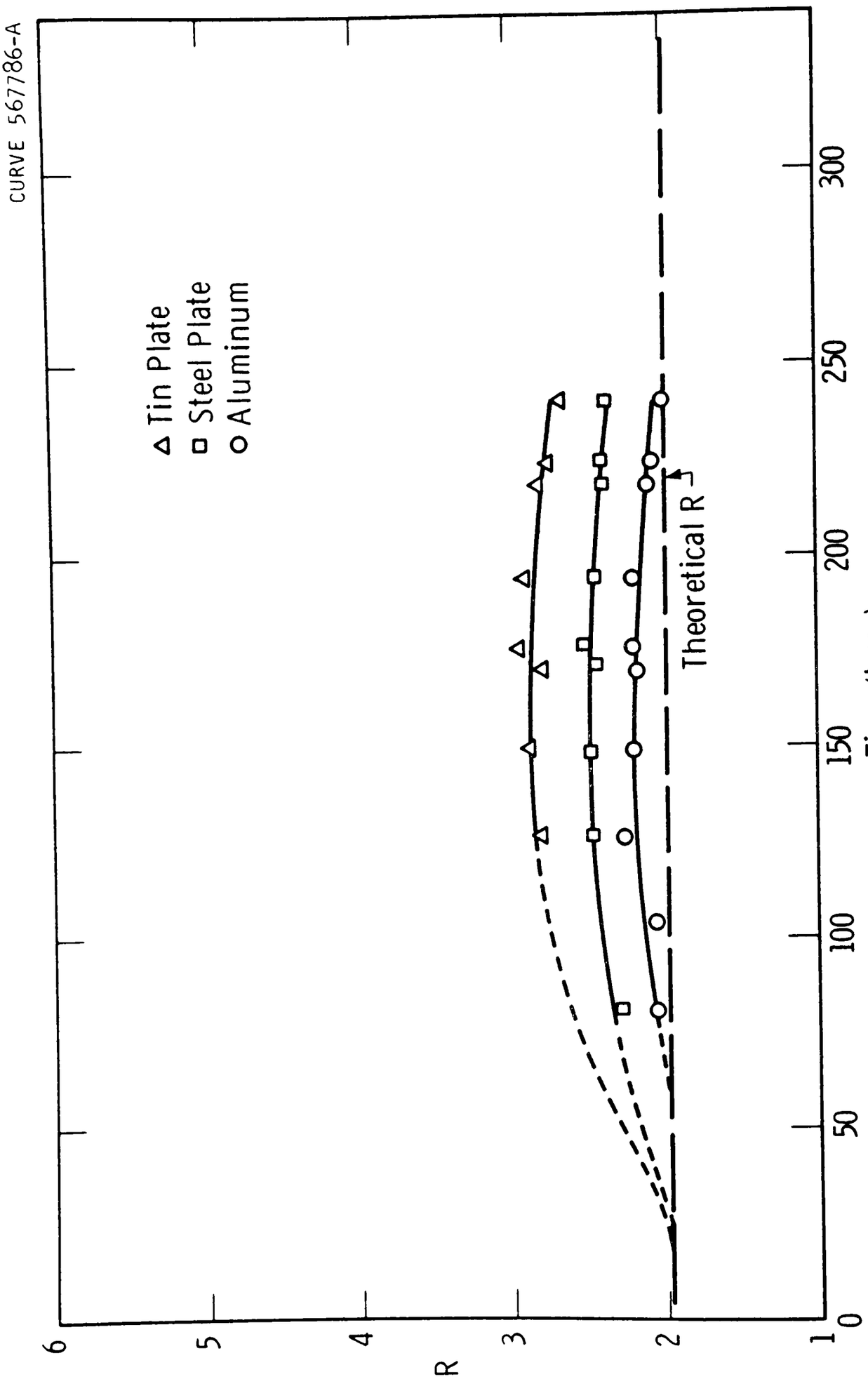

Fig. III-13—Effect of fouling in pH 7.3-7.7 feed water

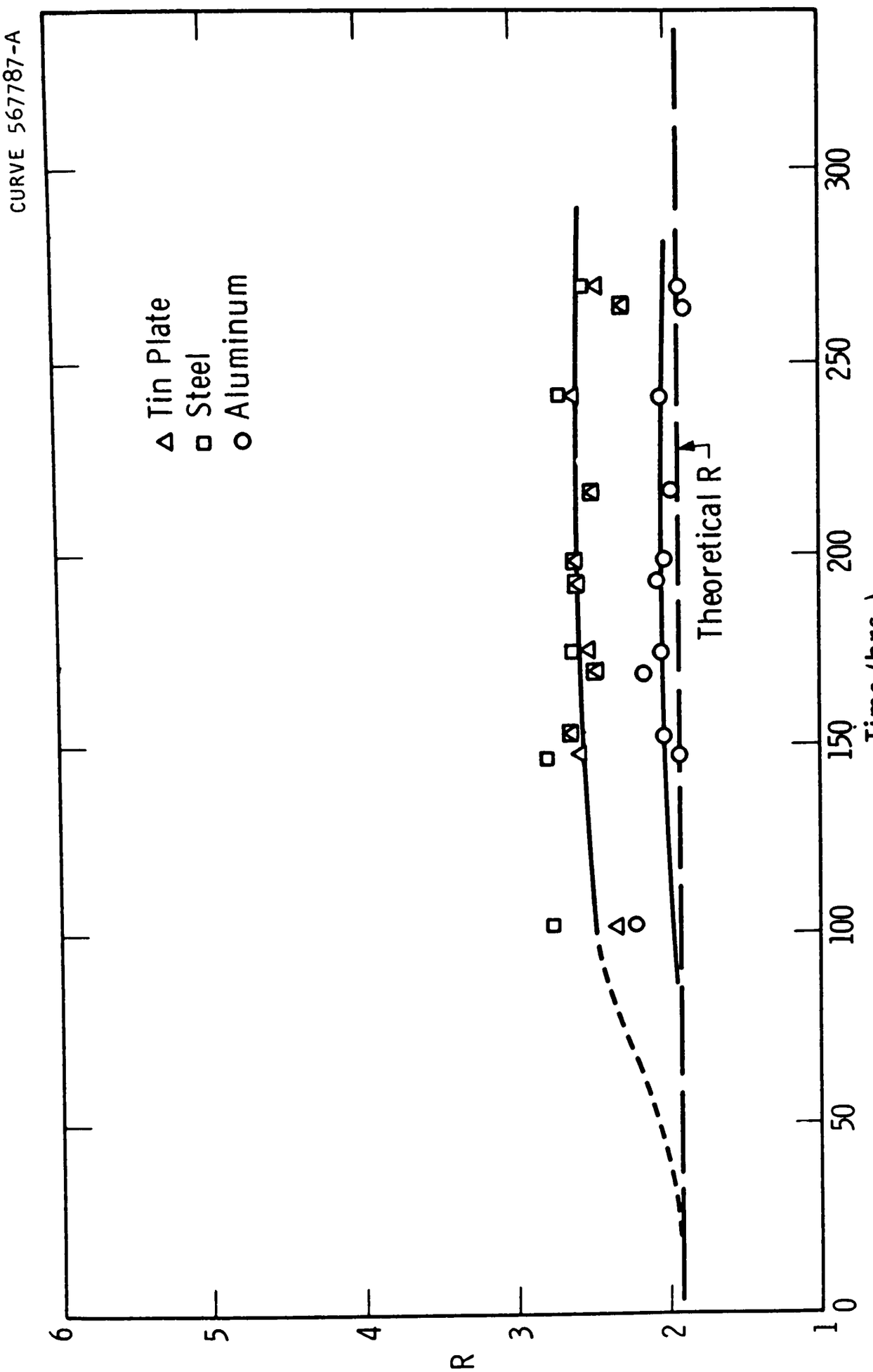

Fig. III-14—Effect of fouling in pH 4.5-6.5 feed water

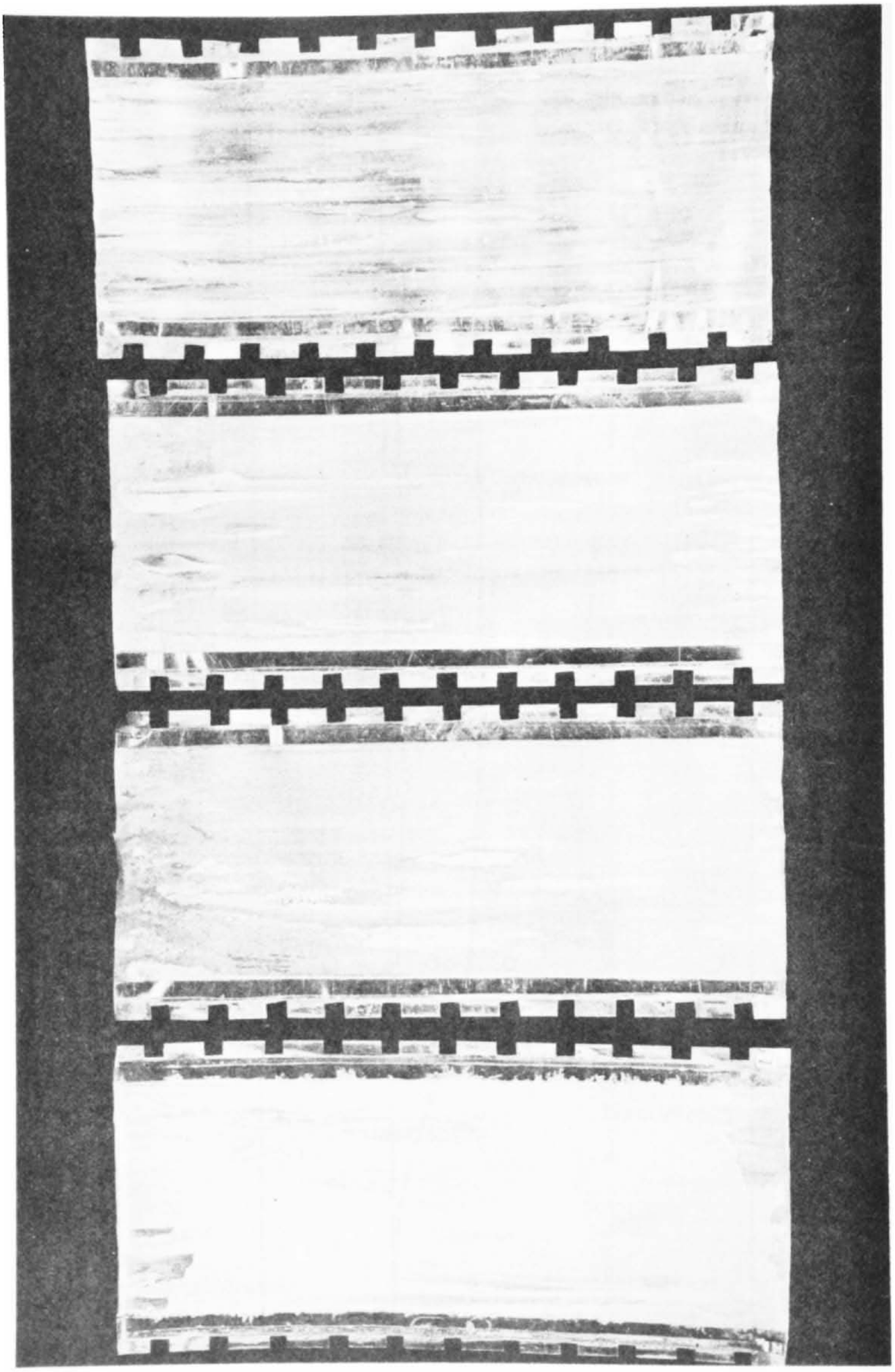

Figure III-15 - Appearance of the evaporating side of aluminum plates after completion of test

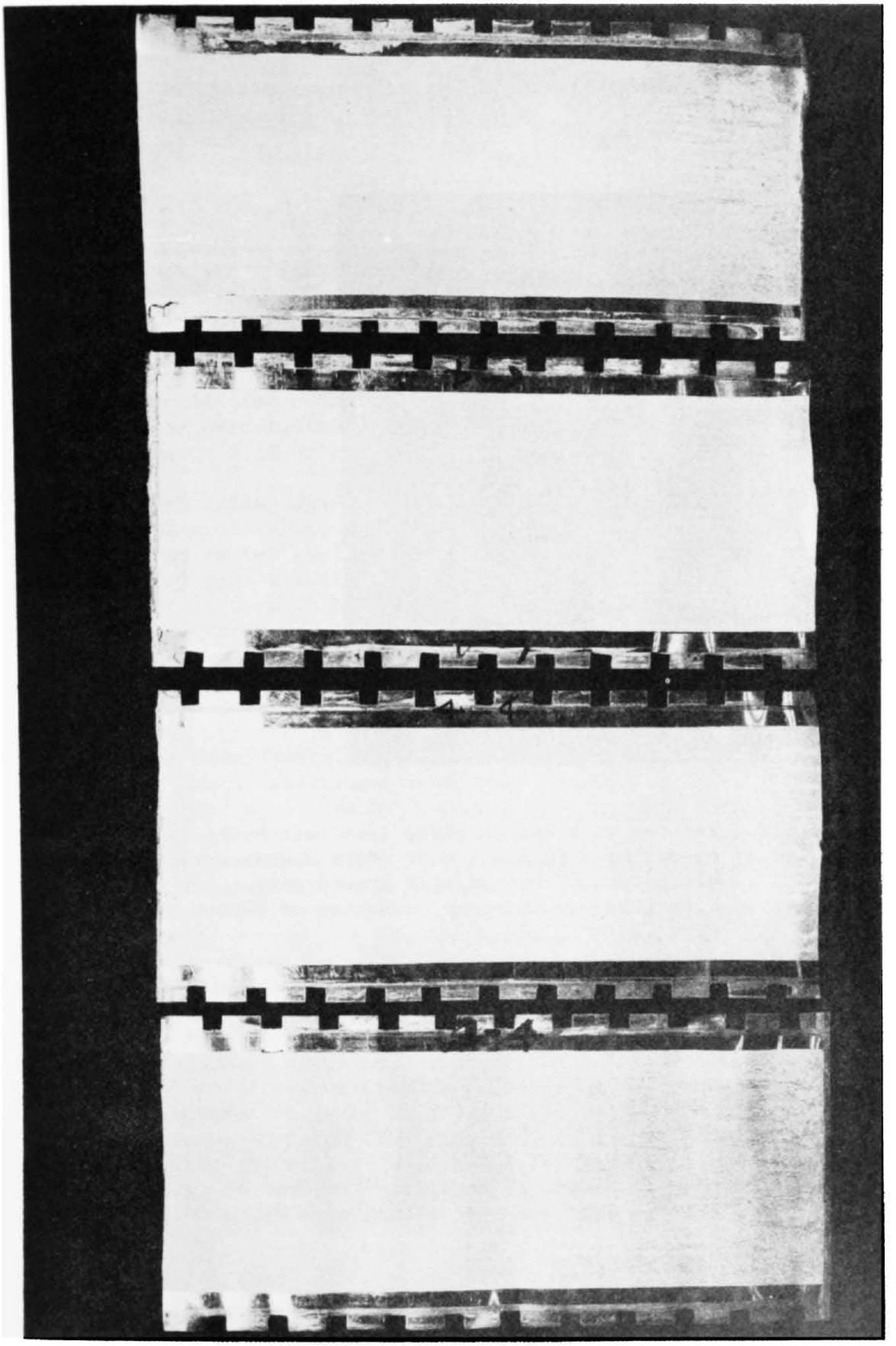

Figure III-16 - Appearance of condensing side of aluminum plates after completion of test

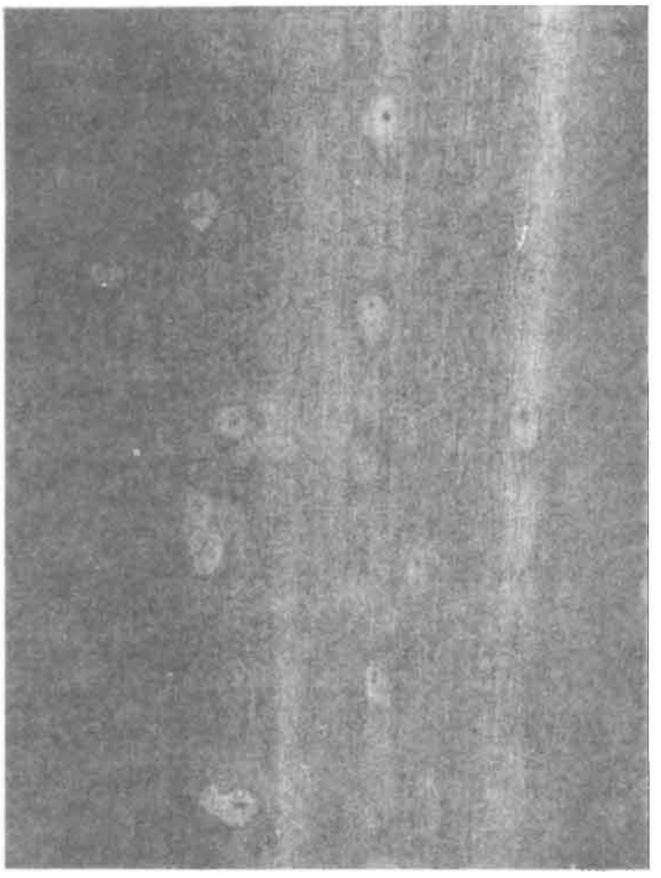

Figure III-17 - Pitting on aluminum plate from test bank operating @ pH 4.5 - 6.5. Note downward elongation of etched area around pits. Film flow was from top to bottom of photo.

Task IV - To Continue Experimental Research Toward Substantial Improvements in Heat Transfer

Description

The goal of Task IV is to conduct experimental research toward the attainment of substantial improvements in heat transfer to evaporating liquid films on vertical surfaces. Attention is to be focused on the evaporator side of a vapor-compression distillation system because, unlike the experimentally well-confirmed Nusselt description of laminar film condensation (Ref. 1), the Nusselt description of film evaporation has not been investigated sufficiently for confident application. Once the heat transfer rates on the two sides are known, the calculation of the over-all coefficients and performance of such a system will be greatly facilitated.

The testing apparatus is to be such that different surfaces can be tested successively. Both flat and contoured surfaces are to be tested, the latter employing the force of surface tension to produce high values of heat transfer coefficients. A single plate mounted in the apparatus is to have a particular surface configuration on the one side, and a coverage by electrical heaters on the other side. The latter side is to be thermally insulated and kept dry. Practically all of the electrically generated heat, therefore, passes through the plate and into the evaporating film.

The experimental program is to be split into three phases. First, experimental measurements of heat transfer coefficients for a flat surface are to be made with steady flow of saturated water from a horizontal feed line at the upper end of the surface. These experiments will ascertain the practical difficulties of film establishment and afford a reliability basis for the apparatus. Satisfactory agreement, if achieved, will then permit the undertaking of more difficult experiments as well as provide a design formulation for steady falling films. Second, using the same flat surface, experiments are to be carried out with periodically interrupted flows, rather than steady flows, that is, flows having various cycle times and on-off ratios. Any resulting correlations should then be usable for predicting the performance of a full-scale apparatus operating with pulsating sprays and falling films. Last, a study of fluted or programmed surfaces employing surface tension to improve evaporation is to be undertaken. These surfaces are similiar to the condensing surfaces of Gregorig (Ref. 2), but with a channel grooved into the top of the ridges to feed the curved evaporating surfaces by weir action. A combined hydrodynamic and heat transfer study is required that is both experimental and theoretical.

Summary

Falling water films were established during evaporating conditions on a 1.7 ft x 3.0 ft vertical plate by feeding from sources located along the smaller, upper edge of the plate. Measurements of heat transfer rates were also made. Good agreement was obtained between experimental and theoretical values for the steady flow heat transfer coefficients.

A second series of test runs using the same surface also was made to check the effect of cyclic flow on heat transfer. These tests were made with a three per cent sucrose solution to avoid dry-spotting which is a serious problem in evaporating pure water films. From the data obtained, it is concluded that pulsed flow does not lead to improved heat transfer on the average in time. However, pulsed flow does not reduce appreciably the heat transfer coefficient; therefore, a pulsed feed system is practical.

The occurrence of dry-spotting on the evaporator surface was observed and rough quantitative estimates of the phenomenon have been found to agree with existing information for condensing systems. The work of Norman and Binns (Ref. 3) is especially to be noted. Adaptation of this work to evaporating films is discussed together with a method of predicting film stability in sea water apparatus.

Equations pertaining to the evaporating film previously developed for a flat plate (Ref. 4) were expanded to include simplified expressions for the heat transfer coefficient in terms of the important design parameters of a programmed surface. The flow in the feed grooves was studied analytically, whereas the flow in the runoff grooves was studied by means of an electrical analog. Results from this analysis, together with a thermal flux plot made in the vicinity of the surface inside the metal, were used to construct an average-performing surface cross section for use in analyzing the experimental data and comparing the data with theory.

An extensive study of the topography of these surfaces was made which verified their being made according to design specifications. Two surfaces, one approximately one-half the scale of the other, were constructed and tested in both bench-type experiments and vaporization tests in the apparatus. The bench tests led to the development of a method of inducing flow simultaneously and uniformly in all the feed grooves of a surface fed by a line of jet streams. They showed that machining burrs along the feed grooves could cause inadequate feeding, and, if removed would permit complete and sustained wetting of the surface. In addition, they revealed in the case of one surface, a bead-like flow pattern covering the surface, which must be associated with a rippling flow phenomenon peculiar to a programmed surface.

The two programmed surfaces were tested under evaporative conditions, but they were not found to achieve their theoretical heat transfer levels. The coarsely grooved surface of the two, gave experimental heat transfer coefficients that were about 50 per cent of those theoretically predicted for the same surface, whereas the finely grooved surface gave coefficients that were 20 per cent of theoretical coefficients. Despite these findings, the heat transfer coefficients obtained were approximately two and three times flat surface coefficients. calculated from the projected areas of the programmed surfaces. Film thickness measurements made under non-evaporating conditions for the coarse surface, agreed roughly with the theoretical thickness of a programmed surface.

Technical Approach

In order to avoid the difficulty of operating a large vaporization apparatus at the reduced pressure corresponding to room temperature, the apparatus was constructed such that the saturated condition for operation would occur at atmospheric pressure, that is, at about 212°F. To maintain this pressure, the apparatus was designed to be open to the atmosphere at several low temperature points. The section on Description of Experimental Apparatus will deal further with this point. Since the primary goal of this research was to measure a heat transfer coefficient (defined as the ratio of heat flux to the temperature difference between the evaporator surface and the ambient vapor), it was obvious that two essential quantities to be measured were heat rate and temperature difference. In addition, both the flow rate and condensate rate had to be measured because these are quantities upon which the heat transfer coefficient itself depends. The equations developed in Appendix A-IV-III for heat transfer through an evaporating film, falling on a vertical surface, show that the heat transfer coefficient depends upon a "runoff factor", defined as the ratio of output flow to input flow under the film.

By far the most difficult quantity to measure during a test run was the temperature difference between the test surface and the ambient vapor. Many differentially connected thermocouples were used which responded directly to local temperature differences along the surface. Each differential thermocouple was arranged so that one of its junctions was located inside the metal near the test surface and the other was located in the vapor, a few tenths of an inch away from the surface. The metal-side junctions were placed inside holes or slots cut into the back of a test plate, thus leaving the test side unmarred. For flat surface testing, the metal-side junctions were inserted and glued firmly in small diameter holes drilled into

a 3/8 inch aluminum test plate. These junctions were about 0.1 inch from the test surface for the steady flow experiments and 0.015 inch for the pulsed flow experiments. A temperature difference correction for the displacement of a thermocouple junction from the surface was made. The test plates on which the programmed surfaces were machined were only 1/4 inch thick. Therefore, to avoid any error due to lead conduction for a metal-side junction, a special technique of laying the junction and its wires in a deep slot cut into the back of the test plate was developed. The junction was made by overlapping and soldering the thermocouple wires. The junction lay at the center of the slot, with its wires extending from either side along the bottom of the slot. Consequently, the wires were equidistant from the test surface for a few inches before being brought out through the back of the test plate. The bottom of a slot was approximately 15 mils from the bottom of the runoff grooves of the test surface. Some of these thermocouple junctions were insulated with a 0.5 mil layer of mylar film, but others were not; however, no difference in performance was noted because of this provision. The slots, which were only 14 mils wide, were then filled with a mating sliver of aluminum, and the assembly then was glued in place. A great advantage was obtained by running the slots across the grooves rather than parallel to them. For in this way, a single junction (0.10 inch long) could average the temperatures of several grooves simultaneously. Copper - constantan thermocouple wires, 5 mils in diameter, insulated with one-mil thick teflon were used, and their only calibration consisted of a measurement of their Seebeck coefficient at 212°F.

The measurement of temperature difference was accomplished by measuring the small e.m.f. output of the differential thermocouple and by converting this e.m.f. to a temperature difference by dividing the measured e.m.f. by the Seebeck coefficient. Because the voltage output of the thermocouple was too small for recorder use, it had to be amplified before being fed to the recorder. A calibration circuit consisting of a precision potentiometer was used to feed a standardizing signal to the recorder. The response of the recorder was found to be linear.

Description of Experimental Apparatus

A schematic drawing of a falling film vaporization test loop is shown in Fig. IV-1. The test plate assembly is part of a demountable container of rectangular cross section that fits into a well of a larger container. The test plate divides

the container into two vapor-tight compartments: on the left side, as shown in the figure, is the vaporization chamber; on the right side is the heat compartment. Electric heaters are screwed or bonded to the back of the test plate. The heater compartment is filled with insulation and is open to the atmosphere at the top. This compartment not only keeps the heaters dry, but it also reduces heat loss from the backs of the heaters to a negligible amount with respect to the total output of the heaters.

The apparatus is designed so that a space of about one inch is left between the walls of the two containers. The well is made long enough so that a 10 inch deep sump is formed in the bottom of the larger container. An immersion heater, located in the bottom of the sump, keeps the sump water at its boiling point during the experimental testing. A water level control is used to maintain the sump approximately two-thirds full at all times. The vapor produced by the sump is essentially at atmospheric pressure, for the system is open to the atmosphere at the reservoir. Vapor fills the entire space above the sump and, because the liquid and vapor have a common pressure and temperature a saturated condition prevails. This space is essentially a guard chamber whose environment matches, and thus, prevents heat loss from the test chamber. When condensate appears at the outlets of the condenser, it is known that sufficient heat is being generated in the sump to allow for losses by condensation to the outer side walls. The whole exterior of the apparatus is insulated, and this keeps the heat loss down to about one kilowatt. Figures IV-2,-3 and 4 are photographs of the apparatus. The large, flat test plate is shown in Figure IV-2 as it appeared before testing. Figure IV-3 is an over-all view of the apparatus, and Figure IV-4 is a view of the inside of the sump. For the testing of programmed plates, the large plate was removed from its frame, and a dummy plate of equal area, having a smaller plate mounted upon it, was installed in the original's place. All test plates and the mounting plate were appropriately insulated with neoprene gaskets. The surface finish of the flat plate was approximately 20 micro-inch; for a programmed surface, it was approximately 30 micro-inch. Both kinds of surfaces were liquid honed, but the programmed surfaces required "polishing" with 2/0 emergy paper to remove burrs along their feed grooves. Many details about the construction of the various surfaces are given in Appendixes A-IV-1 and A-IV-2. Both the inner plate housing and outer enclosure were made from aluminum. All plates, tubing, and hardware were made from aluminum with the exception of the machine screws which were made from stainless steel. The various components outside the outer enclosure were made from copper, brass, stainless steel, and teflon. The outer enclosure was insulated from these parts by the use of Imperial-Eastman Impolene tubing to minimize galvanic action.

The flow system is shown rather generally in the schematic of Figure IV-1, and in some detail in Figure IV-5. The system was designed to produce both steady and pulsed flows. In steady flow operation, valve B was closed and water could be pumped directly from the sump into the line connecting to the spray tube. In pulsed operation, valve B was opened and a timer-actuated solenoidal valve would alternately admit flow to spray tube and sump-return line. The timer was also used to control the ratio of flow times into the two flow lines leading to these components. The spray tube consisted of a 0.5 inch O.D. x 0.032-inch wall aluminum tube with small clean-out plugs at each end. A "flat" approximately 0.1 inch wide, is machined along the length of the tube to make drilling easy. Along this "flat", small equally-spaced 8 mil holes were drilled. The hole spacing for the flat plate tests was 0.75 inch, and for the programmed surface tests it was 0.375 inch.

Various apparatus checks were made during the experimental program. Flow continuity was checked, and heat balances were made from electrical power and condensate measurements. One or more direct temperature-reading thermocouples were located in the vapor of the test chamber, on the spray tube, and on the walls of the test chamber, including the plexiglas window. All thermocouples agreed with the saturation temperature determined from the barometer. That the pressure inside the chamber could be taken equal to the outside pressure was determined in another test. This showed the difference in pressure to be less than 0.1 inch of water. Another test was made to determine the air content of the vapor in the chamber. This was done by connecting an electrochemical cell between the evaporator chamber and the condenser in order to effect a continual flow of sample past the cell. According to the cell response, the residual air in the system during normal operation was less than 0.1 percent by volume.

Such a cell consists of $ZrO_2 \cdot CaO_{20}$ and platinum electrodes. It is described in Ref. 5. The operation of the gauge is as follows: With air at a pressure of 1 atmosphere as a reference of oxygen at one electrode, the voltage output of the cell is proportional to the logarithm of the oxygen pressure at the second electrode. Since the oxygen dissociation pressure of water is extremely small at the operating temperature (850°C) of the gauge, the gauge can be used to measure oxygen concentration in water vapor. The response of the gauge for various relative concentrations of oxygen in one atmosphere of water vapor is shown in Fig. IV-6.

Heat was applied electrically to the backs of the test plates. In all tests except one, strip heaters in various electrical combinations, were screwed to the backs of the test plates. A layer of silicone grease was used to fill any air gaps between the heaters and the plates. In the case of the finely grooved programmed surface, a special heater was constructed in anticipation of very high heat fluxes that could result with its use. This heater consisted of a 0.375 inch thick copper plate having longitudinal

milled slots into which an insulated heating wire, 43 feet long, was inserted and cemented in place. The smooth surface of this plate was then bonded with thermally conducting cement and screwed to the back of the test plate.

Results A. Heat Transfer to a Steady-Falling Film

A comparison of electrically-determined and condensate-determined heat rates is made in Table IV-1 in the two Q-labeled columns. The discrepancy in results is due probably to heat lost at the ends of the twelve horizontal strip heaters on the back of the test plate. Some superheating of the vapor could result in this region. But, since this region borders the test plate and is far from any thermocouple junction, this superheating should not affect the thermocouple responses. The table also illustrates that a satisfactory flow balance was obtained.

Each listed temperature difference, ΔT, of the table is obtained from averaging eight differential measurements. A correction for the temperature drop in the aluminum plate must be subtracted from the average difference to obtain the true average surface-to-vapor temperature difference. Since this correction is relatively small, a single value may be found which is applicable to determining h_{exp} for either electrical or condensate heat rate determinations. With $Q_{av} = (Q_{cond} + Q_{elect})/2$, an expression for the true temperature difference is

$$\Delta T_{corr.} = \Delta T_{meas.} - \frac{Q_{av} d}{k A} \qquad (1)$$

The coefficient, h_{exp}, may be determined for either electrical or condensate heat rates by putting the corresponding Q-values into the equation

$$h_{exp.} = \frac{Q}{f A \Delta T_{corr.}} \qquad (2)$$

The average of these values, one-half the quantity, h_{exp} (elect.) plus h_{exp}(cond.), yields a value $h_{exp\text{-}av}$ which can be compared with h_{theory}, calculated according to Equation (13) of Appendix A-IV-3. A comparison between measured and experimental coefficients is made in the next to last column of Table IV-1. Except for one value, the agreement obtained between theory and experiment is well within 5 percent. Since f is a factor that accounts for unwetted area, it is not surprising that when this factor departs markedly from unity, a large discrepancy should result as happens in Run No. 4.

The last column of Table IV-1 shows the magnitudes of the film thickness encountered in these tests.

This table also includes one nonsteady state flow test, Run No. 5, for which the flow was periodically interrupted while the heat rate to the film was held constant. No improvement was noted over the performance predicted using a time-averaged feed flow rate in the steady state formulations and basing the theoretical value on the measured average runoff.

This series of experiments served to demonstrate an inherent instability of thin evaporating, pure water films, for there was a distinct tendency toward a partially dry surface in all the tests. But this tendency was found to increase in intensity as either the flow was reduced or the heat rate was increased. When the condition of nonwetting occurred, it would manifest itself in the form of dry streaks of various widths and lengths extending vertically from the bottom of the surface.

Norman and Binns (Ref. 3) have investigated the effect of surface tension changes on the minimum wetting flow rates required to keep a surface of a distillation column completely wet. Since they were working with mass-transfer columns (distillation units) they define a surface tension difference, $\Delta\sigma$, between that (σ) of the liquid in equilibrium with the vapor at the liquid-vapor interface and that (σ) of the bulk liquid. They show a dimensional correlation of the variable $\sigma\Delta\sigma$ vs. the film thickness cubes, and give the equation

$$\delta^3\,(cm^3)^{-1} = 1.2 \times 10^{-6} - 1.76 \times 10^{-8}\,\sigma\Delta\sigma\ \ (dynes^2/cm^2) \qquad (3)$$

$$(\text{for} \quad 0 > \sigma\Delta\sigma > -500\ dynes^2/cm^2\ )$$

The data used to formulate Equation (3), that of Fig. 17 of the Norman-Binns article, does not accurately describe the situation in the vicinity of $\Delta\sigma$ and δ equalling zero. It is logical that any description, i.e., equation, should include the point $\Delta\sigma = 0 = \delta$. A fit of the data for $0 \leq \delta \leq 2.0 \times 10^{-5} cm^3$ to include the origin with a linear relationship is

$$\sigma\Delta\sigma\ (dynes^2/cm^2)^{-1} = -20.0 \times 10^{-6}\,\delta^3\,(cm^3)^{-1} \qquad (3a)$$

For water in the vicinity of 212°F and 1 atm., we find that the change in surface tension with temperature is

$$\frac{d\sigma}{dT} = -0.1 \left(dyne/cm\text{-}F^\circ\right) \tag{4}$$

If we reason that $\Delta\sigma$ can be evaluated in terms of the difference in values existing between the wall and the free surface (a discussion of the correct sign for $\Delta\sigma$ is given by Stewart in Ref. 6), then

$$\Delta\sigma = \frac{d\sigma}{dT} \Delta T \tag{5}$$

A comparison of our experimental values of $\sigma\Delta\sigma$ with those of Norman and Binns can be made based on observing that (for a given δ) any experimental value of $\sigma\Delta\sigma$ greater than the value given by the Norman-Binns equation (Equation 3a) should yield a completely wetted plate, while any experimental value of $\sigma\Delta\sigma$ (for a given δ) less than that predicted by the Norman-Binns equation will be associated with a partly dry plate. The results follow:

Table IV-2

Run	δ (in.)	δ^{3*} (cm^3)	ΔT^{**} (F°)	Experimental $\sigma\Delta\sigma$ ($dynes^2/cm^2$)	Norman-Binns $\sigma\Delta\sigma$ ($dynes^2/cm^2$)	% Plate Wet
No. 1	0.0030	442×10^{-9}	0.76	- 4.6	- 8.8	100
No. 2	0.0029	400×10^{-9}	0.94	- 5.6	- 8.0	100
No. 3	0.0027	320×10^{-9}	1.03	- 6.2	- 6.4	95
No. 4	0.0023	200×10^{-9}	1.21	- 7.3	- 4.0	80
No. 5***	0.0026	290×10^{-9}	0.68	- 4.1	- 5.8	80

* Converted from $inches^3$ to cm^3, the values taken from Table I

** Also taken from Table I

***Cyclic water spray feed.

The Norman-Binns relationship, as modified in Equation (3), agrees well with the experimental results for evaporation from the wetted plate with the exception of Run No. 5. However, the results of Run No. 5 apply to a periodically spray-fed film and may deviate from any steady state correlation.

If we ignore the moderating effect of flow on $\Delta\sigma$, we can more simply illustrate the effect of surface tension gradient on stability. In doing this we include the effect of both concentration and temperature. The equation for stability becomes simply

$$\frac{\partial \sigma}{\partial C} |\Delta C| + \frac{\partial \sigma}{\partial T} |\Delta T| > 0 \qquad (6)$$

Now for water, as for other liquids, $\partial\sigma/\partial T$ is always negative; so it follows that a temperature change has a destabilizing effect on the film. This effect can be overcome, however, by a favorable (positive) surface tension gradient with concentration, $\partial\sigma/\partial C$, and a sufficiently large change in concentration. Some numerical values of $\partial\sigma/\partial C$ are illustrated as follows:

Table IV-3

Solution	Temp. (°F)	$\frac{d\sigma}{dC}\left(\frac{\text{dy}}{\text{cm}}\ \frac{\text{gm-water}}{\text{gm-solute}}\right)$
Sea water	77	+ 22
NaCl-water	68	+ 28
Sucrose-water	77	+ 3.5

We, therefore, can predict, using $\partial\sigma/\partial T = -0.07$ dy/cm-°F for a 77°F sea water film, that such a film will be stable if $22\Delta C > 0.075\Delta T$, i.e., $|\Delta T/\Delta C| > 3 \times 10^2$. If, in Equation (6), ΔT is regarded as the temperature difference between evaporator surface and saturated vapor and ΔC, as the maximum increase in concentration possible from the pure liquid state, we may calculate a concentration of sucrose solution such that it can have a stable evaporating film. Using $d\sigma/dT = -0.1$ dy/cm-°F, corresponding to the temperature used in the experimental work, and $\Delta T = 1$°F, we see that ΔC must equal 0.03 gm-sucrose per gm-water at 212°F. Only this one concentration was tried experimentally, and the films produced from its use were remarkably stable as compared with fresh water films.

Results B. Heat Transfer to a Pulse-Fed Falling Film

The use of a 3 percent sucrose solution removed a major obstacle in the way of producing periodically-fed films without the occurrence of dry-spotting. When operated with the sucrose solution, the reservoir (see Fig. 1) was not used for storage and all condensed liquid was returned immediately to the sump through the reservoir jar by keeping the input solenoid open at all times. Both the collected condensate and runoff liquid were returned to the sump after measurement. These procedures were necessary to maintain the concentration level of the sucrose solution. The flow cycle was monitored by making the ball-float of the flow meter come to a stand-still position temporarily during the flow portion of the pulsing cycle. By adjustment of valve "B", shown in Figs. 1 and 2, considerable control over the initial rise rate of the ball-float was possible. To prevent dripping from the spray tube between pulses, it was necessary to tilt the spray tube slightly and to connect a capillary tube to it at its higher end, to bleed off any dissolved air of the liquid that would accumulate there.

The results of the pulsed flow experiments are presented in Table IV-3. Two different spray periods, 10 and 20 seconds were used, and in each period, the pulse time has been varied from 25 percent of the cycle time to full cycle time. In the latter case, the condition of steady flow obtains. Thus, a pulse-to-cycle time ratio was defined

$$\theta = \text{flow time} / \text{cycle time} \qquad (7)$$

which had its experimental values between 0.25 and 1.0. The runoff, R, was varied from 0.54 to 0.83; average temperature differences ranged from 0.51°F to 1.4°F; power input ranged from 1015 watts to 2450 watts; and average total flow ranged from 8.8 lb/hr to 38.3 lb/hr. The next to last column of the Table IV-4 shows values for the ratio, h_{exp}/h_{theory}. The values of h_{theory} were calculated using pure water properties in Equation (13) of Appendix A-IV-3, while the values of h_{exp} were calculated according to Equation (2) with $f = 1$. It must now be mentioned tha, even though the ability of the films for wetting was increased substantially by the sucrose addition to the water, the improvement was not perfect in all cases. For the high power, low runoff cases, a drying tendency appeared. Streaky regions were again seen, but could not be judged as completely dry; and so they seemed to have less thickness than the surrounding fluid. Since the boundaries of these streaky regions were not very discernable, no attempt to determine f-factors was made. The experimental heat transfer coefficient,

h_{exp}, is plotted versus pulse-to-cycle time ratio, θ, in Fig. IV-7. The numbers placed to the right of the plotted points are measured runoff values. If we ignore the lowest runoff points because of the stability reasons given, then it appears that there is only a slight reduction of the heat transfer coefficient due to pulsing. This result agrees with the single result found in Run No. 5 of Table IV-1 obtained for a pure water film. It is also suggested by the analysis of a sinusoidal film given in Appendix A-IV-4 and illustrated in the Table A-IV-4 contained there.

Results C. Heat Transfer to Programmed Surfaces

Most of the essential geometrical details of the two programmed surfaces of this study are contained in Appendixes A-IV-2, part A and B. The hydrodynamic principles of operation are covered in Appendix A-IV-5, and the combined thermal and hydrodynamic principles are covered in Appendix A-IV-6. The bases of construction of a programmed evaporator surface are (1) the alternately spaced, feed and runoff grooves that run vertically along the surface, (2) the uniform taper of the bottom of a feed groove which is used to discharge increments of fluid to either of its sides by weir action, and (3) the specific contour shape (see Ref. 7) employing uniform rate of change of curvature of the surface to produce a constant pressure gradient in the film. Since, for either surface of this study, the pressure gradient, dp/ds, is proportional to a product of factors, $(1/r^2)$ (dr/ds), and a scale factor can only have influence through the first of these factors in determining the ratio $(dp/ds)_{fine}/(dp/ds)_{coarse}$, it is apparent that the pressure gradient of the fine surface (one-half the scale of a coarse surface)is four times that of the coarse surface.

A study of the geometry of the more finely grooved surface was made which essentially involved rechecking the calculated profile. The checked result was then used as a standard for checking the milling cutter and the actual surface profile produced by the cutter. The calculated profile was accurately drawn 100 times actual size on a transparent plastic sheet, and then the combination was used in an optical comparator so that the enlarged profile could be directly compared with images produced either by the cutter or by molded profiles made from the surface. A group of such profiles contained on silastic impressions is shown in Fig. IV-8. There they are arranged with respect to the position along the surface at which they were made. All comparisons agreed extremely well over the major contours, which meant the surface was made essentially as intended. However, along the edges of the feed grooves tiny burrs, about 0.8 mils high, were detected from the silastic impressions. These may be seen in the figure at positions 0.15 in., 8.90 in., and 13.35 in. The remaining cases were obtained after attempting to remove the burrs by hand polishing for the purpose of studying the effectiveness of the polishing technique. On account of this deburring, a surface was produced which remained completely

wet in bench tests and in the apparatus tests; whereas before doing this, only a partially wet surface was obtained in bench testing. Silastic impressions of the coarse surface were not made, but the cutter of this surface was checked against a calculated surface profile and was found to be correct. Machining burrs along the edges of the feed grooves of this surface were discerned with a magnifying glass, and the burrs also were removed by hand polishing. The group of profiles shown in Fig IV-8 uniquely illustrates the construction of a programmed surface, for it shows both the alternating groove pattern of the surface and the taper possessed by the rectangular feed grooves.

Several other geometrical features of a programmed surface pertained to a method of establishing the flow simultaneously in all feed grooves by proper initiation of flow. The same method of initiation was used for both surfaces, and it will be illustrated as part of a discussion centering on the cold flow bench testing of the coarse surface. Figs. IV-9, IV-10 & IV-11 are composed of photographs taken of three contiguous areas of the surface while the surface operated at three different flow rates. The upper frame in each figure shows a spray bar with 3/32 inch spaced, 8 mil holes, spraying liquid onto a flat region of the plate. This region corresponds to the one designated by A in Part (a) of Fig. IV-12. There the various impinging liquid streams coalesce to form a continuous falling sheet of liquid. The minimum vertical length required for this region is roughly equal to the spacing of the streams. To prevent mist formation, the spray bar had to be held close to the surface. The grooved region above the line designated by 1-2 in Fig. IV-12, which corresponds to the region above the stretched wire shown in the upper frame of Figs. IV-9 to IV-11 was used to funnel liquid into the feed grooves. The method was a modification of an alternative method that uses only the funneling grooves with highly dispersed spray droplets instead of the finite liquid streams. Part (b) of Fig. IV-12 gives some additional information about the topography of a programmed surface. The stretched wire was used to divert excess flows laterally to produce a more uniform distribution of flow in the funneling grooves.

In bench testing it was discovered that the coarse surface could be kept uniformly wet over a range of flows that included the theoretical flow. The upper limit of this range was set by a turbulent flow originating at the inlet ends of the feed grooves, and use of the wire extended the maximum operating flow from 1.4 to 4.9 cm^3/sec for the cold flow condition. Figs. IV-9, IV-10, and IV-11 depict a phenomenon associated with the hydrodynamics of a programmed surface. This was the occurrence of a beaded flow pattern that resulted from ripples originating in the feed grooves. The ripples traveled in trains down a groove, but had a short life span; for at any location, a single ripple could be seen to emerge from the liquid surface, move down the groove a few centimeters, and then recede back into

the surface of the liquid. Figs. IV-9 to IV-11 typify the bead patterns obtained throughout the operating range of the surface. The pattern of Fig. IV-10 is for a flow of 2.2 cm^3/sec, which is approximately equal to the theoretical flow, 2.3 cm^3/sec, calculated for a 100°F surface according to Equation (2) of Appendix A-IV-5. The various photographs shown were obtained from a motion picture film made at 1/16th second exposure. According to judgement based on intensity of the patterns in the figures, ripple amplitude increased with flow rate. Further, the figures illustrate that the line of bead inception, an imaginary horizontal line averaging the tops of the patterns, moved upward as the flow increased. It is to be noted that, if the fine surface had a beaded flow pattern, it must have been too faint to be discernable by eye. When the surfaces were installed in the apparatus, the beaded pattern was seen on the coarse surface, but not on the fine surface.

Before presenting the experimental heat transfer results for the programmed surfaces, the procedure used in analyzing the data will be given. The procedure is based on the equations of Appendix A-IV-6 for obtaining the theoretical heat transfer coefficient, and on the equation for the experimental heat transfer coefficient

$$h_{exp.} = \frac{Q}{2n\ell L \Delta T} \qquad (8)$$

The pertinent equations from Appendix A-IV are as follows: Equation (3) - The volume flow rate, V, is a measured quantity that is corrected by Equation (2) of Appendix A-IV-5 for a small efflux of fluid at the end of the feed grooves in only the case of the coarse surface, and dp/ds and L are constants of the surface; δ_o is consequently calculated. Equation (7) - Since the condensate flow rate was measured, as well as the total flow rate (nV), the runoff, R, can be determined from flow continuity; thus δ_{av} can be found knowing δ_o and R. Equation (9) - The theoretical heat transfer coefficient is found by dividing k by δ_{av}.

This method of calculating the theoretical heat transfer coefficient, h_{pr-th}, had several advantages over the use of Equations (10) and (11) of Appendix A-IV-6. Its stepwise character gave information about the film thickness before the calculation was finished, and therefore gave a check as the calculation proceded. Further, it served the more important function of eliminating temperature difference, a measured quantity in greatest doubt, from the theoretical calculation.

The determination of an experimental heat transfer coefficient was not a simple matter for, even though Q could easily be determined from the condensate rate and that ΔT was known from direct measurement, there remained ℓ the film length, to be determined. This length, ℓ, could change downward along the surface because the depth of the liquid flowing in the runoff grooves varied along them. Therefore, a method had to be devised to account for this effect. Another problem pertained to the correction of temperature difference. This problem was complicated by the curving heat flow path lying between a thermocouple junction and the evaporator surface. However, both of these problems were locked together, for in order to determine a shape factor for heat conduction the depth of liquid in the groove had first to be known.

The method used to attack these problems was based on determining a single position along the surface representing an average heat transfer position for the whole surface, that is, one having a film thickness equal to the average thickness for the whole surface. Then from the known flow in the runoff groove at this position, the surface location of the fluid in the groove (meniscus) could be specified. This, in turn, determined the heat flow lines in the metal behind the surface, for it was next assumed that practically no heat flowed through the relatively thick runoff liquid and feed groove liquid.

In Appendix A-IV-5, it is shown that the function $\Phi^{1/3}$ is proportional to the average local film thickness, so that with the use of the curve in Fig. IV-14 giving $\Phi^{1/3}$ vs. $\xi^{-1} = (4/\pi)(t/w)$, the average thickness for the whole plate can be determined. If distance, z, is measured from the inlet end of the grooves, it is found that the position of average film thickness occurs about 64 percent of the way down the test surface. The liquid flowing in a groove at this location, in principle, is equal to the integral of lateral flow increments, dV/dt x dt, for corresponding t-values at z = 0 to z = 0.64L. This integration was carried out graphically using Fig. IV-13.

The meniscus corresponding to this total flow, corrected for the fraction evaporated, was determined by a trial and error electrical analog method. The problem was to fit an arc of a circle, representing the liquid surface, symmetrically above a runoff groove, such that it tangentially intersected the curved metal surfaces on both sides of the runoff groove. Poisson's equation was solved with usual conditions applying at the solid boundary and free surface. Surface tension effects in the z-direction were determined to be small relative to the gravitational body force, so that only the gravitational force was considered. Basically, the analog was constructed from conducting paper which was cut to conform to the shape of the channel bottom and the liquid surface. Along the edge which represented the channel bottom, a narrow strip of conducting paint was applied. Over the surface of the paper stood a resistance

network; all resistors of the system were tied together at one end and made individual contact with the paper at the other end. The resistors were equally spaced and chosen to be 100 times the resistance of the paper. This provision allowed nearly equal amounts of current to be supplied to the paper at all the contact points. The paper was backed up with a sheet of sponge rubber to absorb any inequalities in the lengths of the resistor terminal wires. The bodies of the resistors were clamped between two plastic sheets, giving rigidity to the network. Voltage was applied between the painted strip and the common (tied) ends of the resistors. The total current per area corresponded to the term $\rho g/\mu$, and the voltage measured between the strip and points on the paper corresponded to the velocity of flow. Consequently, by measuring the voltage with respect to the painted strip at each resistor terminal (about 60 in all), and combining the measured values properly, an average voltage was obtained. Upon transforming this voltage together with a proper scale factor, the total volume flow rate was obtained. Values of flow were determined in this way with a new meniscus being tried for each case until the measured value agreed with the desired value.

The results of this study were used to construct the menisci shown in the surface-bearing cross sections of Figs. IV-16 and IV-17. For each surface a theoretical length ℓ was determined lying between the tangent point of the meniscus and the edge of a feed groove. The theoretical film length for the coarse surface was found to be 41.5 mils, while that of the fine surface was 16.6 mils. These values were used in Equation (8) for the calculation of experimental coefficients.

The cross section depicted in Fig IV-16 was determined at 86 percent runoff for the coarse surface. This runoff value was selected because, in the testing of this surface, a great number of duplicating runs were made near the theoretical flow value, and their runoffs averaged about 86 percent. The flow in this group of runs was set at 5.45 cm^3/sec (see Table IV-5A), corresponding to the maximum flow value of the surface judged on uniformity of surface appearance. This flow was only slightly higher than the theoretical value of 5.3 cm^3/sec. The cross section of average film thickness was found to occur at $z = 9.8$ in from the inlet end of the 15.3 inch long surface. In the case of the fine surface, a measured runoff of 80 percent occurred for a theoretical flow setting of 2.3 cm^3/sec (see Table IV-5B), and the cross section of average film thickness was found to occur at $z = 10.2$ in from the inlet end of the 16.25 inch-long surface. This cross section is depicted in Fig. IV-17.

In viewing the cross sections, it should be borne in mind that the aluminum plates on which the programmed surfaces were milled, were of 1/4 inch stock, or about 250 mils thick. The embedded thermocouple junctions are therefore relatively close to their special surfaces. It is also shown by the flux and temperature lines of the figures that, if a uniform flux originates at the back of a plate, the line containing a

thermocouple junction will be practically isothermal. This important fact together with an isothermal surface curve permits the calculation of a shape factor for each programmed surface. These factors are used for calculating the part of the measured temperature difference that occurs in the metal, which must be subtracted from the measured temperature to obtain the true surface to vapor temperature difference. This temperature correction is shown to be

$$\Delta T_{Al} = \frac{Q}{2\pi K L} \frac{N_y}{N_x} \qquad (9)$$

where N_y is the number of square elements in the curvalinear y-direction, and N_x is the number in the curvalinear x-direction for the region between isotherms coinciding with the thermocouple location and surface location. The ratio, Ny/N_x, equals 1.5 for the coarse surface and 2.1 for the fine surface. The temperature corrections, ΔT_{Al}, are shown in Table IV-5, parts A and B, and were determined using these ratios.

The experimental data obtained for the two programmed surfaces are contained in Table IV-5, parts A and B. It will be noted that twenty of the coarse surface runs tabulated in part A were carried out for the maximum (approximately theoretical) flow condition of the surface, and for approximately the same heat rate (same electrical input power). These runs were a bi-product of various performance studies of the apparatus, including a study of the effect on heat transfer by the addition of known amounts of air to the vaporization chamber. But, while such tests were being made—most of them at this one set of conditions—scale deposits were building up on the curved surfaces of the evaporator. These deposits were estimated to be 0.5 mil thick or more. Therefore, this set of twenty runs, together with six others obtained for the same flow rate, gives a history of the performance during scale build up. In Fig. IV-18, values of h_{exp}/h_{pr-th} are plotted vs. the chronological order in which the tests were made. Therefore, some unspecified time is represented by a given run number. It is apparent from the distribution of the plotted points that the scale buildup has no appreciable effect on the heat transfer. This result, however, was explained by the fact that a spectro-chemical analysis of the scale deposit revealed its composition to be 20 percent copper (from the condenser) and 30 percent aluminum, one percent iron, one percent zinc, and the rest oxides and carbonates. Thus, the scale deposit, because of its very high conductivity, can have a relatively inconsequential temperature drop, even though it is of the same general magnitude as the water film thickness. These results also indicated that the scale deposit had no major effect on the surface tension driving characteristics of the surface.

Of the twenty runs, Runs No. 10 to No. 18 were made with various amounts of air admitted to the vaporization chamber. The oxygen gauge was used in these tests. As indicated by the gauge, the vaporization apparatus had a pumping capability sufficient to reduce the air content in the test chamber to about 0.1 percent under normal conditions of operation. Runs No. 10 to No. 18 are included in Fig. IV-18. The various air concentrations associated with each run are designated by the numbers attached to the plotted points. Again, no trend is indicated by the data, and so the conclusion must be drawn that presence of air in the evaporator has no significant effect on the heat transfer rate in the range of air concentrations covered.

Table IV-5A lists values for the measured heat transfer coefficient, h_{exp}, determined under a variety of flow and heat rate conditions for the coarse programmed surface. These values are three to four times as great as those of the flat surface listed in Table I. The values for h_{exp} listed in Table IV-5B for the fine programmed surface are merely comparable to those of the coarse surface, yet the fine surface was designed to produce coefficients roughly 2.7 times as great as those of the coarse surface. This can be readily demonstrated by comparing values of $\delta_{av\text{-}th}$, the theoretical average film thickness, obtained from the two parts of the table for the theoretical flows, 5.45 cm^3/sec (coarse) and 2.26 cm^3/sec (fine). The next to last column of the Table IV-5 gives the ratio, $h_{exp}/h_{pr\text{-}th}$. This ratio is plotted vs. runoff, R, and flow rate in Figs. IV-19 to IV-22. The experimental data were obtained for the coarse surface at and below the theoretical flow rate, while for the fine surface were obtained at and above the theoretical flow rate. This was done for reasons of experimental expediency rather than by plan. The data for the coarse surface at theoretical flow show that the value of the experimental heat transfer coefficient is about 50 percent of the theoretical value. Such data for the fine surface show that the value of the experimental coefficient is about 19 percent of the theoretical value. The points plotted in Figs. IV-19, IV-21 and IV-22 represent all values of $h_{exp}/h_{pr\text{-}th}$ listed in the tables, but the points in Fig. IV-20 represent average values of $h_{exp}/h_{pr\text{-}th}$ for the coarse surface corresponding to the various flow rates shown in the legend of the figure.

The increasing trend of the $h_{exp}/h_{pr\text{-}th}$ values shown in these figures with increasing flow rate and runoff is not necessarily due in any part to an increase in h_{exp}. Since the same film length (either ℓ_c = 41.5 mils or ℓ_f = 16.6 mils) must be used for all flow rates in the calculation of h_{exp} for a given surface, no compensation for a change in theoretical length can occur in the h-ratio. This may be seen better with the aid of Equation (8) and Equation (10) of Appendix A-IV-6. Together they can be used to express the ratio, $h_{exp}/h_{pr\text{-}th}$, as $(Q/\Delta T)V^{1/3}\left[(1-R^{4/3})/(1-R)\right]$. For some of the data $(Q/\Delta T)$ is constant (see Table IV-5A, flow = 21.9 lb/hr); for other data Q is constant, and ΔT is almost constant (see Table IV-5B). The R-factor does not vary appreciably for the range observed, but, if Q is constant, then R is a function of V by Equation (6) of Appendix A-IV-6. Now, if V increases, the factor in brackets may be shown to increase, so that the net result is for the ratio, $h_{exp}/h_{pr\text{-}th}$, to increase.

The results of these experiments can be compared with the performance of flat surfaces (fed along the top edges) of the same projected areas as the programmed surfaces. Equation (11) of Appendix A-IV-6 may be used to give the result

$$\frac{h(\text{prog.})}{h(\text{flat})} = \left(\frac{1}{\rho g} \frac{dp}{dS} \frac{L}{l} \right)^{1/4} \qquad (10)$$

where the comparison is made for the same film temperature difference and runoff. Film thickness and heating rate per unit area, however, will be different for the two surfaces. The ratio has the value of 11 for the fine surface and 6 for the coarse surface. Therefore, by combining the experimental ratio, $h_{exp}/h_{pr\text{-}th}$, with this ratio, the following comparisons can be made:

$$\frac{h_{exp.}}{h(\text{flat})} = \frac{h_{exp.}}{h_{pr\text{-}th}} \times \frac{h(\text{prog.})}{h(\text{flat})}$$

$$\frac{h_{exp.}}{h(\text{flat})} = 0.2 \times 11 = 2.2 \text{ , fine surface}$$

$$\frac{h_{exp}}{h(\text{flat})} = 0.5 \times 6 = 3.0 \text{ , coarse surface}$$

These results show that three times as much heat can be transferred (vapor produced) with the coarse programmed surface, and almost two times as much can be transferred with the fine programmed surfaces as with a flat surface of the same overall dimensions.

Measurements of film thickness were made during cold flow operation of the coarse surface in a bench test, for which the theoretical flow was set corresponding to the measured operating temperature. The method of measurement utilized a machinist's micrometer head having a special needle-shaped shaft ending for probing the film. Contact with the film could be approximated by observing the approach of the needle point toward its

reflection in the liquid surface with a low power microscope. The actual contact was verified, however, by observing a needle deflection of an ohmmeter connected in series with a dry cell between the test plate and probe. Thus, the numerical difference between micrometer readings taken at the liquid surface and at the metallic surface with no liquid present yielded the film thickness. No additive was needed to make the test water conducting, for the normal impurity level in the flow system was sufficient to render the distilled water conducting. On such longitudinal elements of the surface where rippling was occurring, measurements of thickness could not be made because of film movement. Therefore, measurements were made on the elements above points where rippling was originating and further down the surface on a few of the elements for which no rippling was occurring. The measurements obtained averaged about 0.40 mils, a somewhat lower thickness than the theoretical value of 0.52 mils. This theoretical value of film thickness was slightly lower than the theoretical value corresponding to 212°F operation because of the surface tension dependency on temperature.

Another study was made to determine how great an effect curvature of the surface elements had on increasing the film surface temperature above the normal equilibrium saturated value for a flat surface. The result of this study showed the temperature rise, ΔT_i, to be given by

$$\Delta T_i = \frac{\sigma T}{\rho \lambda r} \tag{11}$$

where T is the absolute temperature of the fluid, r is the non-infinite principal radius of curvature of the surface, and the remaining symbols are as given in the Nomenclature, Appendix A-IV. Upon substitution of appropriate values in this expression together with the smallest conceivable radius of curvature of the fine surface, there results a value of δT less than 0.0001°F. This value, compared with a measured value of about 1°F is seen to be insignificant, so that any effect of curvature on measured temperature difference must be negligible. Equation (11) was obtained by combining the Claussius-Clapeyron equation with the thermodynamically calculated pressure rise as given by Equation (18) of Ref. 12, adjusted for a non-spherical surface.

The last column of Table IV-5 gives values of film length calculated from the data by equating the experimental heat transfer coefficient given by Equation (8) with the theoretical coefficient given by Equation (11) of Appendix A-IV-6. It is apparent that these results are lower than those obtained from the meniscus calculation. Graphs of ℓ_c and ℓ_f for the two surfaces are shown in Figs. IV-23 and IV-24. The results in Fig. IV-23 for

the coarse surface are average values for the various flows listed. At the theoretical flow, the value of ℓ_c is roughly 50 percent of the value determined by the meniscus method. For the fine surface, ℓ_c is roughly 20 percent of the value given by the meniscus method. These percentages roughly agree with the percentages by which each surface falls below its theoretical heat transfer achievement, which of course, they should, since the heat transfer coefficient is inversely proportional to a length, ℓ.

It is obvious from Figs. IV-18, IV-19, and IV-21 that the scatter of the coarse surface data is worse than that of the fine surface. This point is illustrated further in Figs. IV-25 and IV-26 which show the measured temperature variations along the surfaces. For the coarse surface, this error can be seen to be as much as $\pm$ 1°F, while for the fine surface, it is only $\pm$ 0.2°F. This improvement in temperature measurement between the two cases is attributed to the improved method of heating of the fine surface, which was explained in the apparatus discussions.

The slopes of the temperature vs. distance curves shown in Figs. IV-25 and IV-26 can be compared with theoretically determined slopes obtained from the use of Fig. IV-14. By making use of the definition of Φ as given in Fig. IV-13, it may be shown that

$$\frac{d\delta}{dz} = \left(\frac{6}{\pi}\right)^{1/3} \left(\frac{dt}{dz}\right)^{4/3} \frac{d\phi^{1/3}}{d\xi^{-1}} \tag{12}$$

Here dt/dz represents the taper (constant) of a feed groove and $d\Phi^{1/3}/d\xi^{-1}$ represents the slope of the curve shown in Fig. IV-14. Further, $d\delta/dz$ is a factor in the differentiated equation of heat conduction in the film

$$\frac{dT}{dz} = \frac{1}{k} \frac{Q}{2\pi\ell L} \frac{d\delta}{dz} \tag{13}$$

And this equation with the aid of Equation (12) may be written

$$\frac{dT}{dz} = \frac{Q}{2\pi k\ell L} \left(\frac{6}{\pi}\right)^{1/3} \left(\frac{dt}{dz}\right)^{4/3} \frac{d\phi^{1/3}}{d\xi^{-1}} \tag{14}$$

This result will be used to calculate theoretical values of dT/dz, which in turn will be compared with experimental values determined from Figs. IV-25 and IV-26. An average value of slope, $d\Phi^{1/3}/d\xi^{-1} = 0.19$, for the coarse surface is given by the secant line occurring along the curve between points B-B of Fig. IV-14, representing the end points of the surface. For the fine surface, it is apparent that the secant does not adequately represent the condition over the surface between points A-A, since the slope is fairly constant over about 80 percent of the surface. Therefore, the slope, $d\Phi^{1/3}/d\xi^{-1} = .067$, is taken as an approximate, representative value. The comparison of results follows:

Table IV-6

Values of dT/dz (F°/in)

Surface	Exp't.	Theory (Equation 14)	
		(meniscus ℓ)	(calculated ℓ)
coarse	0.072	0.052	0.11
fine	0.029	0.022	0.10

That the results agree as well as they do, is a commendation for the hydrodynamic theory as expressed in Figs. IV-13 and IV-14. It is to be noted from the table that the experimental value for either surface is bracketed by theoretical values calculated from the two different ℓ-values of this report, and that the experimental value is closer to, but higher than, the theoretical value calculated from the ℓ-value of the meniscus study. This fact suggests that somewhat higher h_{exp}-values might actually be occurring than have been determined (and reported herein) on the basis of the meniscus study.

Conclusions and Recommendations

The agreement attained between theory and experiment in the steady flow falling-film tests supports use of the underlying assumptions of the theory, and Equation (13) of Appendix A-IV-3 can be used to calculate heat transfer coefficients for steady flow evaporating films to within a few percent.

On the basis of data obtained for pulsed falling films, it may be concluded that pulsed flows do not lead to improved heat transfer, on the average, in time. On the other hand, since pulsed flows do not decrease the heat transfer coefficient, a pulsed feeding system is practical. Further,

the occurrence of dry-spotting that has been reported for the steady flow experiments, due at least in part to adverse surface tension gradients, is qualitatively at least, no more of a problem with pulsed flows than with steady flows in view of the similarity established between sucrose and sea water salts in their effects on stability.

The occurrence of dry-spotting on the evaporating surface has been observed. A rough quantitative criterion of the phenomenon, which takes into account both the effects of temperature and concentration changes in the film (and which is based on existing information for condensing systems) has been formed and found to agree with experiment.

A technique was developed employing silastic castings and an optical comparator for studying the surface profiles of a programmed surface. This technique was an invaluable aid in determining the feed groove depth variation of the fine surface.

Cold flow bench tests using the coarse programmed surface revealed a beaded flow pattern that resulted from trains of ripples moving slowly down the feed grooves. At a distance, the ripples looked to an observer like tiny beads spread uniformly over the surface. Such bead patterns were visible for the coarse surface during the vaporization tests, as well as during the bench tests, but were not visible for the fine surface in either type of tests. In bench tests, as well as in the vaporization tests, no apparent difficulty was noted with dry-spotting of the programmed surfaces using pure test water. Measurements of film thickness were also made in bench tests for the coarse surface which resulted in values slightly lower than calculated theoretically.

A number of vaporization heat transfer tests were made to determine whether air admitted to the test chamber would influence the results. The concentration of air in the evaporator was varied from 0.1 percent—the value during normal operation of the evaporator—to about 16 percent. No effect on the measured heat transfer coefficient could be determined.

Scale deposits accumulated on the curved surface elements of the coarse surface during the testing period. Thickness measurements showed the final deposit to be about 0.5 mil thick in the upper regions of the surface, and to be much larger in the lower regions. Since the deposit was found to be of high metallic content (52 percent), it did not influence the heat transfer coefficients measured. This was demonstrated by a chronological ordering of twenty-six coefficients measured at the same flow rate for which no time dependence was in evidence. The over-all result also served to indicate that the deposit buildup had no significant effect on the film driving characteristics of the surface.

The decrease in temperature difference measured along the two programmed surfaces has been shown to agree with the hydrodynamic theory developed for feed groove operation. Also, the observed scale thickening at the lower part of the coarse surface is qualitatively consistent with a thinner evaporating film as predicted by the hydrodynamic theory for this region. Both of these findings support the use of this theory for design work.

The coarse programmed surface gave experimental evaporation heat transfer coefficients that were about 50 percent as large as those determined from simple programmed surface theory, while the fine programmed surface gave experimental coefficients only 20 percent as large as the theory gave. Yet, a comparison of these experimental coefficients with those obtainable for a flat plate of the same overall dimensions, showed that a three-fold improvement for the coarse plate, and a two-fold improvement for the fine plate had been achieved. These comparisons were made for the same temperature differences and runoffs.

It is instructive to review the various grounds that have been examined in attempting to uncover the reason for the discrepancy existing between the theoretical and measured performance of the programmed surfaces tested. First, the runoff meniscus determinations were made to explain the apparently short effective film lenght, ℓ, needed for agreement between the h-values. Second, film thickness measurements were made on a cold surface at theoretical flow with rippling present. Third, observations were made during vaporization testing to detect dry-spotting on the surface. Fourth, measurements were made as a function of time to determine a history of performance. Fifth, a theoretical check was made to determine whether curvature of the surface could cause an elevation of the film's equilibrium saturation temperature. Sixth, the effect of air concentration was studied by admitting different amounts of air to the system and taking measurements of the heat transfer coefficients.

Any of these studies might have led to a plausible explanation for the discrepancy, but each led to a negative conclusion in its own fashion: the lengths determined from the runoff menisci were larger than required by the theory; the film thickness measurements were nearly correct, even with rippling flow present and were on the low side of the theoretical value—thus further negating this effect; the surfaces always appeared completely and uniformly wet during testing; the measurements of h_{exp} showed no change over a long period of testing; curvature was shown to be far too large to have any effect; and air-vapor concentration had no effect on the measured heat transfer coefficients. All of these studies are discussed in detail in the body of this report.

None of these studies has enabled the explanation of $h_{exp}/h_{pr\text{-}th} < 1$ and an explanation has not yet been found. The explanation may yet be found in such intractable behaviors as low conductivity scale buildup before a time history is taken or undetectable dry-spotting.

Table IV-1 - Flat Surface Results for Pure Water

Run No.	Elect. Power (meas.) watts	Condensate (meas.) lb/hr	Runoff (meas.) lb/hr	Total Flow (calc.) lb/hr	Total Flow (meas.) lb/hr	ΔT (meas.) °F	Q (elect.) Btu/hr	Q (cond.) Btu/hr	Q_{av} (elect. + cond.) Btu/hr	$Q_{av} \cdot (\frac{d}{KA})$ °F	ΔT (corr.) °F	f area corr. factor
1	1600	5.22	32.3	37.5	37.8	0.84	5440	5070	5255	0.087	0.76	1
2	1990	6.64	----	----	37.8	1.04	6790	6440	6615	0.099	0.94	1
3	2246	7.20	16.1	23.3	24.1	1.14	7670	6980	7325	0.11	1.03	0.939
4	2570	8.51	22.8	31.3	31.0	1.34	8775	8250	8513	0.13	1.21	0.803
5 *	1294	4.41	16.9	21.3	pulsed	0.74	4420	4275	4348	0.065	0.675	0.828

* Flow was regularly pulsed: 8.7 sec flow time/19.4 sec period.

Table IV-1 - (Cont'd)

Run No.	h_{exp} (elect.) Btu/hr-ft^2-F°	h_{exp} (cond.) Btu/hr-ft^2-F°	$h_{exp\text{-}av}$ (av. of elect. + cond.) Btu/hr-ft^2-F°	R	$\frac{1-R}{(1-R^{4/3})^{3/4}}$	$(.943)\left(\frac{\lambda \rho^2 k^3 g}{\mu L}\right)^{1/4}$ Btu/hr-ft^2-°F$^{3/4}$	$\left(\frac{1}{\Delta T}\right)^{1/4}$ °F$^{-1/4}$	h_{theory} Btu/hr-ft^2-F°	$\frac{h_{exp\text{-}av}}{h_{theory}}$	$\delta = \frac{k}{h_{exp\text{-}av}}$ inch
1	1369	1276	1323	0.863	0.499	2408	1.071	1287	1.03	0.0030
2	1381	1310	1346	0.824	0.537	2408	1.016	1312	1.03	0.0029
3	1516	1380	1448	0.701	0.621	2408	0.985	1473	1.03	0.0027
4	1727	1623	1675	0.727	0.604	2408	0.954	1388	1.20	0.0023
5 *	1512	1461	1487	0.794	0.557	2408	1.103	1479	1.01	0.0026

* Flow was regularly pulsed: 8.7 sec flow time/19.4 sec period.

Table IV-4 - Pulsed Flow Results

(for a 3 per cent sucrose solution)

Period (Sec.)	Spray Time (Sec.)	Spray / Period	Elect. Power (meas.) watts	Condensate (meas.) lb/hr	Runoff (meas.) lb/hr	Total Flow (calc.) lb/hr	ΔT (meas.) °F	Q (elect.) Btu/hr	Q (cond.) Btu/hr	Q_{av} (elect. + cond.) Btu/hr
20	10	.50	1400	4.59	21.60	26.19	.559	4778	4452	4615
20	5	.25	1015	3.07	6.04	9.07	.514	3464	2978	3721
20	7.5	.375	1160	3.90	7.04	10.94	.571	3959	3783	3871
20	12.5	.625	1410	4.44	18.24	22.68	.514	4812	4307	4560
20	12.5	.625	1425	4.53	12.87	17.40	.600	4864	4394	4629
20	12.5	.625	1335	4.27	8.43	12.70	.657	4556	4142	4349
20	15	.750	1700	5.98	15.60	21.58	.943	5802	5801	5802
20	17.5	.875	1700	5.64	19.17	24.81	.686	5802	5471	5637
20	17.5	.875	1460	4.65	13.40	18.05	.714	4983	4511	4747
20	20	1.00	2000	6.56	31.18	37.74	.886	6826	6363	6595
20	20	1.00	2400	8.08	30.20	38.28	1.057	8191	7838	8015
20	20	1.00	1600	5.35	21.14	26.49	.571	5461	5190	5326
20	20	1.00	1980	6.63	20.47	27.10	.800	6758	6431	6595
10	2.5	.25	1600	5.31	5.89	11.20	.743	5461	5151	5306
10	2.5	.25	1920	6.47	5.18	11.65	1.229	6553	6276	6415
10	2.5	.25	1600	5.38	8.02	13.40	.800	5461	5219	5340
10	5	.500	1850	6.22	21.69	27.91	.629	6314	6033	6174
10	5	.500	2150	7.31	20.20	27.51	.857	7338	7091	7215
10	5	.500	2450	8.29	19.24	27.53	1.029	8362	8041	8202
10	5	.500	2450	7.88	17.24	25.12	1.314	8362	7644	8003
10	5	.500	2150	6.76	18.26	25.02	1.000	7338	6557	6948
10	2.5	.250	1850	6.07	6.92	12.99	1.400	6314	5888	6101
10	2.5	.250	1400	4.62	8.18	12.80	.714	4778	4481	4630
10	2.5	.250	1280	4.23	8.58	12.81	.514	4369	4103	4236
10	2.5	.250	1280	4.07	4.71	8.78	.571	4369	3948	4159

Table IV-4 - (Cont'd)

$\Delta T_{corr.}$ °F	h_{exp} (av. of elect. + cond.) Btu/hr-ft^2-F°	R	$\frac{1-R}{(1-R^{4/3})^{3/4}}$	$(.943)\left(\frac{\lambda\rho^2 k^3 g}{\mu L}\right)^{1/4}$ Btu/hr-ft^2-°F$^{3/4}$	$\left(\frac{1}{\Delta T}\right)^{1/4}$ °F$^{-1/4}$	h_{theory} Btu/hr-ft^2-F°	$\frac{h_{exp}}{h_{theory}}$	$w = \frac{k}{h_{exp}}$ inch
.559	1578	.825	.537	2408	1.156	1495	1.060	.0025
.514	1384	.666	.642	2408	1.180	1824	.760	.0028
.571	1296	.644	.654	2408	1.150	1811	.710	.0030
.514	1696	.804	.554	2408	1.178	1571	1.079	.0023
.600	1475	.740	.597	2408	1.136	1636	.901	.0027
.657	1266	.664	.643	2408	1.113	1723	.735	.0031
.943	1176	.723	.608	2408	1.016	1487	.790	.0033
.686	1571	.773	.572	2408	1.100	1515	1.036	.0025
.714	1271	.742	.596	2408	1.091	1566	.812	.0031
.886	1423	.826	.5345	2408	1.033	1330	1.070	.0028
1.057	1450	.789	.563	2408	.987	1337	1.085	.0027
.571	1741	.798	.556	2408	1.149	1538	1.160	.0023
.800	1576	.755	.587	2408	1.065	1505	1.047	.0025
.743	1365	.526	.716	2408	1.080	1862	.733	.0029
1.229	998	.445	.759	2408	.950	1736	.575	.0039
.800	1276	.599	.677	2408	1.060	1728	.738	.0031
.629	1877	.777	.572	2408	1.124	1548	1.213	.0021
.857	1610	.734	.601	2408	1.042	1508	1.068	.0024
1.029	1524	.699	.623	2408	.992	1488	1.024	.0026
1.314	1165	.686	.631	2408	.934	1419	.821	.0034
1.000	1328	.750	.590	2408	1.000	1421	.935	.0030
1.400	833	.533	.713	2408	.919	1578	.528	.0047
.714	1240	.639	.656	2408	1.090	1722	.720	.0032
.514	1576	.670	.640	2408	1.178	1815	.878	.0025
.571	1393	.536	.712	2408	1.150	1972	.706	.0028

Table IV-5 - Programmed Surface Results

A. Coarse Surface

Run No.	Total Flow (cm^3/sec)	Total Flow (lb/hr)	Cond. Flow (lb/hr)	R	Q Cond. (Btu/hr)	ΔT_{Al} (F°)	$\Delta T_{corr.}$ (F°)	$\delta_{0\text{-th}}$ (Ft x 10^{-5})	$\frac{3}{4}\frac{(1-R)^{4/3}}{1-R}$	$\delta_{av\text{-th}}$ (mils)	$h_{pr\text{-th}}$ Btu/hr-ft^2-F°	h_{exp} Btu/hr-ft^2-F°	$\frac{h_{exp}}{h_{pr\text{-th}}}$	ℓ_c (mils)
1	5.45	41.5	3.56	0.913	3453	0.29	2.06	4.72	0.983	0.557	8469	3280	0.387	15.8
2	5.45	41.5	3.16	0.922	3065	0.26	1.49	4.72	0.991	0.562	8397	4025	0.479	19.7
3	5.45	41.5	5.45	0.866	5287	0.45	3.24	4.72	0.974	0.552	8541	3194	0.374	15.4
4	5.45	41.5	5.53	0.864	5364	0.46	3.71	4.72	0.976	0.553	8526	2829	0.332	13.3
5	5.45	41.5	5.61	0.862	5442	0.46	2.47	4.72	0.973	0.552	8554	4312	0.504	20.4
6	5.45	41.5	5.62	0.862	5451	0.46	3.10	4.72	0.973	0.552	8554	3440	0.402	16.3
7	5.45	41.5	5.53	0.864	5364	0.46	2.98	4.72	0.976	0.553	8526	3522	0.413	16.6
8	4.83	36.8	5.53	0.847	5364	0.46	4.50	4.54	0.971	0.529	8922	2333	0.261	10.9
9	4.25	32.4	5.61	0.822	5442	0.46	2.98	4.34	0.965	0.503	9372	3573	0.381	15.8
10	5.45	41.5	5.53	0.864	5364	0.46	2.34	4.72	0.976	0.553	8526	4485	0.526	21.0
11	5.45	41.5	5.53	0.864	5364	0.46	3.00	4.72	0.976	0.553	8526	3499	0.410	16.4
12	5.45	41.5	5.77	0.858	5597	0.48	2.33	4.72	0.972	0.551	8560	4700	0.549	22.7
13	5.45	41.5	5.77	0.858	5597	0.48	2.42	4.72	0.972	0.551	8560	4526	0.529	21.9
14	5.45	41.5	5.69	0.860	5519	0.47	2.37	4.72	0.975	0.553	8530	4557	0.534	22.1
15	5.45	41.5	5.78	0.858	5607	0.48	2.63	4.72	0.972	0.551	8560	4172	0.487	20.2
16	5.45	41.5	5.72	0.860	5548	0.47	2.58	4.72	0.975	0.553	8530	4208	0.493	20.3
17	5.45	41.5	5.61	0.862	5442	0.46	2.88	4.72	0.973	0.552	8554	5636	0.659	17.5
18	5.45	41.5	5.58	0.862	5413	0.46	2.54	4.72	0.973	0.552	8554	4170	0.487	19.6
19	5.45	41.5	5.45	0.866	5287	0.45	2.13	4.72	0.963	0.546	8640	4857	0.562	23.3
20	5.45	41.5	5.44	0.867	5277	0.45	2.32	4.72	0.976	0.553	8526	4451	0.522	21.6
21	4.83	36.8	5.37	0.851	5209	0.44	2.57	4.54	0.971	0.529	8916	3966	0.445	18.3
22	4.25	32.4	5.37	0.830	5209	0.44	2.73	4.34	0.966	0.503	9364	3734	0.399	16.5
23	3.67	28.0	5.37	0.802	5209	0.44	2.75	4.13	0.962	0.477	9881	3707	0.375	15.4
24	2.65	21.9	5.45	0.720	5287	0.45	2.57	3.80	0.946	0.430	10,950	4026	0.368	14.8
25	1.80	13.7	5.37	0.585	5209	0.44	2.38	3.23	0.922	0.357	13,220	4283	0.324	13.5
26	5.45	41.5	5.31	0.870	5151	0.44	2.58	4.72	0.975	0.553	8530	3907	0.458	18.9
27	4.83	36.8	5.45	0.849	5287	0.45	2.81	4.54	0.968	0.528	8944	3682	0.412	17.0
28	4.25	32.4	5.45	0.828	5287	0.45	2.95	4.34	0.968	0.504	9343	3507	0.375	15.4

Table IV-5 - (Cont'd)

A. Coarse Surface

Run No.	Total Flow (cm^3/sec)	Total Flow (lb/hr)	Cond. Flow (lb/hr)	R	Q Cond. (Btu/hr)	ΔT_{Al} (F°)	$\Delta T_{corr.}$ (F°)	$\delta_{0\text{-th}}$ (Ft x 10^{-5})	$\frac{3}{4}\frac{(1-R)^{4/3}}{1-R}$	$\delta_{av\text{-th}}$ (mils)	$h_{pr\text{-th}}$ Btu/hr-ft^2-F°	h_{exp} Btu/hr-ft^2-F°	$\frac{h_{exp}}{h_{pr\text{-th}}}$	ℓ_c (mils)
29	3.67	28.0	5.45	0.800	5287	0.45	3.05	4.130	.964	.478	9865	3392	.344	14.2
30	2.65	21.9	5.45	0.720	5287	0.45	2.77	3.796	.946	.430	10,950	3725	.341	13.8
31	2.23	17.0	5.53	0.659	5364	0.46	3.54	3.474	.935	.390	12,100	2965	.245	10.2
32	1.60	13.7	5.53	0.573	5364	0.46	4.02	3.225	.917	.355	13,300	2611	.196	8.2
33	5.45	41.5	4.42	0.891	4287	0.37	1.98	4.723	.977	.554	8514	4237	.498	20.5
34	5.45	41.5	6.48	0.841	6286	0.54	3.19	4.723	.967	.548	8607	3856	.448	18.6
35	5.45	41.5	7.58	0.814	7353	0.63	3.37	4.723	.964	.547	8632	4270	.495	20.5
36	2.65	21.9	3.24	0.833	3143	0.27	1.65	3.796	.965	.439	10,720	3728	.348	14.0
37	2.65	21.9	4.50	0.768	4365	0.37	2.26	3.796	.957	.435	10,820	3780	.349	14.0
38	2.65	21.9	5.45	0.720	5287	0.45	2.75	3.796	.946	.430	10,950	3762	.344	13.8
39	2.65	21.9	6.56	0.662	6363	0.54	3.37	3.796	.934	.426	11,100	3695	.333	13.4
40	2.65	21.9	4.50	0.768	4365	0.37	2.50	3.796	.960	.438	10,800	3417	.316	12.6
41	5.45	41.5	5.50	0.865	5335	0.45	2.47	4.723	.978	.555	8507	4227	.497	20.4
42	5.45	41.5	4.58	0.888	4443	0.38	2.11	4.723	.978	.555	8507	4121	.484	19.9
43	5.45	41.5	3.63	0.911	3521	0.30	1.80	4.723	.983	.551	8465	3828	.452	18.4
44	5.45	41.5	2.58	0.937	2503	0.21	1.29	4.723	.989	.561	8416	3797	.451	19.5
45	5.45	41.5	5.54	0.864	5374	0.46	2.64	4.723	.975	.552	8534	3983	.467	19.3
46	5.45	41.5	5.53	0.864	5364	0.46	2.16	4.723	.975	.552	8534	4860	.569	23.5

Table IV-5 - Programmed Surface Results

B. Fine Surface

Run No.	Total Flow (cm^3/sec)	Total Flow (lb/hr)	Cond. Flow (lb/hr)	R	Q Cond. (Btu/hr)	ΔT_{Al} (F°)	$\Delta T_{corr.}$ (F°)	$\delta_{0\text{-}th}$ (Ft x 10^{-5})	$\frac{3}{4}\frac{(1-R)^{4/3}}{1-R}$	$\delta_{av\text{-}th}$ (mils)	$h_{pr\text{-}th}$ Btu/hr-ft^2-F°	h_{exp} Btu/hr-ft^2-F°	$\frac{h_{exp}}{h_{pr\text{-}th}}$	ℓ_f (mils)
1	2.26	17.2	3.33	0.808	3234	0.175	1.61	1.72	0.965	0.199	23,740	4474	0.188	3.17
2	2.26	17.2	4.01	0.767	3893	0.211	1.84	1.72	0.960	0.198	23,860	4712	0.197	3.35
3	7.25	55.1	2.21	0.960	2146	0.116	1.22	2.53	0.994	0.302	15,620	3918	0.251	4.13
4	6.65	50.7	2.21	0.956	2146	0.116	1.21	2.46	0.989	0.292	16,160	3950	0.244	4.07
5	5.75	43.8	2.02	0.954	1961	0.106	1.13	2.34	0.992	0.279	16,900	3864	0.229	3.79
6	5.15	39.2	2.05	0.948	1992	0.108	1.12	2.26	0.995	0.270	17,460	3961	0.227	3.75
7	4.55	34.7	2.05	0.941	1992	0.108	1.15	2.17	0.992	0.258	18,280	3857	0.211	3.51
8	4.00	30.5	2.09	0.931	2023	0.110	1.18	2.08	0.989	0.246	19,120	3817	0.200	3.30
9	3.40	25.9	2.09	0.919	2023	0.110	1.13	1.97	0.991	0.234	20,150	3987	0.198	3.24
10	2.90	22.1	2.09	0.905	2023	0.110	1.08	1.88	0.987	0.221	21,330	4171	0.196	3.21

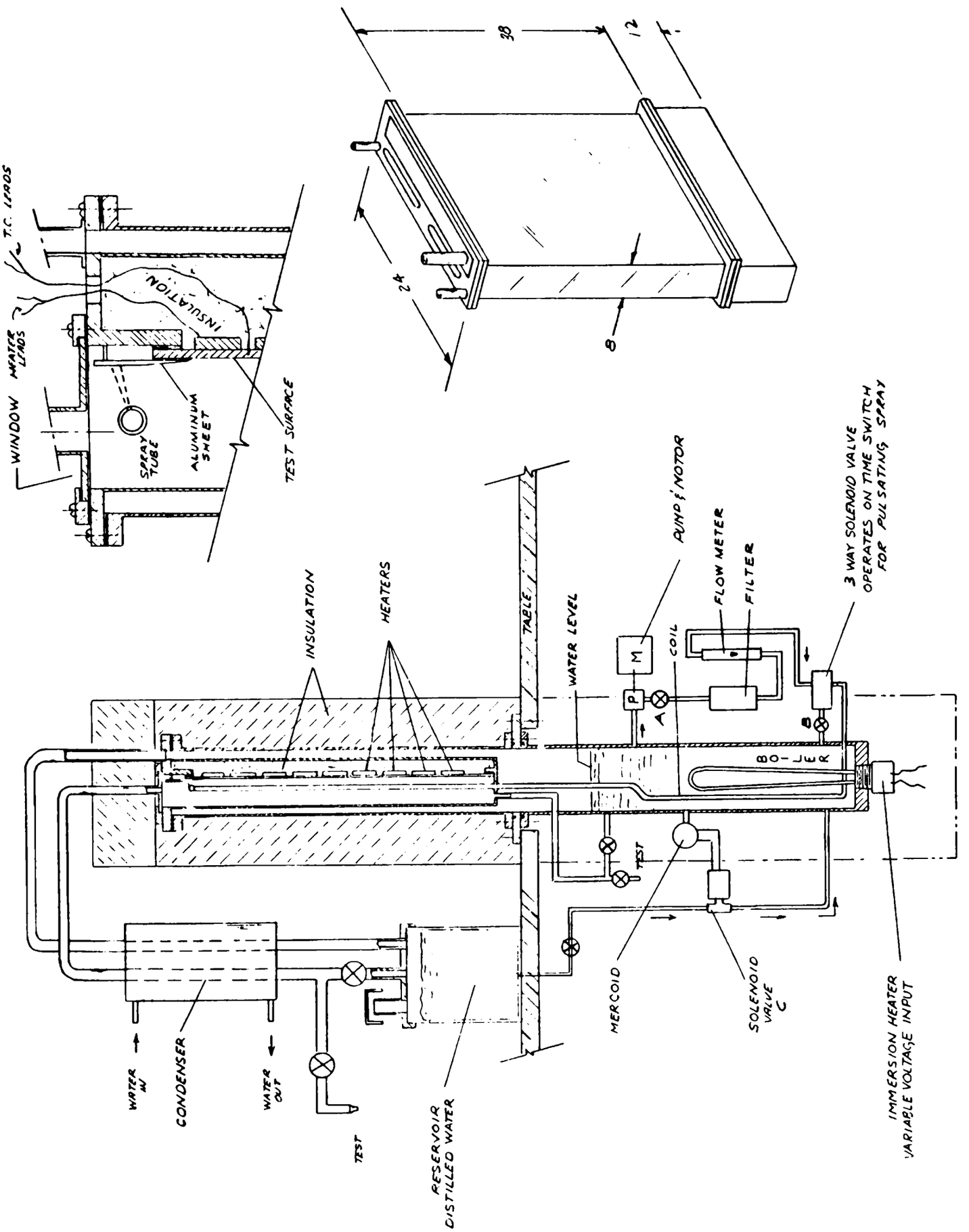

FIG IV-1 SCHEMATIC OF VAPORIZATION TEST APPARATUS

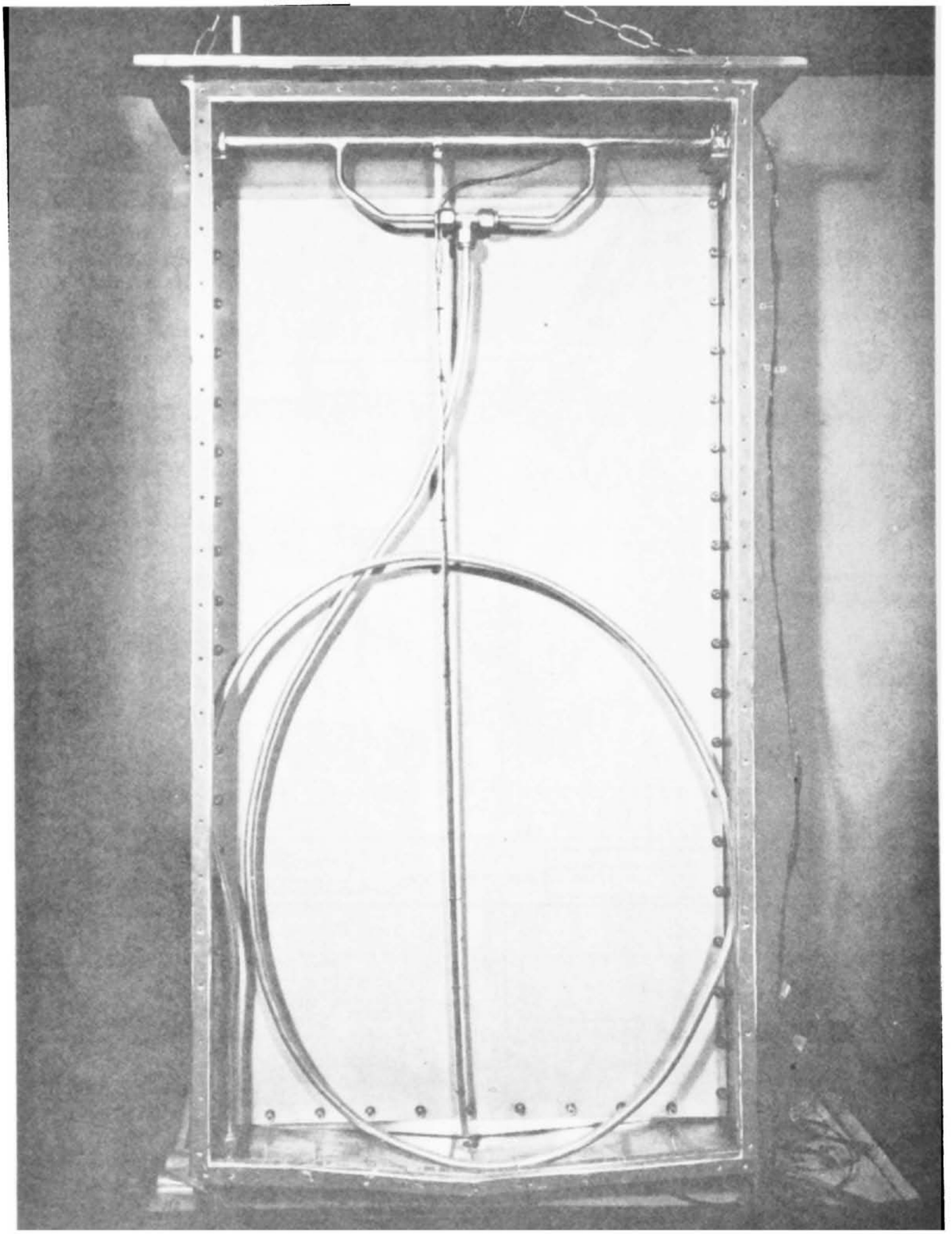

Fig. IV-2

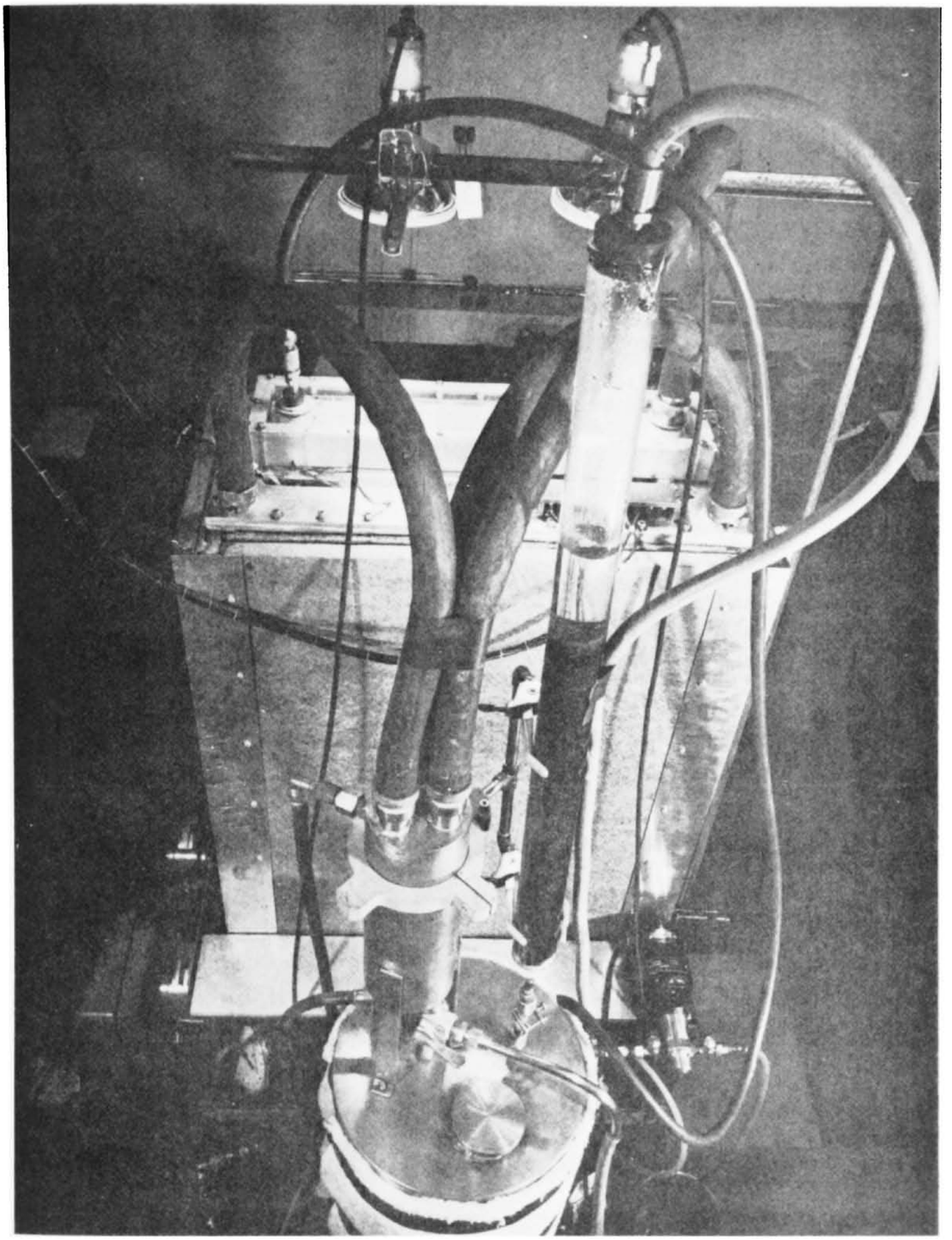

Fig. IV-3

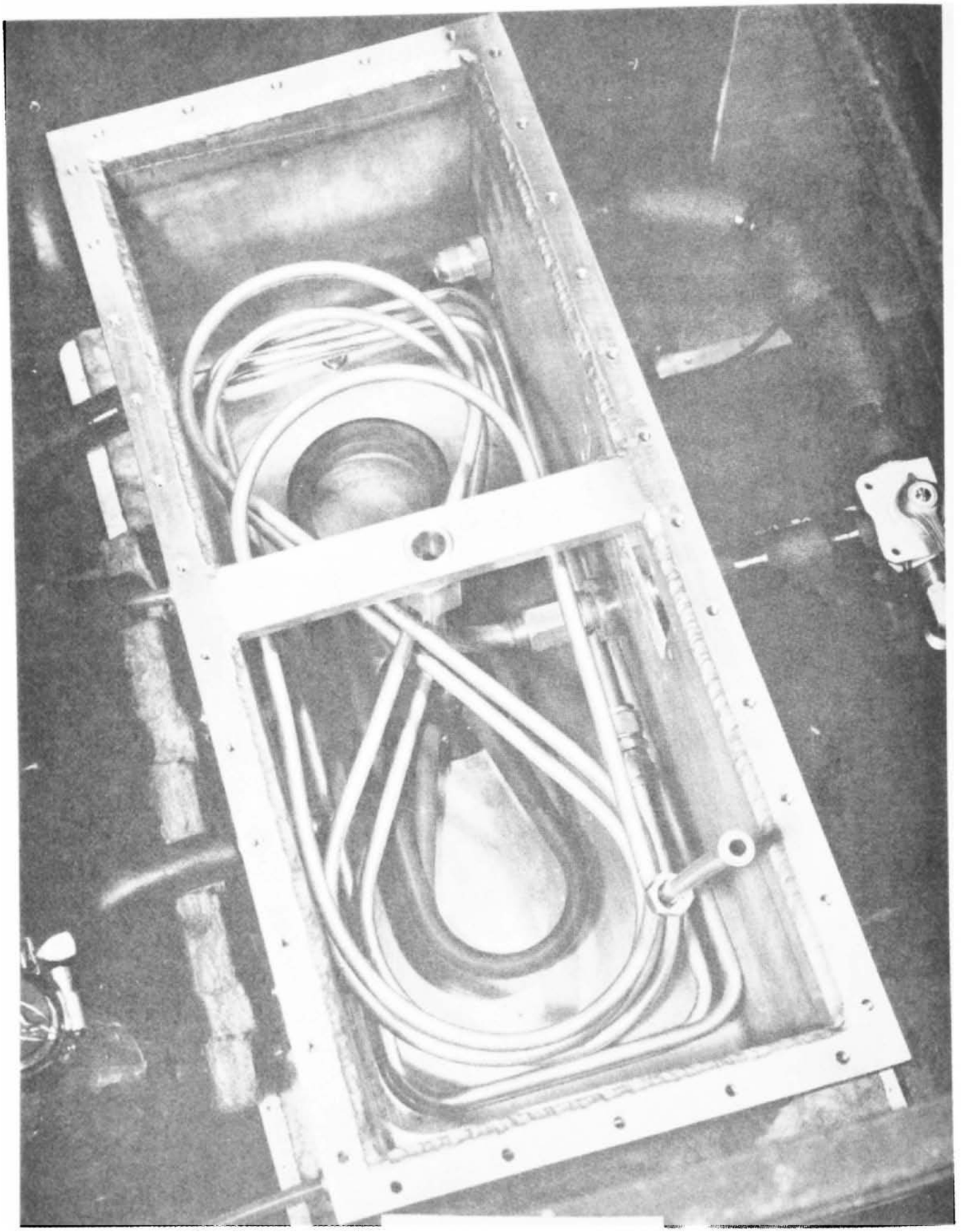

Fig. IV-4

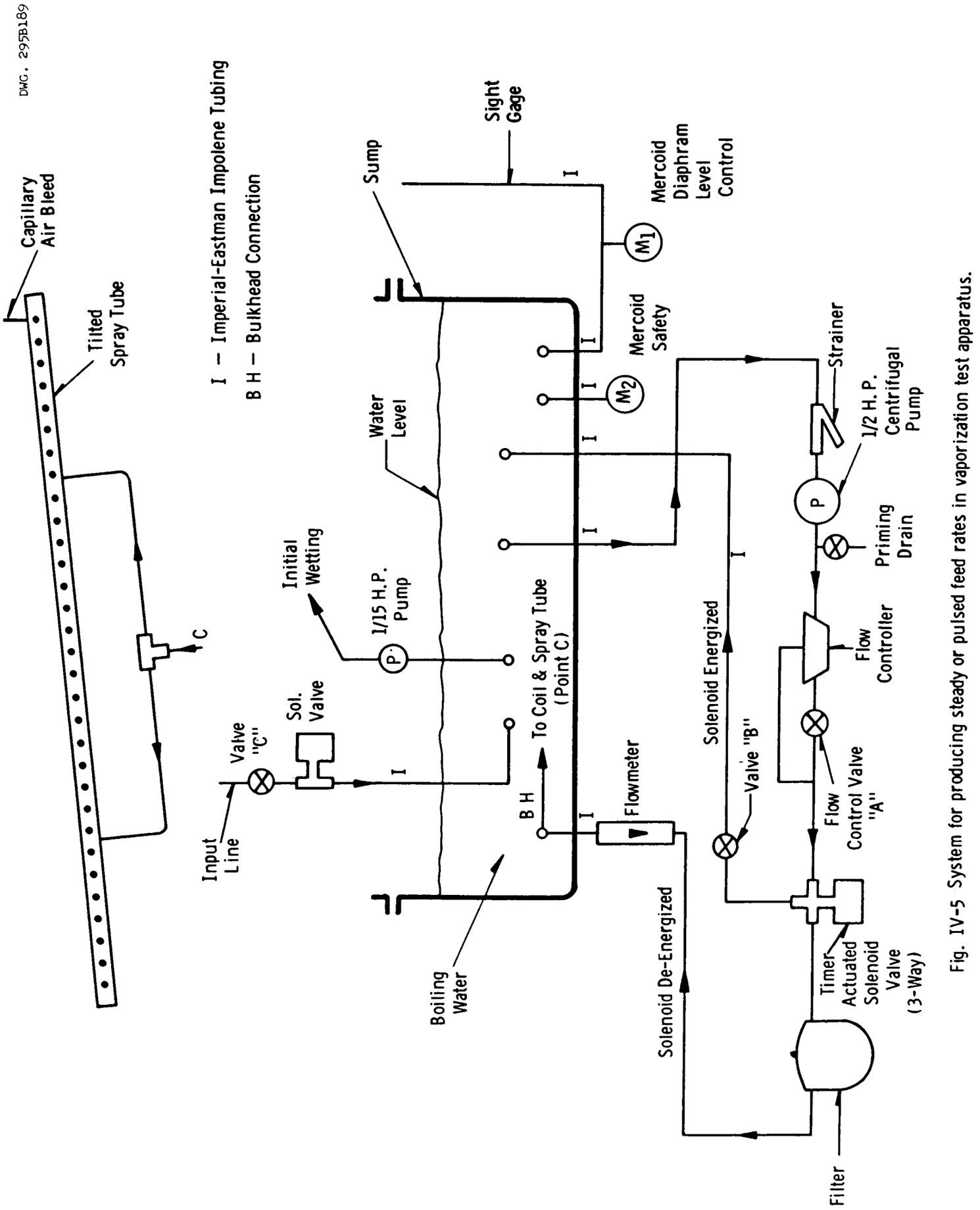

Fig. IV-5 System for producing steady or pulsed feed rates in vaporization test apparatus.

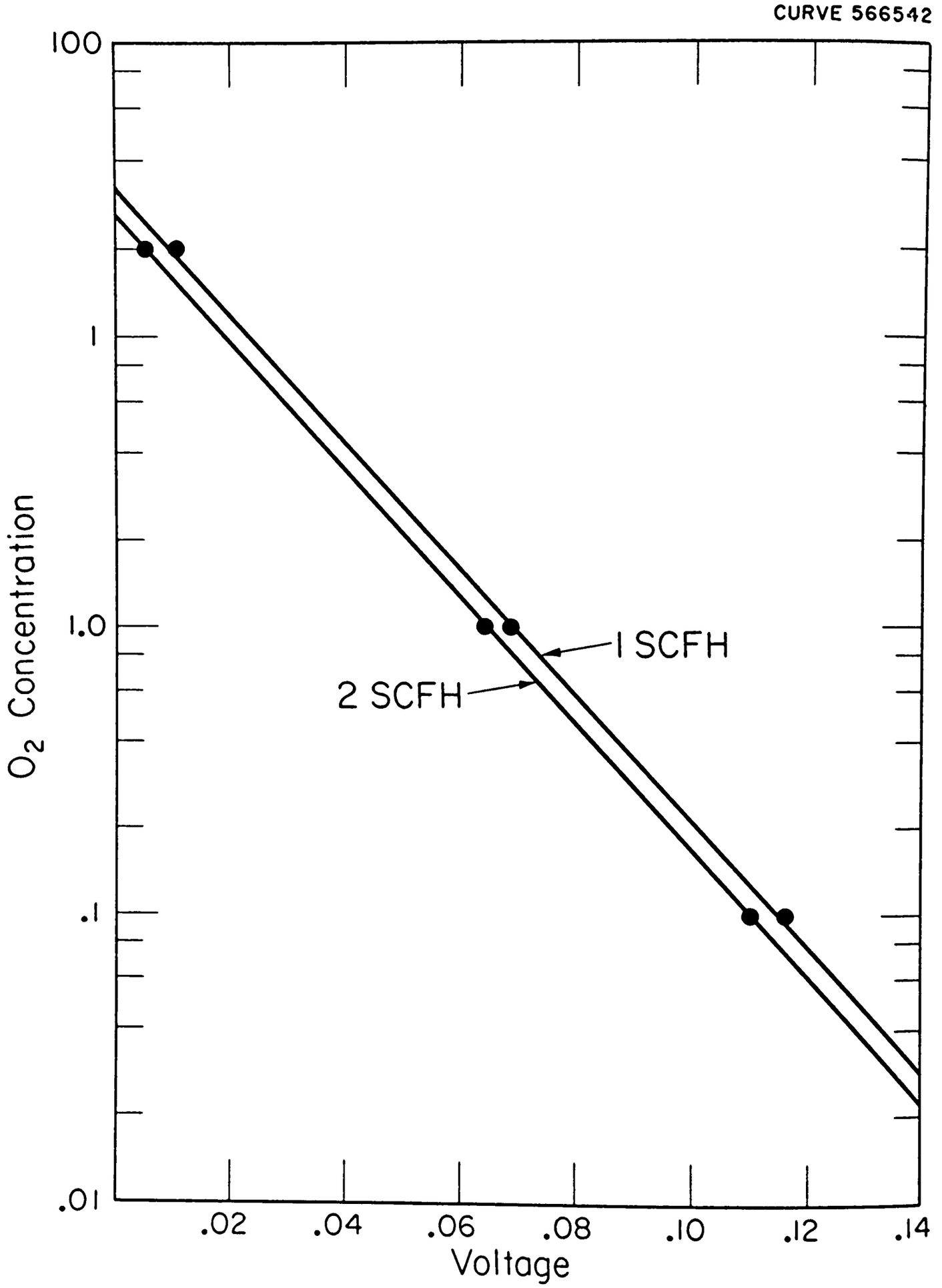

Fig. IV6-Voltage vs O_2 concentration in steam

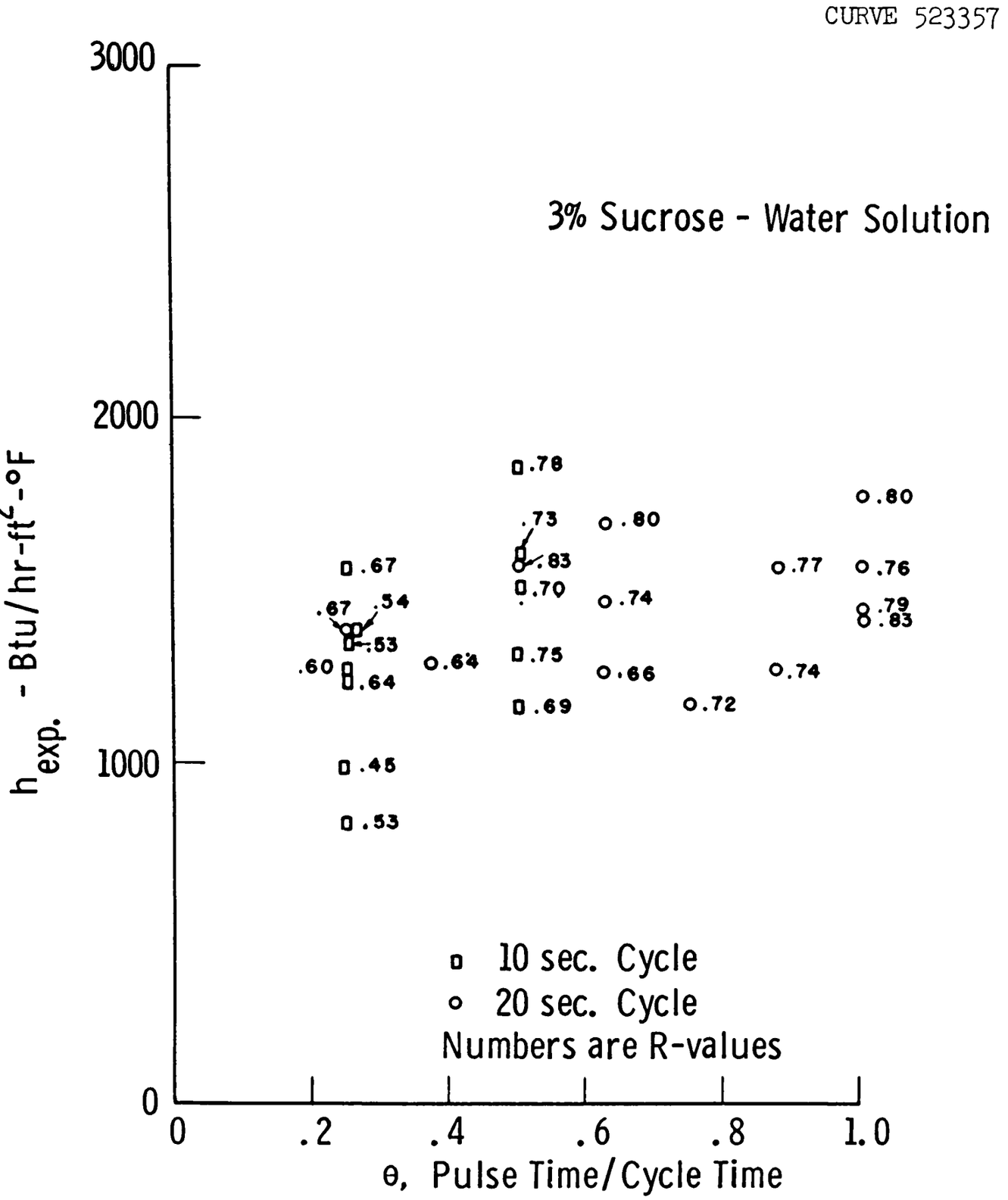

Fig. IV-7 —Effect of pulsed flow on measured heat transfer coefficient

DWG. 626A281

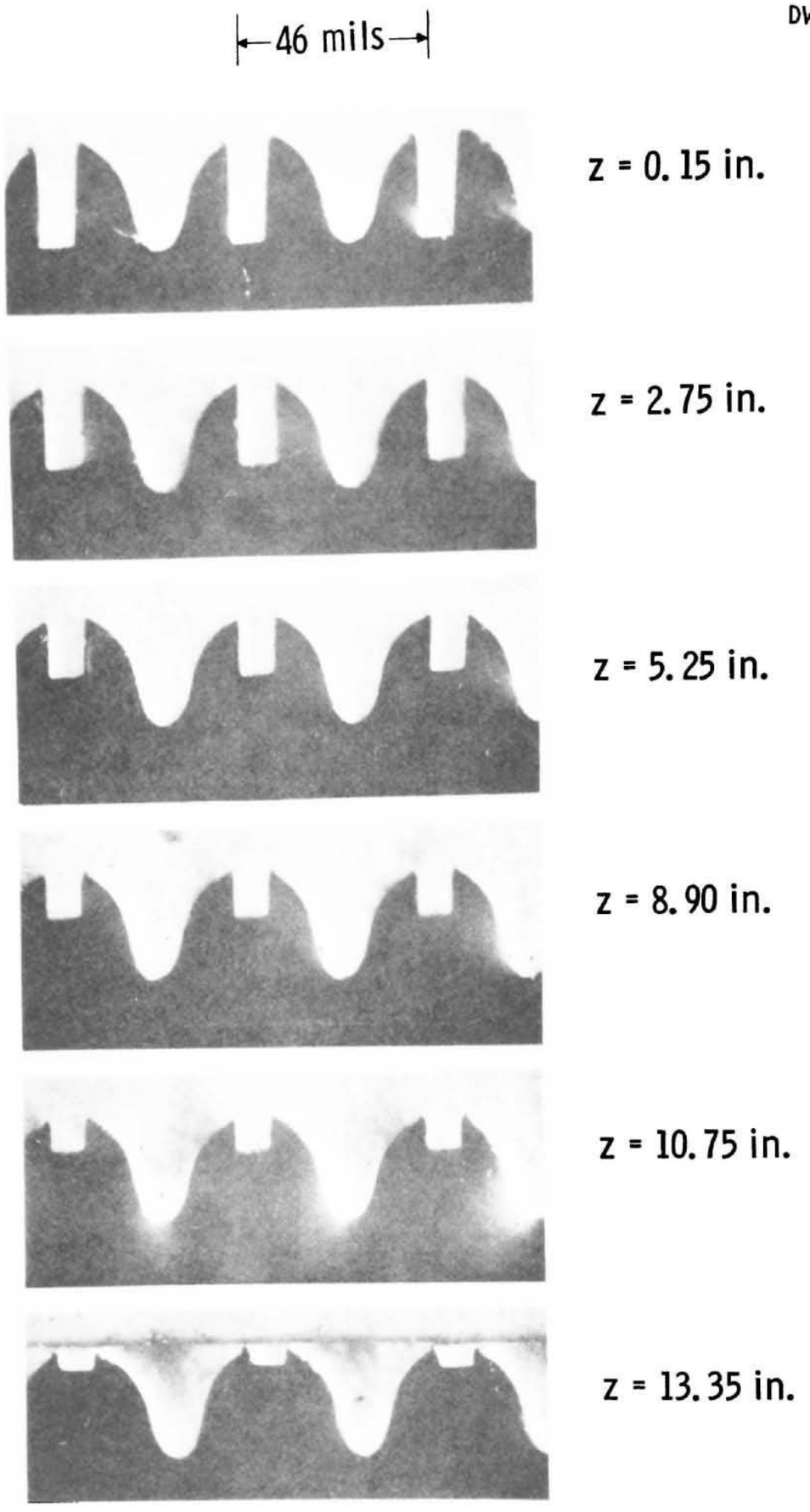

Fig. IV-8—Outlines of an actual programmed evaporator surface obtained from photomacrographs of silastic impressions made at various positions z, along the surface. Flow is initiated at the position z = 0, in the rectangular (feed) grooves.

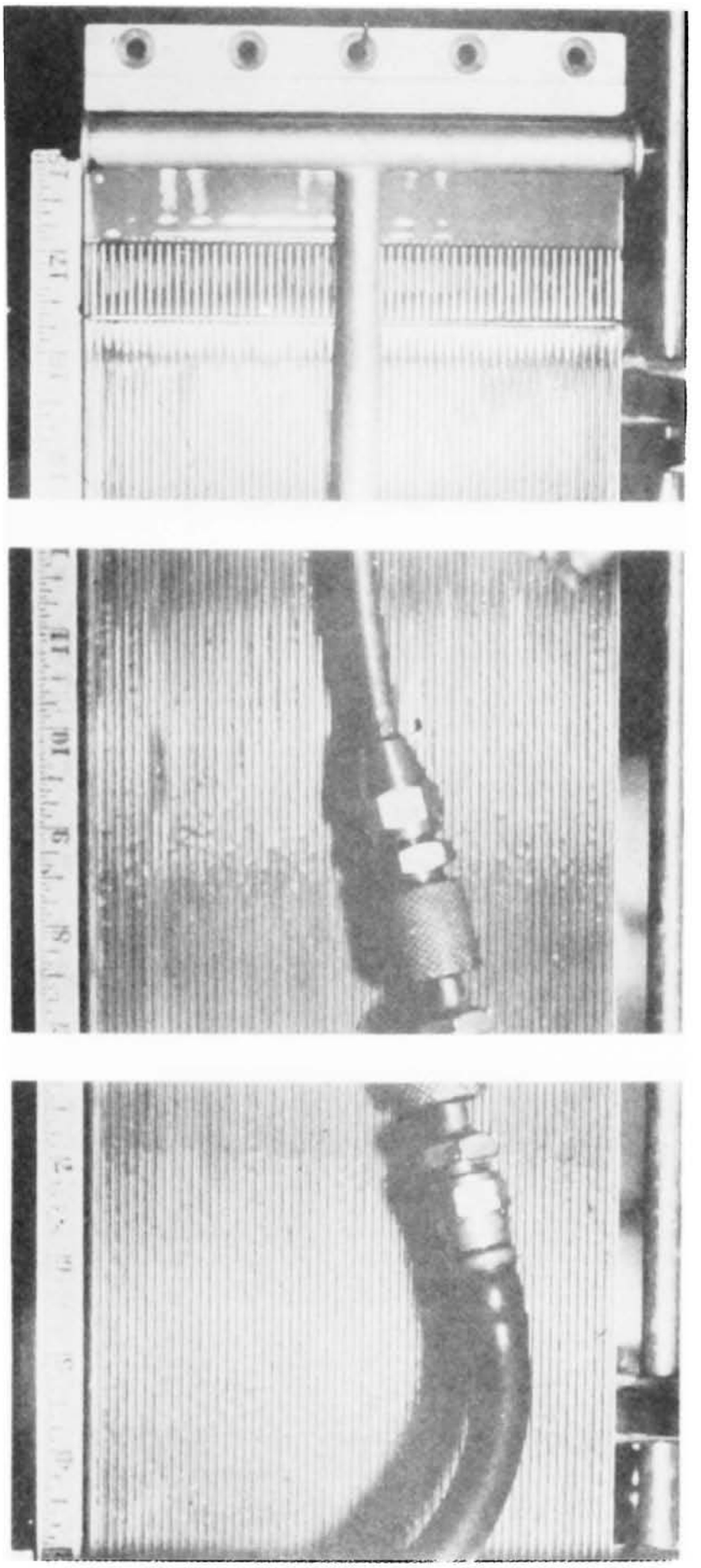

Flow: 1.0 cm^3/sec

Fig. IV-9 Exploded-type view of a programmed evaporator surface operating at a non-evaporating flow condition

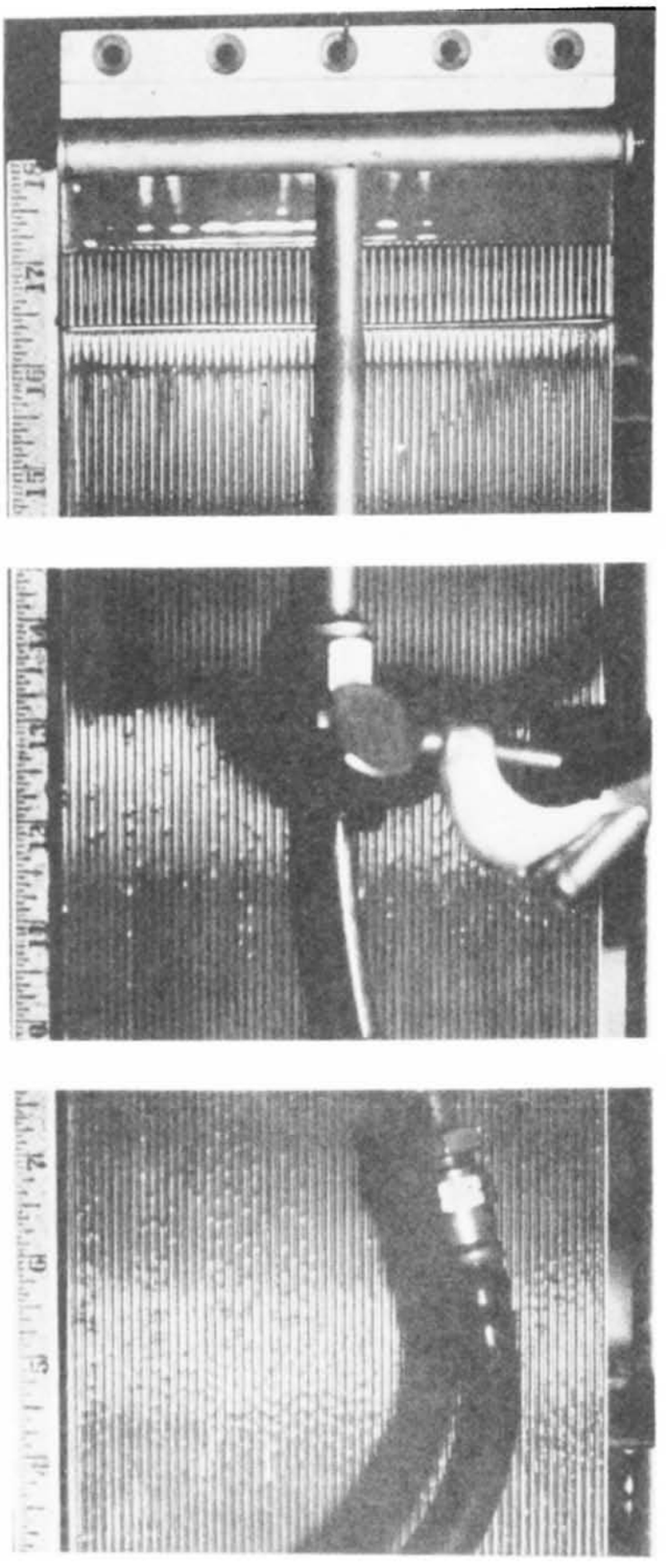

Flow: 2.2 cm^3/sec

Fig. IV-10 -Exploded-type view of a programmed evaporator surface operating at a non-evaporating flow condition

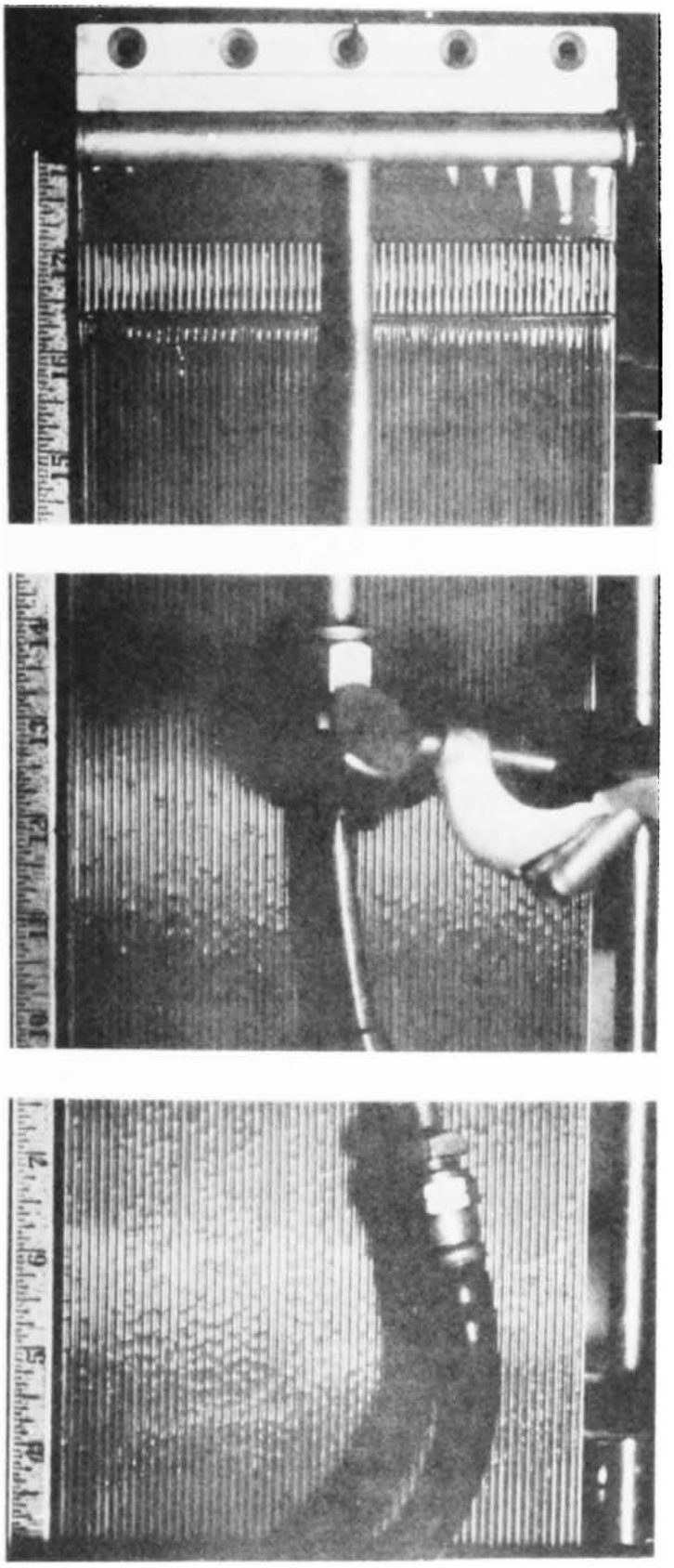

Flow: 4.4 cm^3/sec

Fig. IV-11 -Exploded-type view of a programmed evaporator surface operating at a non-evaporating flow condition

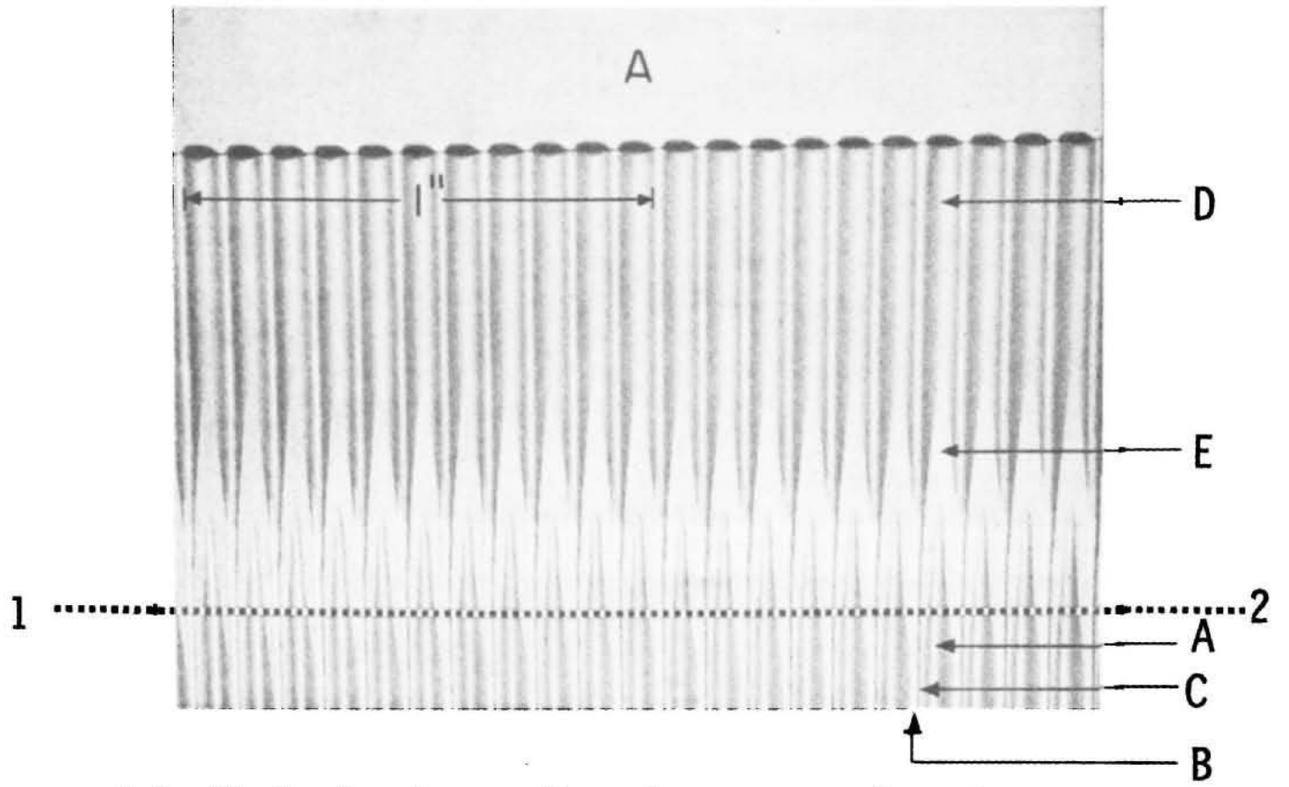

(a)—Photo showing portion of programmed surface and modified flow starter section

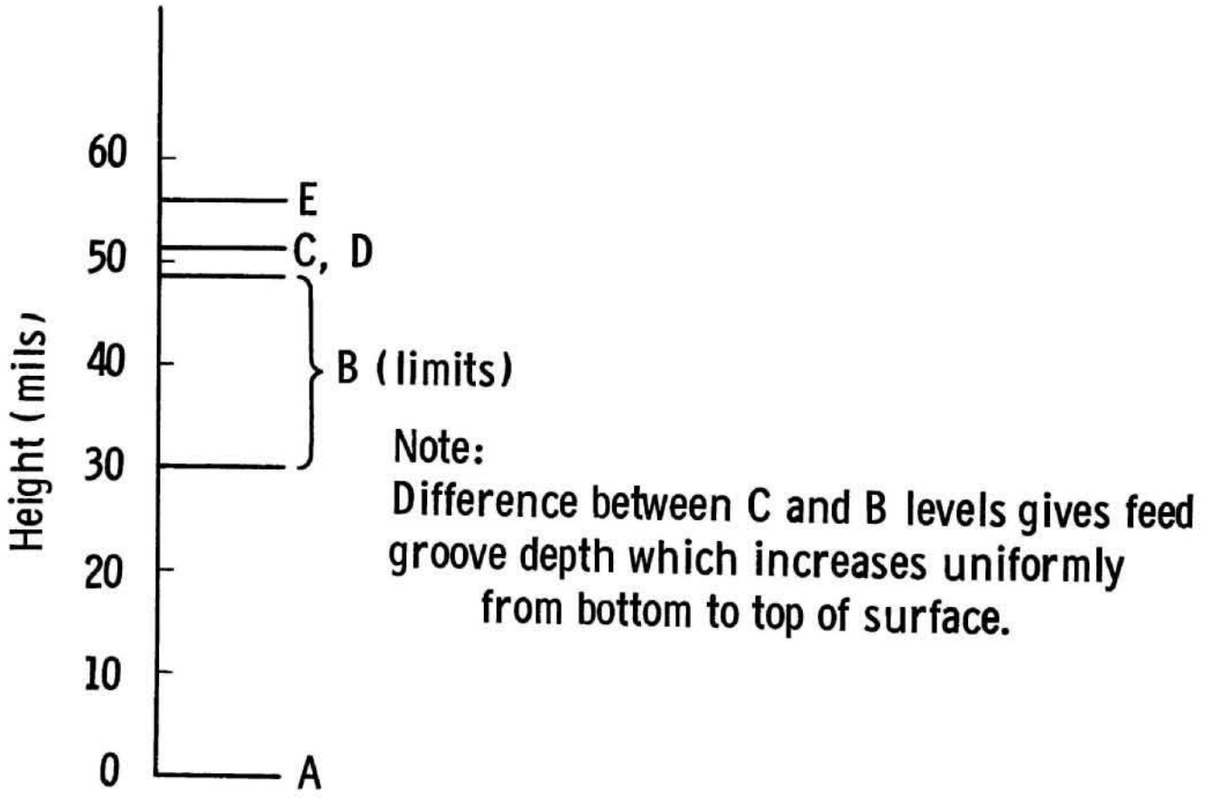

(b)—Level diagram for above surface

Fig. IV-12 -Structural details of an actual programmed evaporator surface

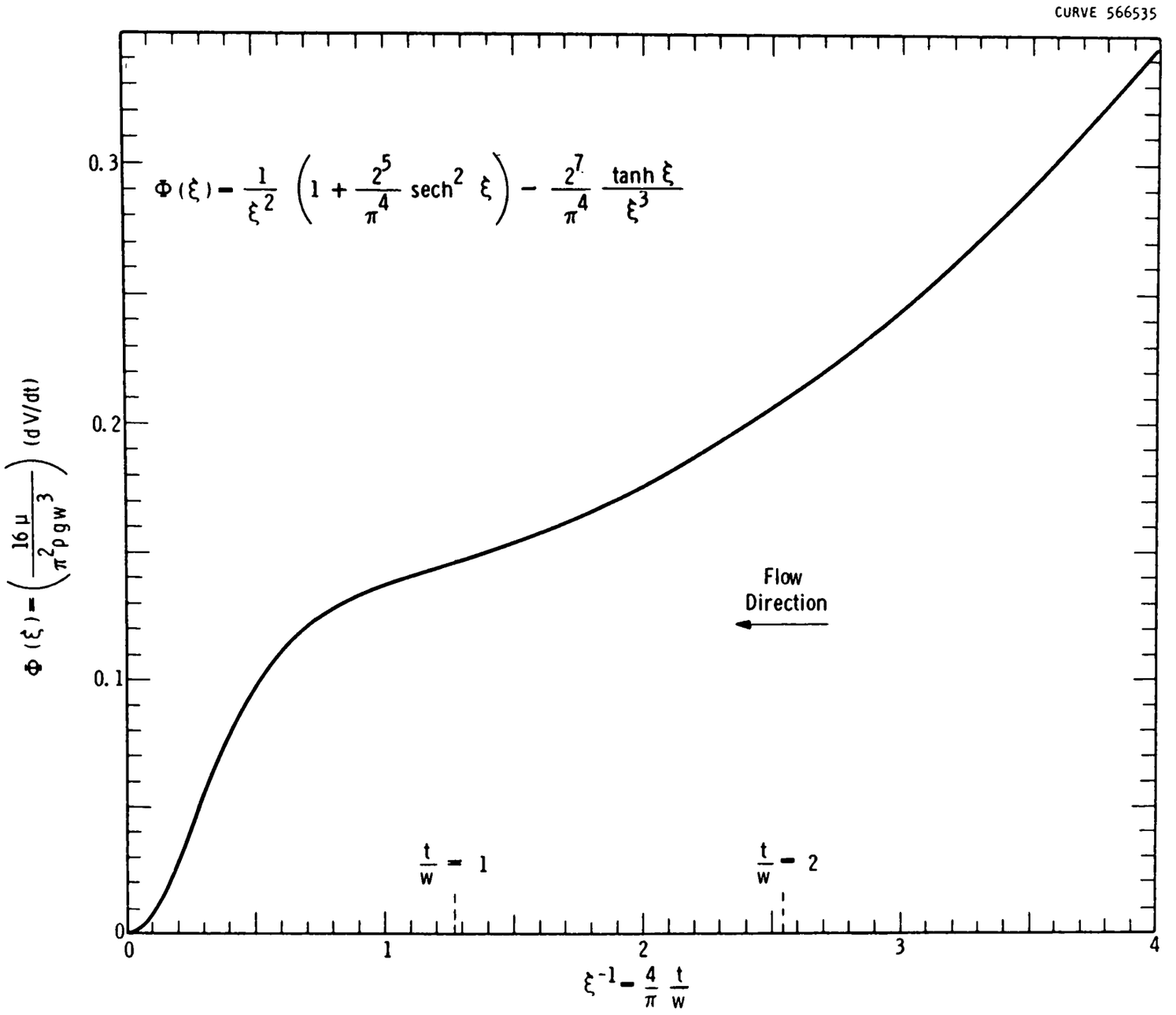

Fig. IV-13—Dimensionless volume-rate function, $\Phi(\xi)$, vs. dimensionless thickness variable, ξ^{-1}.

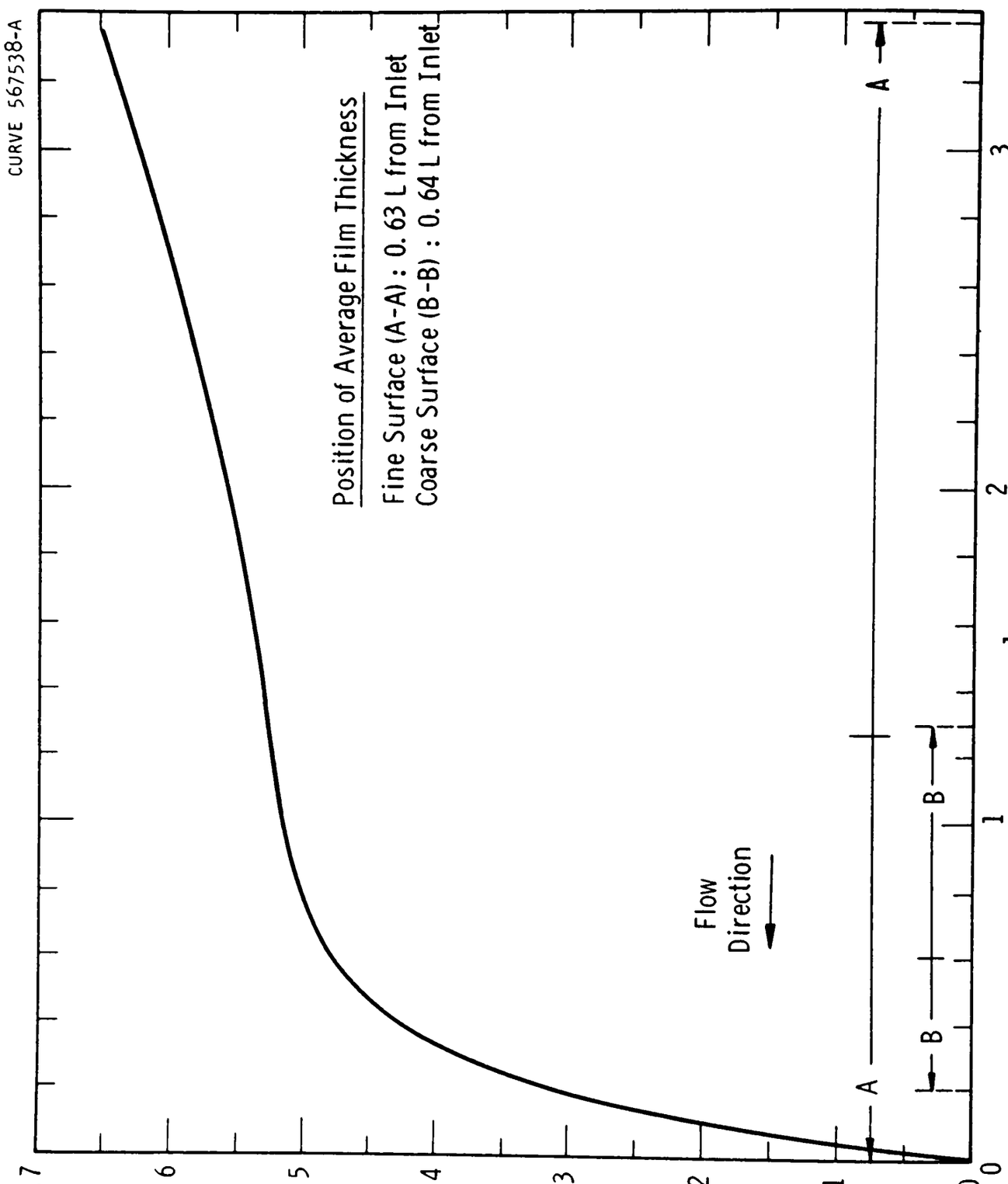

Fig. IV-14—Dimensionless film thickness function, $\Phi^{1/3}$, vs. dimensionless thickness variable, ξ^{-1}

CURVE 565409

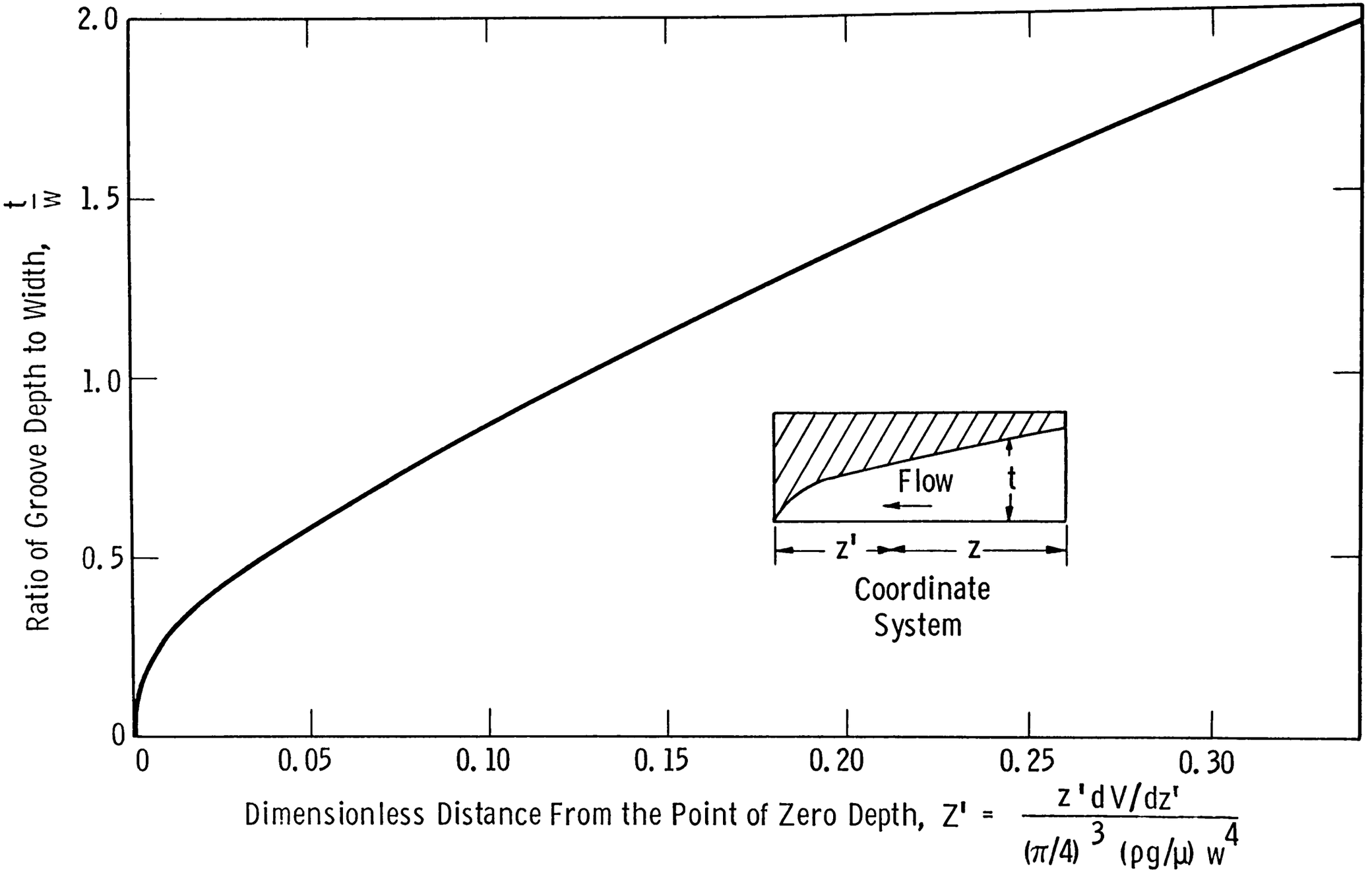

Fig. IV-15—Dimensionless correlation for a feed groove having constant feed rate per unit length, dV/dz', and constant width, w

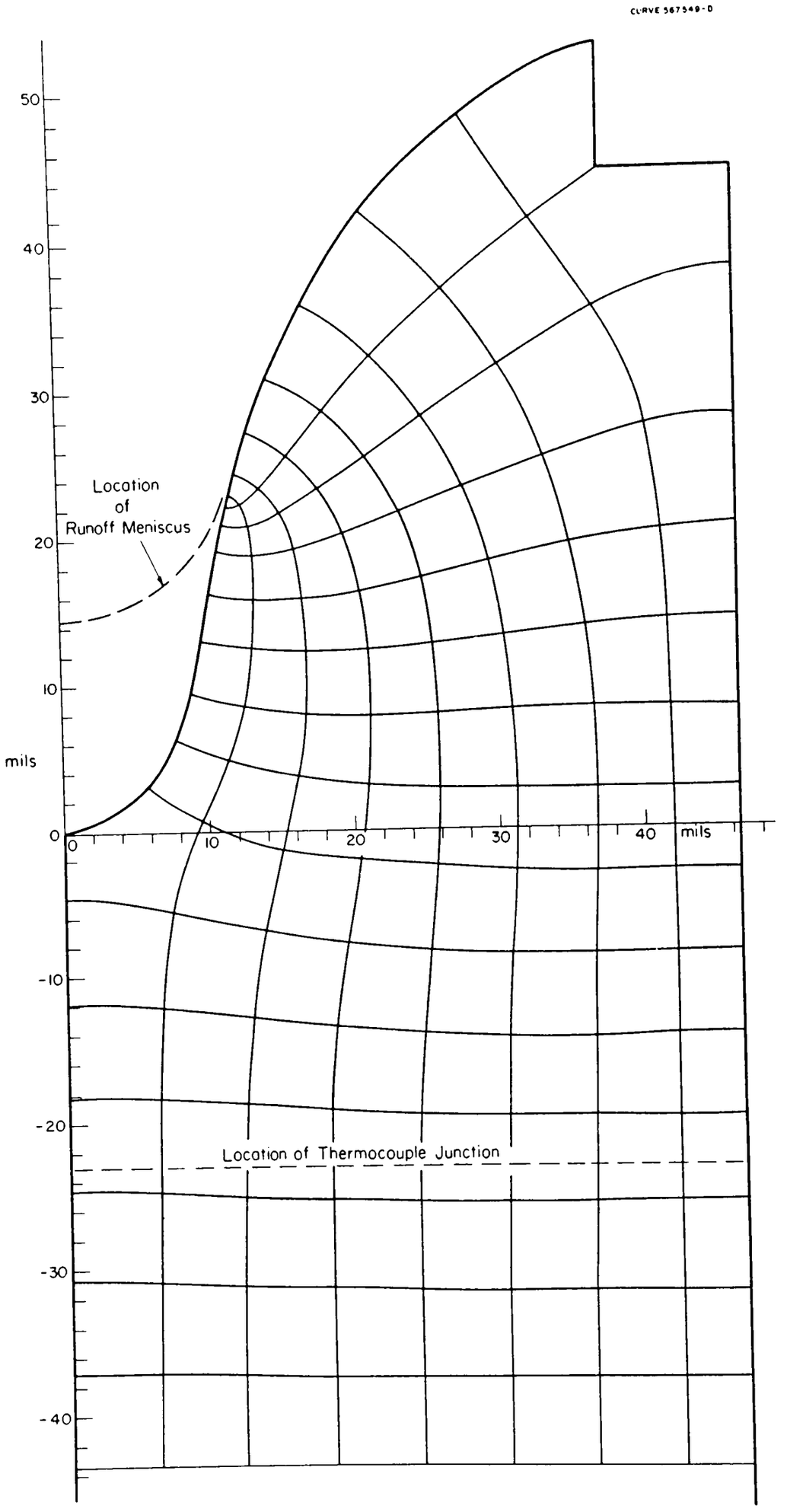

Coarse Surface
86% Runoff
$N_y/N_x = 1.5$
$z_{av} = 9.8$ inch
$L = 15.3$ inch
$\ell = 41.5$ mils

Fig IV 16 - Cross section corresponding to average film thickness position on surface.

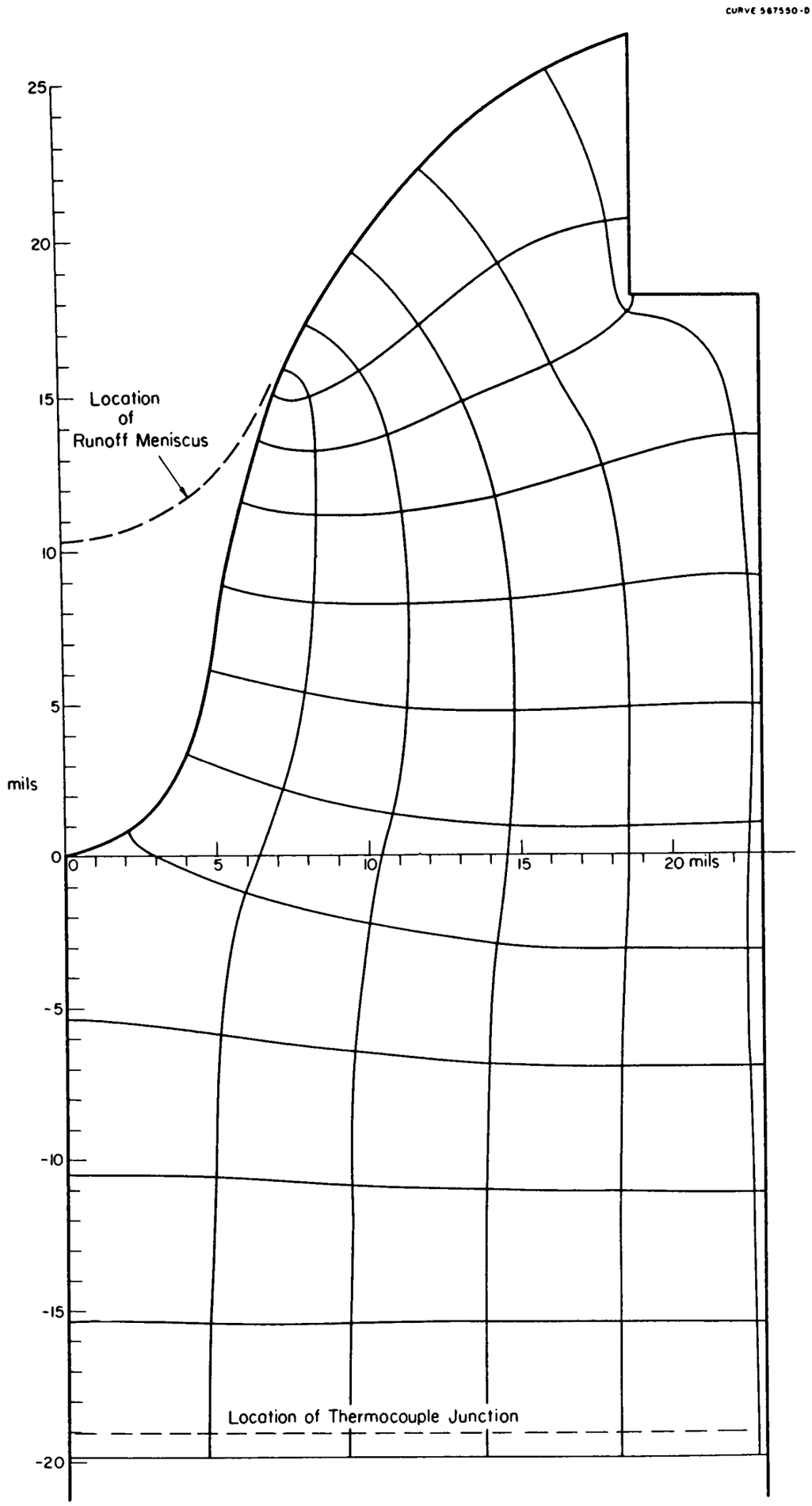

Fine Surface
80 % Runoff
$N_y/N_x = 2.1$
$z_{av} = 10.2$ inch
L = 16.25 inch
$\ell = 16.6$ mils

Fig. IV 17 - Cross section corresponding to average film thickness position on surface.

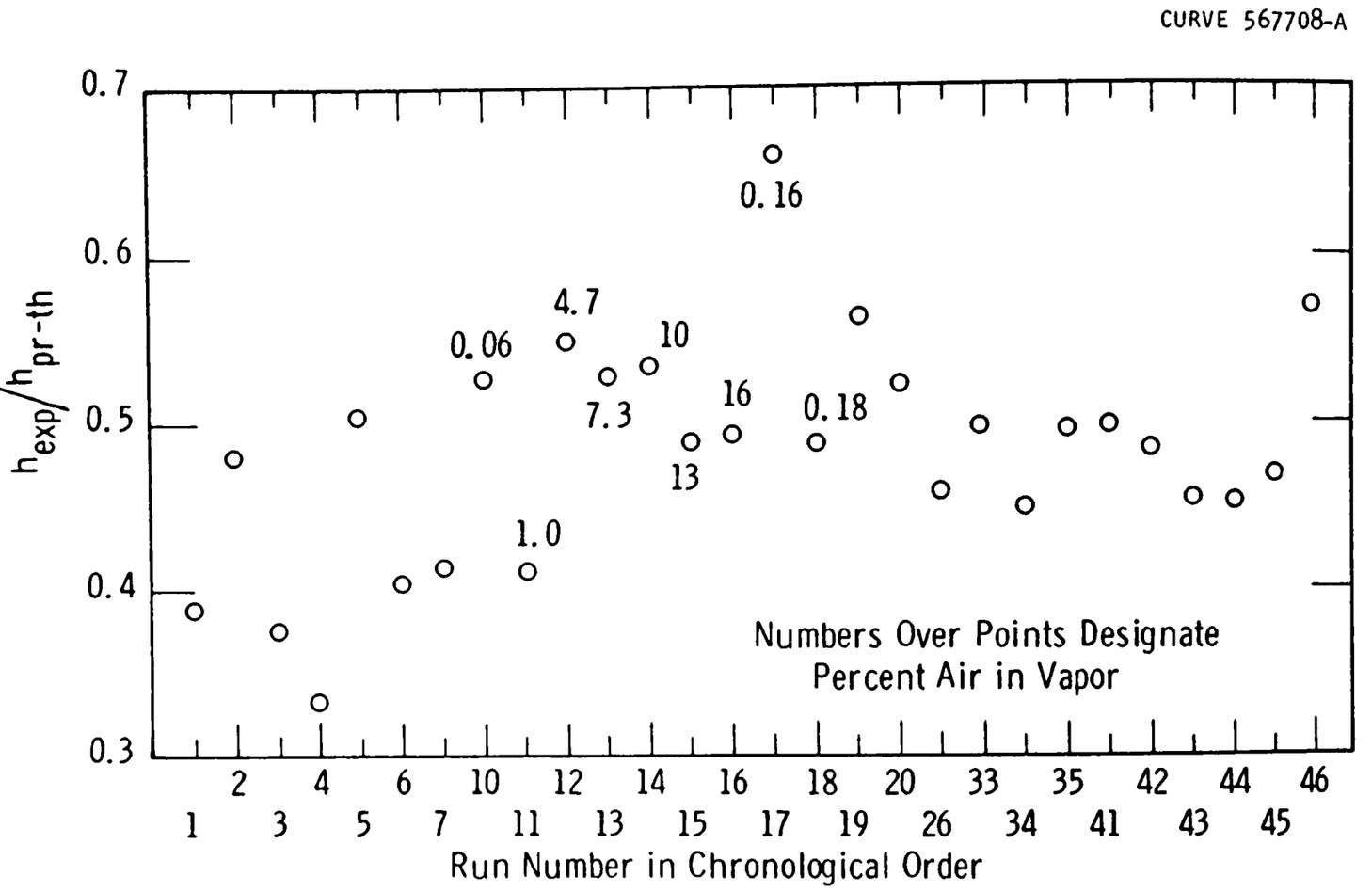

Fig. IV-18—Heat transfer results in chronological order for the coarse surface operating at theoretical flow and at various air - vapor concentrations

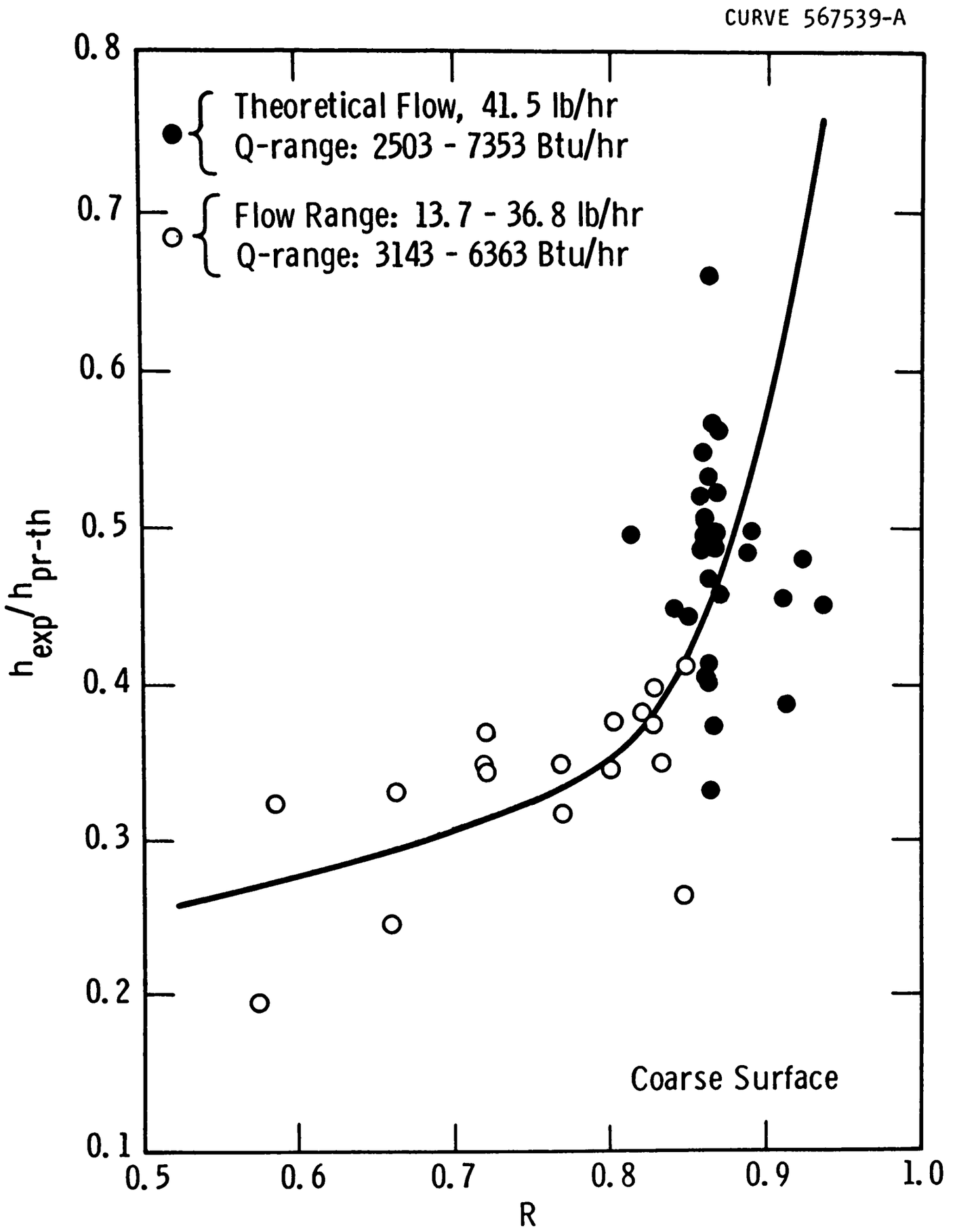

Fig. IV-19—Comparison of experimental with theoretical heat transfer coefficients at various measured runoffs for the 58-groove surface

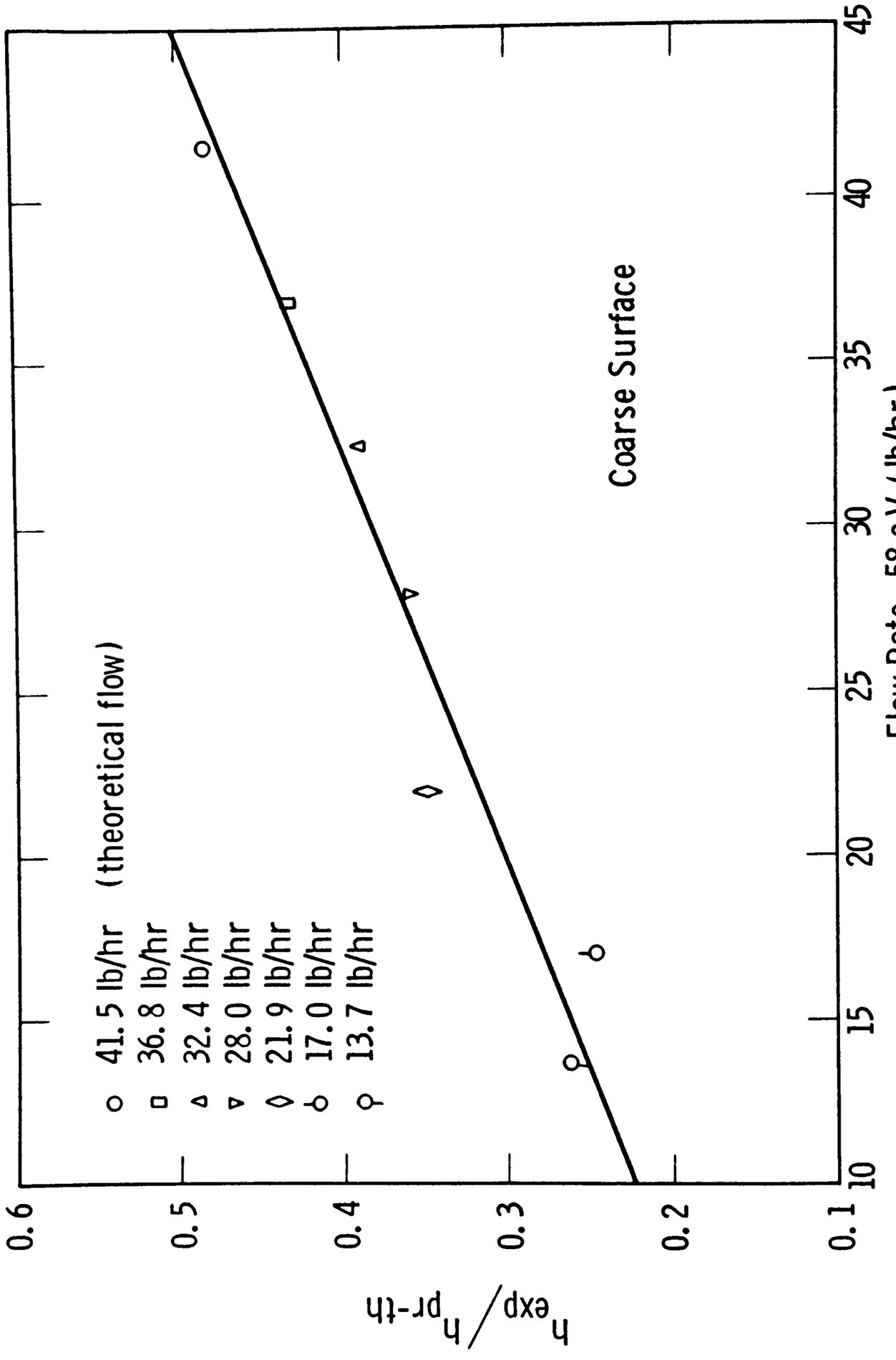

Fig. IV-20—Ratio of heat transfer coefficients $\left(h_{exp}/h_{pr-th}\right)$ vs. total flow over surface

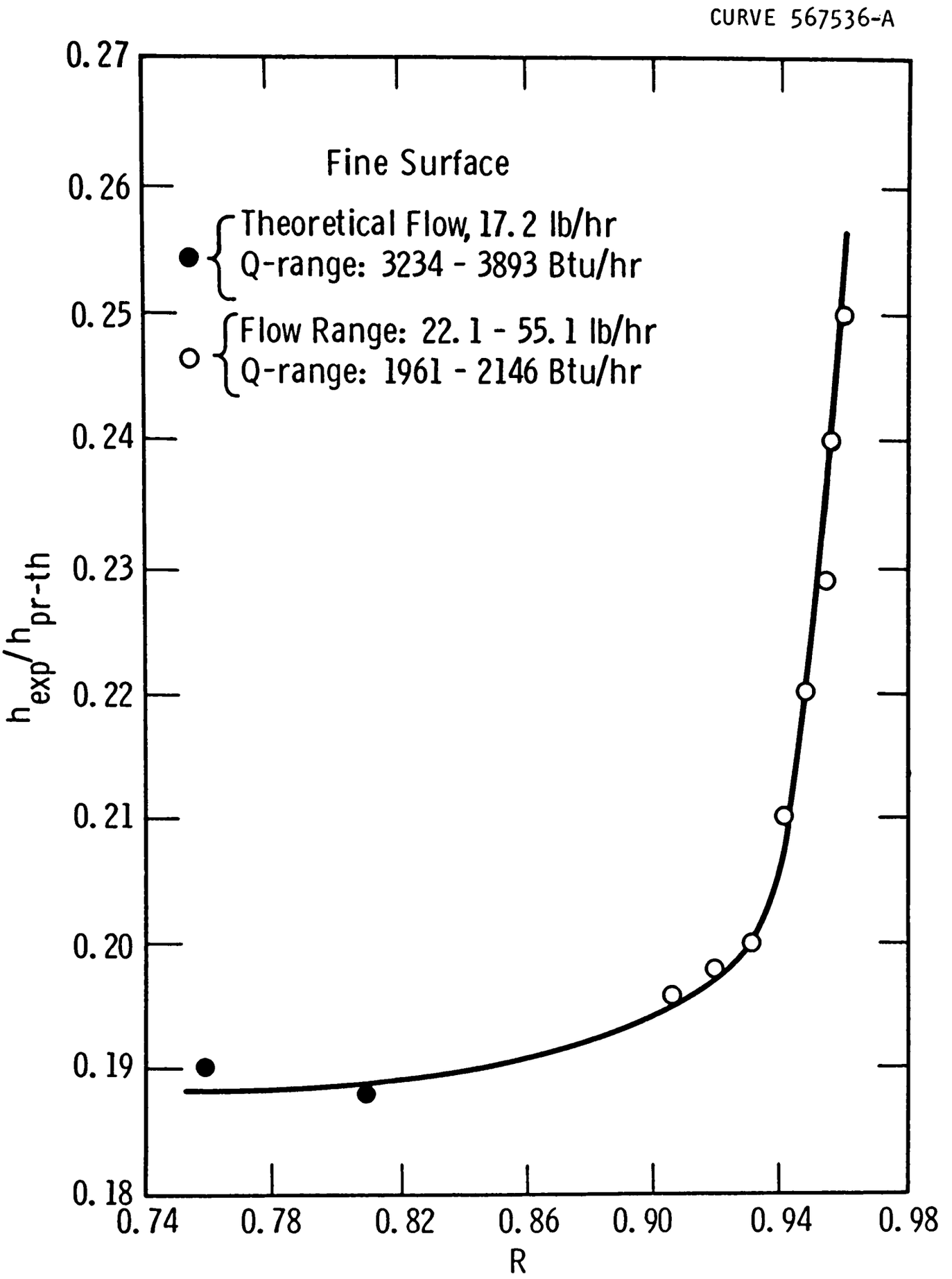

Fig. IV-21—Comparison of experimental with theoretical heat transfer coefficients at various measured runoffs for the 120-groove surface

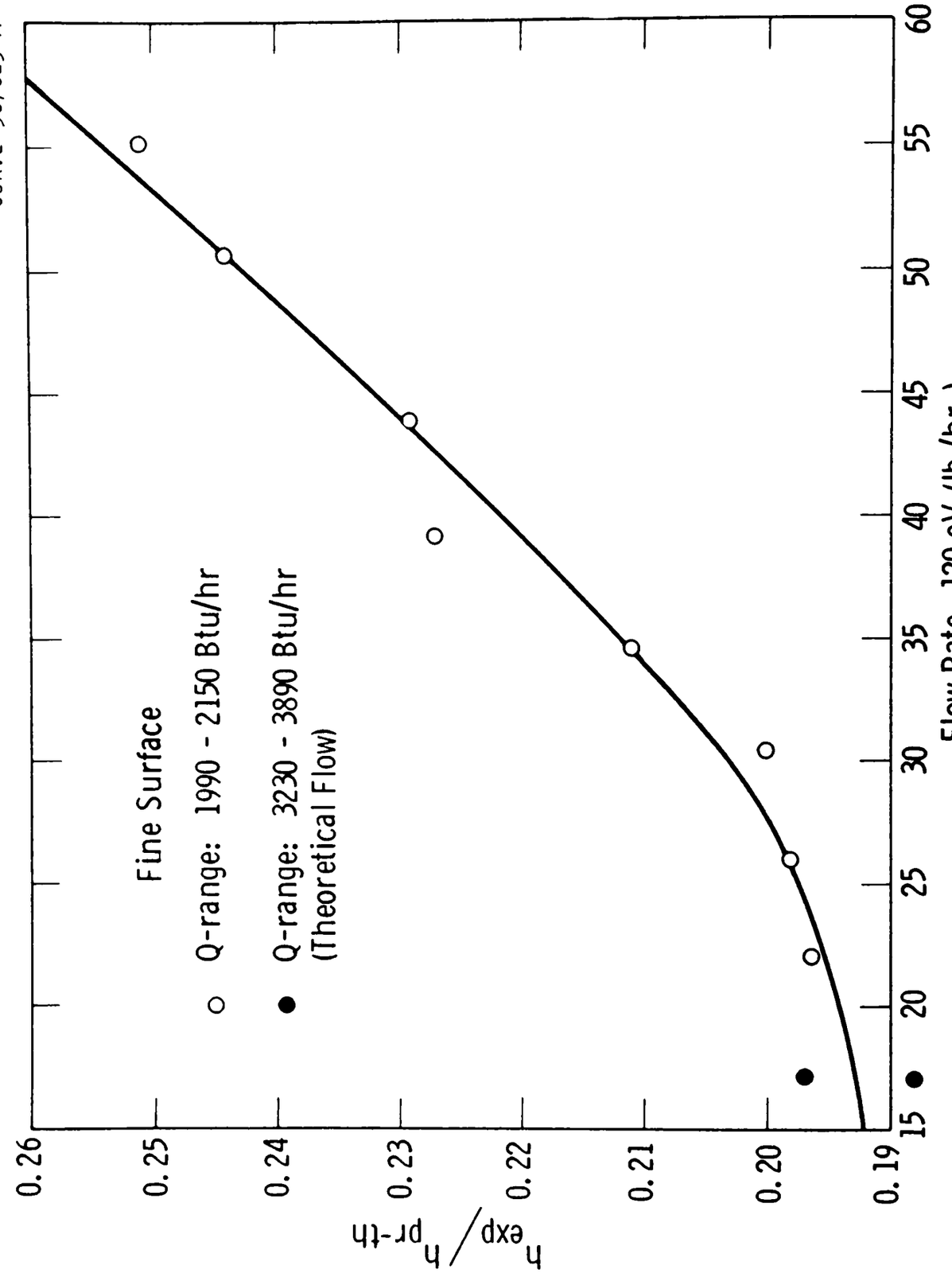

Fig. IV-22—Ratio of heat transfer coefficients $\left(h_{exp}/h_{pr-th}\right)$ vs. total flow over surface

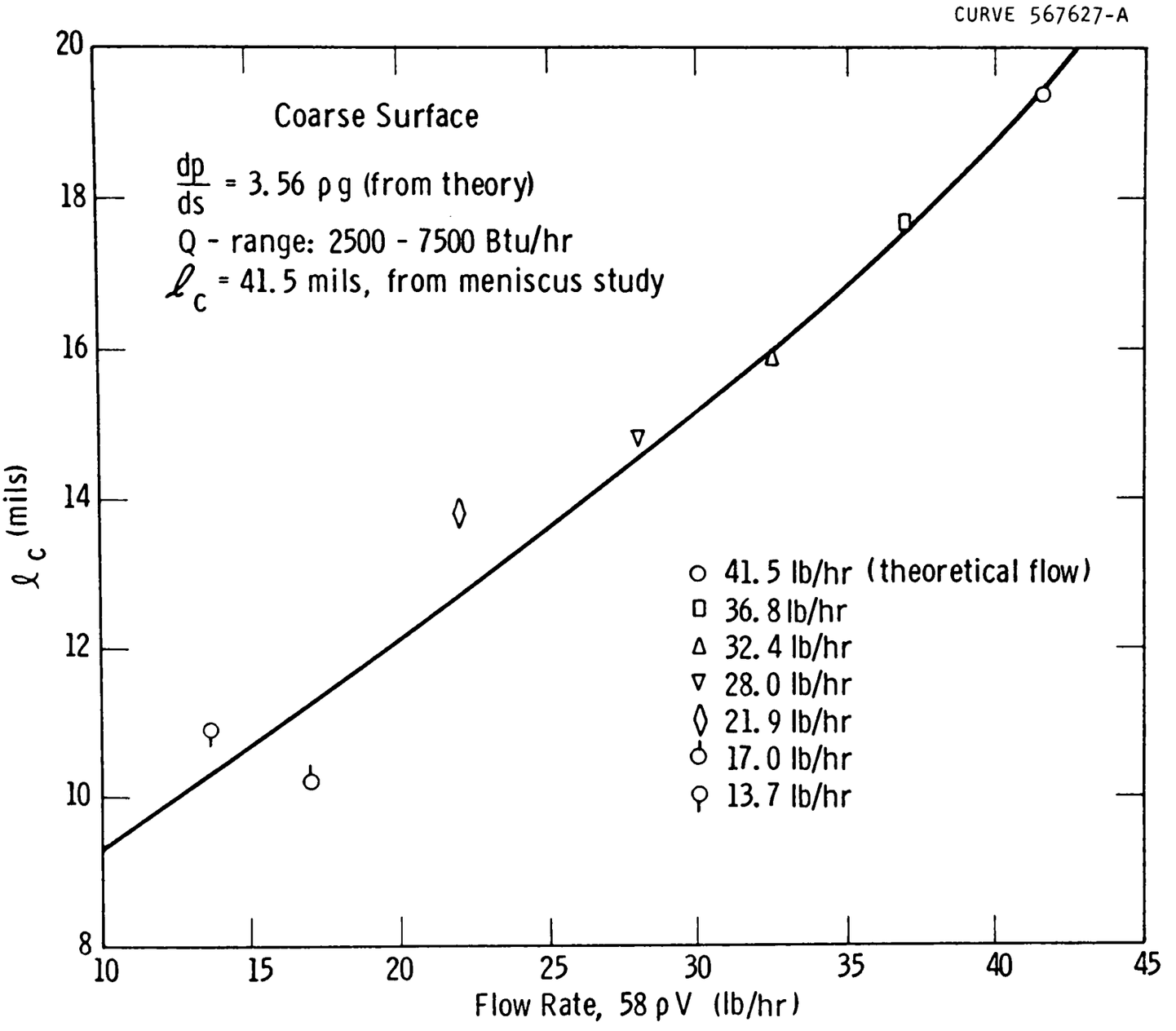

Fig. IV-23—Film length calculated from experimental data by equating h of eq. (11), Appendix V with h of the equation, $h = Q/(116\,\ell_c\,L\Delta T)$

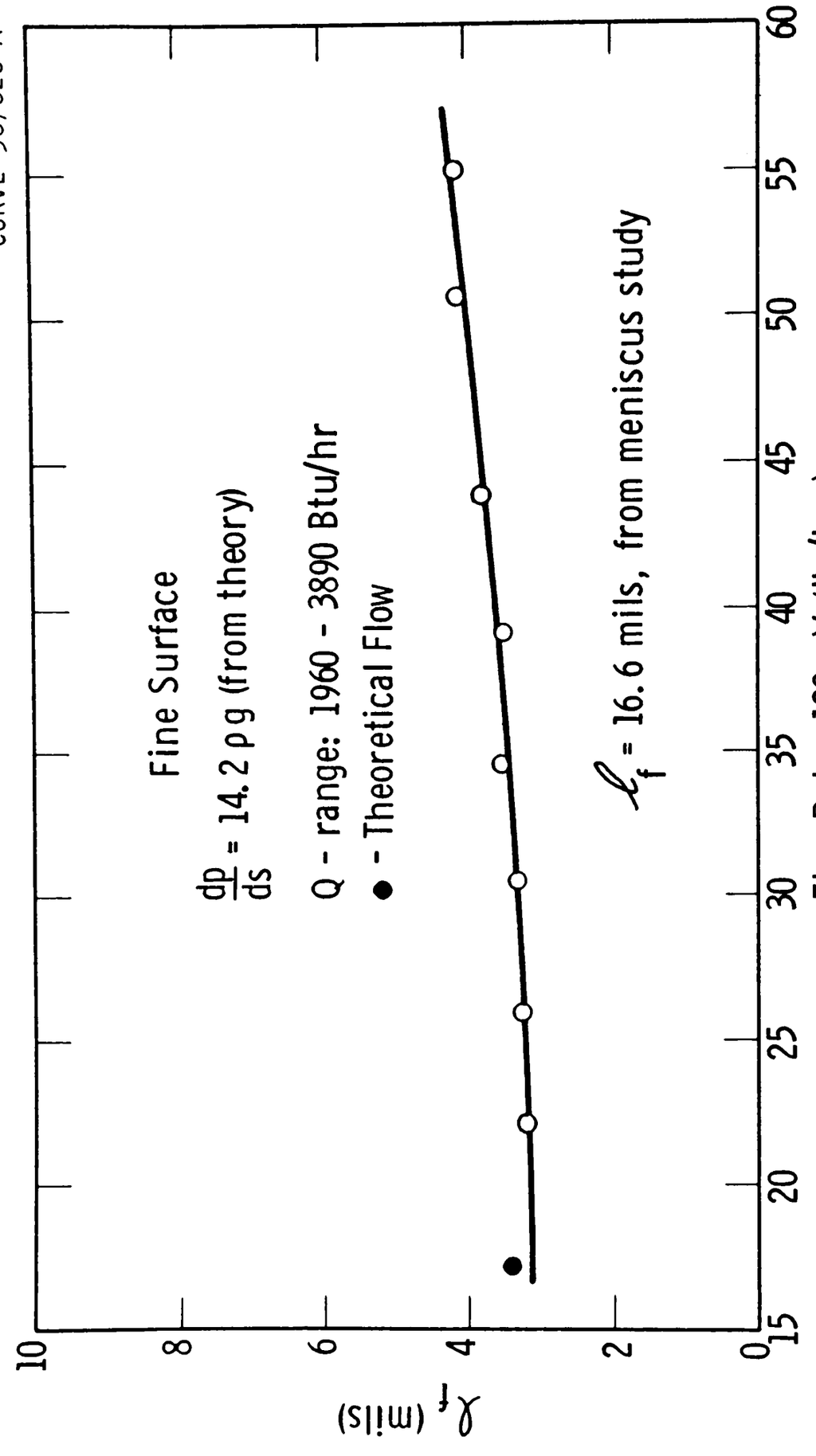

Fig. IV-24—Film length calculated from experimental data by equating h of eq. (11), Appendix V with h of the equation, $h = Q/(240\,\ell_f\,L\Delta T)$

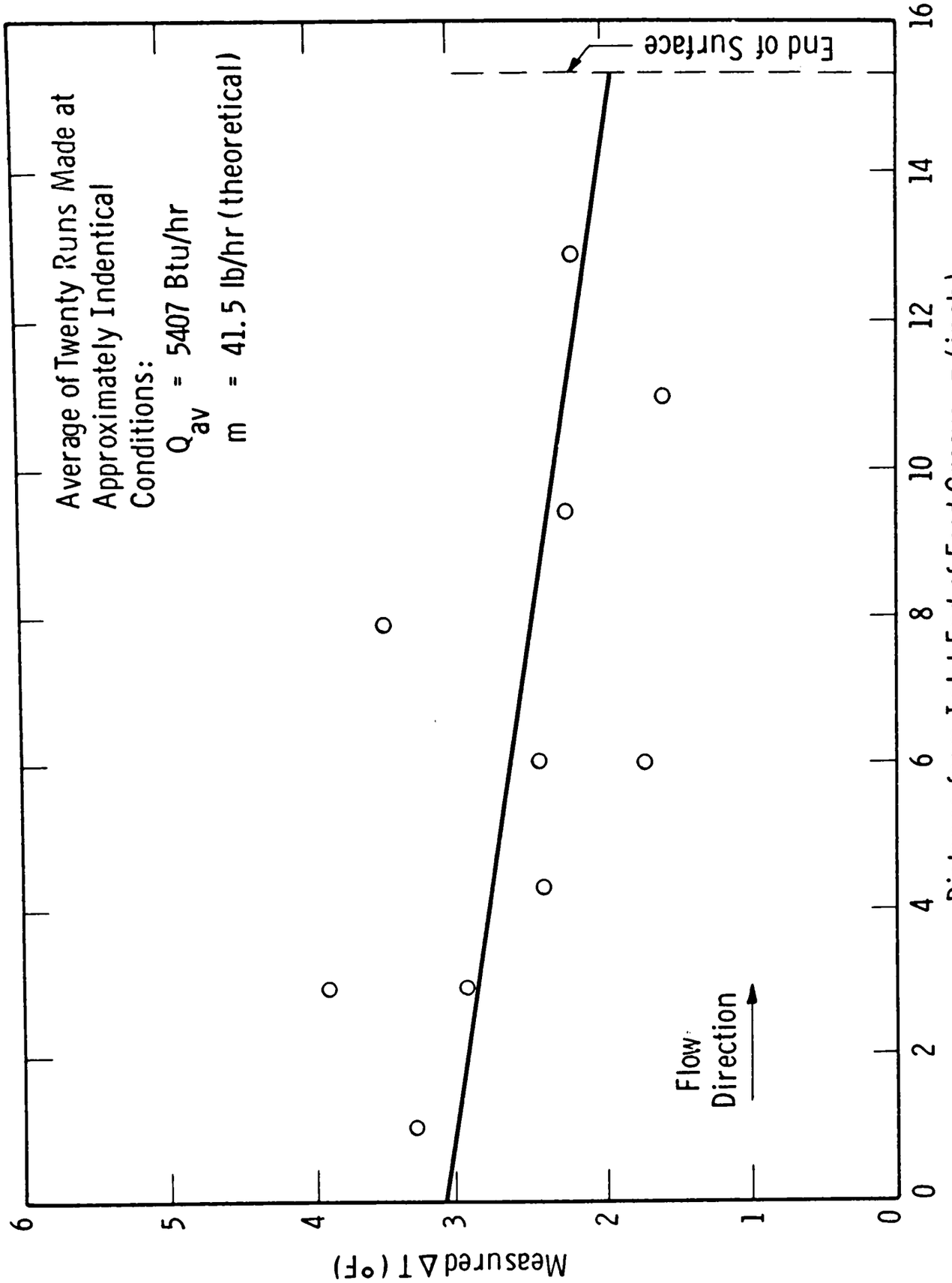

Fig. IV-25—Variation of ΔT along the coarse surface

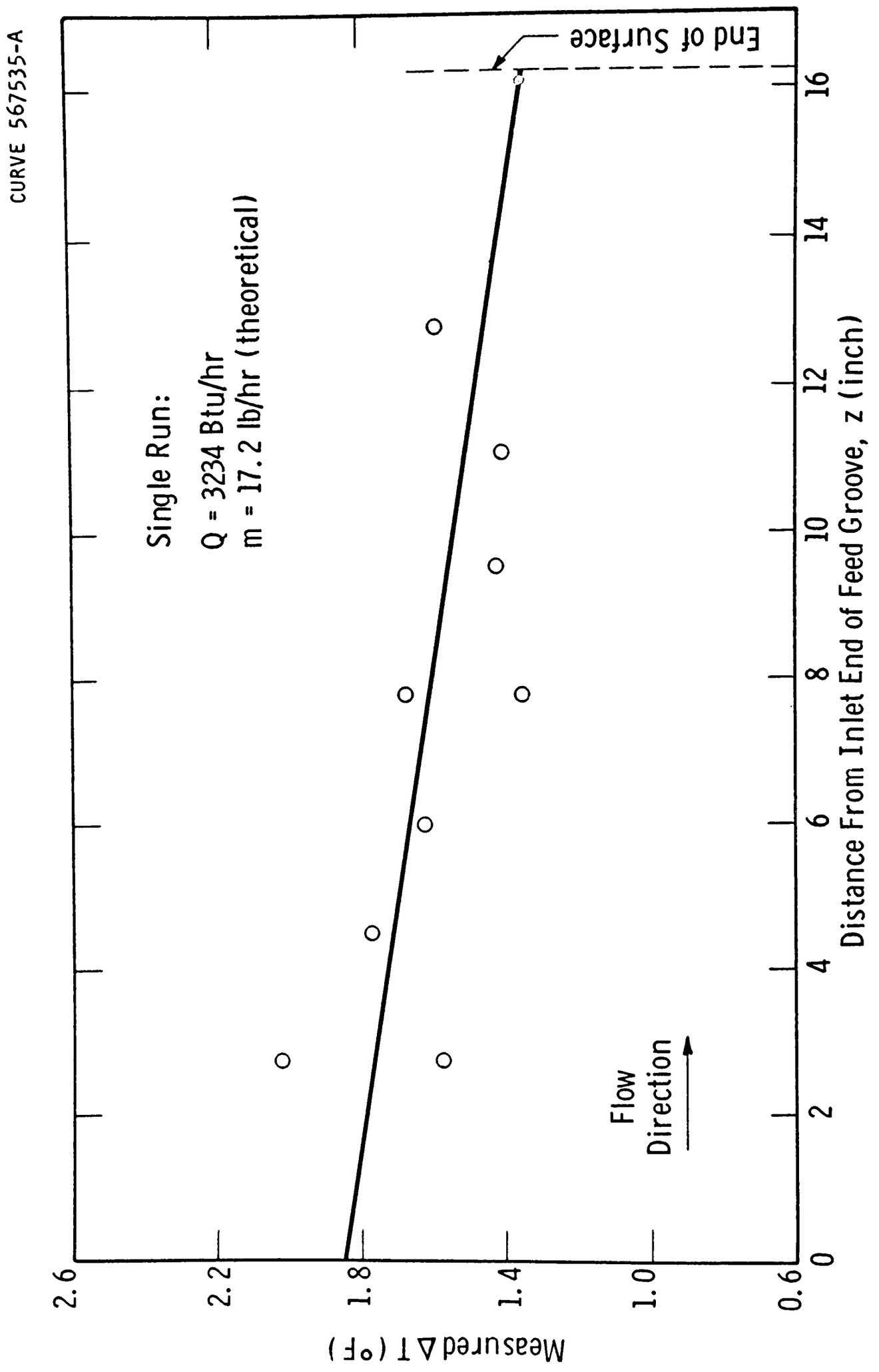

Fig. IV-26—Variation of Δ T along the fine surface

Task V - System Analysis and Surveillance

Task Description

The ultimate goal of this program is the attainment of a low cost saline conversion system. The first cost, life, and operating costs make up the overall water production costs. The accomplishment of the goal of low cost water requires a continuing examination and evaluation of experimental information, new or improved designs, new manufacturing techniques, the results of all tests, and costs and factors which contribute to costs.

The success of the overall program depends on the successful attainment of the individual goals of Tasks I through IV; plus the integration and application of all the acquired technology, material and manufacturing information, and economic factors into a system for producing low cost water. Attainment of the Task I and II goals provides required technology and demonstrates system and component feasibility. The meeting of the Task III goals provides material, economic and technical information. Economic as well as technical information results from the efforts of Task IV. An important piece of information which is not furnished by these other tasks is the required manufacturing and cost information for fabricating the heat transfer module. A major goal of Task V is to obtain this information. The other important goals of Task V include:

1. Evaluation of the results of Tasks I through IV plus the manufacturing data in terms of defining the system operating conditions.
2. Evaluation and integration of the acquired technology and economic factors into an analysis of the system economics.

Summary

Manufacturing studies showed that the conceptual heat transfer module could be fabricated of aluminum or tin plated carbon steel at costs of 0.495$/sq. ft. and 0.370$/sq. ft. respectively. Based on the results obtained from all of the tasks and a re-evaluation of some of the system component costs, the Thin Film Vapor Compression system was re-optimized. The results of this optimization show that the cost per 1,000 gallons is comparable to current multistage flash conversion plants.

Technical Approach

Each of the preceding tasks was concerned with the verification of certain assumptions made in the Westinghouse proposal and/or the acquiring of required technology. Toward this end, experimental apparatus was designed and manufactured, and tests were run.

Unlike the other tasks the approach used in meeting the Task V goals did not require a major hardware development program. Part of the information sought was the verification of the assumption that the heat transfer module could be manufactured in the required geometrical shape at a cost of less than 1.00$/sq. ft. To prove this by actually fabricating a complete module would have been too costly in that only one module could be made, using one material, and one method of manufacture. Since acquiring one piece of hardware would not really satisfy the intended goal; and, since more than one material and method of fabrication were under consideration, it was decided that a broader, though perhaps, slightly less positive approach be used to satisfy the task goal.

The Westinghouse Headquarters Manufacturing Planning group was asked to perform a manufacturing study to determine methods and costs for fabricating the heat transfer module from the four materials under consideration. This study and the results obtained are fully described in the Manufacturing Study Final Report which is included in Appendix B of this report.

The conceptual compressor unit is illustrated in Figures V-1, V-2, and V-3. The capacity of this unit would be about 15,000 GPD.

Conclusions and Recommendations

Based on the experimental results obtained, the technology acquired, the results of the manufacturing study, and the optimization of the system economics, it can be concluded that:

1. A thin film vapor compression pilot plant can be designed.
2. At the completion of a pilot plant development program, a Thin Film Vapor Compression system could be built which would produce potable water at a cost comparable to current multistage flash plants.
3. A compressor would probably have to be developed for the post pilot plant system application.
4. The operating temperature of the system should be between 120° and 150°F and that some further work should be required to permit raising the operating temperature to 150°F.
5. The reduction in total operating cost for temperatures above 150°F are not significant enough to warrant the additional work required to permit operations above 150°F.
6. While the improvement in heat transfer using the programmed surface was significant, it was not substantial enough to warrant the effort required to reduce the concept to a practical heat transfer surface for this application.

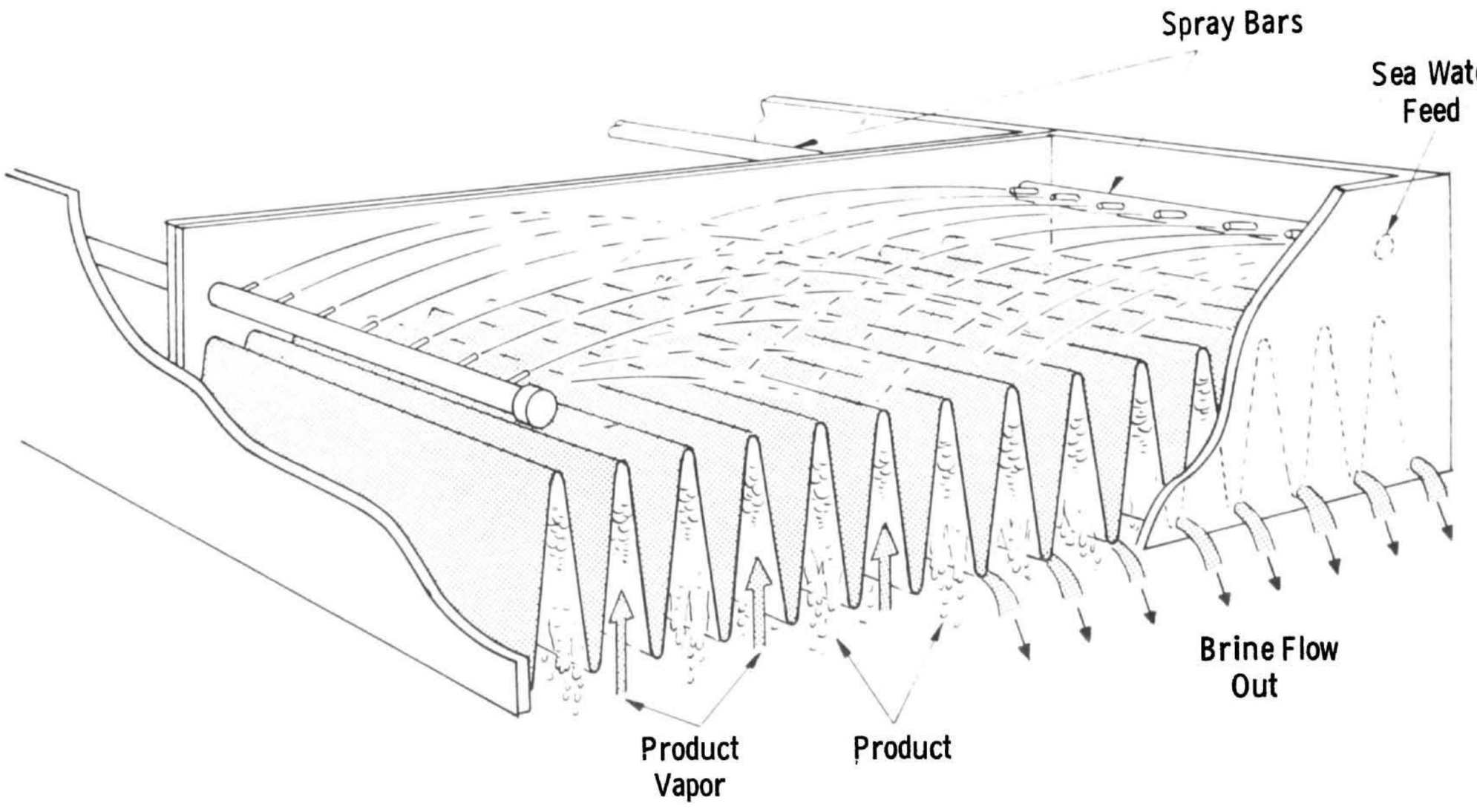

Fig. V-1 —Heat transfer module

DWG. 4498096

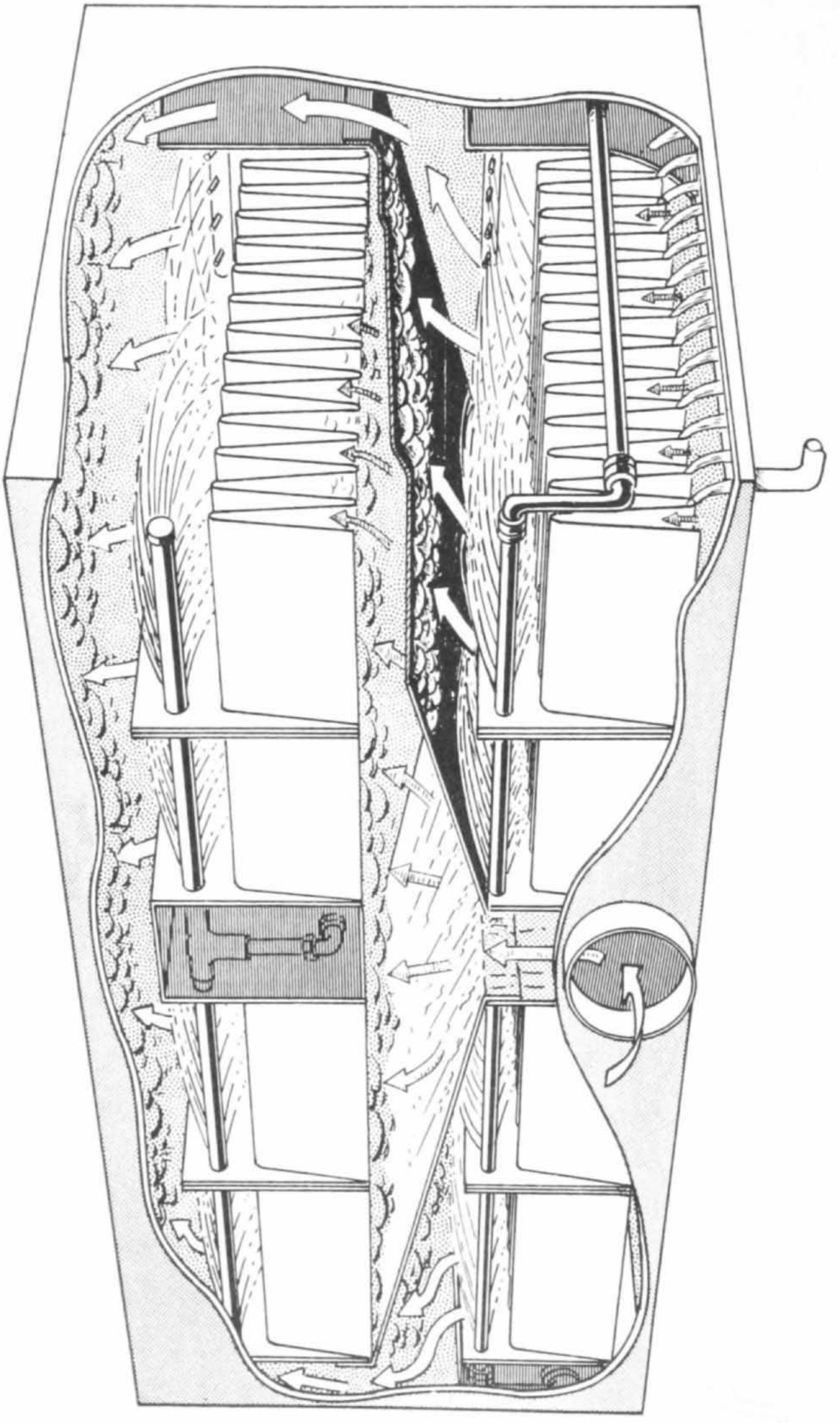

Fig. V-2 —Compressor/heat transfer unit (8 heat transfer modules)

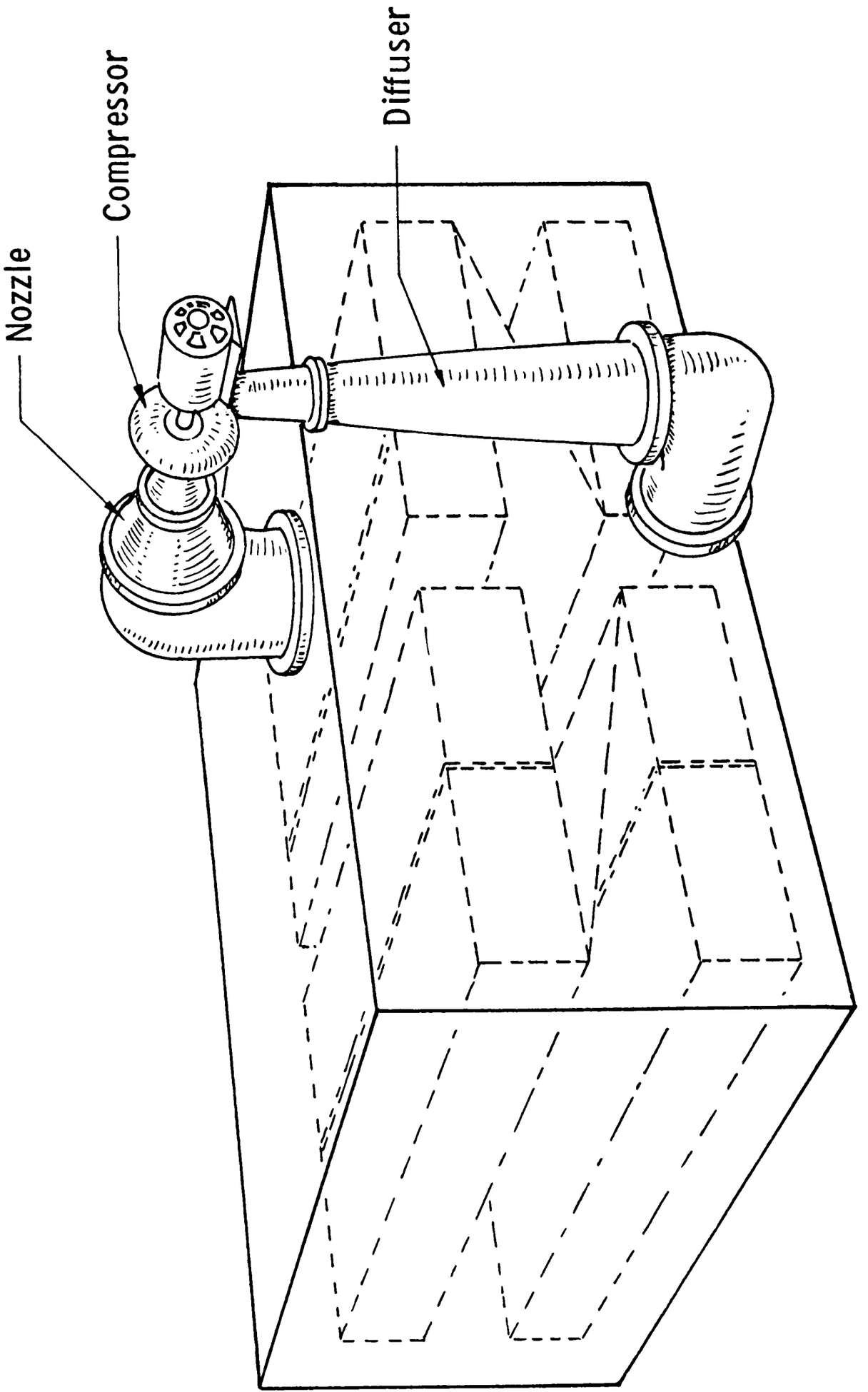

Fig. V-3 –Basic compressor unit

NOMENCLATURE

A	heat transfer surface area	ft^2
B.P.E.	boiling point elevation(1)	F^o
h	film coefficient	$Btu/hr\text{-}ft^2\text{-}F^o$
H	heat transfer surface height	ft
k	thermal conductivity(3)	$Btu/hr\text{-}ft\text{-}F^o$
p	absolute pressure	in. H_2O
ΔP	pressure difference between evaporator and condenser	in. H_2O
Q_i	volume flow of inerts at condenser conditions	cfm
Q_v	volume flow of vapor at condenser conditions	cfm
R	circulation ratio (W_s/W_f)	
R_x	circulation ratio $x_b/(x_b-x_o)$	
T	saturation temperature	°F
Δt_o	overall temperature difference	°F
U_o	overall heat transfer coefficient	$Btu/hr\text{-}ft^2\text{-}°F$
w	fluid mass flow	$lb_m/hr\text{-}ft$
x_{metal}	heat transfer surface thickness	ft
x	brine salinity	%
y	steady state film thickness at any point	ft
λ	latent heat of vaporization(4)	Btu/lb_m
μ	viscosity(5)	centipoise
ρ	density(3)	lb_m/ft^3
σ	surface tension	dynes/cm

Subscripts

b	brine
c	condensation
d	effect of fouling
e	evaporating
f	fresh water
m	mean or mass
o	initial or overall
s	sea water

REFERENCES

1. R. L. Clark, K. J. Nabavian, and L. A. Bromley, A.C.S., Advances in Chemistry Series 27, 21-26 (1960).

2. Jacob, M., "Heat Transfer", Vol. I, John Wiley and Sons, New York, 1958.

3. Office of Saline Water, R&D Progress Report No. 25.

4. Keenan and Keyes, "Thermodynamic Properties of Steam", First Edition, John Wiley and Sons, New York.

5. International Critical Tables.

APPENDIX A-I & II-1

The basic equations used to calculate the performance of the thin film heat transfer module are taken from Nusselt theory as reported by Jakob[2]. They vary slightly from the form, nomenclature and units found in this reference.

They include

$$\gamma = \left(\frac{3\omega\mu}{\rho^2} \times 0.58 \times 10^{-8} \right)^{1/3} \qquad \text{(I-1)}$$

$$\omega_f = \left(\frac{4}{3} \frac{\gamma_{cm}}{.001} \right)^3 \frac{\rho^2}{3\mu} \times .99776 \times 10^{-4} \qquad \text{(I-2)}$$

$$\frac{H}{\left(\frac{4}{3} \frac{\gamma_{cm}}{.001} \right)^3} = \left(\frac{\lambda\rho^2}{3\mu} \right)_f \frac{1}{U_o \Delta t_o} \times .99776 \times 10^{-4} \qquad \text{(I-3)}$$

The overall coefficient was found from:

$$\frac{1}{U_o} = \frac{\gamma_{cm}}{k_f} + \frac{\gamma_{metal}}{k_{metal}} + \frac{1}{h_d} + \frac{\gamma_{em}}{k_{bm}} \qquad \text{(I-4)}$$

for no fouling $1/h_d = 0$.

The relationships between the inlet, mean and outlet concentrations are:

$$x_m = x_o \left(\frac{R - \frac{1}{2}}{R - 1} \right) \tag{I-5}$$

$$x_b = x_o \left(\frac{R}{R - 1} \right) \tag{I-6}$$

The overall driving temperature difference is Δt_o and is the difference between the condensing temperature and the mean surface temperature of the evaporating film.

$$\Delta t_o = T_c - T_{bm} \tag{I-7}$$

where $T_{bm} = T_{sea} + \Delta BPE$ from x_o to x_m evaluated at T_{sea}.

The experimental values of U_o were calculated using the following equation

$$U_o = \frac{\omega_f \lambda}{A \Delta t_o} \tag{I-8}$$

APPENDIX A-I & II-2

In order to verify the theory used in designing the proposed system, the experimental heat transfer surface had to be representative of that of the proposed system. Fouling and corrosion effects, since they were being investigated in Task III, were neglected here. In fact, the surface material (Monel) chosen for Tasks I and II was selected to minimize these considerations.

The operating conditions for which the experimental heat transfer surface was designed were the same as those of the proposed system, i.e., $T_{sea} = 120°F$, $T_c = 122°F$ and a sea water feed rate of 4.60 lb_m/hr-ft. The height of the heat transfer surface for a given set of operating conditions varies with the material selection; and for the materials under consideration, 1.5 ft was a representative height.

Having set the operating conditions, material and surface height, the product flow, W_f, film thicknesses, Y_{em} and Y_{cm}, and therefore the overall heat transfer coefficient could be calculated using Equations I-1, I-2, I-3, and I-4. This is an iterative calculation. Various values of "R" are assumed until Equation I-3 is satisfied. Neglecting the effect of fouling the design values of the overall heat transfer coefficient, product flow, circulation ratio and $\Delta P/P_e$ are:

$$U_o = 842$$

$$w_f = 2.09$$

$$R = 2.2$$

$$\Delta P/P_e = .0737$$

Using the same set of equations and holding the surface height, sea water feed rate, and evaporator temperature, the "off-design" values of the above parameters were also calculated by assuming a range of values for T_c and R. The theoretical variation of U_o with product flow and $\Delta P/P_e$ with circulation ratio are shown in Figures I-9 and I-11.

APPENDIX A-I & II-3

Sample calculation of U_o assuming no fouling for:

T_{sea} = 120°F
x_o = 3.40%
w_s = 4.60 lb_m/hr-ft
R = 2.20

1.	R	2.20
2.	x_o	3.40
3.	x_m	4.82
4.	x_b	6.23
5.	w_s	4.60
6.	w_f	2.09
7.	w_b	2.51
8.	ρ_f	61.675
9.	μ_f	.550
10.	k_f	.370
11.	ρ_s	63.3
12.	μ_s	.598
13.	k_s	.365
14.	ρ_b	64.67
15.	μ_b	.635
16.	k_b	.361
17.	$w_f (3\mu/\rho^2)_f \times .58 \times 10^{-8}$	5.25×10^{-12}
18.	$\sqrt[3]{(17)}$	.000174
19.	$y_{cm} = 3/4$ (18)	.0001305
20.	$w_s (3\mu/\rho^2)_s \times .58 \times 10^{-8}$	11.96×10^{-12}
21.	$y_{eo} = \sqrt[3]{(20)}$	.000229
22.	$w_b (3\mu/\rho^2)_b \times .58 \times 10^{-8}$	6.62×10^{-12}
23.	$y_b = \sqrt[3]{(22)}$	.000188

24.	y_{em}	.000209
25.	x_{metal}	.00025
26.	k_{metal}	9.6
27.	x_{metal}/k_{metal}	.000260
28.	y_{cm}/k_f	.000353
29.	k_{bm}	.363
30.	y_{em}/k_{bm}	.000576
31.	$1/U_o$	.001189
32.	U_o	842.
33.	Δt_o	1.70
34.	B.P.E. @ x_o	.57
35.	B.P.E. @ x_m	.87
36.	$T_{bm} = T_{sea} + \Delta$B.P.E. x_o x_m	120.30
37.	$T_c = T_{bm} + \Delta t_o$	122.00
38.	$\Delta t_{sat} = \Delta t_o$ + B.P.E. @ x_m	2.57
39.	ΔP	3.40
40.	P_e	46.15
41.	$\Delta P/P_e$	.0737

APPENDIX A-I & II-4

Sample Calculation of Experimental Heat Transfer Performance - Tasks I & II.

The data was taken from Task II, Run No. 3, 6-12-63, on sea water.

Items marked with an asterisk were obtained by direct measurement. Salinities were obtained by titration.

All flows are for two 1 foot wide plates 1.5 ft high.

1.	$*w_b$ (cc/min)	39.0
2.	Sp. gr.	1.035
3.	w_b (gms/min)	40.4
4.	w_h (lbs/hr)	5.35
5.	$*w_f$ (cc/min)	31.6
6.	Sp. gr.	.990
7.	w_f (gms/min)	31.3
8.	w_f (lbs/hr)	4.13
9.	w_s (lbs/hr)	9.48
10.	$*x_o$	3.40
11.	x_m	4.71
12.	$*x_b$	6.02
13.	B.P.E. @ x_o (F°)	.57
14.	B.P.E. @ x_m (F°)	.84
15.	B.P.E. @ x_b (F°)	1.15
16.	$R = (w_s/w_f)$	2.30
17.	$R_x = x_b/(x_b-x_o)$	2.30
18.	$*T_{tank}$ (°F)	119.5
19.	T_{sea} (°F)	119.5
20.	$T_{bm} = (T_{sea} + \Delta B.P.E.\ x_o\ \ x_m)$(°F)	119.27
21.	$*\Delta P$ (in. H_2O)	3.35
22.	Δt_{sat} (F°)	2.50

23.	Δt_o (Δt_{sat} - B.P.E. @ x_m) (F°)	1.66
24.	T_c = (T_{bm} + Δt_o) (°F)	122.03
25.	P_{evap} (P_{sat} @ T_{tank})	46.2
26.	$\Delta P/P_{evap}$	.0725
27.	λ	1025.
28.	No-flow area (% by observation)	6.
29.	U_o = $w_f \lambda / A \Delta t_o$ (Btu/hr-ft^{2}F°)	877.

APPENDIX A-I & II-5

DEVELOPMENT OF THE RELATIONSHIP BETWEEN $\Delta P/P_e$ AND THE COMPRESSOR PRESSURE RATIO AND BETWEEN $\Delta P/P_e$ AND COMPRESSOR WORK

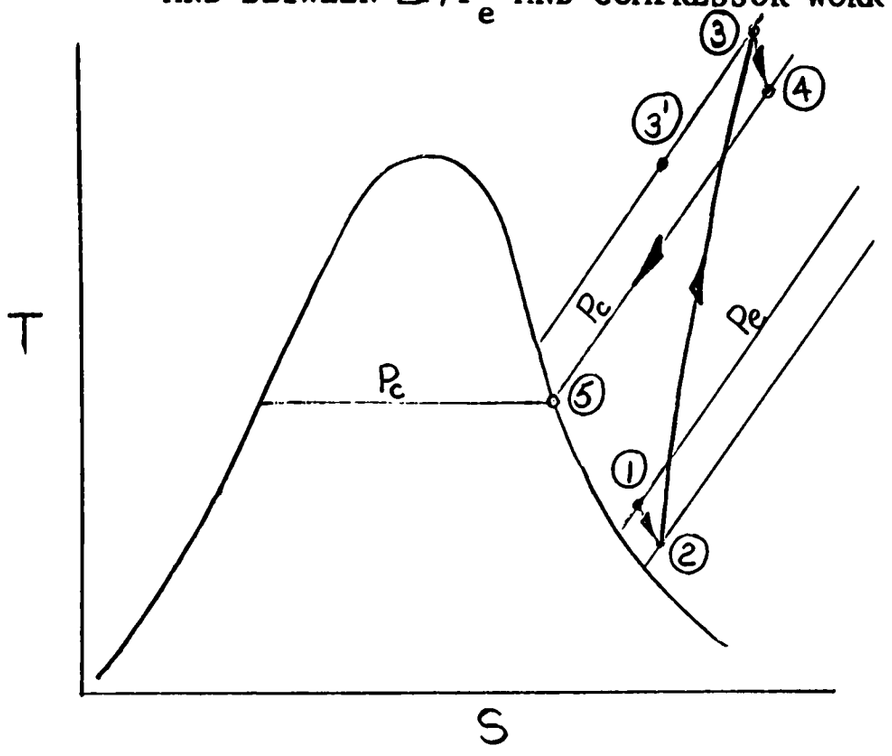

1. State conditions of vapor just after leaving the evaporating film. $P_1 = P_{evaporator} = P_e$ = saturation pressure @ T_{sea}

2. State conditions of vapor at compressor inlet
   P_2-P_1 = ducting pressure losses before compression (adiabatic process assumed)

3. State conditions of vapor after compression
   $\Delta h_c = h_3-h_2$ = work of compression (Btu/#)
   P_3/P_2 = compressor pressure ratio

3'. State conditions of vapor after isentropic compression

$$\Delta h_c' = \eta_c \Delta h_c = h_3' - h_2$$

4. State conditions of vapor at inlet of condenser
   P_3-P_4 = ducting pressure losses after compression (adiabatic process assumed)
   $P_4 = P_5 = P_c$ = saturation pressure @ T_c

$$\Delta P = P_c - P_e = P_4 - P_1$$ By definition

$$\frac{\Delta P}{P_e} = \frac{P_4 - P_1}{P_1} = \frac{P_4}{P_1} - 1$$

$$\therefore \frac{P_4}{P_1} = \frac{\Delta P}{P_e} + 1$$ = compressor pressure ratio with no duct losses since $P_1 = P_2$ and $P_3 = P_4$

but with duct losses

$$\frac{P_3}{P_2} = \frac{P_4}{P_1} \times \frac{P_1}{P_2} \times \frac{P_3}{P_4}$$

$$= \left(\frac{\Delta P}{P_e} + 1\right) \frac{P_1}{P_2} \times \frac{P_3}{P_4}$$ = compressor pressure ratio with losses

The compressor efficiency,

$$\eta_c = \frac{\Delta h_c'}{\Delta h_c} = \frac{c_p(T_3' - T_2)}{c_p(T_3 - T_2)}$$

$$= \frac{T_3'/T_2 - 1}{\frac{\Delta h_c}{T_2}} = \frac{\left[(P_3/P_2)^{\frac{\gamma-1}{\gamma}} - 1\right] c_p}{\frac{\Delta h_c}{T_2}}$$

$$\therefore \Delta h_c = \frac{C_p T_2 \left[\left(P_3/P_2 \right)^{\frac{\gamma-1}{\gamma}} - 1 \right]}{\eta_c}$$

$$= \frac{C_p T_2}{\eta_c} \left[\left(\frac{P_4}{P_1} \times \frac{P_1}{P_2} \times \frac{P_3}{P_4} \right)^{\frac{\gamma-1}{\gamma}} - 1 \right]$$

or $$\Delta h_c = \frac{C_p T_2}{\eta_c} \left[\left\{ \left(\frac{\Delta P}{P_e} + 1 \right) \frac{P_1}{P_2} \times \frac{P_3}{P_4} \right\}^{\frac{\gamma-1}{\gamma}} - 1 \right] \qquad \text{(I \& II-3-1)}$$

for the minimum work of compression (no duct losses).

$$\Delta h_{c\,MIN} = \frac{C_p T_2}{\eta_c} \left[\left(\frac{\Delta P}{P_e} + 1 \right)^{\frac{\gamma-1}{\gamma}} - 1 \right] \qquad \text{(I and II-3-2)}$$

Equations (I & II-3-1) and (I & II-3-2) show the relationship between the parameter, $\Delta P/P_e$, and the compressor work.

NOMENCLATURE

$\mathcal{A}$	amplitude growth factor
A	area of flat test surface
c	wave velocity; also, concentration
d	distance of thermocouple junction from flat surface inside metal
f	fraction of flat plate area wetted
F	function symbol
g	acceleration of gravity (= 4.18×10^8 ft/hr^2)
h	evaporation heat transfer coefficient
k	thermal conductivity of liquid (= 0.393 Btu/hr-ft-F°)
K	thermal conductivity of test plates (= 119 Btu/hr-ft-F°)
l	film length
L	vertical length of test surface
m	mass flow rate
n	number of feed grooves
N_y/N_x	shape factor used for programmed surface temperature difference correction
q	heat flux
Q	total heat rate
r	radius of curvature
R	runoff - defined as the fraction of inlet flow occurring at the outlet end of the film
s	coordinate along curved programmed surface normal to feed groove
t	depth of feed groove
T	temperature
$\mathcal{T}$	period of a cycle

$\mathcal{U}$	unit step function
u_o	flow velocity at free surface of film
V	volume flow rate in a single feed groove
w	width of feed groove (constant)
x,y,z	length coordinates; z is measured from inlet end of groove
z'	length coordinate along a feed groove measured from point where t = o and directed opposite to z
Z,Z'	dimensionless distances
$\frac{dp}{ds}$	pressure gradient in film (constant along s)
$\frac{dV}{dz}$	volume flow rate per unit groove length for a single groove
ΔT	temperature difference across film
α,β	temperature correction factors for the programmed surfaces (= 1/(2nKL))
δ	film thickness
ξ	dimensionless variable (= $\frac{\pi}{4}\frac{w}{t}$)
θ	pulse time ratio: flow time divided by period of cycle
λ	latent heat of vaporization (= 970 Btu/lb)
μ	coefficient of viscosity (= 0.684 lb/hr-ft)
ν	kinematic viscosity (μ/ρ)
ρ	density of liquid (= 60 lb/ft^3)
σ	surface tension
$\Delta\sigma$	surface tension difference: that evaluated at the temperature of the free surface minus that evaluated at the wall
$\tilde{\tau}$	time
ϕ	volume feed rate function

(Subscripts)

exp	shows that h is experimentally determined
th	shows that h is theoretically determined
pr	refers to a programmed surface
o,oe	o refers to the inlet thickness of a steady film, except in Appendix A-IV-4, where o refers to the local steady film thickness and oe refers to the inlet thickness of the same film
av	refers to an average
c	refers to the coarse surface
f	refers to the fine surface

REFERENCES

1. Nusselt, W., Z. Ver. Dent. Ingr., Vol. 60, p. 541 (1961); also, E. R. G. Eckert, Heat and Mass Transfer, pp. 334-336, McGraw-Hill (1959).

2. Gregorig, R., Z. Ang. Math and Physik, Vol. X, pp. 36-49 (1954).

3. Norman, W. S., and Binns, W. T., "The Effect of Surface Tension Changes on the Minimum Wetting Rates in a Wetted Rod Distillation Column," Trans. Inst. Chem. Engrs., Vol. 38, pp. 294-300 (1960).

4. "A Minimum Cost Method of Obtaining Fresh Water from the Ocean," Westinghouse Research Report 007-H000-R1X - C. Zener and E. V. Somers.

5. "Gauge for Monitoring Oxygen Content of Helium," Westinghouse Research Report 62-172-564-R1 - W. M. Hickam, et al.

6. "Effect of Surface Tension Gradient on Thin Liquid Film Stability," Research Memo 62-118-542-M1 - W. A. Stewart.

7. Westinghouse Proposal for Research and Development of Thin Film Vapor Compression Saline Water Conversion System - To OSW, Dept. Interior, Washington, D.C., October 1961, Appendix B, Report 7.

8. McAdams, W. H., Heat Transmission, McGraw-Hill, 3rd ed., p. 330 (1954).

9. Brooke-Benjamin, T., "Wave Formation in Laminar Flow Down an Inclined Plate," Jnl. Fluid Mechanics, Vol. 2, pp. 554-574, (1957).

10. Carslaw, H. S., and Jaeger, J. C., Conduction of Heat in Solids, Oxford, 2nd ed. 1959, p. 171, eq. (6); also Dryden, H. L., et al, Hydrodynamics, Dover, 1956, p. 197.

11. "Design Criteria for Uniform Vapor Production on a Programmed Evaporator Surface," Westinghouse Research Report 63-965-416-R1 - J. A. Cyphers.

12. Adam, N. K., The Physics and Chemistry of Surfaces, Oxford, 3rd ed., p. 14 (1941).

Appendix A-IV-1

Geometrical Factors for the Flat Surface.
Numerical Values Used in the Preparation of Tables IV-1, IV-2 and IV-4

$A = 5.23$ ft (37 in x 20-3/8 in)

$d = 0.11/12$ ft

$L = 3.08$ ft

$d/KA = 1.5 \times 10^{-5}$ F°/Btu-hr

Appendix A-IV-2

Programmed Surface Geometrical Factors. Numerical Values Used in the Preparation of Table IV-5

A. Coarse Surface

width of test surface: 5.5 in.
length of feed grooves (L): 15.3 in.
width of feed grooves (w): 0.018 in.
pitch of feed grooves: 0.0937 in.
number of feed grooves (n): 58
taper of feed grooves: 1 mil per in.
formula for feed groove depth (t):

$$t = 18.3 \text{ mils} - z \frac{\text{mils}}{\text{in}} \quad (o \leq z \leq 15.3 \text{ in})$$

film length from Fig. IV-16 (l): 41.5 mils
shape factor (N_y/N_x): 1.5
total film area based on l: 0.511 ft^2
total projected plate area: 0.584 ft^2
theoretical total mass loss from end of feed groove (Δm): 0.76 lb/hr
temperature correction factor (β):

$$\beta = 1/(116 \text{ KL}) = 5.682 \times 10^{-5} \text{ hr F°/Btu}$$

pressure gradient (dp/ds): $3.56 \rho g$

B. Fine Surface

width of test surface: 5.5 in.
length of feed grooves (L): 16.25 in.
width of feed grooves (w): 0.0084 in.
pitch of feed grooves: 0.046 in.
number of feed grooves (n): 120
taper of feed grooves: 1.37 mils/in
formula for feed groove depth (t):

$$t = 22.25 \text{ mil} - 1.37 \text{ z mil/in} \quad (o \leq z \leq 16.25 \text{ in})$$

film length from Fig. IV-17 (l): 16.6 mils
shape factor (N_y/N_x): 2.1
total film area based on l: 0.449 ft^2
total projected plate area: 0.621 ft^2
theoretical total mass loss from end of feed groove (Δm): 0 lb/hr
temperature correction factor (α):

$$\alpha = 1/(240 \text{ KL}) = 2.586 \times 10^{-5} \text{ hr F°/Btu}$$

pressure gradient (dp/ds): $14.2 \rho g$

Appendix A-IV-3

Development of the Equation for the Heat Transfer Coefficient Applying to an Evaporating, Falling Liquid Film

Nusselt's hypothesis readily provides the basic expression for a vertically falling liquid film undergoing evaporation at constant wall temperature and constant, but lower, vapor temperature:

$$\frac{\rho g}{\mu} \delta^2 \frac{\partial \delta}{\partial z} + \frac{k \Delta T}{\lambda \rho} \frac{1}{\delta} = - \frac{\partial \delta}{\partial \tau} \qquad (1)$$

Here δ is the film thickness and is a function of the vertical position, z, and the time, τ . In developing this equation, the usual assumptions regarding momentum, continuity, and energy transfer have been made. For the steady state case, this equation reduces to the separable form,

$$\frac{\rho g}{\mu} \delta^3 \frac{d\delta}{dz} + \frac{k \Delta T}{\lambda \rho} = 0 \qquad (2)$$

which has for its solution,

$$\delta^4 - \delta_o^4 = - C z \qquad (3)$$

Here δ_0 is the inlet thickness and $C \left(= \frac{4 \mu k \Delta T}{\rho^2 g \lambda}\right)$ is a constant. The meanings of the various symbols are given in the Nomenclature.

In order to derive an expression for the film coefficient applicable to the whole plate, i.e., for $0 \leq z \leq L$, we must define an average heat transfer coefficient, h, in terms of local values of δ along the plate. We therefore set

$$h = k \left(\frac{1}{\delta}\right)_{av} = \frac{k}{L} \int_0^L \frac{1}{\delta} dz \qquad (4)$$

We now can express h in terms of volume flow rate or (constant density) mass flow rate. Since the average flow velocity at any point along the plate is proportional to the square of the film thickness, that is, proportional to δ^2 (as a consequence of the assumed parabolic flow) and since the throughput area per unit plate width is proportional to δ , the average flow rate must be proportional to δ^3. We now define a runoff term, designating it by the symbol, R, as the ratio of the flow rate at z = L to the flow rate at z = 0. The previous discussion thus leads to the expression

$$R = \left(\frac{\delta_L}{\delta_0}\right)^3 \tag{9}$$

Inserting this result in equation (8b) gives

$$h = k\,\frac{4}{3}\left(\frac{1}{CL}\right)^{1/4}\frac{1-R}{(1-R^{4/3})^{3/4}} \tag{10}$$

For the no-runoff case, we see that

$$h_{no\text{-}runoff} = k\,\frac{4}{3}\left(\frac{1}{CL}\right)^{1/4} \tag{11}$$

and that the ratio,

$$\frac{h}{h_{no\text{-}runoff}} = \frac{1-R}{(1-R^{4/3})^{3/4}} \tag{12}$$

Equation (11) is of interest because it is identical with the Nusselt result for film condensation (Ref. 1). This result also shows that the maximum value of h obtainable with an evaporating film is given by the Nusselt equation. Equation (10) shows how the Nusselt result may be modified by a runoff factor to apply to evaporating films.

The complete expression for the average film coefficient for any falling liquid film under evaporating conditions may now be written by inserting $C = \frac{4\mu k \Delta T}{\rho^2 g \lambda}$ in equation (10). Thus,

$$h = 0.943 \left(\frac{\rho^2 g \lambda k^3}{\mu \Delta T L} \right)^{1/4} \frac{(1-R)}{(1-R^{4/3})^{3/4}} \qquad (13a)$$

or alternatively,

$$h = 0.943 \left(\frac{\lambda \rho^2 k^3}{\mu} \right)^{1/4} \left(\frac{g}{\Delta T L} \right)^{1/4} \frac{(1-R)}{(1-R^{4/3})^{3/4}} \qquad (13b)$$

This last form is useful because it separates the previous result into three groups of variables. The first two of which, one a physical properties group and the other an operating and geometry group, are employed by McAdams (Ref. 8) in an alignment chart prepared for quick estimation of film-condensation coefficients. By application of the third group, the runoff factor, $(1-R)/(1-R^{4/3})^{3/4}$, to the h-value determined from this chart, we can use this chart for evaporating films as well as condensing films, for all the many fluids contained in the chart.

Appendix A-IV-4

Unsteady Falling Liquid Films.

In this section some important formulas are developed pertaining to pulsed and periodic flow phenomena.

A simple theoretical treatment bearing on evaporating, pulse feed, falling films will be given and compared, as far as possible, with existing unsteady film theory. The method of small disturbances will be applied to equation (1) of Appendix A-IV-3. This equation may be written in the form

$$\frac{\rho g}{\mu} \delta^3 \frac{\partial \delta}{\partial z} + \frac{k \Delta T}{\lambda \rho} = - \delta \frac{\partial \delta}{\partial \tau} \qquad (1)$$

If now the conditions,

$$\delta = \delta_0 + \delta_1 \qquad \frac{\partial \delta_0}{\partial \tau} = 0 \; ; \quad \delta_1 << \delta_0 \qquad (2)$$

and

$$\delta_0^4 = \delta_{0e}^4 - \frac{4 \mu k \Delta T}{\rho^2 g \lambda} z \qquad (3)$$

are applied, equation (1) may be transformed to

$$\frac{\rho g \delta_0^2}{\mu} \frac{\partial \delta_1}{\partial z} - \frac{3 k \Delta T}{\delta_0^2 \lambda \rho} \delta_1 = - \frac{\partial \delta_1}{\partial \tau} \qquad (4)$$

Consider now an arbitrary disturbance function $\delta_1 (z, \tau)$ whose inlet value is $\delta_1 (o, \tau)$. Upon taking the Laplace transform of equation (4) and using the Second Shifting Theorem, the solution is found to be

$$\delta_1 (z, \tau) = \left(\frac{\delta_{0e}}{\delta_0} \right)^3 \delta_1 (o, \tau - \tau') \; \mathcal{U}(\tau - \tau') \qquad (5)$$

where $\mathcal{U}$ is the unit step function and

$$\tau' = \frac{\lambda \rho}{2 k \Delta T} \left(\delta_{oe}^2 - \delta_o^2 \right) \tag{6}$$

The speed of descent of the pulse is given by

$$\frac{dz}{d\tau'} = \frac{\rho g}{\mu} \delta_o^2 = 2 u_o \tag{7}$$

with

$$u_o = \frac{1}{2} \frac{\rho g}{\mu} \delta_o^2 \tag{8}$$

This result shows that the speed of descent is twice the speed of the undisturbed surface, a well-known result in non-heated film analyses. The amplitude factor, $A = (\delta_{oe}/\delta_o)^3$, changes with the movement of the disturbance. From its form it is easy to see that it may also be expressed as a ratio of the volume flow rate at inlet divided by the local value at the pulse location. It may additionally be expressed

$$A = \left(1 + \frac{2 k \Delta T}{\lambda \rho \delta_o^2} \tau \right)^{3/2} \tag{9}$$

And this expression may be approximated

$$A = e^{\gamma_1 \tau} \tag{10}$$

where

$$\gamma_1 = \frac{3 k \Delta T}{\lambda \rho \delta_o^2} \tag{11}$$

This amplitude factor is described in terms of thermal and hydrodynamic quantities. It may now be compared with a result of Brooke-Benjamin (Ref. 9) for the amplitude factor of a non-heated falling film influenced by surface tension. His result, obtained from a stability analysis based on the Orr-Summerfeld equation, describes the wave character of the most prominent wave of a film. The results follow:

$$A = e^{\gamma_2 \tau} \tag{12}$$

$$\gamma_2 = \frac{32}{75} \frac{u_o^4 \rho}{g \sigma} = \frac{2}{75} \frac{g^3}{\nu^4} \frac{\rho}{\sigma} \delta_o^8 \tag{13}$$

$$t = \frac{z}{2 u_o} \quad ; \quad u_o = \frac{1}{2} \frac{\rho g}{\mu} \delta_o^2 \tag{14}$$

$$\lambda = \frac{\sqrt{5}\, \pi\, \delta_o^{1/2} \sigma^{1/2}}{\rho^{1/2} u_o} \tag{15}$$

$$T = \frac{\lambda}{2 u_o} \tag{16}$$

When property values pertinent to pure water at 212°F and a film thickness of 3 mils are used with the last two equations, there results a wave length, λ, equal to 5 ft and a period, T, of 8 seconds. Therefore, on the basis of these hydrodynamic equations, it is evident that the most effective pulse feed frequency would be one corresponding to the natural period of 8 seconds.

A most simple evaluation of the effect of a periodically changing film amplitude on heat transfer will now be given. In this approach the film thickness is represented by a sinusoidal component superposed on a fixed component. The thickness of the film can then be expressed

$$\delta = \delta_0 + \delta_1 \cos \frac{2\pi}{\lambda}(z - ct) \tag{17}$$

where it is implied that $C = (\rho g/\mu)\delta_0^2$. Now, for such a film, the heat flux averaged over one time cycle may be written

$$q = \frac{1}{\tau}\int_t^{t+\tau} \frac{k\,\Delta T\, d\xi}{\delta_0 + \delta_1 \cos \frac{2\pi}{\lambda}(z - c\xi)} \tag{18}$$

Next, the integrated result of this equation is expressed in terms of the heat flux pertaining to the undisturbed film by the ratio

$$\frac{q}{q_0} = \frac{h}{h_0} = \frac{\delta_0}{(\delta_0^2 - \delta_1^2)^{1/2}} \tag{19}$$

This equation also shows the correspondence existing between heat flux and heat transfer coefficient when the same temperature differences exist for the two film conditions. Equation (19), therefore, yields the effective heat transfer thickness of a sinusoidal film

$$\delta = (\delta_0^2 - \delta_1^2)^{1/2} \tag{20}$$

The following table illustrates the effect of the amplitude ratio, δ_1/δ_0 on the heat transfer coefficient ratio, h/h_0:

Table A-IV-4

$\frac{\delta_1}{\delta_o}$	$\frac{h}{h_o}$
0.0	1.000
0.05	1.00
0.10	1.005
0.20	1.02
0.40	1.09
0.50	1.15

Thus it is shown that, in order to achieve an appreciable increase in h in cyclic operation, it is necessary to change the amplitude by 40 per cent or more.

Appendix IV-5

Hydrodynamic Study of a Feed Groove

Equations were developed in Appendix A-IV-3 for the heat transfer rate to a falling liquid film on a flat, vertical surface during evaporative conditions. These equations may be adapted ideally to the case of film feeding from the vertical grooves of a programmed evaporator surface by employing the assumption that the flow of liquid over the contoured surface elements is strictly normal to the feed grooves and their companion runoff grooves. Such a flow condition would be well approximated when the pressure gradient within the film, arising from surface tension, would be very large compared with the gravitational body force of the flat plate case. To employ the flat plate equations we must (1) substitute the path length along the curved surface element for the plate length, and (2) substitute the pressure gradient derived from the surface tension for the gravitational body force. The calculation of the forces associated with a surface tension driving contour are discussed in Ref. 7.

Since the feed groove is a rectangular channel of varying depth, t, it is important to consider the flow behavior in such a groove, specifically, the rate of volume discharged (dV) from it per unit length (dz) of groove. In the analysis, surface tension and inertial forces are to be neglected, and the overflowing liquid is assumed to be of negligible thickness relative to the groove depth. The analytical solution for rate of volume flow in a rectangular channel of constant width, w, and constant thickness, t, can be shown to be (see Ref. 10)

$$V = \frac{\rho g}{\mu}\left[\frac{1}{3} w t^3 - \frac{2^7}{\pi^5} t^4 \sum_{j=0}^{\infty} \frac{\tanh \frac{(2j+1)\pi w}{4t}}{(2j+1)^5}\right] \qquad (1)$$

The first term of this expression $(\rho g w t^3/(3\mu))$ may be recognized as the volume flow rate on a vertical surface having no edge effects; thus, the second term represents side-wall drag on the flow. Now, since the tanh-function is limited to values between 0 and 1, we can with negligible error use equation (1) in the form

$$V = \frac{\rho g}{\mu}\left[\frac{1}{3} w t^3 - \frac{2^7}{\pi^5} t^4 \tanh \frac{\pi w}{4t}\right] \qquad (2)$$

using only the first term of the indicated summation.

Now, by considering the exact expression for V, we may deduce the feed rate per unit length of channel (feed groove). The result will be obtained from the fundamental relationship

$$\frac{dV}{dz} = \frac{dV}{dt} \cdot \frac{dt}{dz} \tag{3}$$

Here $\frac{dV}{dz}$ represents the feed rate per unit length of groove and is in general a variable, being dependent on both, $\frac{dV}{dt}$ and $\frac{dt}{dz}$. The following approximation is obtained upon differentiating equation (1) and applying the conditions - (1) boundness of the tanh-function, and (2) the trend toward decreasing values possessed by the sech^2-function with increasing j-values:

$$\frac{dV}{dt} = \frac{\rho g}{\mu} \frac{\pi^2 \omega^3}{4^2} \left[\frac{1}{\xi^2} \left(1 + \frac{2^5}{\pi^4} \operatorname{sech}^2 \xi \right) - \frac{2^7}{\pi^4} \frac{\tanh \xi}{\xi^3} \right] \tag{4}$$

where $\xi = \frac{\pi}{4} \frac{\omega}{t}$. A dimensionless plot of equation (4) is given in Fig. IV-13.

When the taper of a feed groove is constant - as it is for the test surfaces of this study - the function $\phi(\xi)$ is proportional to the volume feed rate per unit length of surface. Thus, the nature of the local feed along the surface is depicted by the graph in Fig. IV-13 since dt is proportional to dz, and t varies essentially like z.

Now since ϕ is a volume rate function at the film's inlet end, equation (3) of Appendix IV-6 shows that the inlet thickness is proportional to $\phi^{1/3}$. Furthermore, since R is a constant for a particular film, equation (7) of Appendix IV-6 shows that δ_{av} is proportional to δ_o, the inlet thickness. Consequently, $\phi^{1/3}$ is proportional to δ_{av}, which in turn may be related to t, the groove depth. Fig. IV-14 gives the relationship between $\phi^{1/3}$ and ξ^{-1}, where $\xi^{-1} = \frac{4}{\pi} \frac{t}{\omega}$.

For the constant feed rate case, namely dV/dz = constant, equation (4) may be substituted into equation (3), and the resulting equation integrated to give a shape of the channel bottom that is not linear. If distance, z', is measured from the point of the groove where t=o, instead of from the inlet end, the result obtains:

$$\frac{1}{3\xi^3} - \frac{z^5 \tanh \xi}{\pi^4 \xi^4} = \frac{z'(dV/dz')}{(\pi/4)^3(\rho g/\mu)w^4} \quad (5)$$

where z' + z = L, and L is the length of a channel that terminates at zero depth. Fig. IV-15 is a dimensionless plot of equation (5). A more complete discussion of the equation is given in Ref. 11.

Appendix A-IV-6

Thermal-Hydrodynamic Equations of a Programmed Surface

The basic equations and parameters applying to programmed evaporator design can now be developed. A useful expression for the total volume rate of discharge from a single feed groove may be obtained using equation (2), Appendix A-IV-5, which is

$$V = \frac{\rho g w^4}{\mu}\left[F(t/w)_{in} - F(t/w)_{out}\right] \qquad (1)$$

wherein

$$F = \frac{1}{3}\left(\frac{t}{w}\right)^3 - \frac{2^7}{\pi^5}\left(\frac{t}{w}\right)^4 \tanh\left(\frac{\pi t}{4 w}\right)^{-1} \qquad (2)$$

However, $F(t/w)_{out}$ can be made negligible compared with $F(t/w)_{in}$ for practical application. Next, the equation for viscous flow over a flat surface under the action of a constant pressure gradient is applied along the surface. This equation is

$$V = \frac{2}{3}\frac{dp}{ds}\frac{\delta_o^3}{\mu} L \qquad (3)$$

in which flow to both sides of the feed groove is taken into account. The pressure gradient, dp/ds, may be calculated according to the method outlined in Ref. 7, in which dp/ds is made constant by choosing a linearly changing surface curvature with respect to the surface coordinate. The 58-groove (coarse) surface and 120-groove (fine) surface have dp/ds values equalling 3.56 and 14.2, respectively, but are reduced from the pure water values, 4 and 16, respectively, because of unavoidable contamination occurring inside the apparatus.

An equation for δ_o may be deduced by equating equations (6) and (13) of Appendix A-IV-3 and combining the result with the runoff factor

$$R = \left(\frac{\delta_L}{\delta_o}\right)^3 \qquad (4)$$

This operation gives

$$\delta_o = \left[\frac{4 \mu k \ell \Delta T}{\lambda \rho (dp/ds)(1 - R^{4/3})} \right] \qquad (5)$$

The equation for Q may most simply be written as

$$Q = \lambda \rho n V (1 - R) \qquad (6)$$

Equations (1) through (6) include most of the important design variables. Aside from variables pertaining only to the liquid, these six equations contain twelve variables:

$$l,\ w,\ \frac{dp}{ds},\ t,\ L,\ n,\ V,\ \delta_o,\ R,\ \Delta T,\ Q \text{ and } F$$

Consequently, for design practice, six of these variables may be selected arbitrarily in choosing a surface configuration.

It is important to note, in considering equations (1) through (6), that R is entirely dependent on ΔT for a given surface and groove design. Equation (5) shows that decreasing R, which corresponds to increasing the amount of liquid evaporated, requires a larger ΔT. Also, equation (6) shows that Q is increased. Now, if we permit a change in the groove shape, but keep the same surface geometry, we can, for a given ΔT, reduce R by reducing δ_o (see equations (1) and (3)). But reducing δ_o means reducing V, and this in turn means reducing the groove taper. Thus, a lower R, and its associated higher Q, could be achieved for the given temperature difference and the same surface geometry only by reducing the groove taper.

In practical design work δ_o will be chosen as small as is consistent with a good film condition, that is, one that is stable and uniform over the working surface. Then, ΔT and R can both be small, as is required by the thermodynamics of a vapor-compression distillation system, for both ΔT and R work in cooperating directions in the ratio $\Delta T/(1-R^{4/3})$ of equation (5). This equation also shows the effect of surface geometry in the factor, l/dp/ds. These two factors must be balanced against each other to give a practical surface geometry. The volume flow rate and feed groove taper can then be found from equations (1), (2) and (3).

Further insight into the evaporation process may be gained by noting that the average film thickness, δ_{av}, may also be included among the collective variables by replacing equation (6) by the following two equations:

$$\delta_{av} = \frac{3}{4} \frac{(1-R^{4/3})}{(1-R)} \delta_o \tag{7}$$

and

$$Q = \frac{2\pi k \ell L \Delta T}{\delta_{av}} \tag{8}$$

Here δ_{av} is defined so as to be consistent with the relation

$$h = \frac{k}{\delta_{av}} \tag{9}$$

where h is given by equation (13) of Appendix A-IV-3 with L replaced by 1. It is apparent from equations (7) and (9) that h may be expressed in different forms depending on whether δ_o is substituted in equation (7) from equation (3) or equation (5). The results of these substitutions are:

$$h = \frac{2^{7/3}}{3^{4/3}} \left(\frac{k^3 L \, dp/ds}{\mu V} \right)^{1/3} \frac{1-R}{1-R^{4/3}} \tag{10}$$

and

$$h = \frac{4^{3/4}}{3} \left(\frac{\lambda \rho k^3 \, dp/ds}{\mu \Delta T \ell} \right) \frac{1-R}{(1-R^{4/3})^{3/4}} \tag{11}$$

MANUFACTURING PROCESSES AND COST ESTIMATES FOR MANUFACTURING THIN FILM VAPOR COMPRESSION HEAT TRANSFER MODULES

Appendix B

SUMMARY

Investigation and experimental work was done to determine expected costs for manufacturing Thin Film Vapor Compression heat transfer modules. These costs were determined after a method of manufacturing was established.

Estimated costs for heat transfer module production are well below the one dollar per square foot laid out in the proposal.

These estimated costs are:

1. for aluminum module - $.495 per sq. ft. of evaporative surface
2. for tin plate module - $.370 per sq. ft. of evaporative surface
3. no estimate for low carbon steel module is made, as a suitable joining method has not been determined.

Recommended joining method for aluminum is adhesive bonding with Epon 422 which is made by Shell Chemical Co. The life of the joint is not predictable by known means, and application experience over a number of years will be required before actual life characteristics can be determined. Investigation by adhesive manufacturers and aluminum producers should be encouraged for better adhesives under sea water immersion.

The recommended joining method for tin plate is by soldering. Here again, life of the joint is indeterminate.

No recommendation for steel is presently made. Silver brazing in a hydrogen atmosphere can be done but is not expected to be low cost. Insufficient work has been done by steel suppliers and adhesive manufacturers to recommend adhesive bonding low carbon steel. Mechanical fastening using gasketing materials is another method of making steel modules but this will need further investigation.

Appendix B

The methods and costs outlined in this report are based on a folded evaporator sheet as described in the proposal to the Office of Saline Water dated October 1961. Other configurations are possible that may result in less costly production and these should be considered when the design of the module is being made.

Appendix B

PURPOSE AND ASSUMPTIONS

The manufacturing studies and investigations described in this report were performed to meet certain requirements of the Thin Film Vapor Compression System R&D Contract 14-01-0001-273. The manufacturing effort was carried out under Task V of the contract program.

The purpose of the manufacturing studies and investigations was two-fold:

1. To determine how to manufacture a low cost, long life Thin Film Vapor Compression Heat Transfer module using materials and fabricating techniques consistent with its operating environmental conditions.
2. To estimate as accurately as possible the cost of producing these modules.

The investigations into manufacturing costs have been based on future methods of manufacture. These methods are supported by prior practice, or, development at Headquarters Manufacturing Laboratory. Costs also are available from prior practice and are more accurately estimated once the methods are determined. The same is true for capital equipment costs.

Methods, plant and equipment are dependent on the size of sea-water conversion plant, in what time it must be produced, and how many plants will be built.

The conversion plant is assumed to be the 10 million gallon per day water plant mentioned in the introduction of the Proposal. The time required to produce modules for this plant is assumed to be six months. The cost of this manufacturing equipment is assumed to be amortized over this one production run.

The amount of surface required to produce 10 million gallons of fresh water per day is determined as follows.

The production of fresh water 1.22 lb. per hr.

per sq. ft. of evaporative area

or 3.515 gal. per day

Number of sq. ft. required = $\frac{10,000,000}{3.515}$ = 2,845,000 sq. ft.

In the development of manufacturing methods, it was decided that a 3 foot wide module would be most practical; wider ones being difficult to manufacture and handle while narrower ones being more costly.

With a 3 foot wide module, the number of feet of coil stock = 1/3 of 2,845,000 = 948,333 ft.

The length of the corrugated module is taken as 5 feet. This may be changed as the spray distance is developed beyond this length. Nominal height of the module is 18 inches. Actual flat height for steel is 1.518 ft. and for aluminum is 1.439 ft.

The approximate length of 1 corrugated sheet in a module is

$$\frac{5 \text{ ft. x } 12 \text{ in.}}{1/2 \text{ in. pitch}} \times \frac{18 \text{ inch height}}{12 \text{ inch/ft.}} = 180 \text{ feet}$$

The approximate heat transfer surface area of the module is 180 ft. x 3 ft. = 540 sq. ft.

The number of modules required = $\frac{2,845,000 \text{ sq. ft.}}{540 \text{ sq. ft./module}}$ = 5,270 modules

Production rate = $\frac{5,270}{1,000 \text{ hrs./6 months}}$ = 5.27 per hr.

or 11.38 minutes per module

Estimated production efficiency is 75% due to maintenance, downtime, absenteeism, etc.

Therefore required production time = .75 x 11.38 minutes

= 8.54 minutes per module

For in-line processing evaporator sheet such as de-reeling, washing, etc. the rate of sheet travel will be $\frac{180 \text{ ft.}}{8.54 \text{ min.}}$

$$= \underline{21.1 \text{ ft. per min.}}$$

Rate of side sheet production for 2 sheets per module is

$$\frac{5 \text{ ft.} \times 2}{8.54 \text{ min.}} = \underline{1.17 \text{ ft. per min.}}$$

Rate of folding operation is 120 folds per 8.54 minutes or 14.08 folds per minute or 4.26 seconds per fold.

Appendix B

OPERATING CONDITIONS OF MODULE

During operation the evaporating surface of the module is subjected to the intermittent spray of sea water near the top of the surface and the flow of a thin film of evaporating sea water over the entire surface. The condensing side is subjected to the flow of a thin film of distilled water over the entire surface. The pertinent fluid properties of the flowing films are:

	Evaporating Side	Condensing Side
Temperature	120 - 120.4°F	122°F
Pressure	3.39 in.Hg. abs.	3.64 in Hg. abs.
Salinity	3.5 - 7%	0 to 10 ppm
O_2 Content	0.1 ppm	0.0 ppm

The joints separating the evaporating and condensing sides are to:

(1) serve as a seal

(2) serve as bonding means between side sheet and evaporating sheet.

Item (2) can be considered as an optional requirement as the side sheets could be held in place by mechanical means i.e., clamping with tie-rods.

The required strength of the joint is governed by handling procedure rather than by the operating load conditions of 0.1228 p.s.i. The desired life of the joint is ten years. The actual life can be determined only by building a module or modules and testing it under the actual operating conditions for extended periods of time.

Appendix B

MANUFACTURING PROCESSES

Introduction

Since the manufacturing studies were started in parallel with the rest of the thin Film Vapor Compression program many of the factors affecting the manufacture of the module were not completely defined. Factors such as the heat transfer surface material and the final geometrical configuration of the module could not be selected until after the appropriate heat transfer and corrosion tests had been conducted. As a result, the manufacturing studies had to provide for a range of materials and possible design configurations. Some of the other factors which could not be evaluated or defined early in the program were:

1. The required surface finish and condition of the heat transfer surface for adequate wetting characteristics.
2. The effect of the sea water on the various types of joining materials under consideration.

One of the most important goals of the manufacturing studies was the attainment of a cost estimate for the manufacture of the heat transfer module. In order to achieve this goal within the time and funding budgeted for this effort it was obviously impossible to wait until all of the above factors had been evaluated experimentally. By judiciously screening the many possibilities and based on the experimental evidence available, two of the basic materials with their most promising joining techniques were selected for cost analysis purposes. At the same time a module configuration and size were also chosen. The dimensions of this module have already been described in a previous section. In the sections which follow the materials, joining techniques and all manufacturing processes involved in making the module will be described.

Materials

The materials originally selected for consideration were:

1. Low carbon steel SAE 1010 or 1020
2. Aluminum 1100, commercially pure
3. Aluminum 3003
4. Copper

These materials were chosen on an economic and a resistance to corrosion basis with little or no consideration given to their heat transfer characteristics. Ordinarily the corrosion resistance of low carbon steel is rather poor in a sea water environment but with the low temperature and low oxygen content of the sea water in the application there is a reasonable chance that its corrosion characteristics will be adequate. The low cost of this material however, is its greatest virtue.

The aluminums were chosen for their relatively low cost and their resistance to corrosion characteristics.

Copper which is relatively high in cost was chosen for its resistance to sea water corrosion.

All of these materials are available in coil form and with the exception of copper, are available in thicknesses close to 0.030 inches and widths up to 36 inches and greater. In order to make copper competitive in cost its thickness could not exceed 0.010 inches. Copper is not available in coil stock in widths greater than 20 inches.

The statistics on tolerances and cost additions for these materials are listed in Appendix C.

Subsequent contacts with the various metal suppliers indicated that the original selection of materials could be improved upon. The steel suppliers recommended that a tin plated low carbon steel or a chromized steel be used either as replacements for or in additions to the low carbon steel. The aluminum supplier recommended the use of 3003 clad with high purity 1188 as a replacement for the clad material originally chosen and either a 5050 or 5052 alloy as the alternate material.

As a result of these recommendations the selection of proposed materials was re-evaluated. The anticipated problems associated with handling and joining the very thin gage copper were significant factors in eliminating copper as a possible material. The four materials selected as a result of the re-evaluation were:

1. Low carbon steel 1010 or 1020
2. Tin plated carbon steel
3. Aluminum 5050
4. Aluminum 3003 clad with 1188

A comprehensive discussion of the material selection is given in the Task III section of the program final report. It is sufficient to state here that for the low carbon steels - rimmed steel should be considered because of its low cost and that aluminum killed steel is desirable for welding considerations. It should also be noted that the tin plate lends itself readily to soldering as a joining technique.

The table below shows a cross index of materials with the joining methods considered.

	Steel	Aluminum	Copper
Braze	Yes	Yes	Yes
Oxy-weld	Yes	No	No
Arc-weld	Yes	Yes	No
Electron Beam Weld	Yes	Yes	Yes
Solder	Yes	No	Yes
Adhesive Bond	Yes	Yes	Yes
Mechanical Fastening	Yes	Yes	No

Processes

The manufacturing processes described in this section are aimed at producing the required heat transfer modules at as low a cost as possible. Three materials with their most promising methods of joining were chosen for the manufacturing process analysis.

The module configuration chosen for the process analysis is shown in Figure 1. The processes for the different materials are shown in block diagrams as indicated below:

Aluminum Module, Epoxy Bonded	Figure 2
Tin Plated Module, Soldered	Figure 3
Steel Module, Brazed	Figure 4

The following manufacturing processes have been investigated for inclusion in the production of a module.

(a) De-Reel, Straighten and Feed

(b) Punch, Draw

(c) Detergent Wash

(d) rinse

(e) dry

(f) shear

(g) sand blast

(h) form evaporator sheets

(i) weld

(k) solder

(l) epoxy bond

(m) braze

(n) etch

(o) leak test

(p) fixture, clamp & cure

(q) package

A description of where and how these processes may be used is described below; also included are the estimated costs of the required capital equipment.

DE-REEL, STRAIGHTEN & FEED

Equipment for de-reeling, straightening and feeding is commercial and standard. It can be obtained from a large number of manufacturers such as Rowe Machinery and Manufacturing Inc. of Dallas, Texas. The equipment should be capable of handling steel or aluminum with a width capacity of 36 inches or more and coil diameter of 50 inches.

Suggested Equipment and Estimated Costs are:

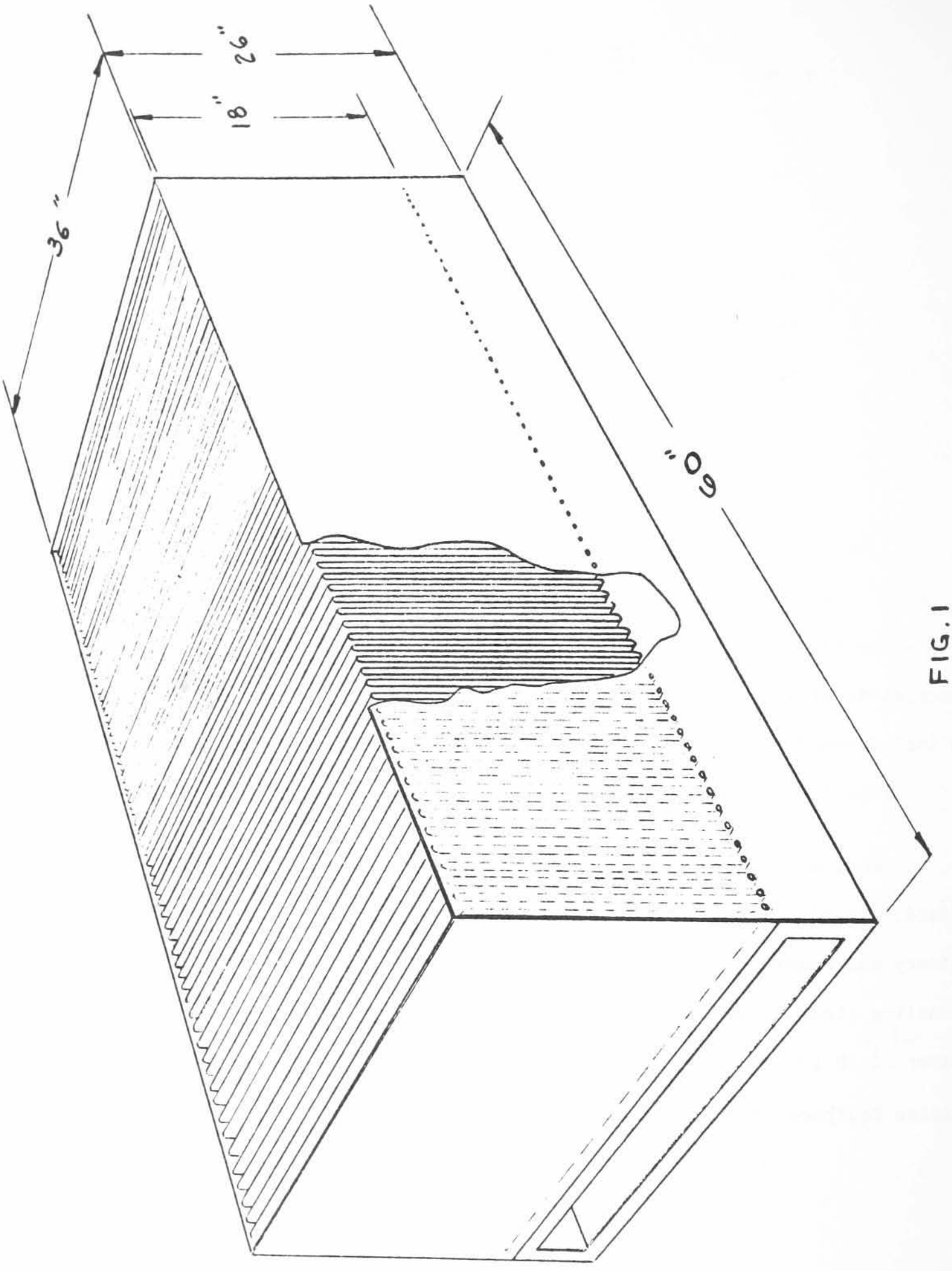

FIG. 1

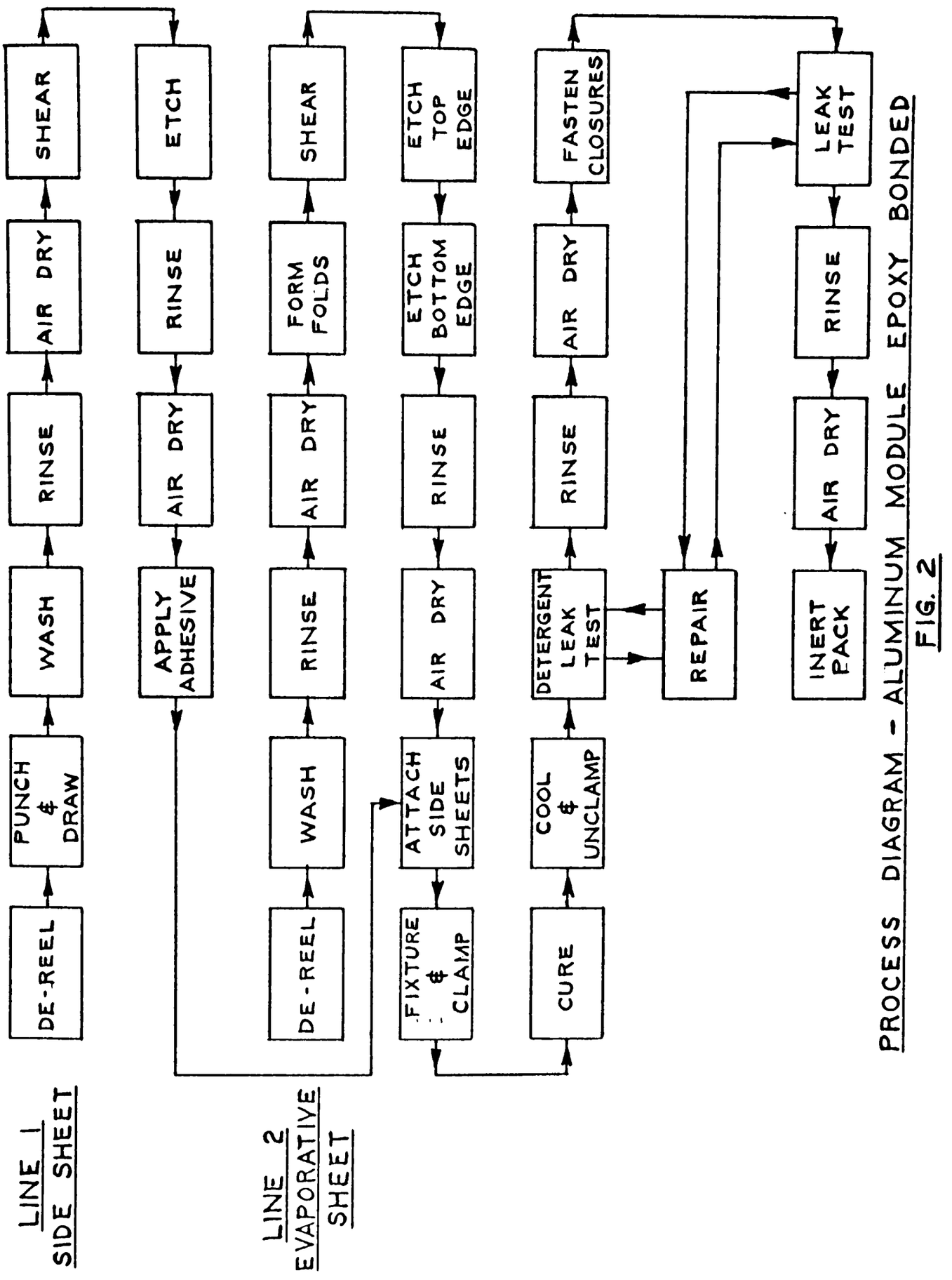

PROCESS DIAGRAM - ALUMINUM MODULE EPOXY BONDED

FIG. 2

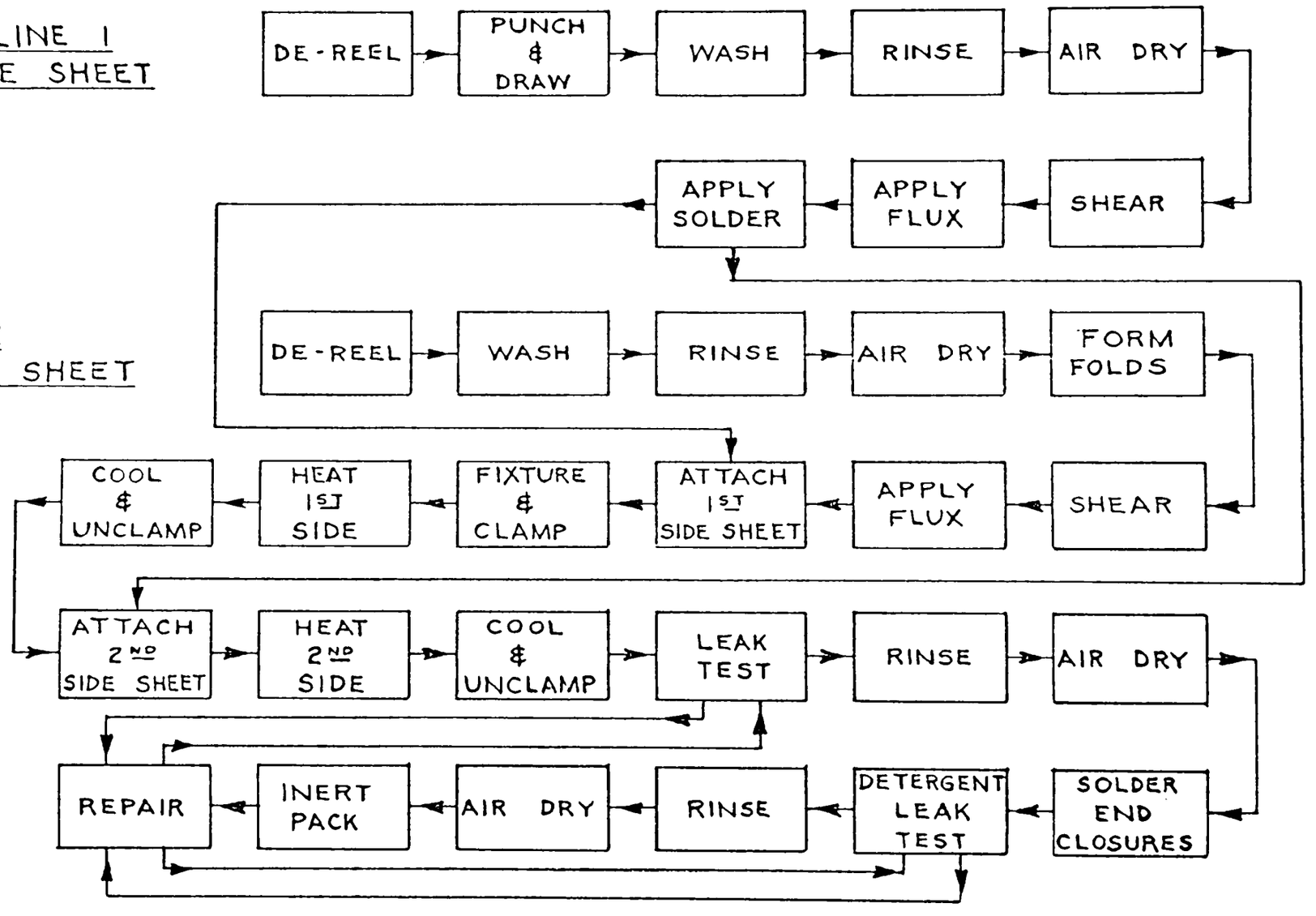

PROCESS DIAGRAM - TIN PLATE MODULE SOLDERED

FIG. 3

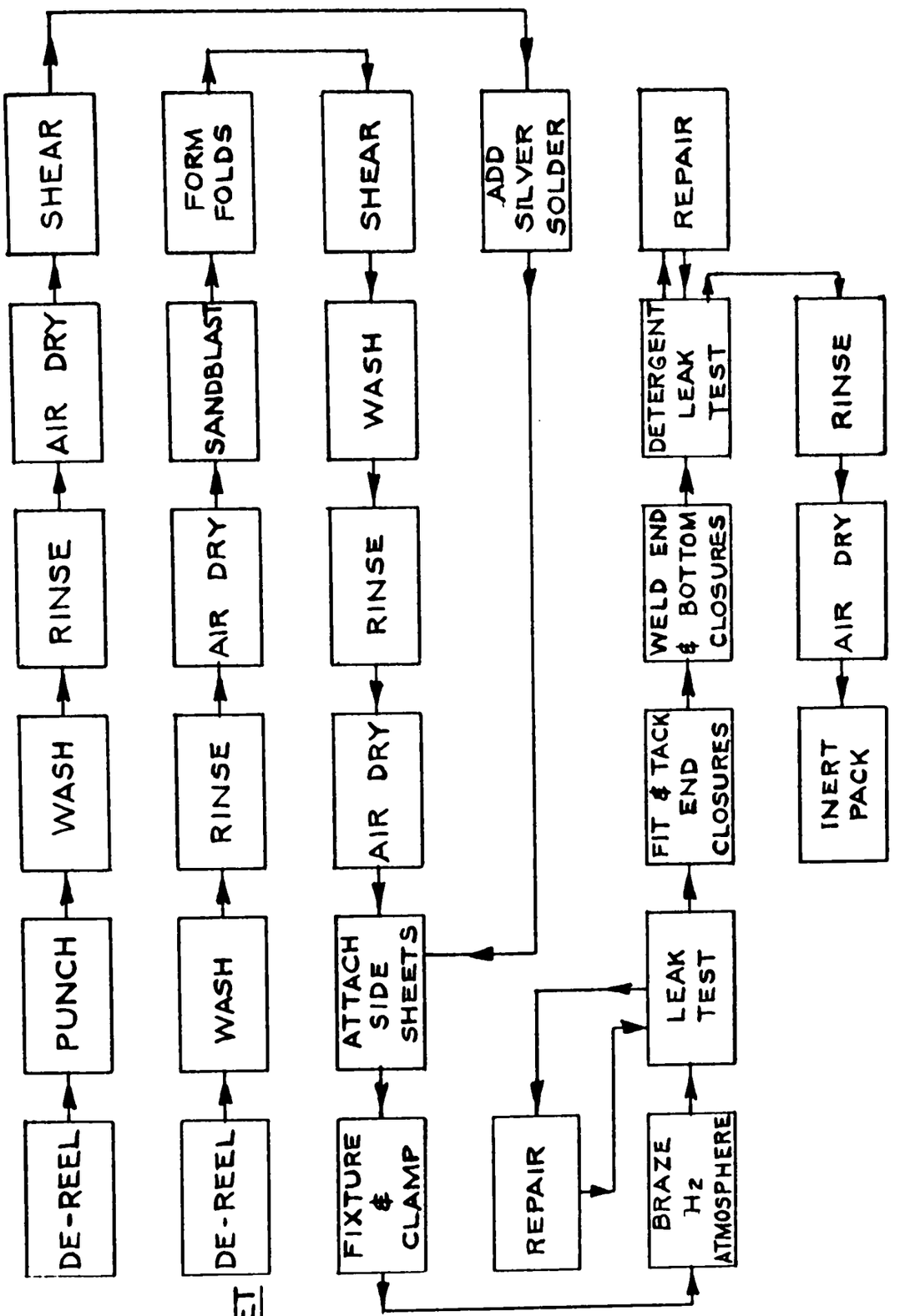

PROCESS DIAGRAM – STEEL MODULE BRAZED

FIG. 4

Power de-reeler	$ 4,065
Cradle is not recommended because of possible surface damage	
Loading dolly	3,760
Peel table and clamp roll for automatic coil start	1,520
Straightener	6,730
Feeder	7,310
Pivot table and feed control	400
Total	$23,785

Costs of this equipment will depend on the final quotations but will probably be near those shown above.

PUNCH, DRAW

Three configurations of side sheets were under consideration depending on the joining method to be used. These were:

(1) Embossed side sheet with drain holes as shown in Figure 5, (drawing D-HML-0.60). This style is recommended for adhesive bonded or soldered modules. It also can be used for brazed modules. The resulting joint will be stronger then (2) below. It will have more joint area and joint volume to resist corrosion and will allow for greater tolerances in manufacturing than that of (2).

(2) Plain side sheet with drain holes as shown in Figure 6, (drawing D-HML-0.63). This configuration could be used for adhesive bonded or brazed modules.

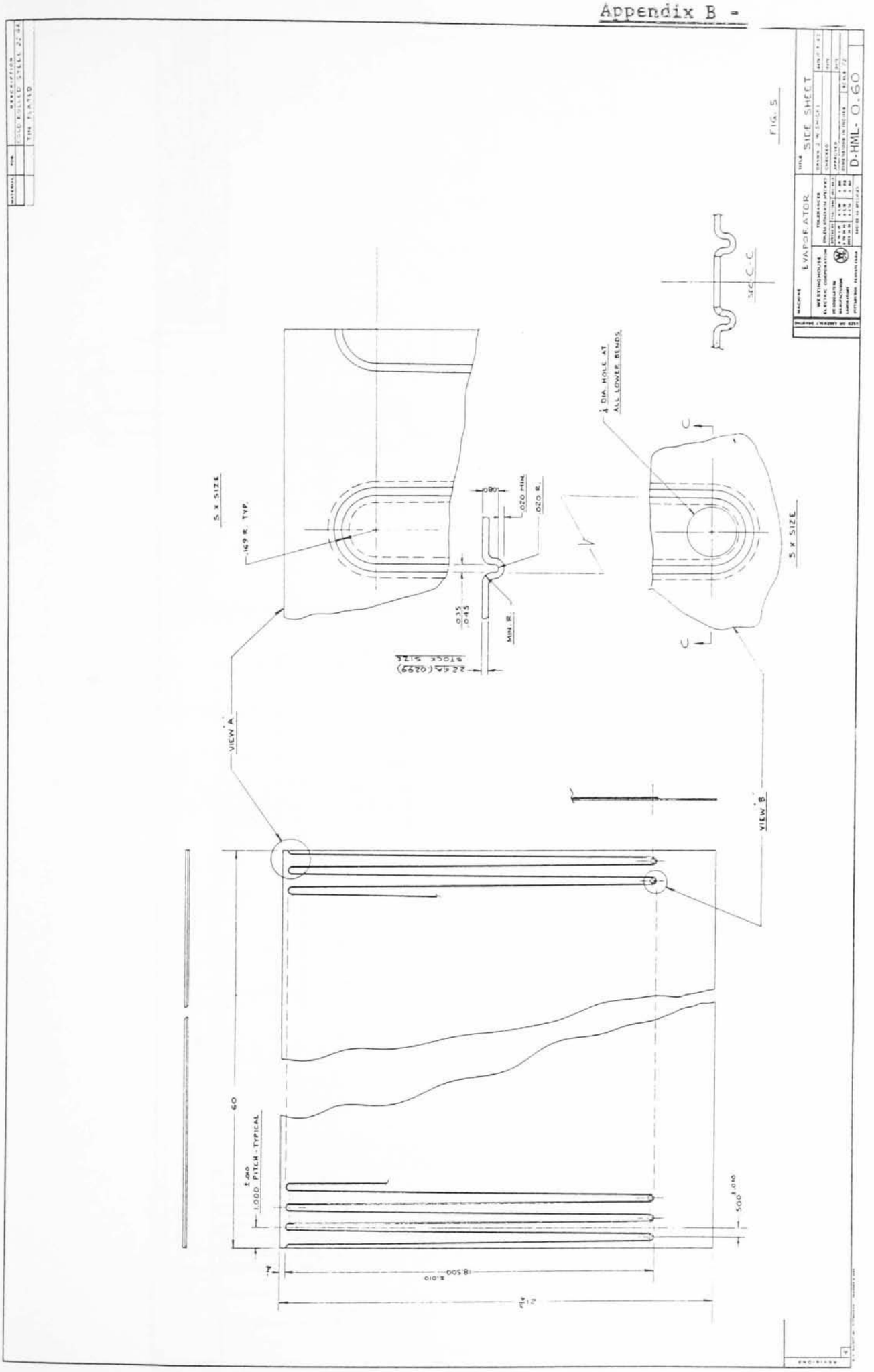
MATERIAL
DESCRIPTION
COLD ROLLED STEEL 22 GA
TIN PLATED
MACHINE
EVAPORATOR
TITLE
SIDE SHEET
WESTINGHOUSE
ELECTRIC CORPORATION
MANUFACTURING
D-HML-0.60
SEE C-C
4 DIA. HOLE AT
ALL LOWER BENDS
5 X SIZE
.169 R. TYP.
.020 MIN.
.020 R.
.035
.045
MIN. R.
22 GA (.0299)
STOCK SIZE
VIEW A
VIEW B
60
1.000 PITCH - TYPICAL
18.500
21.12

FIG. 5

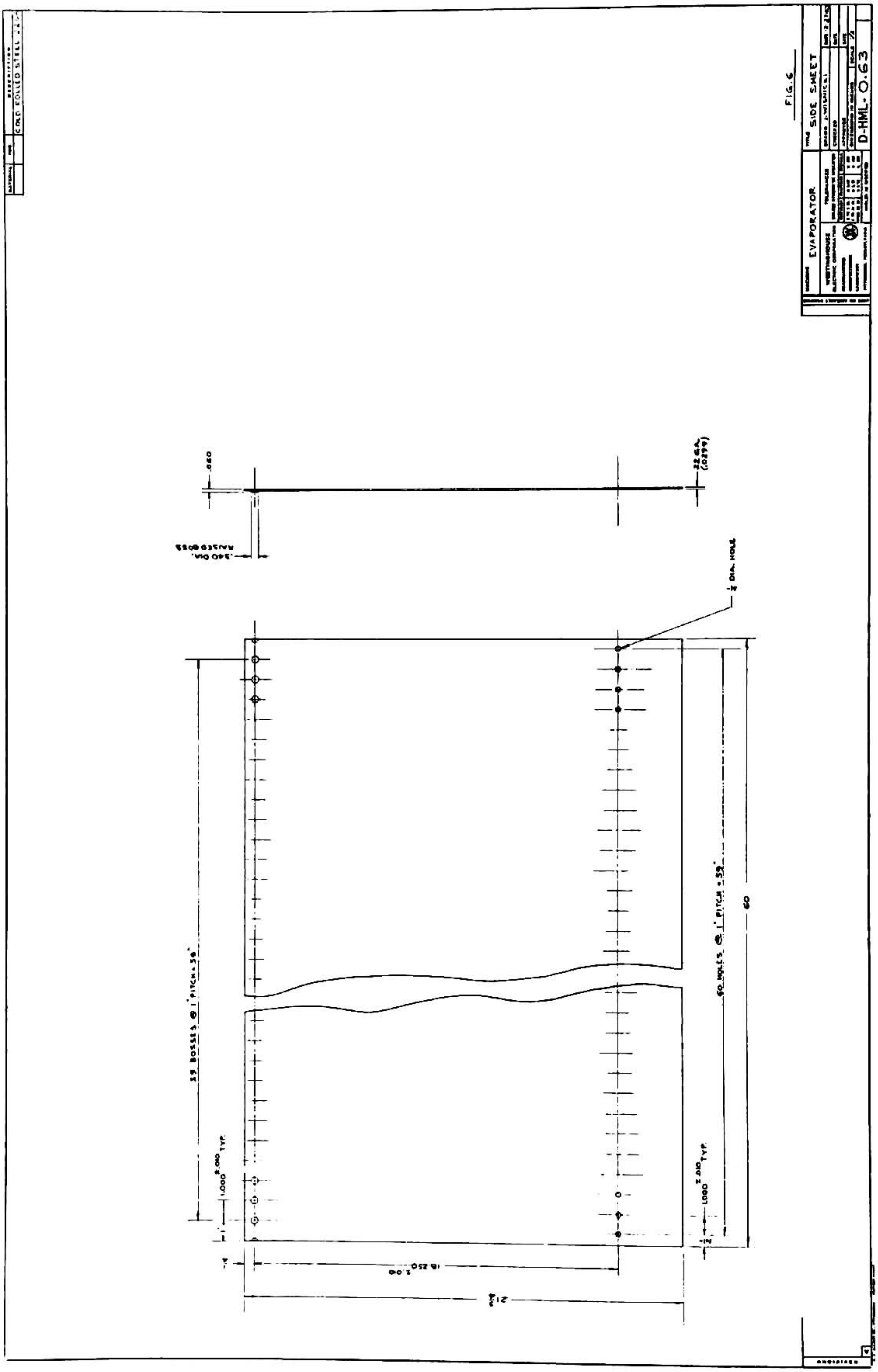
FIG. 6
EVAPORATOR
SIDE SHEET
D-HML-0.63
COLD ROLLED STEEL
59 BOSSES @ 1" PITCH = 58"
60 HOLES @ 1" PITCH = 59"
60
DIA. HOLE
22 GA. (.0299)
RAISED BOSS
1.000
TYP.
18.250

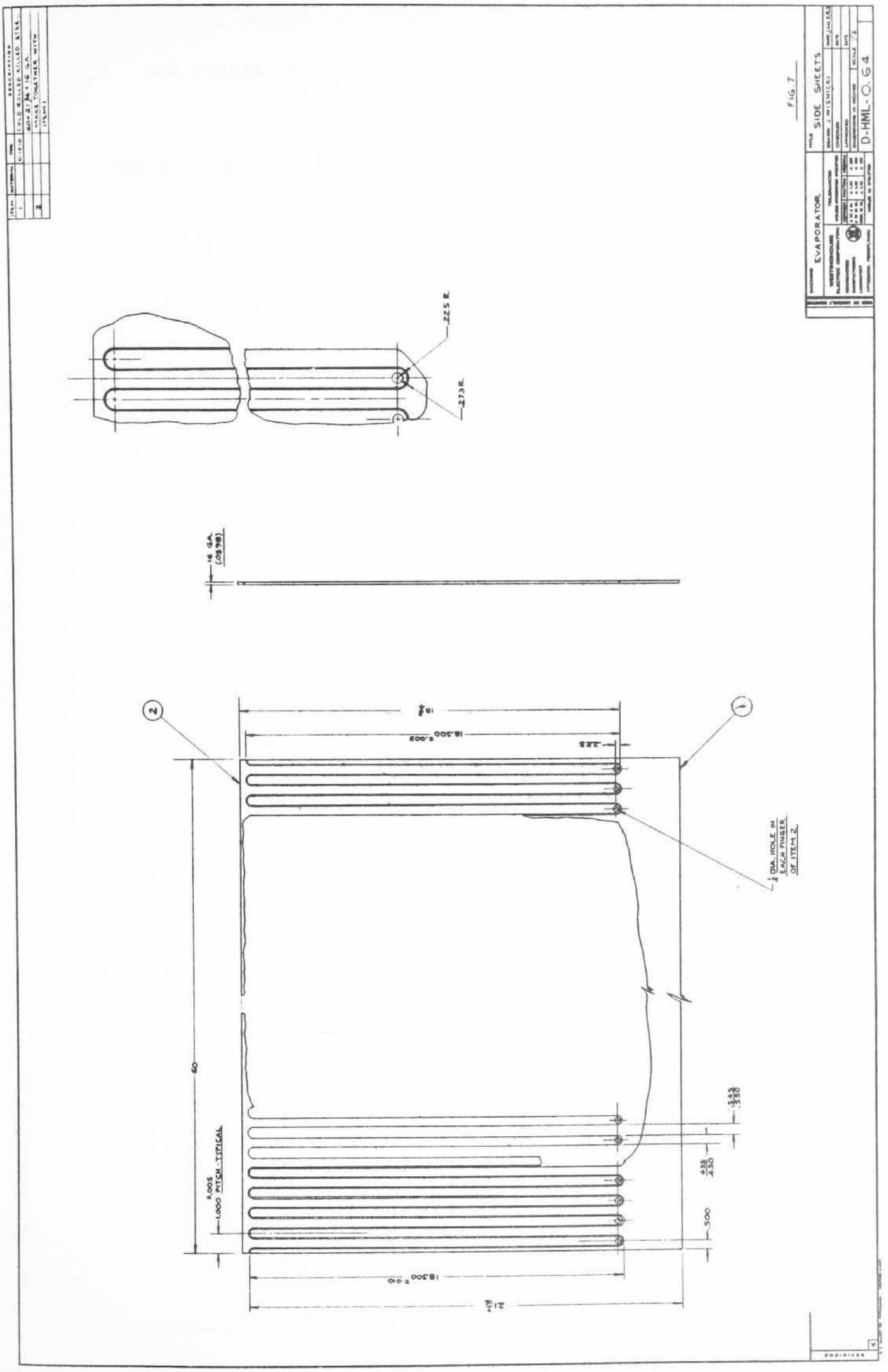
EVAPORATOR
SIDE SHEETS
D-HML-0.64
FIG. 7
.225 R.
.273 R.
18 GA (.0598)
18.300 ±.005
18.300 ±.010
.228
DIA. HOLE IN EACH FINGER OF ITEM 2
60
1.000 ±.005 PITCH - TYPICAL
.500

(3) Split side sheet with drain holes as shown in Figure 7 (drawing D-HML-0.64). This configuration was found necessary for welded steel modules.

Press size for these items will be controlled by the width of the sheet rather than by the tonnage. A four-poster or straight side press will be required. Minster Machine Company of Minster, Ohio are manufacturers of such equipment. Cost of a 20 ton press capable of handling up to 36 inch wide stock is about $14,000.

Tooling can be made to form and stamp one complete side sheet per stroke but this would require a large die. The side sheet can also be made by progressively feeding the sheet through a short section of die to keep tooling costs to a minimum.

The die for side sheet of configuration 1 will be a combination of punch and draw. This is the one recommended for bonded or soldered modules. By keeping the punch and draw operation limited to one pitch, the die cost can be kept to a minimum. It is expected that the draw operation can be done in a single stroke and a single stage die will be sufficient. Depth of draw is shown on drawing D-HML-0.60. Estimated die cost is $ 3,500.

The die for side sheet of configuration 2 will consist of a hole punch and an embossing punch. It will have a stripper plate, strip guides and a finger stop. A sketch of this type of die is shown in Figure 8. Its cost will be about $2,000.

Tooling was investigated for side sheet of configuration 3. This will involve a 3 stage blanking operation consisting of:

(1) punch drain hole

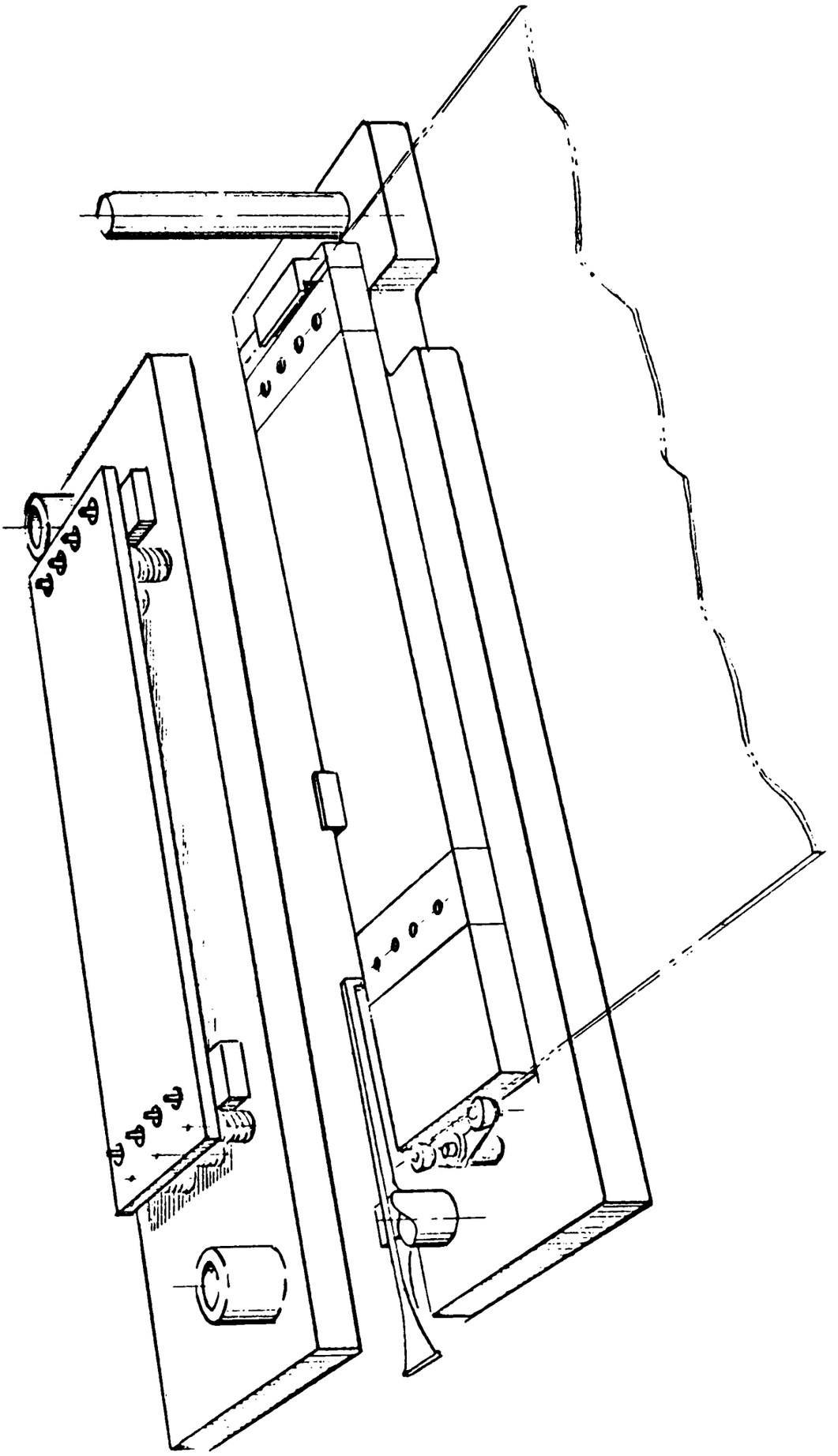

FIG. 8

(2) punch out vertical strip

(3) punch out combined reverse bend and vertical strip

The two side sheets can be produced from one sheet as shown on drawing D-HML-0.64. This is suitable for a steel rule punch with tool steel die and appropriate stripper. Press required would be a single action mechanical press of 50 ton capacity. The stages of blanking the coil stock are shown in Figure 9. Estimated die cost is $1,500.

DETERGENT WASH

Washing operations are necessary for: (1) cleaning prior to a specific manufacturing operation and (2) final cleaning prior to packaging. Each metal will require washing at different intervals in the process. Cleaning methods for each metal are outlined below.

Aluminum

In manufacturing the side sheet, washing is required after the press operation. Lubrication is used in drawing and, in addition, handling will deposit dirt on the side sheet. Prior to the press operation no cleaning is necessary. The detergent wash will assure a clean sheet for the etch operation and prolong the life of the etchant solution.

In manufacturing the evaporative sheet the washing operation is placed before the folding operation because no lubrication is planned for folding and the folded form presents a more difficult shape for efficient cleaning. Leak testing after joining will also serve as a wash operation as it will be done with a detergent solution.

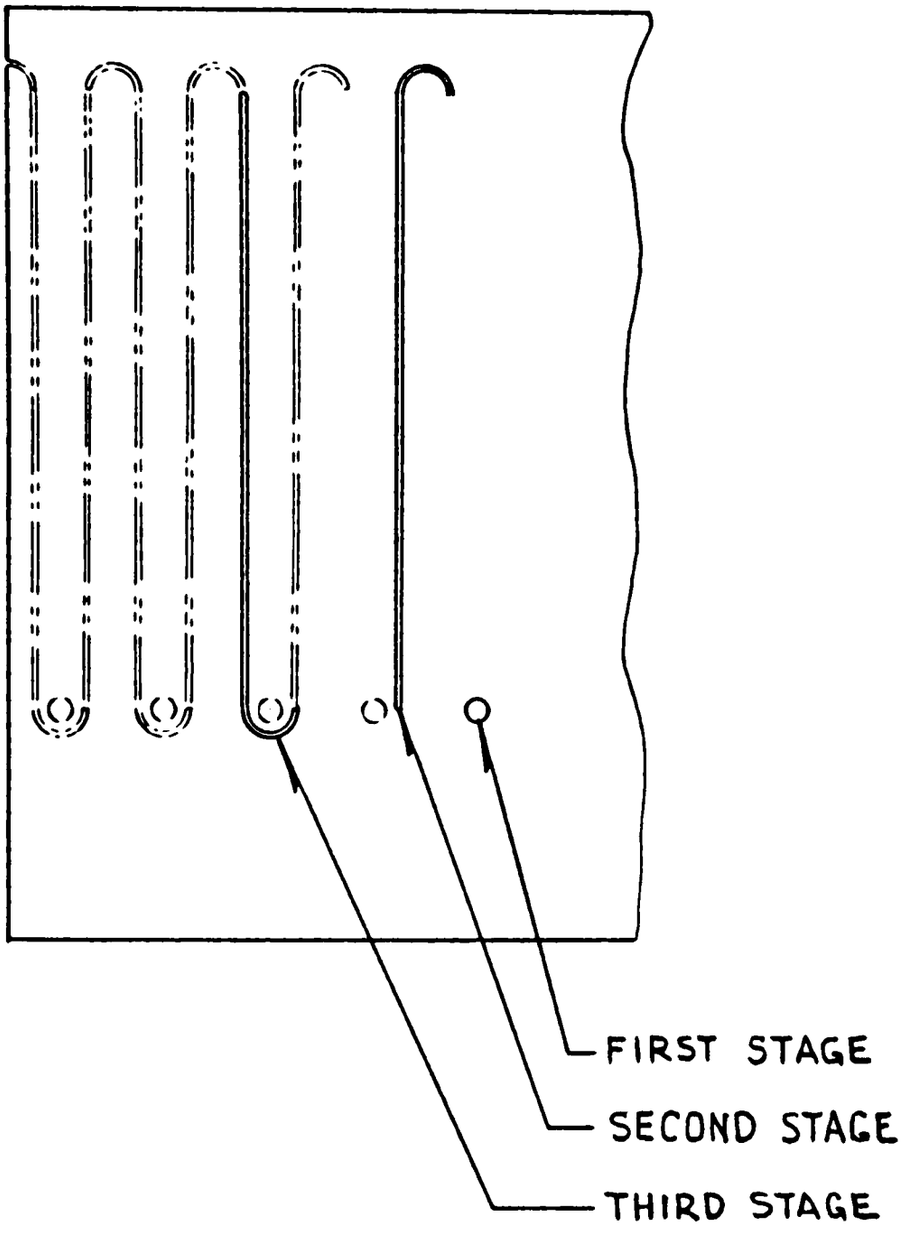

FIG. 9

The recommended wash process is:

Cleaning Medium -	5% aqueous solution of Oakite 61 or 164
Temperature -	155°F ± 10°
Time -	1 minute
Mechanical Cleaning -	Fibre or Scotch-Brite brushes

Kaiser Aluminum recommends the Oakite 61 while Oakite representatives suggest 164 as being more suitable for the water in the Pittsburgh area. Both have been tried in the laboratory with equal success. Oakite 61 has been used to get clean wettable surfaces on evaporative sheets in laboratory heat transfer tests. Clean surfaces will allow wetting of the surface with water with no breaks in the water layer and with small contact angles between water and metal. See page 8 of bibliography (1).

Tin Plate

Washing recommendations for tin plate are the same as with aluminum except that Scotch Brite brushes are not recommended. These remove a small layer of surface metal and could remove an unacceptable amount of tin plating. (A common grade of tinplate, No. 25, has a plating thickness of 0.000015 inches). The aluminum cleaners noted above have been found to give equally wettable surfaces on tin.

Steel

Cleaning tests were conducted on steel when adhesive bonding for this material was under consideration. Sandblasted surfaces gave best results for bonding and gave good wettability. Prior to sandblasting it was found desirable

to wash the metal with solvent so that the blasting grit would not become contaminated. Detergent wash after blasting is recommended to remove dust particles and residual oils. A 3% solution at 150°F of Northwest Chemical detergent number 63 has been found to be adequate. The grit used was steel G-25.

Washing Equipment

Washing of coil stock on a continuous operation could be done on one piece of equipment. This could include guide rolls, heating system for the detergent solution and rinse water, spray nozzles, brushes, and pumps, rinse water and air blowers for drying. Such equipment is shown on Figure 10 (Pennsalt Chemical drawing S-736) and would be suitable for this application. Capital cost of this system is $25,000.

Minnesota Mining and Manufacturing are makers of Scotch-Brite brushes. These are nylon matting brushes impregnated with resin and silicon carbide. The manufacturer claims that this method is supplanting sandblasting in many cases. Its ability to create clean surfaces has not been verified at the laboratory since the other methods were found satisfactory.

Washing of side sheets could be done using rotary scrub brushes. These would be done on an individual basis rather than on a continuous sheet. Drag out of wash solution for production requirements is estimated by Oakite at 2000 gallons per month and this will have to be made up on a daily basis.

RINSE

Water rinsing would be required after washing and after etching operations. Most recommendations call for rinsing in water below 150°F, and ordinary

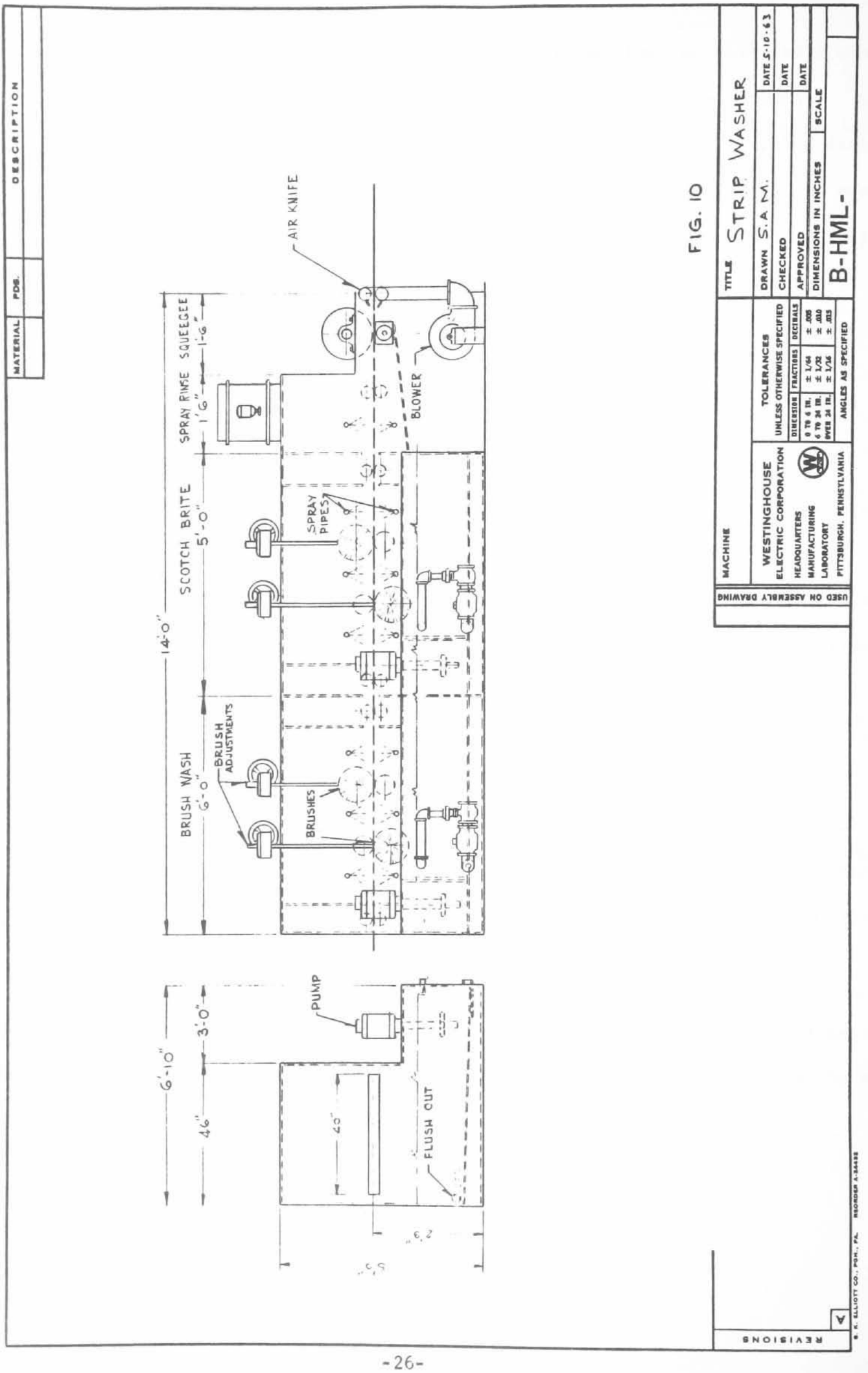
AIR KNIFE
BLOWER
SPRAY RINSE SQUEEGEE
1'-6"
1'-6"
SCOTCH BRITE
5'-0"
SPRAY PIPES
14'-0"
BRUSH WASH
6'-0"
BRUSH ADJUSTMENTS
BRUSHES
PUMP
6'-10"
3'-0"
46"
40"
FLUSH CUT
MATERIAL
PDS.
DESCRIPTION
USED ON ASSEMBLY DRAWING
MACHINE
WESTINGHOUSE
ELECTRIC CORPORATION
HEADQUARTERS
MANUFACTURING
LABORATORY
PITTSBURGH, PENNSYLVANIA
TOLERANCES
UNLESS OTHERWISE SPECIFIED
DIMENSION
FRACTIONS
DECIMALS
0 TO 6 IN.
± 1/64
± .005
6 TO 24 IN.
± 1/32
± .010
OVER 24 IN.
± 1/16
± .015
ANGLES AS SPECIFIED
TITLE STRIP WASHER
DRAWN S.A.M.
DATE 5-10-63
CHECKED
DATE
APPROVED
DATE
DIMENSIONS IN INCHES
SCALE
B-HML-
REVISIONS
E. E. ELLIOTT CO., PGH., PA. REORDER A-34488

FIG. 10

tap water temperature is usually satisfactory. No recommendation could be obtained on the amount of flushing water required or the purity of the water. In our flushing operations, it was estimated that we used one-tenth gallon of water per square foot of surface. This would be about 40 times the amount of wash solution left on an etched shot-blasted surface and was found to give adequate rinsing. Water would be sprayed on the surfaces through nozzles at a pressure of 75 psi. Normal city supply water seems to be suitable. Distilled water is not recommended because of its high cost, (20 cents per gallon in truck lots.)

DRY

Two methods of drying are proposed. One would use ambient temperature air for drying flat sheets, and folded evaporator sheets. The second would use heated air to dry the completed module. Experiments have been run both ways to determine the time, heat, and air necessary to do the job. In both cases air would be propelled by blowers.

On the coil line, drying will be a combination of blowing-off excess water and evaporation. Air will be directed at the passing sheet, through a long thin nozzle to give a knife-edge effect to the air. The minimum velocity of the air should be 3000 feet per minute at exit of the nozzle. Both intake and exhaust air should be ducted. Intake air will be filtered.

Folded evaporator sheets should be passed over the blower on edge to allow the air to reach both sides of the sheet. Evaporator sheets with sides shall be passed with the wet side facing down and air directed upward.

Intake filters will cost about $1100 each, ducting depends on plant layout, but is estimated at $1000 each system.

SHEAR

In the production of evaporator sheets on a special machine for continuous folding, the shearing operation could be done by an abrasive cut-off wheel. It would be incorporated into the folding equipment.

In the production of side sheets, shearing could be done on a standard shear of 20 ton minimum capacity. The shorn sheet is 0.030 inches by 26 inches in cross-section. Shearing could be operator controlled against a fixed stop. Cost of such a shear is about $5000.

SANDBLAST

Sandblasting was strongly considered for epoxy bonded modules. This is the method of surface preparation usually recommended for steel and our tests also have shown it to be superior to detergent washing, sonic cleaning or solvent washing. A steel grit, size G-40 or G-50 is recommended for maximum rotor life. Larger shot may distort the sheet during blasting.

Equipment for sandblasting is shown in Figures 11 and 12 which are from Pangborn drawing M/L-590588 and M/SM-62108. Figure 11 would be for side sheet production and would blast one side only. Figure 12 would be for evaporator sheet production and would blast both sides.

Cost of the small unit (side sheets) is	$13,800
Cost of the large unit is	17,000
Cost of the dust collector is	3,400
	$34,200

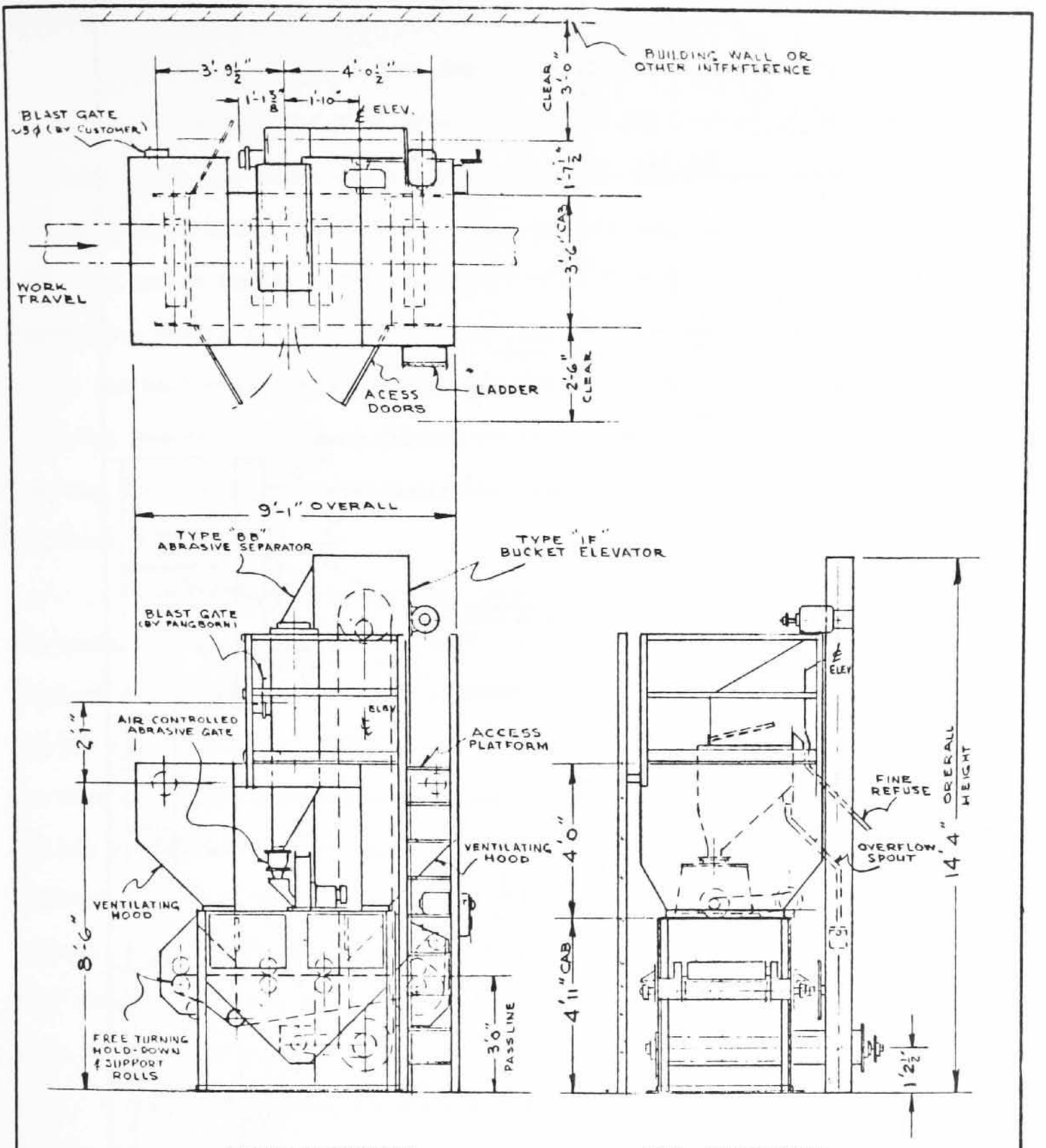

GENERAL ARRANGEMENT
TYPE ES-783 ROTOBLAST CLEANING CABINET

FIG. 11

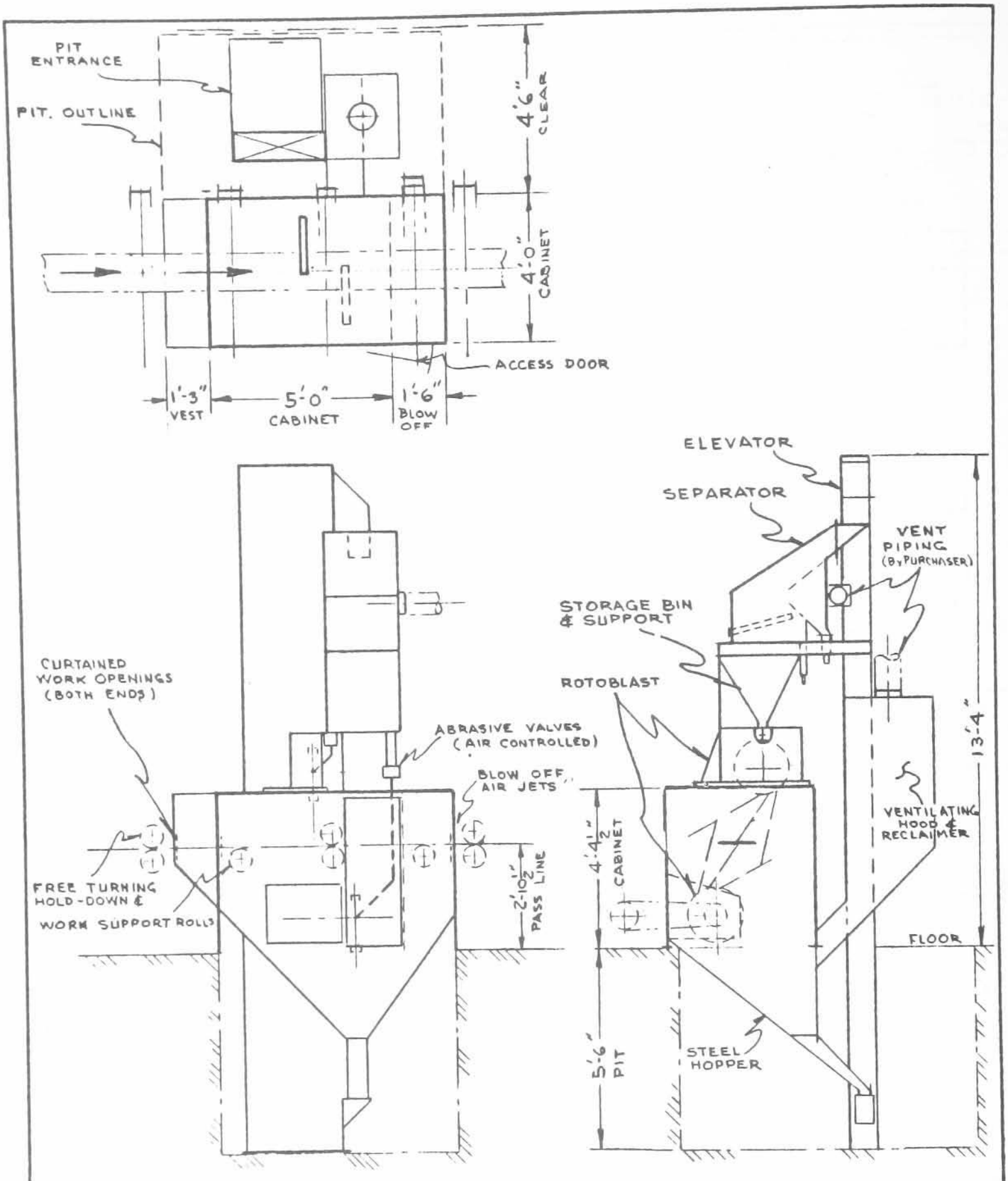

FIG. 12

PROPOSED ARRANGEMENT
TYPE "ES" ROTOBLAST MACHINE FOR STEEL COILS

Appendix B

FORM EVAPORATOR SHEETS

The proposal of October 1961 shows a continuously folded evaporator sheet. The height of the flat area of the fold has been given as 1.518 feet (18.216 inches) for steel and 1.439 feet (17.268 inches) for aluminum. To these heights must be added the forming radius at both top and bottom which should be 3/16 inch inside radius. The respective overall heights of the steel and aluminum evaporative sheets are 18.65 and 17.693 inches. The configuration of the return bends at top and bottom of the module are not fixed and can be varied to suit the manufacturing process. However, the bottom reverse bend must accommodate a means of removing the concentrated brine and the upper reverse bends must accommodate ports for inert gas removal.

Some configurations of top bends and bottom bends that were considered are shown in Figure 13. To date there has been no reason to deviate from the original radius bend as shown in Figures 13 (a) and 13 (e). Using bends (b) and (f) will complicate the drainage of concentrated brine from the bottom and the ducting of inert gases from the top. A bottom bend as shown in Figure 13 (h) can result in crevices which tend to form oxygen concentration cells. The bottom bends shown in 13 (e), (g) and (h) have best characteristics for brine drainage through the side sheet as a hole of adequate size can be made in the side sheet within this bend. The calculation of hole size for drainage is given in Appendix D.

Page 16, drawing 623A035 of the Westinghouse's proposal to the O.S.W. shows a continuous folding operation to form the evaporative sheet. A continuous

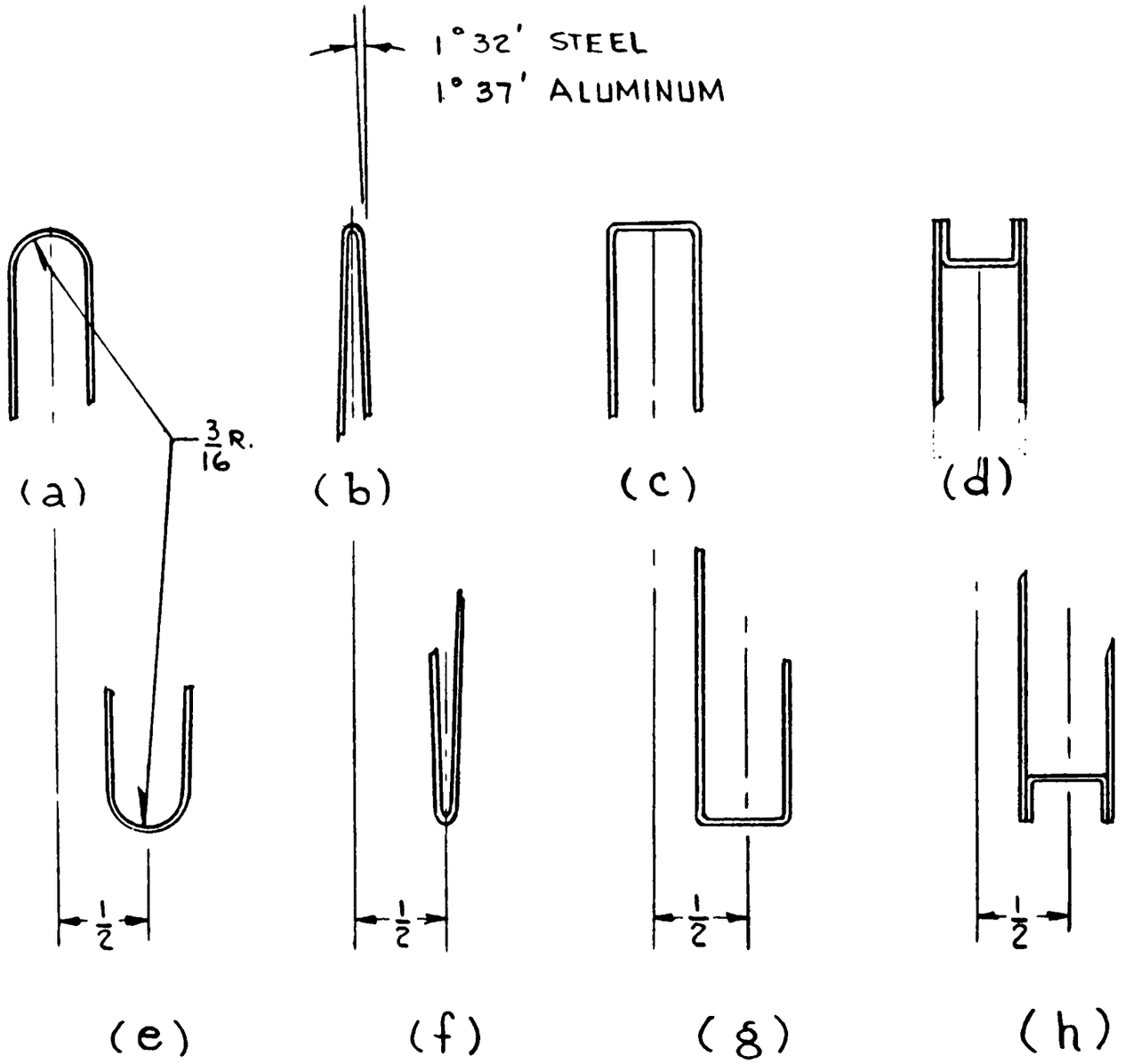

STYLES of BENDS for
EVAPORATIVE SHEETS

FIG. 13

process is definitely possible, but it will have to be done differently from that shown in the proposal.

The tooth and groove arrangement shown in this drawing can be used to make a reverse 180° bend except that the entrance and exit from this groove must be gradual so that an abrupt permanent deformation does not take place in the sheet. With .030 thick steel, the entrance and exit must be such as not to bend the steel through a radius smaller than 9 inches, otherwise permanent deformation will take place. The configuration of rolls shown in the proposal is shown here in Figure 14 together with the resulting form of the evaporative sheet.

Figure 15 shows the cut-out necessary in the rolls to prevent the unwanted deformation. However, by doing this, the rolls would lose control of the sheet upsetting the concept of the rolls.

Feed rolls could be used on either side of the forming rolls, but control between these would be lost. The effect would be similar to a press brake with rotary action.

A superior method for continuously folding was similarly proposed by two firms. One of these firms, the Taylor-Winfield Corporation proposed a method of folding and stretch-sizing. This corporation works in the field of special equipment for sheet metal forming, stamping and welding. Their method includes partial creasing at the fold, folding to near 180° bends, and then stretching the folds to a linear reproducible dimension. Their estimated cost of the equipment is $112,000. However, since this equipment is unique and therefor would require extensive development and debugging a figure of $150,000 would seem more realistic.

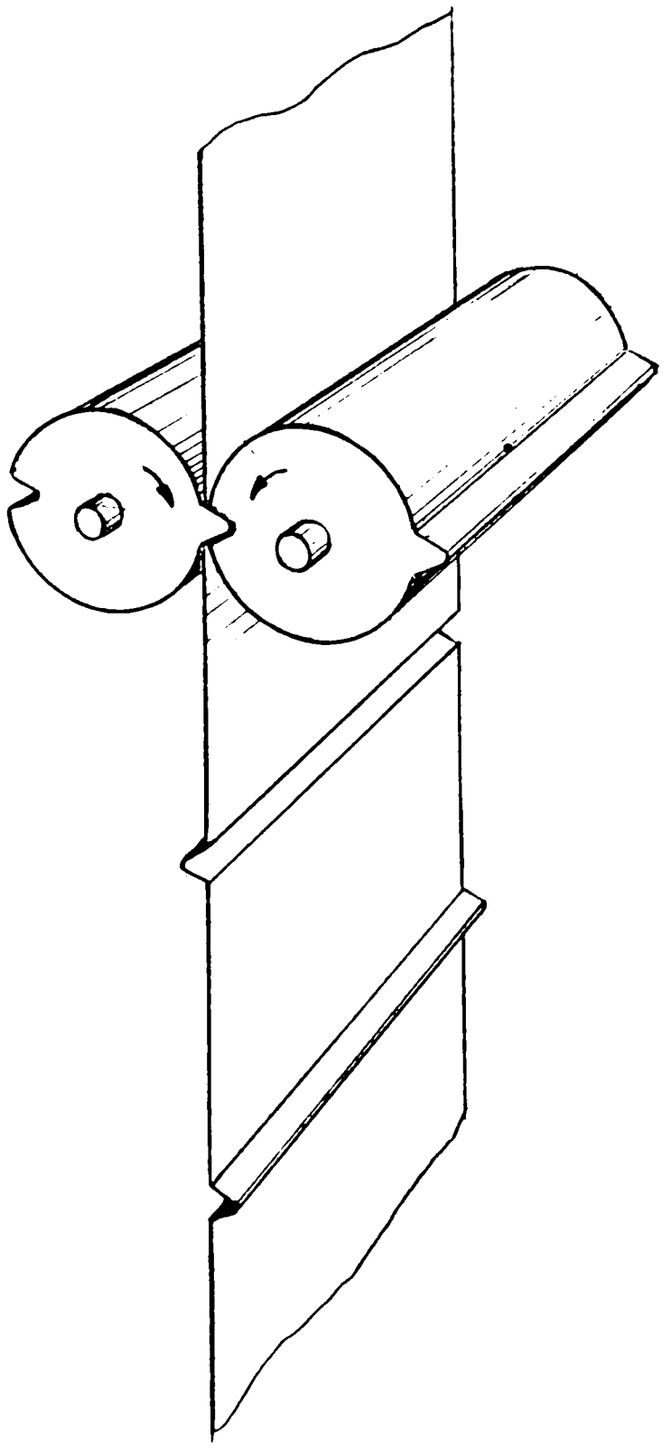

FIG. 14

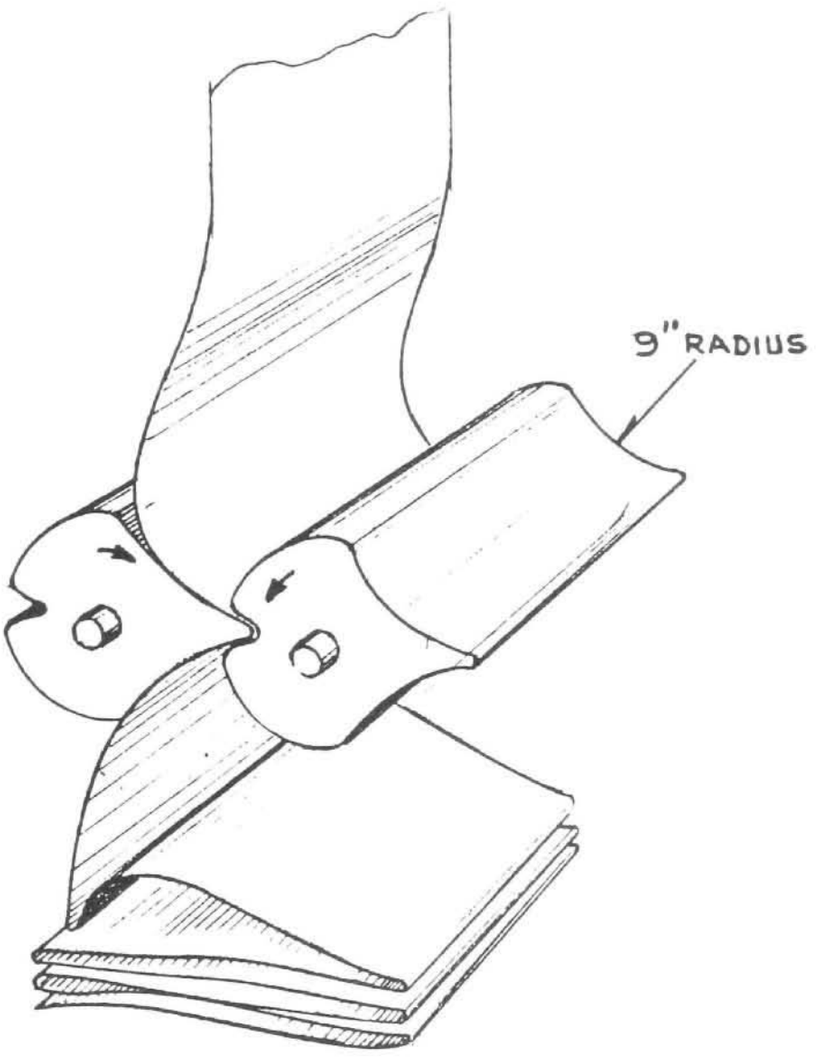

FIG. 15

A sketch of the equipment is shown in Figure 16. Such equipment could be suitable either for steel or aluminum modules and is recommended where production of modules for more than one 10,000,000 g.p.d. conversion plant is anticipated.

SAE 1010 has an elongation of 35% in 2 inches and would be desirable because of the stretching operation. SAE 1020 has an elongation of 22% in 2 inches and would also be suitable.

Tin has an elongation of 35% in 2 inches and this would make it compatible with either of the above steels in the stretching operation. There should be no cracking or rupture of the plating.

For limited production, the module can be most economically made from pieces joined together. Configurations of this type are shown in Figure 17. They can be formed on a press brake with simple dies. Making and sealing the joint can be done by soldering if tin plate is used. For aluminum adhesive bonding is the recommended method of joining. Brazing of steel can be effected provided heat is applied only to the joint and not to the complete sheet, otherwise unacceptable distortion will result.

WELD

Welding was investigated as a good possibility for joining steel. To date it has proved unsuccessful due to distortion of the evaporator sheet caused by heating during welding.

Killed steel is preferable to other steels as it gives a more uniform porous free weld, and was used in our experimentation. Rimmed steel is less costly than aluminum killed steel by about $.75 per hundred lbs., but is not recommended.

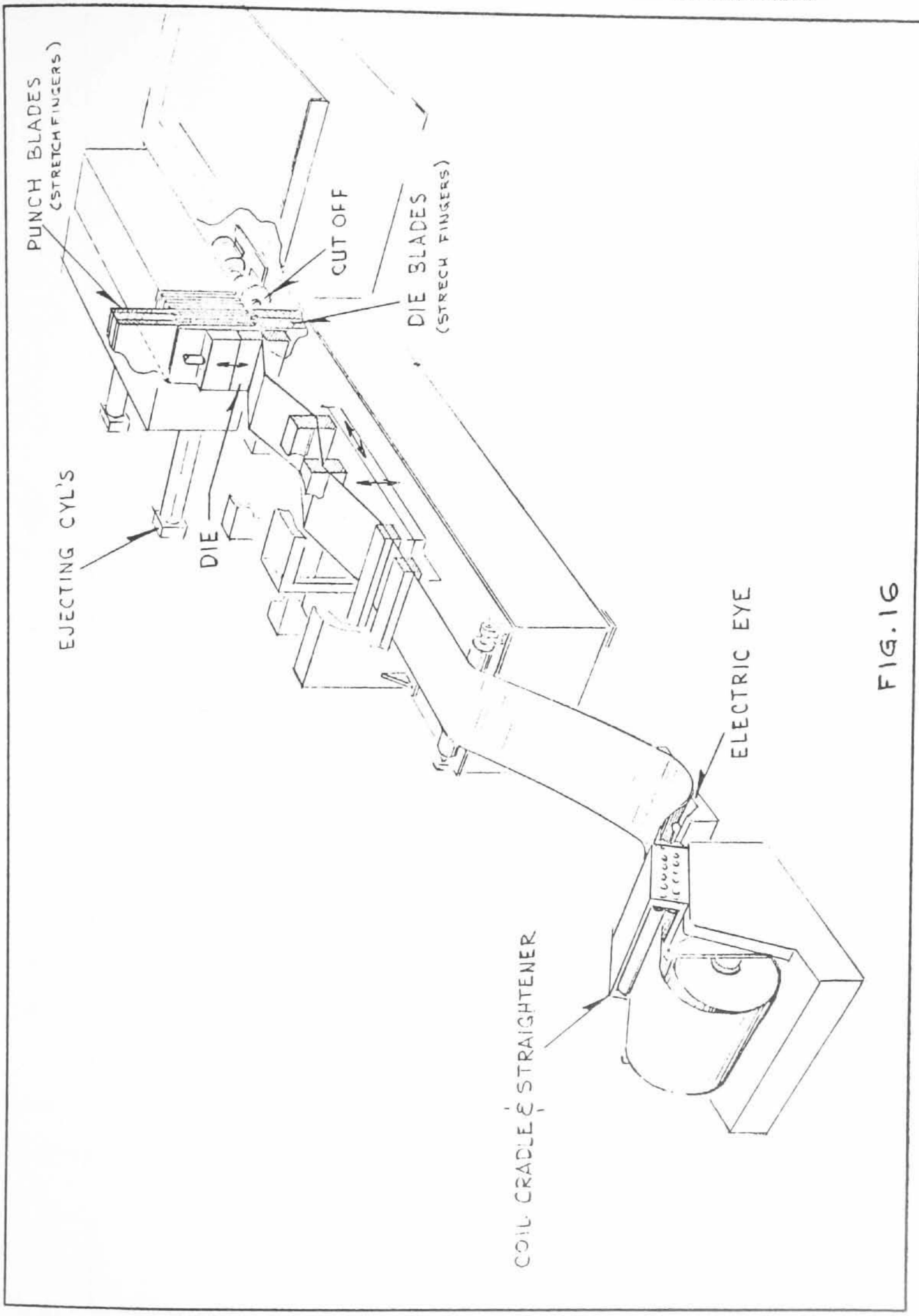
PUNCH BLADES
(STRETCH FINGERS)
CUT OFF
DIE BLADES
(STRECH FINGERS)
EJECTING CYL'S
DIE
ELECTRIC EYE
COIL CRADLE & STRAIGHTENER

FIG. 16

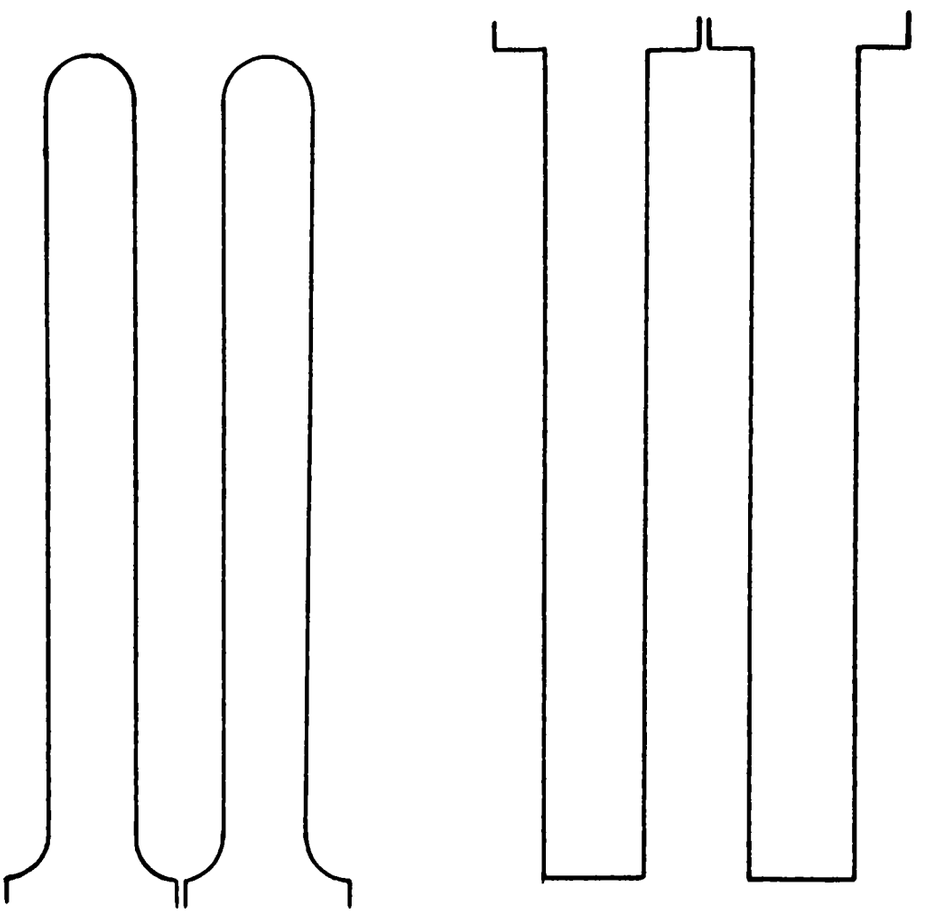

FIG. 17

EVAPORATOR SHEET SECTION
MULTIPLE SHEET DESIGN

Welding the flat side sheet shown in Figure 6, drawing D-HML-0.63, would require melt-through welding. This method of welding is being done on stainless steel for B-70 skin panels for .040 to .072 inch thick stock using T.I.G. This method is described in Item 5 of the bibliography. Due to the problem of blind tracking the joint and to the developmental work involved it was decided to drop this approach and try an edge joint as shown in Figure 18. In this joint design the edge of the evaporator sheet protrudes through the side sheet. A photograph of a sample weld section is shown in Figure 19.

Experimental work in welding this type of joint showed that the optimum side sheet thickness for full weld penetration was 0.0598 inches (16 gage). M.I.G. welding was used with the following conditions:

Westinghouse R. C. D. welder; SA-120 Westing-Gun, SA33 control

Gas: Argon 30 C.F.H., CO_2 - 10 C.F.H.

Wire MS-21 - .035 dia.

Voltage 17 volts, Current 100 amps.

Welding of a sample module section shown in the photograph of Figure 20 resulted in good welds but the heat input caused distortion of the evaporative sheet. Such distortion makes the module unacceptable as it may upset the thin film of sea water and cause dry spots. The fixturing for welding included copper back-up bars and aluminum heat sink plates to minimize distortion. A sketch of this fixturing is shown in Figure 21.

Another joint design that was considered is shown in Figure 22. This joint uses the side sheet shown on drawing B-HML-0.55 Figure 23. This design was discarded for 2 reasons.

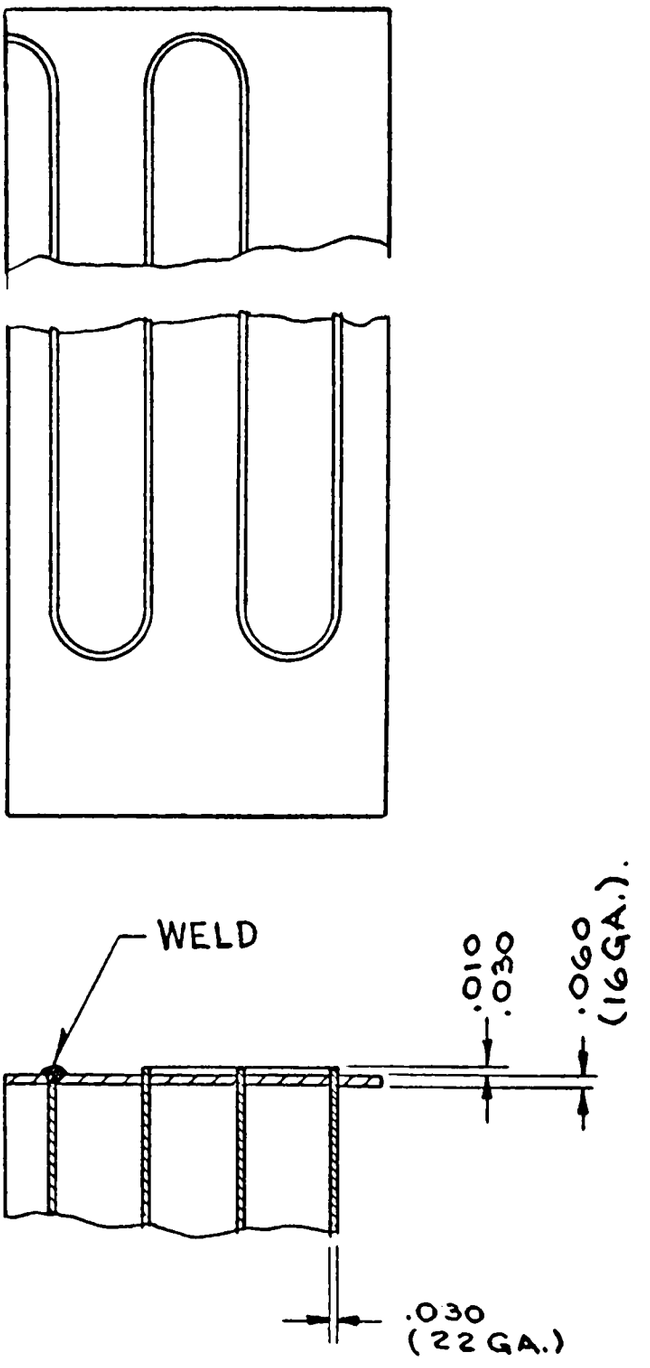

FIG. 18

WELD JOINT - STEEL MODULES

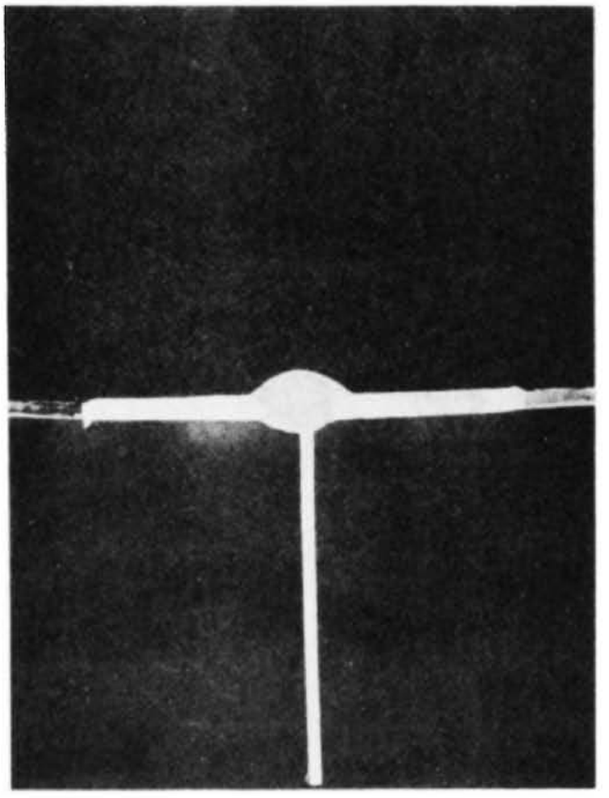

FIG. 19

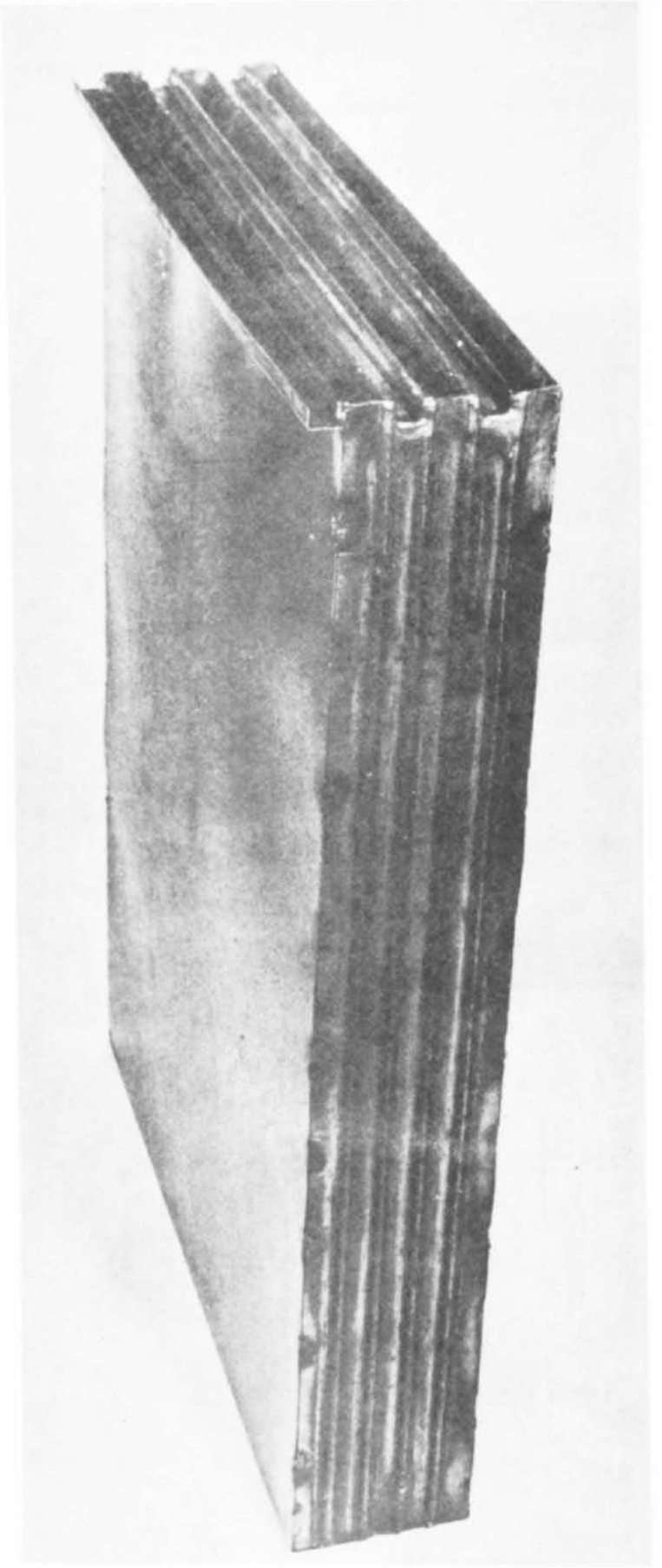

FIG. 20

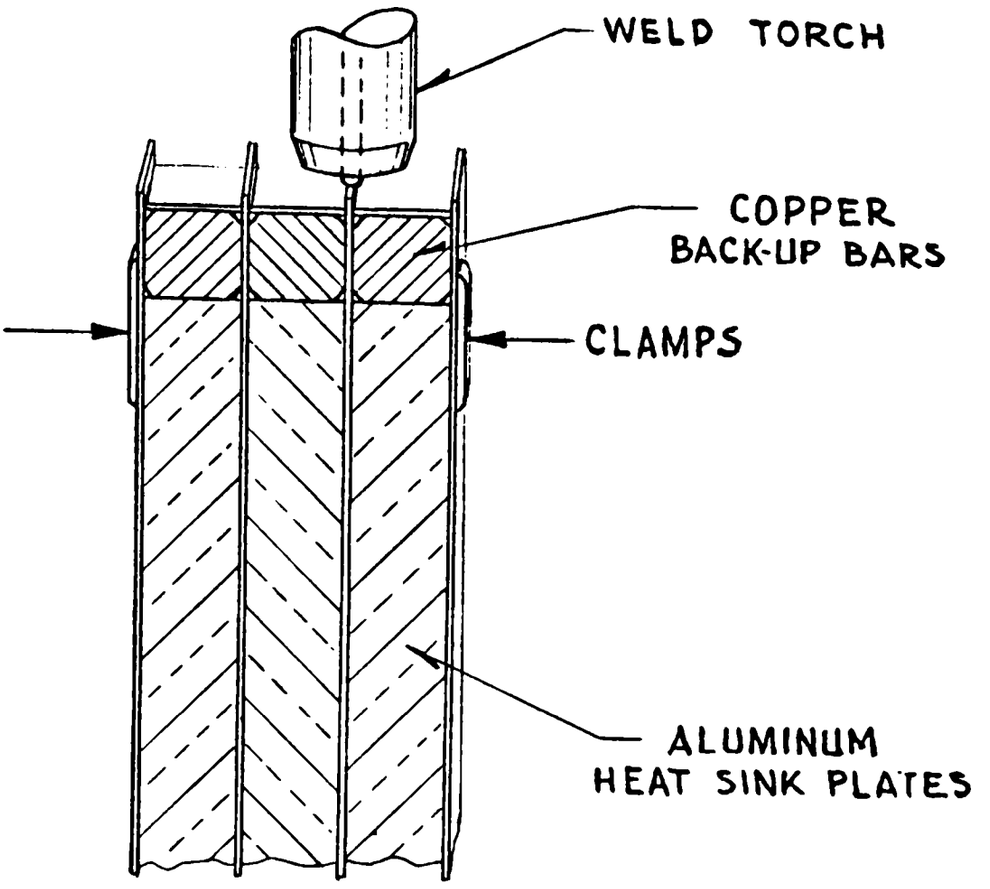

FIXTURING METHOD USED
FOR MIG. WELDING

FIG. 21

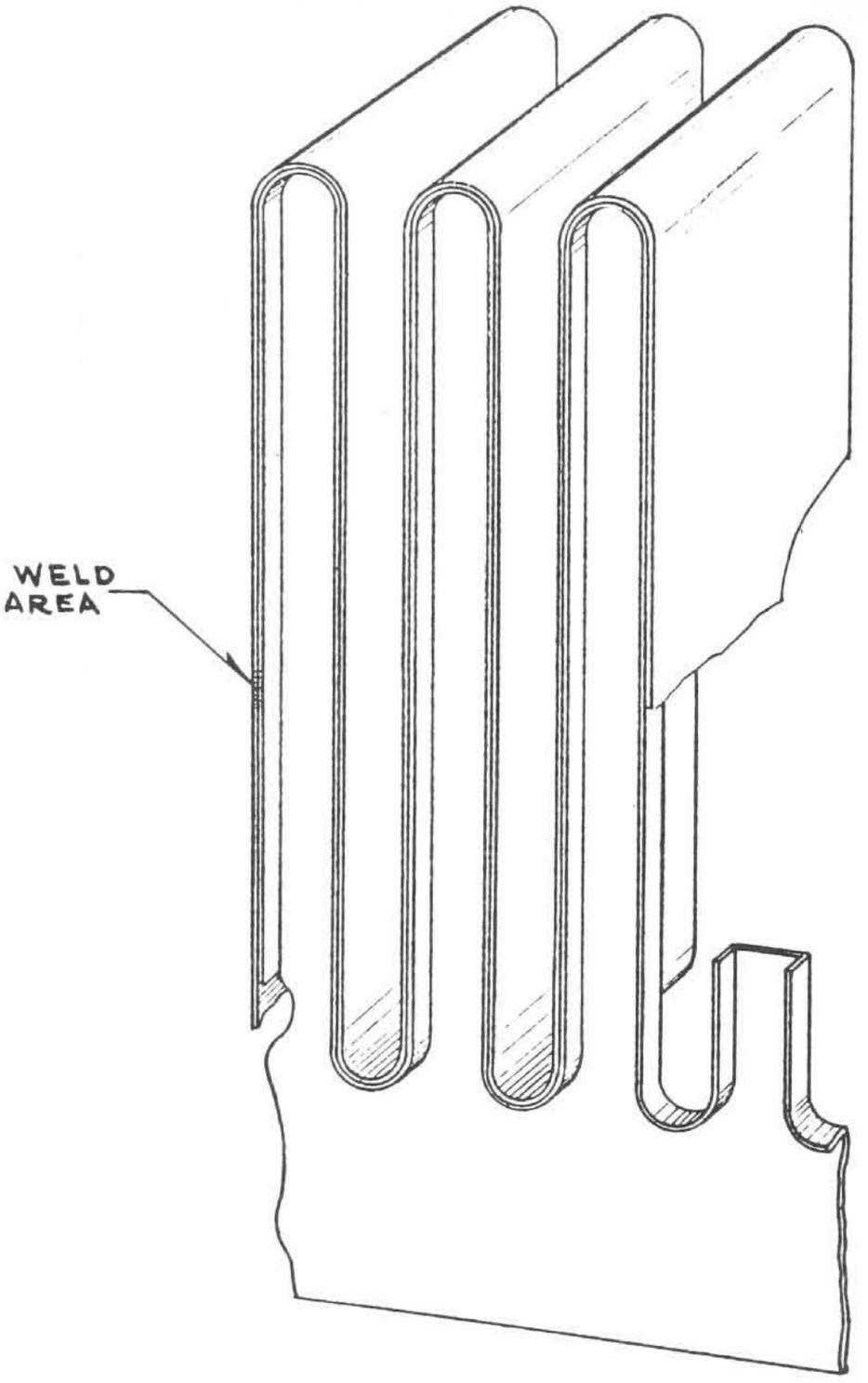

WELDED JOINT DESIGN WITH
FLARED SIDE SHEETS

FIG. 22

MATERIAL	PDS.	DESCRIPTION
STEEL		LOW CARBON PICKELED & OILED SHEET

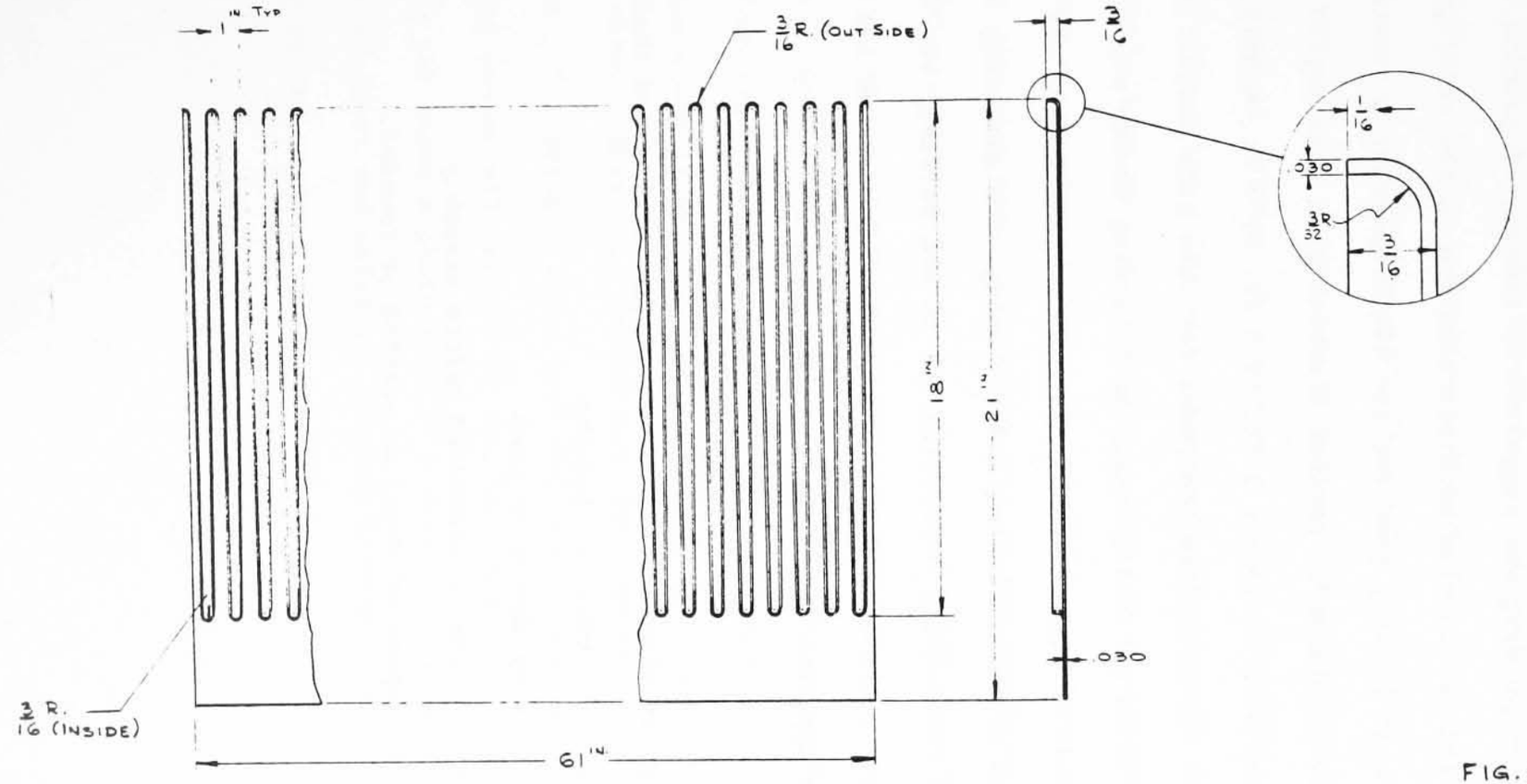

FIG. 23

REVISIONS

A

USED ON ASSEMBLY DRAWING

MACHINE

WESTINGHOUSE ELECTRIC CORPORATION
HEADQUARTERS
MANUFACTURING
LABORATORY
PITTSBURGH, PENNSYLVANIA

TOLERANCES UNLESS OTHERWISE SPECIFIED

DIMENSION	FRACTIONS	DECIMALS
0 TO 6 IN.	± 1/64	± .005
6 TO 24 IN.	± 1/32	± .010
OVER 24 IN.	± 1/16	± .015

ANGLES AS SPECIFIED

TITLE: SIDE SHEET

DRAWN S.Q. Malinoski DATE 8-29-62
CHECKED DATE
APPROVED DATE
DIMENSIONS IN INCHES SCALE

B-HML-0.55

S. K. ELLIOTT CO., PGH., PA. REORDER A-24432

(1) It creates crevices that may give rise to oxygen concentration cells.

(2) Development of the die for producing the side sheet with the necessary close fit-up requirements would be a formidable task.

Electron beam welding was suggested as a means of joining for melt through welding and this would give no distortion due to the welding process. However, the fit-up must be very good for the electron-beam; intimate metal to metal contact must be maintained. Another drawback with this method is the size of vacuum chamber needed to enclose a 3 ft. by 5 ft. by 2 ft. module.

The cost of Electron Beam equipment for this size product is in the area of $200,000. In addition a blind tracking or following device would have to be provided and this would add approximately $50,000 to the cost of the equipment.

Suggestions of super cooling and fixturing with annealing have been advanced as means of eliminating distortion due to arc welding, but these create large costs in equipment and have not been followed. To date no low cost successful welding means is apparent and none is recommended.

SOLDER

When making tin plated steel modules it is recommended that:

(1) soldering be used for joining

(2) embossed side sheets be used

(3) solder and flux be preplaced before assembly

(4) edge of evaporator sheet be scarfed or rounded.

A plain "T" joint would not have sufficient mechanical strength and would require close control of tolerances and fit-up. The grooved joint as shown on drawing D-HML-0.60 Figure 5 will allow more joint area and more tolerance in fit-up. It is estimated that the cross-sectional length (C-D-E) of joint on the evaporator sheet will be about 0.200 inches long assuming a fillet radius of .030 inches. This will be equivalent to a lap joint with a leg of .150 inches, see Figure 24.

All soldering is done below 800°F (A.S.M.E. - Metals Engineering Processes) and the temperature range used here would be about 500°F to 550°F depending on the choice of solder. In choosing a solder the corrosion characteristics of the solder tin plate joint will have to be considered. Solders of 40%Pb.- 60%Sn. would be best to start with since they are reasonably low cost and solidify rapidly on cooling. A rosin flux should be used and this could be applied by spray on the side sheet and on the edge of the evaporator sheet. Since rosin is non-corrosive at the operating temperature of 122°F no effort need be expended to remove it unless it presents a wetting problem.

Heat can be applied by gang torch, furnace, infra-red lamps, induction coils, resistance heating or hot platten. The hot platten press is recommended for this application since it will heat only the side sheet and a short section of the evaporator sheet. This will insure that the evaporator sheet does not distort due to heat. Soldering will be done one side at a time, in a horizontal plane so that molten solder will remain in the joint are.

Figure 25 (a) shows a photograph of a section of a soldered joint made with an embossed side sheet and using hot platten heating. (Figure 25 (b) is an enlargement of the center joint.

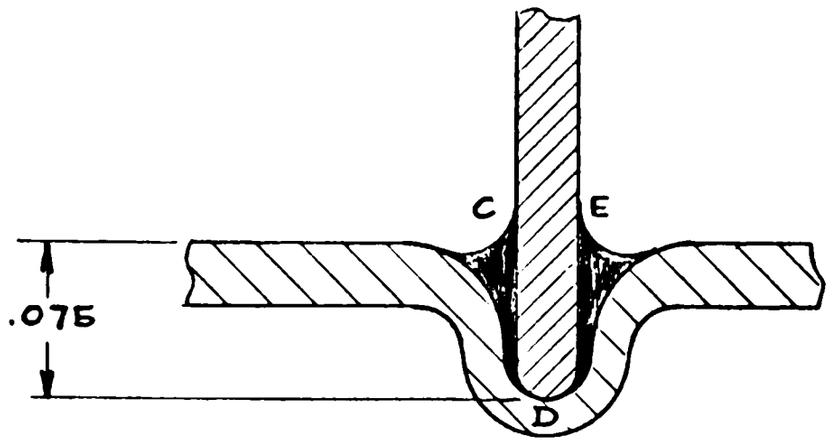

(a)

RECOMMENDED MODIFIED
"T" JOINT

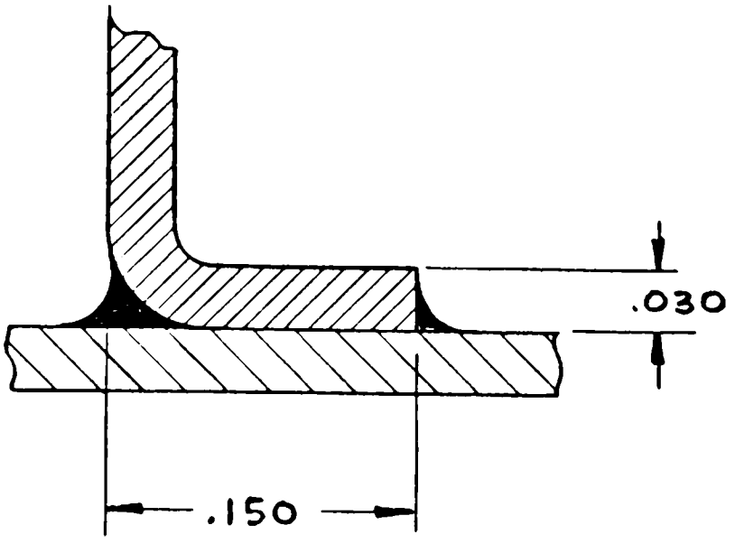

(b)

EQUIVALENT LAP JOINT
FOR SURFACE AREA CONTACT

FIG.24

FIG. 25 (b)

38 x Size

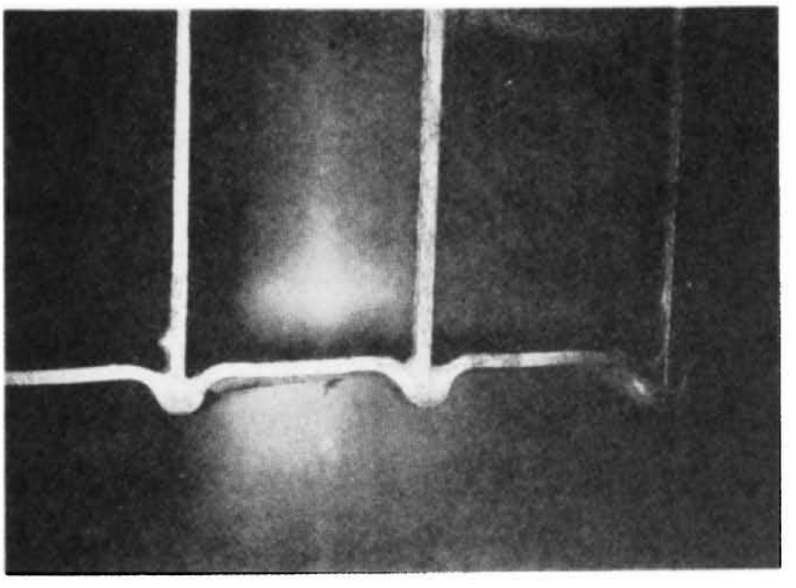

FIG. 25 (a)

2-1/4 x Size

EPOXY BOND

During the course of the manufacturing studies more effort was expended on investigating adhesive bonding as a joining technique than on any of the other joining methods. The reasons for this were threefold:

1. Adhesive or epoxy bonding apparently offered a low cost, method of joining which could be applied to several materials.
2. The temperatures required in the curing cycles were low enough so that distortion and oxidation problems were minimized.
3. This was the method originally proposed in the system concept.

A complete description of the adhesive bonding program is given in Appendix E. For our purposes here it will be sufficient to summarize the findings of the investigation.

The adhesive bonding joining technique was tried using two of the basic heat transfer surface materials - low carbon steel and aluminum. Although many combinations of surface preparations and epoxies were tried with these two materials, the adhesive bonding was found to be successful only with the aluminum. What were apparently satisfactory steel joints after curing suffered serious delamination after immersion in deaerated sea water at 125°F.

Successful aluminum joints were made using Shell Epon 422 (an epoxy phenolic formulation). This epoxy was recommended by the Kaiser Aluminum Co. as being the best adhesive for aluminum for these conditions. Test sample lap joints (bonded with Epon 422) have shown no evidence of delamination after exposure to synthetic sea water at room temperature for periods of time in excess of 18 months. These tests were and still are part of an extensive adhesive bond/aluminum

program conducted by the Kaiser Aluminum Company's Research Laboratories. Although these continuing life tests can not be used to predict the desired 10 year life for epoxy joined aluminum they do show that this method of joining aluminum has definite promise. For this reason an epoxy bonded aluminum module would be recommended for a pilot plant application.

The recommended pretreatment for the aluminum prior to bonding with Epon 422 is a chromic-sulfuric acid etch. The recommended joint geometry is the modified "T" joint formed with the embossed side sheet. See Figure 24 (a). The complete cure cycle for Epon 422 is described in Appendix C. The top temperature is 340°F and curing time is 135 minutes.

BRAZE

Brazing of both aluminum and steel modules was tried and presently is not recommended.

Steel

A steel module 12 inches wide by 18 inches high x 6-1/2 inches long was made and furnace brazed. Solder used was Handy and Harman No. 3 silver solder. Flux was Handy and Harman borax type.

Due to the mass of the oven it took 5-1/2 hours to heat the module to a brazing temperature of 1400°F. Gradual heating was necessary to prevent distortion. Module was cherry red and allowed to cool in the oven overnight. The poor quality of the joint was assumed to be due to deterioration of the flux over the long heat-up period. Some distortion was evident in the evaporator sheets, but not enough to be considered objectionable. The long heating time, and cooling time, and the need for a reducing furnace atmosphere makes this method of joining unattractive.

A photo of this module is seen in Figure 26. Original fit-up between evaporator sheet and side sheet was .005 inch maximum.

The photo in Figure 27 shows a steel module 12" wide x 18" deep by 1-1/2" wide that was induction brazed. This used the same solder and flux as above. The upper edge of the module was brazed by pre-coating with flux, applying sheet of silver solder, fixturing using transite spacers and passing slowly over an induction coil. The lower edge of the module was brazed the same way except that steel spacers were used instead of transite. With the use of steel spacers there was very little distortion and the joint was contiinuous. With this type of brazing there is a problem of cleaning out the flux. Manual scrubbing seems to be the most certain way of cleaning. This is difficult with the folds spaced at 1/2 inch and 18 inches deep. Induction brazing probably could be developed in a reducing atmosphere to eliminate the flux and the cleaning problem. However, it is felt that the cost of the brazing material and the development of the coil and furnace would make this method expensive.

Aluminum

The big problem with brazing aluminum is that the operation involves high temperatures of 1100°F and this leads to unacceptable distortion in the module. Alcoa Aluminum was of the opinion that the module could be brazed using brazing stock for side sheets. Brazing stock is an aluminum sheet covered with a 5% (More or less as desired) thickness of brazing alloy.

A sample module 12 inches wide by 18 inches high by 9 inches long was folded and fixtured for salt bath brazing. This is shown in the photo of Figure 28.

FIG. 26

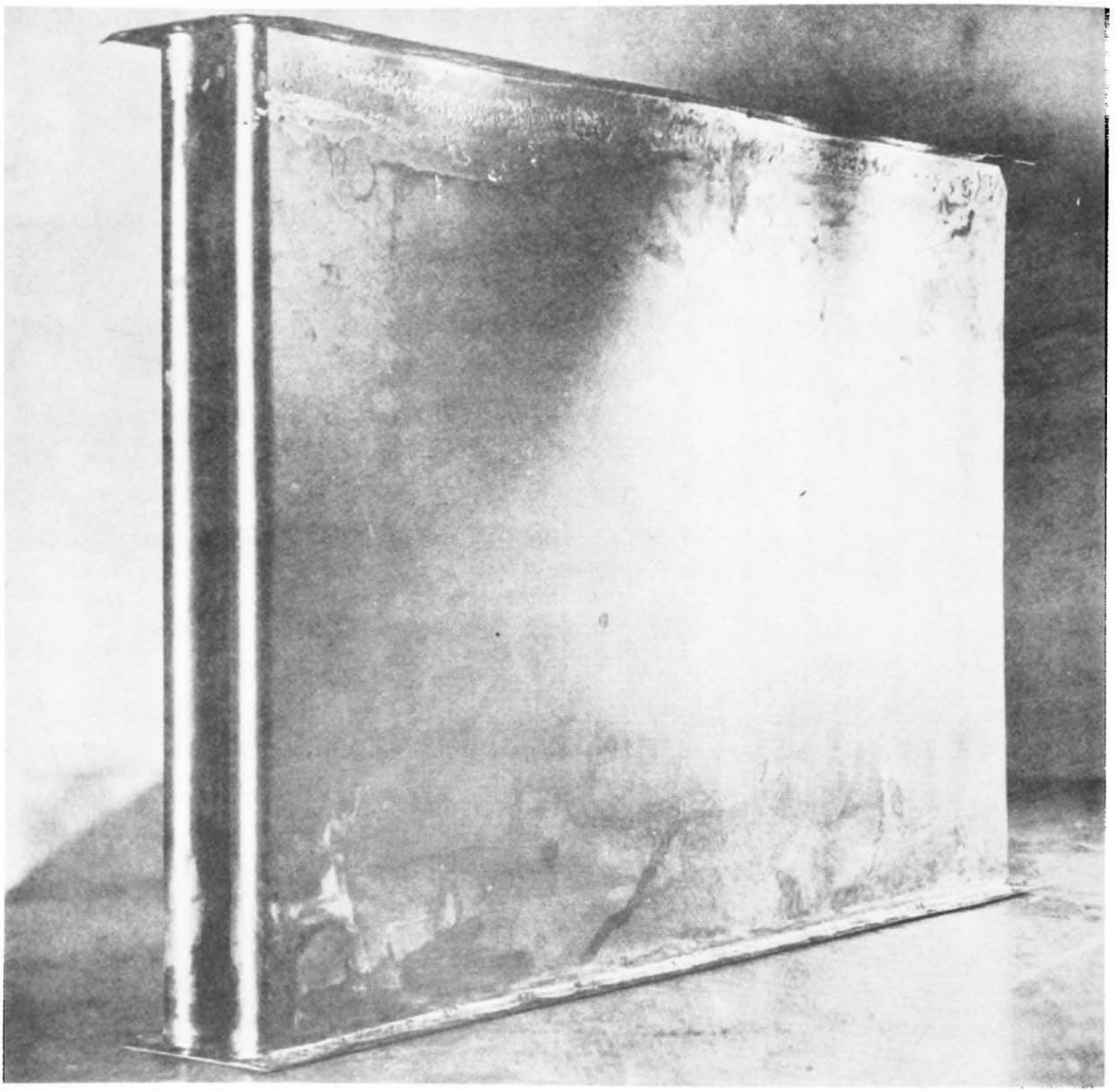

FIG. 27

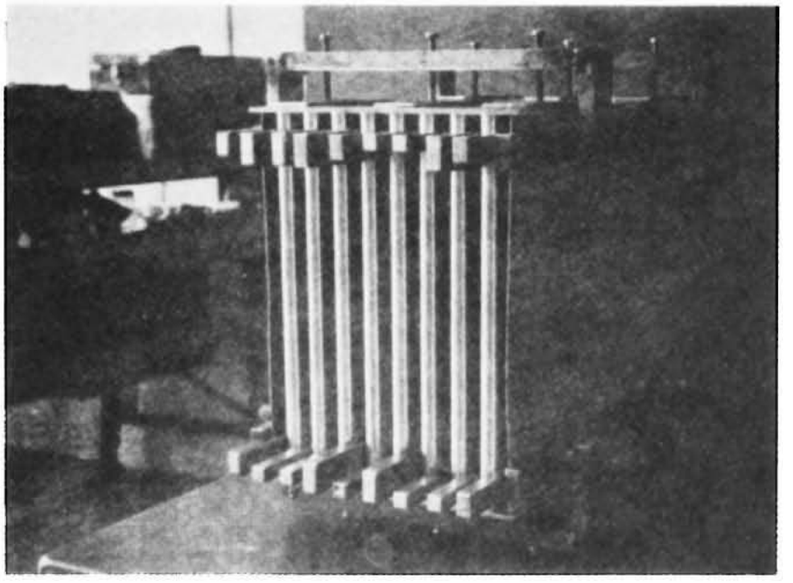

FIG. 28

The sample was taken to the Alcoa Laboratory for brazing. Upon preheating in an oven to 700°F the folded sheet warped to such a degree that further heating and brazing was pointless. It was felt by the Alcoa people that modules could be successfully brazed after doing developmental work on fixturing with, perhaps, some changes to the module design. These changes might encompass multiple piece construction, extruded sections for some of these pieces and possibly locating and holding tabs and notches.

Kaiser Aluminum also felt that the module could be brazed, but thought that this could be done best by inert gas furnace brazing. A pre-heat tunnel type oven with graduated heat zones was considered necessary. Preheat time would be from one to two hours. The module would require a carefully designed fixture to hold the module parts and at the same time allow variable expansion of the parts during preheat and brazing.

Photos were seen of brazed products of a size similar to the heat transfer module, but none had similar high ratios of unsupported surface area to metal thickness. Fit up requirements spelled out in Alcoa's Brazing Manual call for maximum gaps between mating parts of 0.010 inches for lap joints. No fit up is given for "T" joints. Kaiser representatives have had filleting of gaps up to 0.030 inches, and believe that embossed side sheets would improve filleting.

Experimenting with fixturing and module design would be too expensive in time and money for this study and was not pursued.

Appendix B

ETCH

For adhesive bonding of aluminum, the surface treatment recommended is a chromic-sulfuric etch. This is recommended by Kaiser Aluminum and by Shell Chemical for treatment prior to bonding with Epon 422. Superiority of an etched surface is supported by Elmund Thelen in his article on "Adherend Surface Preparation" published in "Symposium on Adhesives for Structural Applications" - bibliography (4) where he says chromium ions are necessary for maximum joint strength with aluminum or magnesium. Surface cleaniness can be determined by the wettability of the cleaned materials.

After etching, the metal should be flushed with cold tap water and air dried at 150°F or less.

Surfaces that are etched, washed and dried should not be allowed to stand unprotected for any length of time (no more than 2 hours) otherwise they will adsorb moisture, oils and even dust which will be detrimental to the joint strength.

Composition of etchant solution:

2 parts by weight sodium dichromate ($Na_2Cr_2O_7 2H_2O$)

7 parts by weight of 96% sulphuric acid

17 parts by weight of distilled water.

To mix, dissolve the dichromate in most of the water, add sulphuric acid, stirring carefully and then add the remaining water.

Recommended etching time, 10 minutes

Recommended etching temperature, 155°F $\pm$ 10°

The life of the etchant will depend on the actual operating conditions. It is estimated that one cubic foot of etchant will suffice for 10 modules.

The side sheets shall be totally immersed in solution for etching. The evaporator sheets shall be etched, one edge at a time for a depth up to 1 inch.

Tanks for etching solution together with electrical heating means and temperature control will cost $2,500 each. Coated exhaust ducting for etchant vapors is estimated at a cost of $2,000.

Two tanks and exhausts will be required, - one for the side sheets and one for the evaporator sheets. The tank for the side sheet should be able to accommodate 2 at a time. The tank for the evaporator sheet should be able to accommodate 4 at a time.

LEAK TEST

Regardless of the method of joining modules they must be tested for leakage. If there are leaks in a module it will have to be scrapped or repaired, the latter disposition being preferable.

Methods of Leak Testing

Liquid or gas under pressure applied to one side of the heat transfer module can be used. The presence of leaks can be determined by:

(1) visual observation

(2) pressure drop

(3) gas pass-through with gas detector or bubbles through liquid

(4) volume drop

When checking for leakage, the location as well as the existence of the leak must be determined. In addition the clean surface condition of the module must not be disturbed or, of disturbed must be cleaned again. This cleaniness is necessary

for system operation rather than production, that is, it must not be allowed to rust, or be coated with oils or grease.

A simple static water test using detergent solutions is an approach that would be most suitable here. Subsequent rinsing and drying will be required.

Volume of module = 3/2 ft. x 5/2 ft. x 3 ft. = 11-1/4 cu. ft.
= 84 Gallons

Flow 30 p.s.i. - 1" nozzle = .37 c.f.s. = 22.20 cfm

Time required to fill module = 1/2 minute

Soak time = 1 minute

Leakage check time = 2 minutes

Dump water time = 1 minute

Total = 4-1/2 minutes

Associated handling time will raise this to 8.54 minutes per module.

Pumping and associated equipment will cost about $15,000 which includes pumps, valves, piping lines, gauges, fixture stand, crane.

Recommended liquid:

for aluminum - water with detergent

for steel - water with about 1/2% phosphoric acid

FIXTURE, CLAMP & CURE

Fixturing and clamping will be based on the curing method in the case of aluminum and on the soldering method in the case of tin plate. Platen

heating is recommended for both these materials and fixturing will be similar in both cases.

Standard platen presses can be fixtured for locating side sheets and evaporator sheets. Due to the long cure cycle of 135 minutes approximately 15 individual presses would be required. The cost of these would be about $6,000 each. Fixturing alterations would be $1,000 each. For a total of $7,000 each. Cost for 15 such presses = 15 x 7,000 = $105,000.

Dunning and Boschert Corporation of Syracuse, New York, have platen presses suitable for this application.

PACKAGE

Packaging of individual modules will be necessary to:

(1) facilitate handling

(2) prevent damage to the module

(3) prevent deterioration of the clean evaporator surface of the module

Items (1) and (2) are taken care of by normal crating or boxing methods. Item (3) will be taken care of by enclosing the module with a plastic bag, adding a desiccant and heat sealing. The plastic bag will be partially evacuated before sealing.

The following detailed packaging procedures are recommended. See Figure 29 for illustration.

1. Place expendable pallet in packaging area.

2. Place bottom stitched tray open side up on pallet.

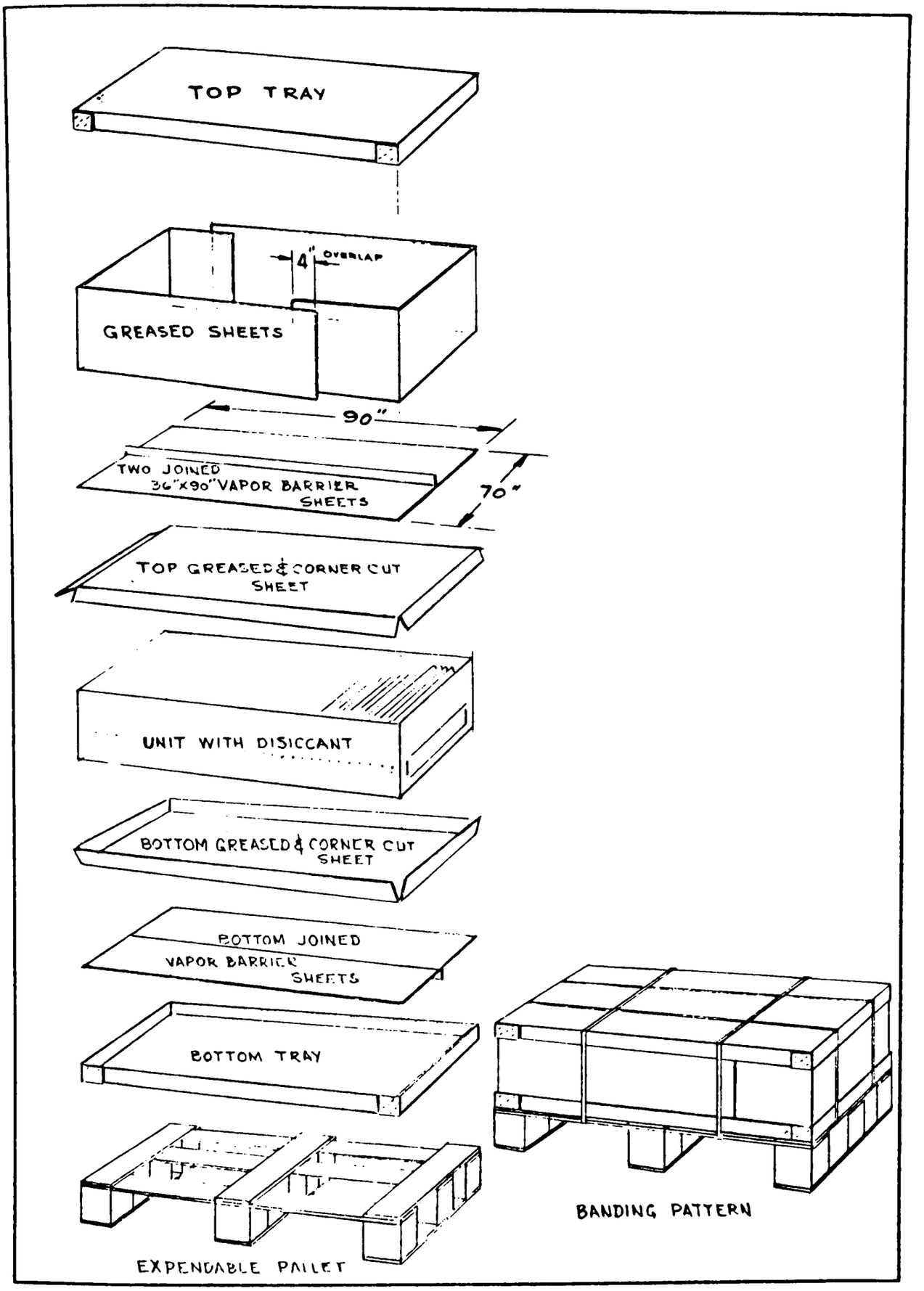
TOP TRAY
4" OVERLAP
GREASED SHEETS
90"
TWO JOINED
36"x90" VAPOR BARRIER
SHEETS
70"
TOP GREASED & CORNER CUT
SHEET
UNIT WITH DISICCANT
BOTTOM GREASED & CORNER CUT
SHEET
BOTTOM JOINED
VAPOR BARRIER
SHEETS
BOTTOM TRAY
EXPENDABLE PALLET
BANDING PATTERN

FIG. 29

3. Join two 36 inch x 90 inch sheets of vapor barrier material to form one sheet 70 inches x 90 inches and center this sheet onver stitched tray.
4. Place bottom creased and corner-cut sheet on top of vapor barrier and line up with inside of tray. Push down, making sure the vapor barrier and corner-cut pad conform to inside of tray.
5. Distribute desiccant packages evenly throughout unit and place unit in tray.
6. Place top creased and corner-cut sheet over unit and initially fold down flanges to pre-break creases.
7. Place second 70 inch x 90 inch barrier sheet over unit and seal edge to bottom sheet with rotary hand operated sealer, leaving a 2 inch diameter hole at one corner for partial evacuation. After evacuation, completely seal hole.
8. Place creased sheets around unit inside of bottom tray so that they overlap 4 inches at the end of each sheet.
9. Place top tray over tube created by creased sheets and band as per illustration.

COST ANALYSIS OF MANUFACTURING PROCESSES

In the section on Manufacturing Processes the techniques of applying a given process and the equipment required were described. In this section, the costs of each of the processes is analyzed from a material and labor standpoint. The production requirements are the same as those described in the section on Purpose and Assumptions.

The cost estimates of this report are based on an average direct labor rate of $3.00 per hour. Overhead is added at 100% to cover supporting indirect labor office help, supervision and fringe benefits. Plant and equipment costs are treated as separate expense items. The dollar figures for costs are based on a "per module" basis except for the "Summary of Module Costs on a Square Foot Basis" which is based on a square foot of evaporative surface of the module.

DE-REEL, STRAIGHTEN & FEED

De-Reel - Side sheet

There will be no direct labor or material costs in de-reeling the coil stock for the side sheet. The operation of loading the fresh coils of steel or aluminum on the reel will be done by the punch press operator.

De-Reel - Evaporator sheet

This equipment will be part of the folding line and will require no direct labor in operation. Loading fresh coils will be done by the material handler who unloads folded evaporator sheets from the folding machine.

Appendix B

PUNCH AND DRAW

Using a 1 inch section of die equivalent to one pitch will require 60 strokes of the press for production of one side sheet. At a conservative press speed of 30 strokes per minute the actual press time is 2 minutes. Maximum drawing speed for carbon steel is 35 f.p.m. and this is well within the above 30 strokes per minute. Allowing for a production efficiency of 75% the production time required is $\frac{2}{.75}$ = 2-2/3 minutes per side sheet.

Time for 2 sides sheets per module = 5-1/3 minutes.

Cost of direct labor at $3.00 per hour = $.267/module.

This estimate is supported by a quotation from McCauley Metal Products, Inc. of Buffalo which gives a price of $.463 per side sheet or $.926 per module.

For a comparable basis of the quotation with the direct labor cost estimate, overhead, equipment depreciation and gross profit margin should be added to the labor costs.

Direct labor	$.267/module
Overhead at 100%	.267/module
Press depreciation, 5 year term rate for 5-1/3 minutes, $14,000 capital cost	.124/module
SUB TOTAL	$.658/module
Gross Profit @ 40%	.263
TOTAL SELLING PRICE	$.921/module

Appendix B

DETERGENT WASH

Chemical Costs (Oakite Products) = $.09/thousand sq. ft. metal surface

Heat costs = 9 x chemical costs

= $.81/thousand sq. ft.

Time cycle 30 seconds detergent wash

5 seconds cold rinse

10 seconds hot rinse

Rate of strip feed = 24 ft. per minute

Solution dragout = 2000 gal. per month

Amount of strip cleaned per month

= 8 hrs. per day x 22 days x 60 min./hrs. x 24 x 3 sq. ft./min.

= 760,000 sq. ft.

Solution cost:

Water 2000 gal. at $1.00/thousand gal. = $ 2.00

Chemical 2 oz./gal. x $\frac{2{,}000 \text{ gal. x } 16 \text{ cents/lb.}}{16 \text{ oz./lb.}}$ = $40.00

Total solution cost = $42.00

Cost of solution change = $\frac{\$\ 42.00}{760{,}000 \text{ sq. ft.}}$ = $ .055/M. sq.ft.

Total material cost = $.81 + .055 = $ .865/M. sq.ft.

Cost per module = $\frac{\$.865}{1{,}000 \text{ sq.ft.}}$ x 2(541.6 sq.ft. + 2 x 12-1/2 sq.ft.

= $ .981/module

Since the wash operation will be carried on automatically, there will be no direct labor involved. However, we will allow for 1 man to monitor the washing, rinse and dry line.

RINSE

Amount of rinse water required = 1/10 gallon per sq.ft.

No. of sq.ft. of metal in module = 566.6

No. of sq.ft. rinsed = 2 x 566.6 = 1133.2 sq.ft.

Amount of rinse water used per module = 1133.2 x 1/10 = 113 gallons

Cost of water at $1.00 M. gals. = $.113 per module

DRY

Two experiments were run on drying sandblasted aluminum plate that was wet with water. One used heated air at 800°F at blower exit. Air velocity at blower exit was 3000 ft. per min. Drying time fore the sample was 1-1/2 minutes.

The second drying method used room temperature air blowing at 3000 ft. per min. Drying time for this sample was 6-1/2 minutes. Relative humidity 45% air temperature 73°F. In both cases sample size was 6-3/4 in. x 18-5/8 x .025 inches.

Since the unheated air drying is less costly, it will be used for flat sheet, folded sheet and partially assembled modules. Heated air will be used for completed modules due to the complex shape and reduced drying efficiency.

$$\text{Surface area dried} = 6.75 \times 18.625 \times \frac{2 \text{ sides}}{144} = 1.748 \text{ sq.ft.}$$

Ambient Air

Air exit area of blower:

Nozzle diameter = 1-3/16 inches

Gross nozzle area = $\frac{\pi}{4}$ x $(1\text{-}3/16)^2$ = 2.77 sq. in.

Wire mesh area = (14 + 14) wires/sq.inch x 1 in. long x .015 diameter

= .42 sq. inches/sq.in.

% open area = 100 - 42 = 58%

Net nozzle area = 2.77 sq.in. x .58 = 1.608 sq.in.

Air volume = 3000 ft./min. x $\frac{1.608}{144}$ sq.ft. = 33.5 c.f.m.

Total air volume per sq.ft. of sheet

$$= \frac{33.5 \text{ cfm} \times 6\text{-}1/2 \text{ min.}}{1.748 \text{ sq.ft.}} = 128.1 \text{ cu.ft. air/sq.ft. sheet}$$

Production requirements

= (541.6 sq.ft. evaporator sheet + 2 x 10 sq.ft. sides) x 2 sides of sheets = 1,123.2 sq.ft. per module

Production time per module = 8.54 min.

Drying rate = $\frac{1,123.2}{8.54}$ = 131.8 sq.ft./min.

Air volume required = 128.1 x 131.8 = 16,880 c.f.m.

Blower of 1 hp. delivers 1200 c.f.m. air at 1-1/2" water static pressure.

No. of hp. required = $\frac{16,880}{1200}$ = 14 hp.

Cost of electric power = $.01 per Kwh or $.01/effective hp.

Drying costs (power) = 14 x $.01 = $.14 per hour = $\frac{\$.14 \times 8.54}{60}$ = $.020/module

Heated Air

Drying time 1-1/2 minutes

Air temperature from gun 800° F at exit

Air velocity 3000 ft. per min. using same gun as above

$$\text{Air volume per sq.ft. of sheet} = \frac{33.5 \text{ c.f.m.} \times 1\text{-}1/2 \text{ min.}}{1.748 \text{ sq.ft.}}$$

$$= 28.8 \text{ c.f.m./sq.ft.}$$

Heat Required

Specific heat of air = .242 BTU/lb.°F

Weight of air at 800°F = .0314 lbs./cu.ft.

Amount of heat required = .242 BTU (800-72)°F x .0314 lbs./cu.ft.

x 28.8 cu.ft. = 159 BTU/sq.ft. of surface area

$$\text{No. of kw} = 159 \times .01758 \frac{\text{kw}}{\text{BTU}} = 2.79 \text{ kw/sq.ft. surface area}$$

Production = 541.6 sq.ft. evaporative sheet + 2 x 11 sq.ft. sides

x 3 x 5 bottom + 2 x 3 x 2 ends = 591 sq.ft.

Production time = 8.54 min. per module

No. of kw. per module = 591 sq.ft. x 2.79 kw./sq.ft. = 1,649 kw.

$$\text{No. of kw. hrs.} = 1{,}659 \times \frac{8.54 \text{ min.}}{60 \text{ min./hr.}} = 235 \text{ kw. hr.}$$

Heat power cost at $.01 per kw.hr. = $2.35/module

$$\text{Air required} = 28.8 \text{ cu.ft./sq.ft.} \times \frac{591 \text{ sq.ft.}}{8.54 \text{ min.}} = 1993 \text{ c.f.m.}$$

This is equivalent to 2 hp. at 1-1/2 inches static pressure.

SHEAR

The shear operation on the side sheet will be done by the same operator that controlls the press. The allowed production time for 2 side sheets per module is 5.33 minutes. The requirement in production is 8.54 minutes for 2 sheets. The remaining 3.21 minutes are available and more than sufficient for the shearing operation.

The cost of direct labor at $3.00/hr. = $.161 per module

SAND BLAST

The following operating costs are based on information received from Pangborn Corporation.

Evaporative Sheet Line

Operating speed - 21.1 linear ft. per min.

operating costs for equipment - labor not included, (Power, shot, replacement parts) = $2.50 per hour

Length of evaporator sheet per module = 180.5 ft. (steel)

Time required for blasting = $\frac{180.5 \text{ ft.}}{21.1 \text{ f.p.m.}}$ = 8.55 minutes

Cost per module = $8.55 \times \frac{\$2.60}{60}$ = $.356 per module

Side Sheet Line

Operating speed required = 1.17 ft. per minute

Operating costs = $1.00 per hour (From Pangborn)

Length of sheet per module = 2 x 5 ft. = 10 ft.

Time required for blasting = $\frac{10 \text{ ft.}}{1.17 \text{ f.p.m.}}$ = 8.55 minutes

Cost per module = 8.55 min. x $\frac{\$1.00/\text{hr.}}{60 \text{ min.}}$ = $.42 per module

Total blasting costs per module = $.356 + .142 = $.498 per module

As this will be a continuous automatic operation no direct labor is required.

ETCH

Recommended etchant

2 parts/w sodium dichromate ($Na_2 Cr_2 O_7 \cdot 2H_2O$)

7 parts/w 96% sulphuric acid

17 parts/w distilled water

26

Size of etching tank per module = 6 ft. long by 3 ft. wide by 6 in. deep

Specific gravity of water = 1.0

of sulphuric acid = 1.84

of sodium dichromate = 2.52

Weight of solution per cu.ft.

Water = $\frac{17}{26}$ x 62.4 lbs./cu. ft. = 40.8 lbs.

Sulphuric = $\frac{7}{26}$ x (1.84 x 62.4 lbs./cu.ft.) = 30.9 lbs.

Sodium Dichromate = $\frac{2}{26}$ x (2.52 x 62.4 lbs./cu.ft.) = 12.1 lbs.

Total = 83.8 lb./cu.ft.

Weight required for 9 cu.ft.

Water = 9 x 40.8 = 367.2 lbs. or 44.1 gallons

Sulphuric = 9 x 30.9 = 278.1 lbs.

Sodium Dichromate = 9 x 12.1 = 108.9 lbs.

Costs

Distilled Water = $1.10 per 5 gallon bottle = $.22/gal.

Sulphuric Acid 96% = $6.05 per 100 lbs.

Sodium Dichromate = $.35 per lb.

Costs per batch: (9 cu.ft.)

Distilled water 44.1 gal. at $.22/gal.	= $ 9.69
Sulphuric 278.1 lbs. at $6.05	= 16.81
Sodium Dichromate 108.9 lbs. at $.35/lb.	= 38.10
TOTAL	= $64.60

Estimated Life of Solution

Assume a 10 mil layer will be suitable for etching and that this will be used during one etching. Coverable area of 9 cu.ft. etchant =

$$9 \text{ cu. ft.} \times \frac{12 \text{ in.}}{.01 \text{ in.}} = 10{,}800 \text{ sq.ft.}$$

$$\text{Area covered per module} = (3 \text{ ft.} \times 5 \text{ ft.} \times 4 \text{ sides}) + 180 \text{ ft.} \times \frac{1 \text{ ft.}}{12} \times 4 \text{ sides}$$

$$= 120 \text{ sq.ft.}$$

$$\text{No. of modules} = \frac{10{,}800}{120} = 90 \text{ modules}$$

$$\text{Cost of etchant per module} = \frac{\$64.60}{90} = \$.718/\text{module}$$

Etchant cost per sq. ft. of evaporative surface = $.139

Although this operation could be automated one operator would be sufficient for loading folded evaporator sheets into the etchant tanks. He would also be available for loading and unloading side sheets in the etchant tank.

Direct labor cost for this operation would be 8.54 minutes per module at $3.00/hr. = $.427/module

Appendix B

FORM EVAPORATOR SHEETS

The special equipment for forming folds is estimated to operate at the required rate of 1 module every 8.54 minutes.

There will be one operator required for the operation of the machine plus one operator for loading, handling crates, and unloading folded evaporators.

Direct labor costs for these operations would be 2 x 8.54 minutes per module at $3.00/hr. = $.854/module

WELD

Although welding steel for modules has not proved successful some figures on costs are laid down for future information.

Oxy-Acetylene Welding with Filler Rod

Oxygen consumption 2.4 cu.ft./hr. - cost $.01 per cu.ft.

Acetylene consumption 2.3 cu.ft./hr. - cost $.02 per cu.ft.

Rod consumption .23 lbs./hr. - cost $.345/hr. @ $1.50/lb.

Welding speed - manual - 4 inches per minute

T. I. G. Welding

Argon consumption 12 cu.ft. - cost at $.07 per cu.ft.

Welding speed - manual - 6 inches per minute

M. I. G. Welding

Argon consumption 30 cu.ft. /hr. - cost $.07 per cu.ft.

CO_2 consumption 10 cu.ft./hr. - cost $.01 per cu.ft.

Wire feed 12-1/2 inches wire per inch of weld

Welding speed - automatic 12 inches per minute

Wire feed = 12-1/2 x 12 = 150 inches per minute or 150 x .000272 lb./in.

= .0408 lb./min.

Oxy-Acetylene - Material and Labor Costs

Length of welds - sides to evaporator sheets = 2 at 180-1/2ft. = 361 ft.

- bottom closures 2 (3 + 5) ft. = 16 ft. = 16 ft.

- end closures 2 at $(\frac{26}{12} + 3)$ 2 = 20.7 ft. = 20.7 ft.

TOTAL = 397.7 ft. = 397.7 ft.

Welding speed = 4 inches/min.

Welding time = $\frac{397.7 \text{ ft.}}{4 \text{ in.} \times 60 \text{ min.}}$ x 12 inches = 19.89 hours

Oxygen cost = 19.89 x 2.4 c.f.h. at $.01/c.f. = $.477

Acetylene cost = 19.89 x 2.3 c.f.h. at $.02/c.f. = .915

Rod cost = 19.89 x .23 lbs./hr. at $1.50/lb. =$6.862

Welding material cost = $8.25/module

Labor cost $\frac{397.7 \text{ ft.}}{4 \text{ in./min.}}$ x 12 in. x $\frac{\$3.00/\text{hr.}}{60 \text{ min.}}$ = $59.66/module

T.I.G. - Material and Labor Cost

Length of welds 397.7 ft.

Welding speed 6 inches per minute

Welding time = $\frac{397.7 \times 12 \text{ in.}}{6 \text{ in.} \times 60 \text{ min.}}$ = 13.26 hours

Argon cost 13.26 x 12 c.f.h. at $.07/c.f. = $11.138/module

Labor cost 13.26 hrs. at $3.00 hr. $39.78/module

M.I.G. - Material and Labor Cost

Length of welds 397.7 ft.

Welding speed 12 inches per minute

Welding time = $\frac{397.7 \times 12 \text{ inches}}{12 \qquad 60}$ = 6.63 hours

Argon cost = 6.63 x 30 c.f.h. at $.07/c.f. = $13.92

CO_2 cost = 6.63 x 10 c.f.h. at $.01/c.f. = .663

Wire cost = 6.63 x .0408 lb./min. x 60 min. at $.307/lb.

= $ 4.98

Total Material Cost/Module = $19.56/module

Welding will be done automatically. It is estimated that set-up time per module will be 1 hour therefore labor cost = 1/6 x 6.63 hrs. at $3.00/hr. = $ 3.32/module

SOLDER

Side Sheets

Cross-sectional area to be filled with solder = .0023 sq. inches

Volume of solder per module = .0023 x 180.5 ft. x 12 in. x 2 sides

= 9.96 cu. inches.

Weight of solder required = 9.96 cu. in. x .33 lb./cu.in. = 3.29 lbs.

Cost of solder per lb. = $.725

Cost of solder per module = 3.29 at $.725 = $2.385

Assume a 5 mil coating of flux.

Flux area (5 ft. x 3/2 ft. x 2 sides + 180.5 ft. x 1/2 in. x 1/12 x 2 sides) = 30.04 sq.ft.

Flux volume = 30.04 x 144 x .005 = 21.63 cu. inches

Number of modules covered per gallon flux = $\frac{231}{21.63}$ = 10.68 modules

Cost of flux per gallon = $9.10

Cost of flux per module = $\frac{\$\ 9.10}{10.68}$ = $.852

Labor

Flux application with standard spray gun:

Speed of gun travel = 30 ft. per min.

Swath of spray = 8 inches

Coverage rate = $\frac{8\ ft.}{12}$ x 30 ft./min. = 20 sq.ft./min.

Spray time = $\frac{30.04\ sq.ft.}{20\ sq.ft./min.}$ = 1.5 minutes

Assume operator efficiency of 67%, therefore, production rate

= 1.5 x $\frac{1}{0.61}$ = 2.25 minutes

Labor cost at $3.00/hr. = 2.25 x $\frac{\$3.00}{60}$ = $.113/module

Solder Application

Solder will be preformed in flat strips and "U" shaped from a free length of 19 inches with 1/2 inch between legs. There will be 120 pieces required for each side of the module. Time to position 120 pieces at 4 secs. each = $\frac{120 \times 4}{60}$ = 8 minutes.

Time required per module = 2 x 8 = 16 minutes

This requires 2 men for the production of 1 module every 8.54 minutes.

Labor cost for solder application = 2 x 8.54 x $\frac{\$3.00}{60}$ =$.854 per module

Bottom and End Closures

Joint area of bottom closure = 1/12 ft. x (5 + 3) ft. x 2

= 1. 33 sq.ft.

Joint area of end closure 1/12 ft. x 2 ($\frac{26}{12}$ + 3) ft. x 2

= 1.72 sq.ft.

Joint area of flanges = 1/12 x 2 x 2 (3 ft. + 1/2 ft.)

= 1.33 sq.ft.

TOTAL = 4.38 sq.ft.

Flux volume = 12 (4.38 sq.ft. + 50% overspray) x .005 in.

= .394 cu.in.

Flux cost at \$9.10/gal. = .394 x $\frac{\$9.10}{231}$ = \$.016/module

Solder cross sectional area = .010 sq. inches (size of .040 thick x .250 wide strip)

Volume of solder = .010 in. x 36-2/3 ft. joint length x 12 in.

= 4.28 cu. inches

Weight of solder = 4.28 x .33 lb./cu.in. = 1.41 lbs.

Solder cost at \$.725 per lb. = \$1.023/module

Flux spray time at 30 ft. per minute = 1.222 minutes

Labor cost at \$3.00 per hour = \$0.061/module

Solder placement estimated at 10 ft. per minute

Solder placement time = $\frac{36.60 \text{ ft.}}{10 \text{ ft./min.}}$ = 3.666 min.

Labor cost at \$3.00 per hr. = \$0.183/module

Summary of Soldering Costs

Material, Flux	$ .854
	.016
Solder	2.385
	1.023
Total Material Cost per Module	$4.278/module
Labor	$ .113
	.854
	.061
	.183
Total Labor Cost per Module for Soldering Operation	$1.211/module

Platen Loading and Unloading

Each module will be loaded into the platen, unloaded, turned over, re-loaded and unloaded again.

It is estimated that 2 men can load side sheet and evaporator sheet and secure them in position on the platen in 4.27 minutes or 8.54 minutes per module.

Labor cost for loading - unloading = 2 x 8.54 min. x $\frac{\$3.00}{60}$

= $.854/module

EPOXY BOND

Length of aluminum evaporator sheet = 175.2 ft.

Adhesive to be used - Epon 422 paste by Shell Chemical Co.

Cross-sectional area of groove to be filled with adhesive

= .0038 sq.in.

Volume of adhesive in groove = 175.2 ft. x 12 in./ft. x .0038 sq.in.

= 7.99 cu.in.

Volume on surface of side sheet = 20 in. width x 60 in. long x 2 sides

x .005 thick = 12.00 cu.in.

Total adhesive volume per side sheet = 19.99 cu.in.

Total per module = 2 x 19.99 = 39.98 cu.in.

Weight of Epon 422 = 6 lbs. per gallon or .026 lbs./cu.in.

Weight of Epon 422 per module = 39.98 x .026 = 1.04 lbs.

Cost of Epon 422 = $3.40 per lb. (quantity lots)

Cost of Epon 422 = 1.04 lbs. at $3.40 = $3.536/module

The above assumes a trowel application of adhesive. A bead application will reduce the amount of adhesive required.

It is estimated that an operator can trowel 6 sq.ft. of area per minute. Area to be covered = 2 sides x $\frac{20 \text{ ft.}}{12}$ x 5 ft. = 16.7 sq.ft.

Time required = $\frac{16.7 \text{ sq.ft.}}{6 \text{ sq.ft./min.}}$ = 2.78 minutes

Labor cost = $\frac{2.78}{60}$ x $3.00 = $.139/module

Appendix B

BRAZE

Assuming the use of a flat side sheet, the brazing material will be laid down in a sheet form of 10 mil thickness. The evaporator sheet will be placed on the brazing sheet.

Area of brazing sheet is (5 x 12) inches x 18.7 in. x 2 sides = 2,250 sq. in.

Volume of brazing sheet = 2,250 x .01 in. = 22.5 in.

Solder to be used is silver solder weighing .34 lbs. per cu. in.

Weight required per module = 22.5 x .34 = 7.65 lbs.

Solder Cost = 7.65 lbs. x 14.58 troy.oz./lbs. at $.74 per troy oz.

= $82.50/module

Flux required = 18 gms per sq. ft.

Total flux weight = $18 \times 5 \text{ ft.} \times \frac{18.7 \text{ ft.}}{12} \times \frac{4 \text{ layers}}{454 \text{ gms/lb}} = 1.24 \text{ lbs.}$

Cost of flux at $.70/lbs. = 1.24 x $.70 = $.87 per module

Total material cost per module = $82.50 + .87 = $83.37/module

This is compared to material cost of $3.54 for adhesive and $3.23 for solder for similar joining operations.

LEAK TEST

The description of the leak test indicated a 5 minute cycle time for filling, checking and dumping water. Allowing the operator time to load and unload the module brings the cycle time up to the standard of 8.54 min. per module.

Labor cost = 8.54 min. at $\frac{\$3.00}{60}$ = $.4270/module

No material costs are involved since the test water with detergent will be re-used.

FIXTURE, CLAMP & CURE

Fixture, Clamp & Cure for Epoxy

These are estimated to be the same as for the soldered modules and are

Labor $.854 per module

Although the bottom and end closures for the module are not designed it is assumed that these will be bonded. The bonds are assumed to be 1/2 inch double lap joints giving a total joint cross-sectional length of one inch. The end flanges are assumed to be bonded face to face to the end closure.

Joint area of bottom closure = 1/12 x (5 ft. + 3 ft.) 2

= 1.33 sq.ft.

Joint area end closure 1/12 x 2 $(\frac{26}{12}$ + 3 ft.) 2

= 1.72 sq.ft.

Joint area flanges = 1/12 x 2 x 2 (3 ft. + 1/2 ft.)

= 1.33 sq.ft.

Total joint area = 4.38 sq.ft.

Adhesive volume at .010 inch thick = 4.38 x 144 x .010 = 6.31 cu.in.

Weight of adhesive = 6.31 cu.in. x .026 lbs./cu.in.

= .164 lbs.

Cost at $3.40/lb. = $ .557/module

It is assumed that labor costs for applying the adhesive and loading is the same as for side sheet assembly.

These are:

Adhesive application labor = $ .14 per module

Assembly and loading labor = $ .854 per module

Fixture & Clamp for Soldering

These costs are included in loading and unloading in the heated platen press.

PACKAGE

Material Estimate	Costs - $ Each	Total/Ctn.
1 - Expendable Pallet 9 Post, 4 way entry	$ 1.60	$ 1.60
2 - Corrugated Fiber Board Stitched trays I.D. 61-1/2" x 37-1/2" x 4" 200# Single wall "C" or "A" flute	.30	.60
2 - Corrugated Fiber Board Creased sheets Creased 42" - 37" - 22" Sheet size 101" x 26" 200# single wall "C" or "A" flute	.25	.50
4 - Bands as per illustration approximately 600" of 1/2" x .015 banding used		.25
10 sq. yd. of MIL-B-131 Polyethylene - Foil - Cotton scrim vapor barrier sheet @ $46.50/roll in 100 yd. rolls 36" wide		4.65
6.4# Desiccant in .916# Bags MIL-3464B	.35	2.45
2 - Corrugated Fiber Board Creased & corner cut sheets Creased 4 - 36-1/8 - 4 Creased 4 - 60-1/8 - 4 Sheet size 44-1/8 x 68-1/8 Non test "C" or "A" flute	.24	.48
Total Material Cost Per Module	=	$10.53

Labor Estimate

It is estimated that one man will be sufficient to pack the unit as described in package within the 8.54 minutes allowed per module.

Labor Costs = $8.54 \times \frac{\$3.00}{60} = \$.427$/module

Aluminum - Metal Costs

Module - 3 ft. wide by 5 ft. long x 1.429 ft. vertical surface. Folds at 1/2 inch spacing.

Length of evaporator sheet = 120 folds x 1.439 x 12 in. + $1/2 \cdot \frac{\pi}{2}$ = 120 x 18.053 = 2166.4 inches = 180.53 ft.

Material thickness of evaporator sheet = .025 inch

Material weight of .025 thick aluminum = .361 lbs/sq. ft.

Area of evaporative sheet = 3 ft. x 180.53 ft. = 541.6 sq. ft.

Weight of evaporative sheet = 541.6 x 361 = 195.5 lbs.

Side sheet 5 ft. long by 26 in. wide by .032 in. thick

Weight of 2 side sheets at .456 lbs. per sq. ft. = $2 \times 5 \times \frac{26}{12} \times .456$ = 9.9 lbs.

Bottom sheet 3 ft. by 5 ft. by .032 inch thick

Weight of bottom sheet at .456 lbs. per sq. ft. = 6.8 lbs.

End sheet $\frac{26}{12}$ ft. by 3 ft. by .032 in. thick plus end flanges of 1 ft. by 3 ft.

Weight of 2 end sheets at .456 lbs. per sq. ft. = 2 x (6.5+3) x .456 = 8.7 lbs.

Total calculated aluminum weight = 195.5 + 9.9 + 6.8 + 8.7 = 220.9 lbs.

Allow 5% for scrap and ends = 11.1 lbs.

Total aluminum used per module = 232.0 lbs.

Price of alclad coil stock = $.43 per lbs.

Cost of aluminum per module = $99.76

Steel - Metal Costs

Module - 3 ft. wide by 5 ft. long x 1.518 ft. vertical surface folds at 1/2 inch spacing.

Number of folds = 120

Evaporative surface length = 120×1.518 ft. $\times$ 12 in. + $1/2 \cdot \frac{\pi}{2} \cdot \frac{1}{2}$ = 2280 in. or 190 ft.

Material thickness of evaporator sheet = .0299 in.

Material weight of .0299 thick stock = 1.25 lbs./sq. ft.

Area of evaporative sheet = 3 x 190 ft. = 570 sq. ft.

Weight of evaporator sheet = 570 x 1.25 lbs. = 712.5 lbs.

Side sheet 5 ft. long x 26 in. wide x .0299 in. thick

Weight of 2 side sheets = $\frac{26 \text{ ft.}}{12} \cdot$ x 5 ft. x 1.25 lbs./sq. ft. = 13.5 lbs.

Bottom sheet 5 ft. long x 3 ft. wide x .0299 in. thick

Weight of bottom sheet = 3 x 5 x 1.25 = 18.8 lbs.

End sheets 26 in. x 3 ft. x .0299 in. thick plus end flanges of 1 ft. x 3 ft.

Weight of end sheets = $2(\frac{26}{12} \times 3 + 1x3)\ 1.25 = 23.8$ lbs.

Total steel weight = 712.5 + 13.5 + 18.8 + 23.8 = 768.6 lbs.

Steel cost - low carbon, killed steel, pickled and oiled at 8-3/4 cents per lb.

Steel cost for module = 768.6 x 8-3/4 cents = $67.25

Tin Plate

Tin plate costs at the present will be the same as steel costs. = $67.25 per module.

Appendix B

SUMMARY OF ALUMINUM MODULE COSTS

Item	Material Cost	Direct Labor Cost @ $3.00/hour
Metal-evaporator sheet, side sheet, end closures.	$99.76	--
Punch and Draw Side Sheets	--	.267
Form folds-evaporator sheet, incl. de-reel, straighten, fold, stretch, shear	--	.854
Detergent wash-side sheets and evaporator sheets-coil lines	.981	--
Water rinse side sheets and evaporator sheet - coil lines	.113	--
Air dry - side sheets and evaporator sheet - coil lines	.020	--
Shear side sheet		.161
Monitor Coil lines	--	.427
Etch side sheets and evaporator sheets	.718	.427
Rinse side sheets and evaporator sheets	.113	
Air dry-side sheet and evaporator sheets	.020	
Monitor rinse lines		.427
Apply adhesive to side sheet	3.536	.139
Attach evaporator sheet, fixture and clamp in heat press		.854
Detergent leak test		.427
Rinse sub-assembly	.113	
Air dry sub-assembly	.020	
Monitor rinse and dry line	--	.427

Appendix B

End Closures		Material Cost	Direct Labor Cost @ $3.00/hour
Etch end closures	same as side sheets	.718	.427
Rinse end closures	same as side sheets	.113	
Dry end closurures	same as side sheets	.020	
Attach, fixture and clamp end closures			.427
Platen load and unload			.427
Detergent leak test			.427
Rinse module		.113	
Hot air dry module		2.35	
Monitor rinse and dry line			.427
Package module		10.53	.427
Total		119.238	6.972
Manufacture of Bottom closure			.75
Manufacture of (2) end closures			1.50
Stud Weld fasteners 40 at .05		2.00	.50
		121.238	9.722

The labor content of the above is equivalent to 23 men and is based on the production of 2,845,000 sq. ft. in six months time.

If pressure curing would be required as mentioned previously under adhesive bonding, ar additional 2 operators would be necessary to load and unload the autoclaves.

SUMMARY OF TIN PLATE MODULE COSTS

Item	Material Cost	Direct Labor Cost @ $3.00 / hour
Metal-evaporator sheet, side sheets, end closures	67.25	
Punch and draw side sheets	--	.267
Form folds evaporator sheet incl. de-reel, straighten, fold, stretch, shear	--	.854
Detergent wash side sheets and evaporator Sheet - coil lines	.113	--
Air dry side sheets and evaporator sheet - coil lines	.020	--
Shear side sheet	--	.161
Monitor coil lines	--	.427
Apply flux to side sheet and evaporator sheet	.854	.113
Apply solder to side sheets	2.385	.854
Attach evaporator sheet, fixture and clamp in heat press	--	.854
Detergen leak test		.427
Rinse module	.113	
Air dry module	.020	
Monitor "rinse and dry line"		.427
Apply flux to end closures	.016	.061
Apply solder to joint grooves	1.023	.183
Attach fixture and clamp end closures		.427

Appendix B

Item	Material Cost	Direct Labor Cost @ $3.00 / hour
Platen load and unload		.427
Detergent leak test		.427
Rinse module	.113	--
Hot air dry module	2.350	
Monitor "rinse and dry line"		.427
Package module	10.53	.427
	84.787	6.763
Manufacture of Bottom closure		.75
Manufacture of 2 end closures		1.50
Stud weld fasteners 40 to .03	1.20	.50
	85.987	9.513

The labor content of the above is equivalent to 23 men and is based on the production of 2,845,000 sq. ft. in six months time.

EQUIPMENT AND PLANT COSTS

Item	Description	Cost	Floor Area
	Side Sheet Line		
(1)	De-reeler with automatic feed and straightener, dolly & peel table	$23,785	15 ft. x 5 ft.
(2)	Press - straight side	14,000	6 ft. x 5 ft.
(3)	Die for press	3,500	--
(4)	Wash rinse, dry line	25,000	14 ft. x 5 ft.
(5)	Duct work filter	2,100	--
(6)	Shear, 20 ton	5,000	5 ft. x 5 ft.
(7)	Etchant tank heated and with controls	4,500	12 ft. x 5 ft.
(8)	Handling rack for etching	1,000	--
(9)	Rinse tank with water spray, air blowers and conveyor chain	15,000	14 ft. x 5 ft.
(10)	Duct work filter	2,100	--
(11)	Adhesive applicator - conveyor - table (or flux spray with feed)	8,000	8 ft. x 5 ft.
(12)	Storage rack	1,000	12 ft. x 5 ft.
	Evaporator Sheet Line		
(13)	De-reeler with automatic feed and straightener, dolly, peel table	23,785	
(14)	Wash, rinse, dry line	25,000	14 ft. x 5 ft.
(15)	Duct work filter	2,100	
(16)	Form fold, stretch, shear to length	150,000	32 ft. x 5 ft.
(17)	Racks for unloading from forming machine	6,000	--

EQUIPMENT AND PLANT COSTS

Item	Description	Cost	Floor Area
	Evaporator Sheet Line		
(18)	Etchant tank, heated and with controls	$ 4,500	12 ft. x 5 ft.
(19)	Handling platform with roll-over for etchant tank	6,000	--
(20)	Rinse tank with pumps, jets, blowers	20,000	14 ft. x 5 ft.
(21)	Duct work, filter	2,100	
(22)	Handling rake for crane	2,000	--
(23)	Heating platens for soldering and curing or autoclaves for pressure curring 15 platens or 2 autoclaves	105,000	20 ft. x 20 ft.
(24)	Locating fixtures for platens or clamping fixtures for autoclaves	30,000	--
(25)	Roll over fixtures for platen soldering	2,000	--
(26)	Leak test pump, nozzle, storage tank	2,500	18 ft. x 5 ft.
(27)	Rinse tank with pumps, jets, blowers	20,000	14 ft. x 5 ft.
(28)	Duct work, filter	2,100	
(29)	Epoxy applicators or flux spray-manual	600	12 ft. x 5 ft.
(30)	Infra-red oven for curing or soldering end closures	19,000	
(31)	Leak test pump, nozzle, storage tank	2,500	18 ft. x 5 ft.
(32)	Rinse tank with pump nozzle	1,500	14 ft. x 5 ft.
(33)	Blower with heating element, filter, duct	5,000	14 ft. x 5 ft.
(34)	Packaging equipment	5,000	18 ft. x 5 ft.
(35)	Connecting conveyors	50,000	120 ft. x 5 ft.
		$ 591,670	2,890 sq. ft.
	Storage for 100 modules 3 high		700 sq. ft.
			3,590 sq. ft.

Plant operating area required = 2-1/2 times equipment area = 8,975 sq. ft.

Plant rental costs 8,975 sq. ft. x $1.50/sq. ft. per year x 1/2 yr. = $6,730

Plant rental per module = $ 6,730/5,166 = $1.30

Total estimated equipment cost = $591,670

Capitalized over one 10 million g.p.d. plant (5,166 modules) gives equipment cost per module of $114.53.

Appendix B

SUMMARY OF TOTAL COSTS

	Aluminum Module		Tin Plate Module	
Material	$ 121.24		$ 67.25	
Labor	9.72		9.51	
Overhead at 100%	9.72		9.51	
Plant rental	1.30	141.98	1.30	87.57
Equipment cost	114.53		114.53	
	$ 256.51		$ 202.10	
Evaporative area	518.0 sq. ft.		546.5 sq. ft.	
Cost per sq. ft.	$.495 per sq.ft.		$.370 per sq. ft.	

These estimates are believed to be correct and production costs probably will not vary more than 25% in either direction except as governed by final design and changes in basic material and labor costs.

It may be interesting to note that Auel Industries of Herminie, Pa. quoted 60 tin plate modules with some design changes at a price of $148.50 each plus $2,867 tool costs. This is equivalent to $.36 per sq. ft.

Appendix B

SUMMARY OF TOTAL COSTS ON A SQUARE FOOT BASIS

	Aluminum	Tin Plate
Material	$ .234	$ .123
Labor	.019	.017
Overhead at 100%	.019	.017
Plant Rental	.003	.002
Equipment Cost	.221	.209
Cost per sq. ft. of evaporator surface	$ .496 per sq. ft.	$ .368 per sq. ft.

DESIGN RECOMMENDATIONS

During the course of the investigation into manufacturing processes and manufacturing costs, several alternate designs were proposed. However, none of the proposed designs would result in a substantial reduction of production costs. Refinements of the design could result in trimming labor costs and equipment costs but these would need to be investigated before any decision could be reached. Two of the most promising changes are:

(1) A module designed to have evaporating sheets made from pieces joined together as shown in Figure 17 (a).

(2) A module designed to be made from flat tubes as shown in Figure 30.

The advantages associated with (1) would be:

(a) The elimination of the capital equipment investment in a special folding machine. This amounts to $150,000. Simple equipment and tooling of the order of $25,000 would be substituted for cutting and forming the individual sheets.

(b) The increase in freedom to make design changes without making obsolete expensive capital equipment.

(c) The reduction of lead time in setting up the production plant because the special equipment involved in forming the continuous sheet will require extensive design, development and construction time.

Disadvantages of this modification would be the creation of more potential sources of leaks and oxygen concentration cells due to the increased length of joints.

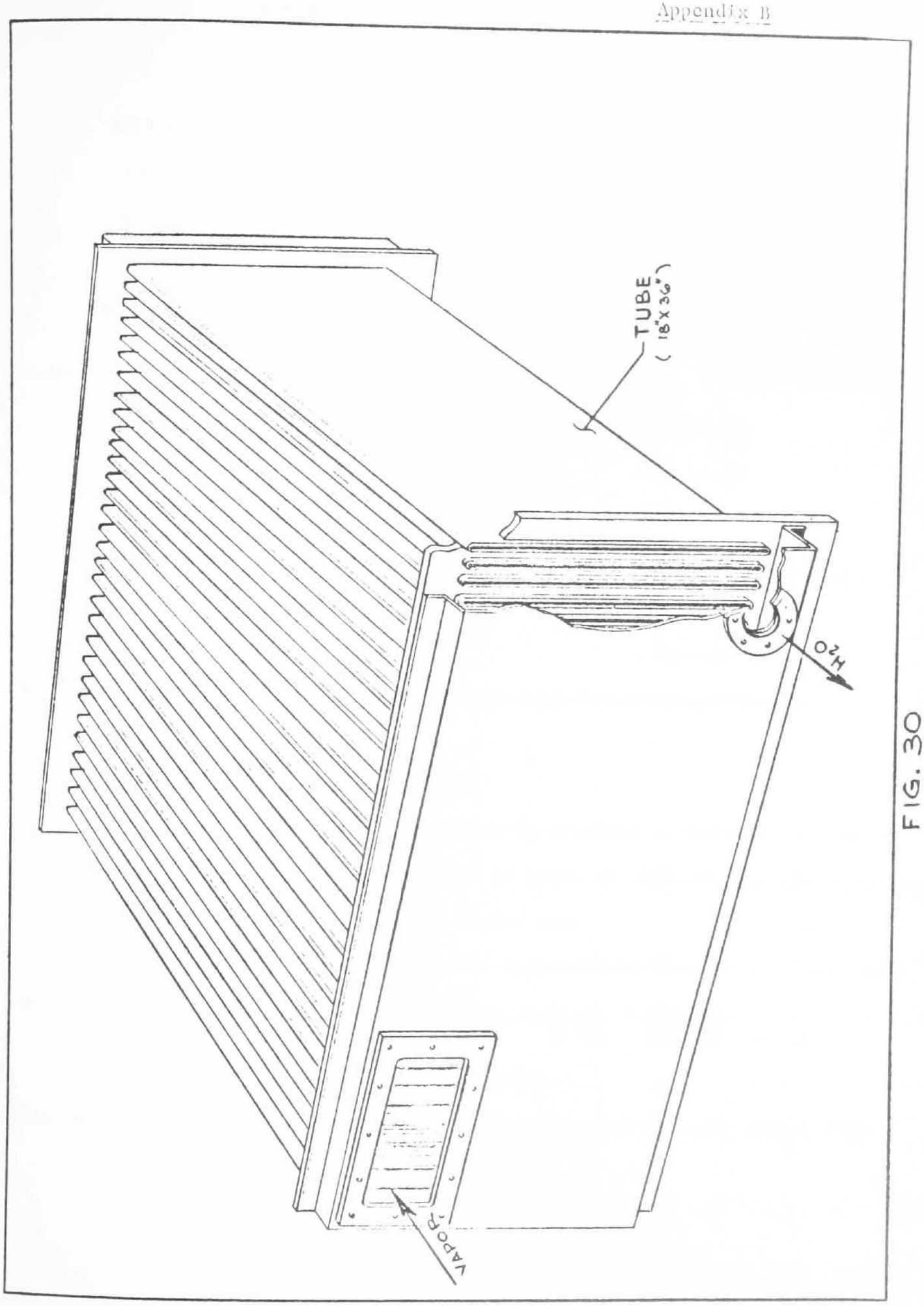

FIG. 30

The flat tube design has the same basic advantages and disadvantages as those just outlined. However, it does have the additional disadvantage of requiring headers (tube sheets) similar to those found in shell and tube heat exchangers.

These design changes should be given serious consideration before any plant design is finalized.

Coil Stock Material Tolerances

Steel

The steels are available in most gages and in widths to 48 inches or more. Tin plate widths are available up to 36 inches in the thickness area of .030 inch. Chromized steel is still under development, and no sizes are commercially available.

TOLERANCES - STEEL

Thickness 22 gage (.0299 in.)	±.003 inch
Length	coil stock
Width for 36 inch wide sheet	
commercial tolerance	+ 1/4 inch - 0
slit tolerance	±.020 inch
camber	1 inch/20 ft. length

Cost extra for aluminum killed steel is $.50 to $.75 per hundred pounds.

TOLERANCES - TIN PLATE

These are the same as for steel

Thickness of tin plate coating can be obtained as desired. Number 50 plate equals .0366 oz. tin per square foot of metal or .000,030 inch thick plating. The standard width of tin plate coil is 33-5/8 inch.

Cost extra for tin plate would be approximately that of tin costs which is $1.15 per lb. This is equal to $\frac{.0366 \text{ oz.}}{\text{sq. ft.}} \times \frac{\$1.15}{16 \text{ oz.}} \times \frac{100 \text{ lbs.}}{1.25 \text{ lb./sq. ft.}}$

= $.21 per hundred lbs.

However, pricing policy by producers shows no extra cost over low carbon steel.

Aluminum

Aluminum coil stock is available in alclad 3003, alclad 7372 and aluminum 1100-0. Standard widths are 12, 18, 24, 36, and 48 inches. Thicknesses range from .016 inches up. Standard thicknesses are .025 and .032 inches.

TOLERANCES

Thickness	±.0025 inch
Length	coil stock
Width for 36 inch wide sheet	
commercial	± 3/64 inch
special at $.0005/lb. extra	± .032 inch
special at $.011/lb. extra	± .016 inch
special at $.044/lb. extra	± .005 inch

Copper

Information from Williams and Co. and from Hussey Copper and Brass indicates that the width of copper coil stock is limited to 20 inches for stock .010 inch thick.

TOLERANCES

Thickness .010	± .0018
Length	coil stock
Width for 20 inch wide sheet	± 1/64 inch
Camber	± 3/8 inch per 6 ft.

Pressure Head of Brine

To determine height of concentrated brine at bottom of fold with a drain hole in the side sheet of 1/4 inch diameter.

Circulation ratio R = 2.5 lb. sea water/lb. fresh water.

Fresh water production per sq. ft. of heat transfer surface = 1.22 lb./hr.

Amount of sea water input = 2.5 x 1.22 = 3.05 lb./hr.-sq. ft.

Amount of brine output = 3.05 - 1.22 = 1.83 lb./hr. - sq. ft.

No. of sq. ft. in one "U" fold, assuming a 3 ft. wide module = 3 ft. x 1-1/2 ft. high x 2 sides = 9 sq. ft.

Amount of brine output per "U" fold = 1.83 x 9 = 16.47 lb./hr.

Initial brine concentration = 3%

Final brine concentration = 5%

Water weight = 62.5 lb./cu. ft.

Specific gravity of 5% NaCl in H_2O = $\frac{(1.0268 + 1.0413)}{2}$ = 1.034

(Handbook of Chem. and Phys. Page 1887)

Weight of 5% brine 62.5 x 1.034 = 64.6 lb./cu. ft.

Vol. of concentrated brine/hr./U plate = $\frac{16.47}{64.6}$ cu. ft./hr. = .255 cu.ft./hr.

Vol. of concentrated brine through one opening = 1/2 x .255 c.f.h. = .1275 c.f.h.

From Crane Bulletin 410 Page 3-14

$$q = 0.0438\ do^2 \cdot C \cdot \sqrt{h} = .525 do^2\ C \sqrt{\frac{\Delta P}{\rho}}$$

q = rate of flow - c.f.s. = $\frac{.1275\ c.f./h.}{3600\ sec/h}$ = .0000354 c.f.s.

C = flow coeff. - assume = 1.0

d = orifice dia. - inches = .25 inches

P = pressure - p.s.i., ΔP = Pressure drop across orifice

ρ = weight density - lbs./cu. ft. = 64.6 lb./cu. ft.

$$q = .525 do^2 \cdot C \cdot \sqrt{\frac{\Delta P}{\rho}} \; ; \quad \frac{q}{.525(do)^2 \cdot C} = \sqrt{\frac{\Delta P}{\rho}}$$

$$\Delta P = \left(\frac{q}{.525(do)^2 \cdot C} \right)^2 \cdot \rho$$

$$= \left(\frac{.0000354}{.525 \ (1/4)^2 \times 1} \right)^2 \times 64.6 = \left(\frac{.0000354 \times 16}{.525} \right)^2 \times 64.6$$

$\Delta P = (.00108)^2 \times 64.6 = .0000753$ p.s.i.

ΔP = press. drop or head required for flow rate

1 cu. ft. brine weighs 64.6 lbs.

1 cu. in. brine weighs $\frac{64.6}{1728} = .0374$ p.s.i.

Height of brine = $\frac{.0000753}{.0374} = .00201$ inches

This says that the 1/4 inch opening in the side sheet will be sufficient to drain the concentrated brine without raising an appreciable head of brine between the folds of the evaporator sheets.

APPENDIX E

Detail of Work on Epoxy Bonding

At the start of the epoxy adhesive program many suppliers of epoxies were contacted for their recommendations of adhesive and their estimate of joint life under the conditions that the module would operate. In addition, metals producers were contacted for similar recommendations. Epoxy adhesives have not been in use so long that data on 10 year life was available. The operating conditions of partial vacuum, elevated temperature and de-aerated sea water was unique. The answer culled from these contacts is best summed up by saying that building some joints and testing them over a period of time is the only sure way of determining joint life.

Epoxies

The following manufacturers of epoxy adhesives were contacted.

Minnesota Mining and Manufacturing

B. and B. Chemical Company

Shell Chemical Company

Devcon Corporation

G. C. Electronics

Woodhill Chemical Company

Borden Chemical Company

The Epoxylite Corporation

Fybroh Industries

H. B. Fuller Company

U. S. Stoneware Company

Inert Chemical Corporation

Mr. Bob Parkinson of U. S. Steel Research recommended Minnesota Mining and Manufacturing No's. 1386 or 2086. Alternate recommendations were Angiers Division of Inert Chemical and General Mills. Alcoa Aluminum recommended U. S. Stoneware, Shell Chemical, H. B. Fuller and Minesota Mining and Manufacturing No's. 2086, AF41, EC1595 and EC1630. Kaiser Aluminum recommended Epon 422 by Shell Chemical.

Minnesota Mining and Manufacturing recommended EC1386 or EC2054 (a 2 part epoxy). Their data sheet gave methods of preparation and application.

Devcon Corporation recommended their No. 101, a 2 part epoxy, but indicated that under prolonged exposure to water, delamination was bound to occur with any epoxy known to them. The process of delamination is not fully understood. Kaiser Aluminum reported that they found delamination of bonds occurring under prolonged immersion in salt water with most epoxies. No figures are available from anyone on joint life under conditions of salt water immersion at elevated temperatures.

The following epoxies were tried:

1. G. C. Electronics Pliobond
2. 3 M's EC2054
3. 3 M's EC1386
4. 3 M's EC2086
5. Shells Epon 422 Paste
6. Shells Epon 422 Film

Minnesota Mining and Manufacturing, U. S. Steel and Alcoa agreed that single part thermosetting epoxies are superior to 2 part catalytic type.

Surface Preparation for Bonding

Various methods of surface preparation were recommended by U. S. Steel, Alcoa and 3 M. These included degreasing, detergent wash, etching and sand blasting. Sandblast, detergent wash and sonic cleaning were tried and evaluated.

Metals

Metals considered were low carbon steel, tin plate, 1100 aluminum and alclad 3003 aluminum.

Procedure

With the above 17 epoxies, 4 methods of surface preparation and 4 materials to consider there would be 272 possible combinations. To prepare and test samples of all combinations of these joints including life tests, would be a project larger in scope and time than possible here. We decided to limit epoxy choice to a few highly recommended ones; choose one of these from test samples and use this in determination of joint preparations.

Because low carbon steel was considered definitely as a control sample, it was used to determine epoxy choice and effect of salt water immersion.

Test samples were made on a small scale similar to the actual evaporator module, see Figure 31 (a). The 2 pieces were cleaned, epoxy applied to one or both and they were clamped together while curing the epoxy. After curing, the space between folds was filled with low temperature cerrobend alloy to permit cutting into test sections as shown in Figure 31 (b).

Some sections were tested after cutting while others were immersed in salt water solution prior to testing. The test was a measurement of load versus deflection utilizing the section as a cantilever beam. The test fixture used is shown in Figure 32.

Test Results for Bonded Samples

Pliobond

Two samples were made with sandblasted pieces. These samples were identified by the letter "C". After curing they were inspected visually and the joint was found to be plastic under light load. The adhesive would tear away.

EC-2054

Two samples were made with sandblasted pieces. These samples were identified by the letter "B". One of the samples broke at the joint while dismantling from the fixture. The other cracked while testing manually the strength of the joint.

EC-1386

Samples made of this were identified by the letter "A".

Group I - EC-1386

The test pieces were washed in thinners, sandblasted with G-25 shot, sonic cleaned, rinsed in distilled water and dried. Epoxy was applied to the flat sheet about .005 to .010 thick and also to the edges of the corrugated sheet. The test pieces were clamped and cured at 375°F for 50 minutes. After sawing, 1 piece was given a load-deflection test and two pieces were immersed in a 10% solution of N_aCl in water at 140°F for 24 hours. The load deflection test was then made. Results of Group I tests are shown on Curve I, Figure 33.

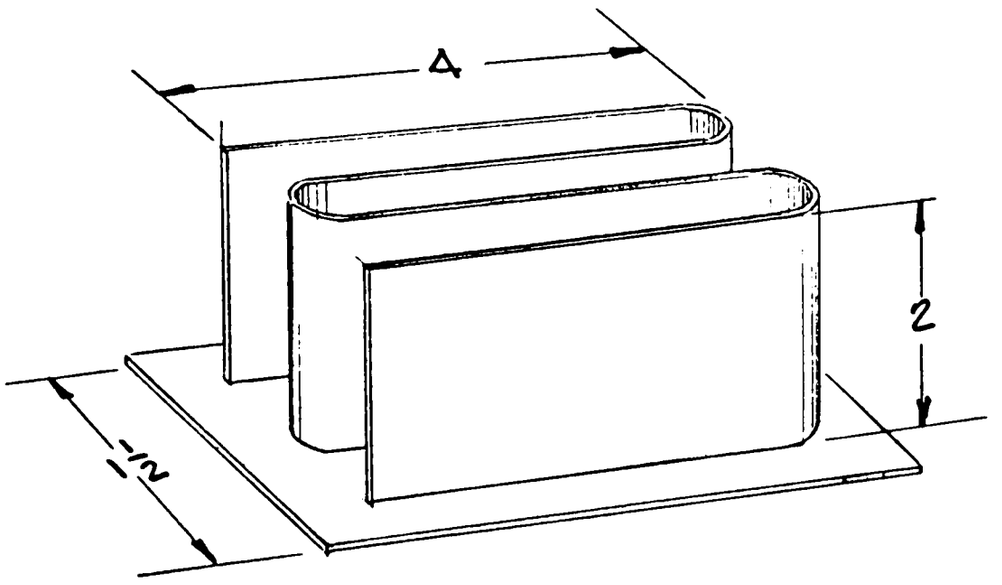

FIG. 31 (a)

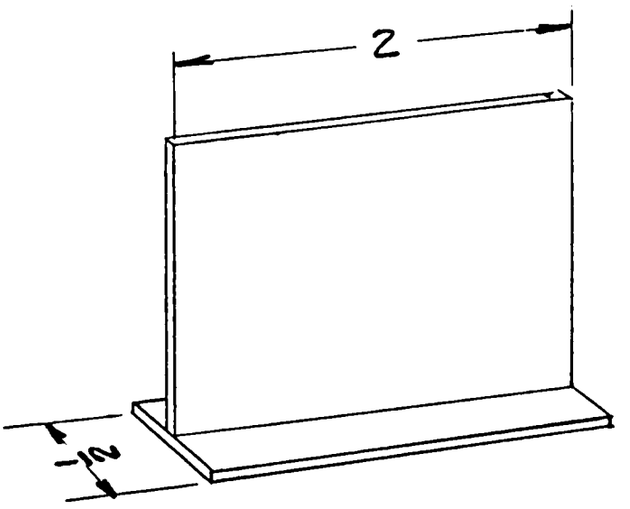

FIG 31 (b)

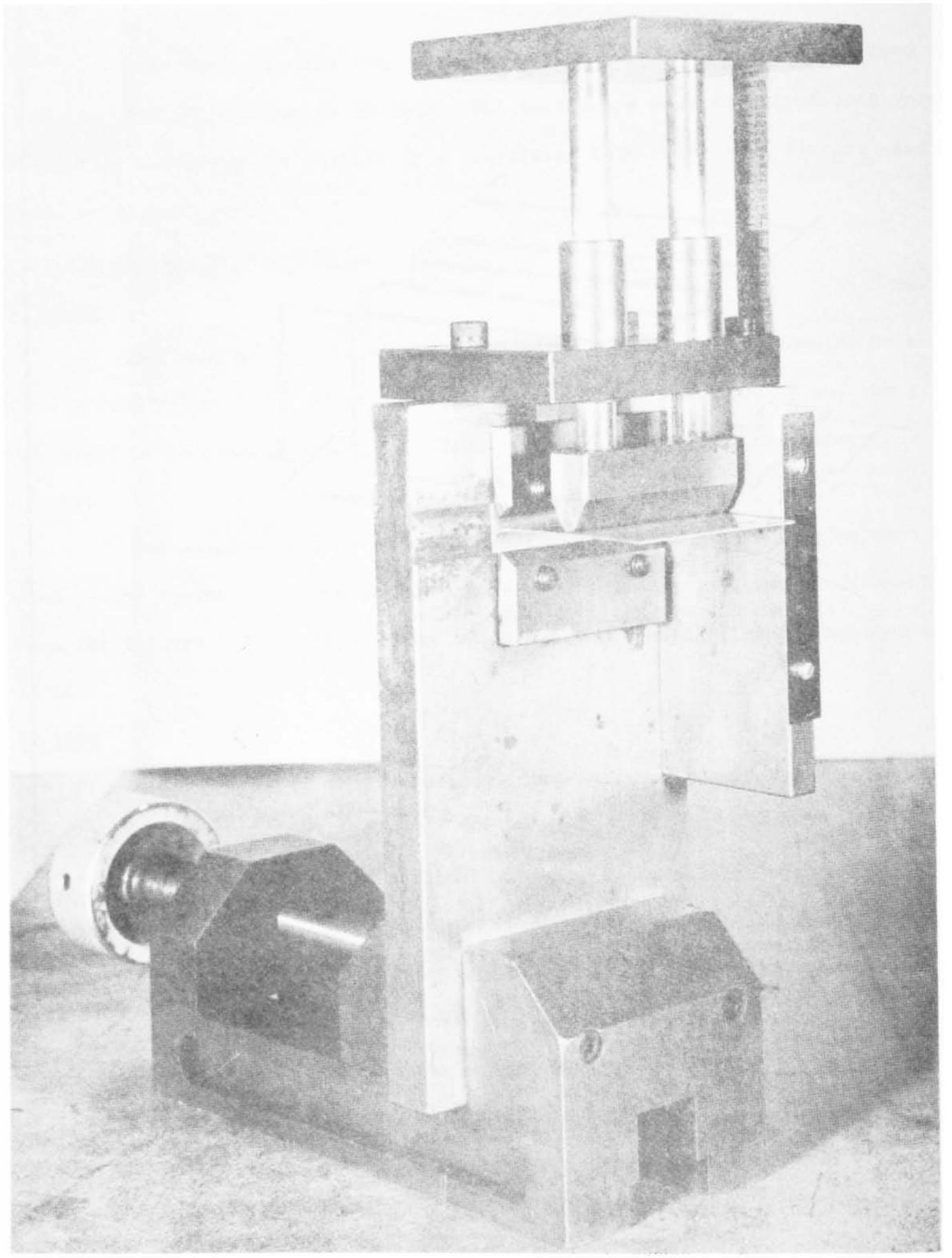

FIG. 32

LOAD-DEFLECTION CURVE I

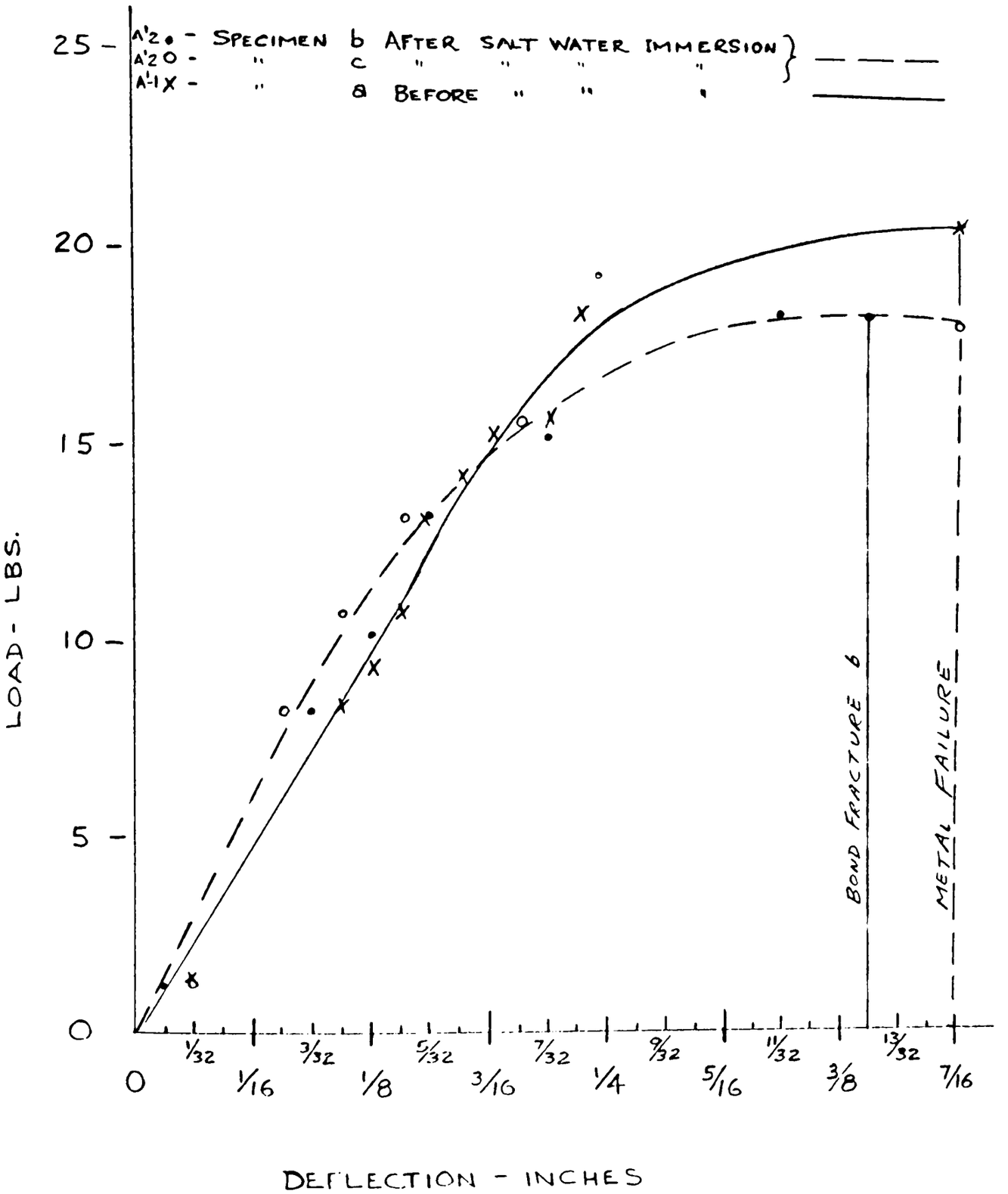

FIG. 33

Group II - EC-1386

The joint preparation here was the same as in Group I except that epoxy was applied to the flat sheet only. Tests were conducted the same way. Results of Group II tests are shown on Curve II, Figure 34.

Group III

The joint preparation here was the same as in Group I except that the flat sheet only was sandblasted. Tests were conducted the same way. Results of Group III tests are shown on Curve III, Figure 35.

Group IV

The joint preparation here was the same as in Group I except that sandblast was ommitted. Tests were conducted the same way. Results of Group IV, Figure 36.

Group V

The joint preparation used here was the same as in Group I except that detergent wash was substituted for sandblast. The detergent used was 2 oz. of Northwest Chemical Company No. 63 in 1 gallon of water at room temperature. Results of Group V test are shown on Curve V, Figure 37.

Extended Salt Water Immersion

Two samples, No's A2 and A4 were immersed in 140°F of 20% N_aCl solution for one month. Sample A2 was a sandblasted sample and sample A4 was sonic cleaned. The test was terminated when the solution was accidentally brought to a boil. Sample A2 showed partial delamination, about 20% by area, between epoxy and metal. Sample A4 showed complete delamination.

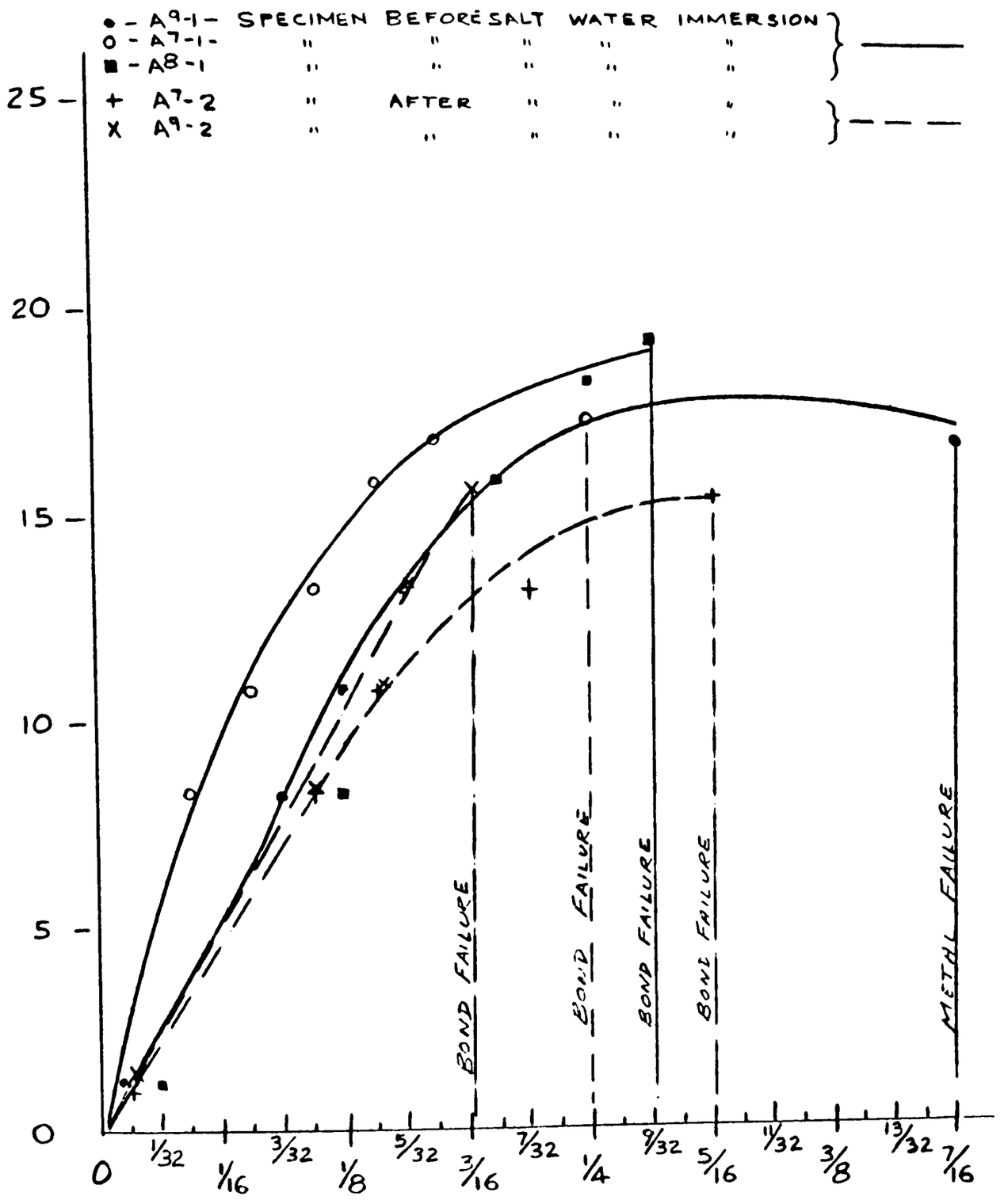
LOAD-DEFLECTION CURVE II
● - A9-1 - SPECIMEN BEFORE SALT WATER IMMERSION
○ - A7-1 - " " " " "
■ - A8-1 " " " " "
+ A7-2 " AFTER " " "
X A9-2 " " " " "
25
20
15
10
5
0
0
1/32
1/16
3/32
1/8
5/32
3/16
7/32
1/4
9/32
5/16
11/32
3/8
13/32
7/16
BOND FAILURE
BOND FAILURE
BOND FAILURE
BOND FAILURE
METAL FAILURE

FIG. 34

LOAD-DEFLECTION CURVE III

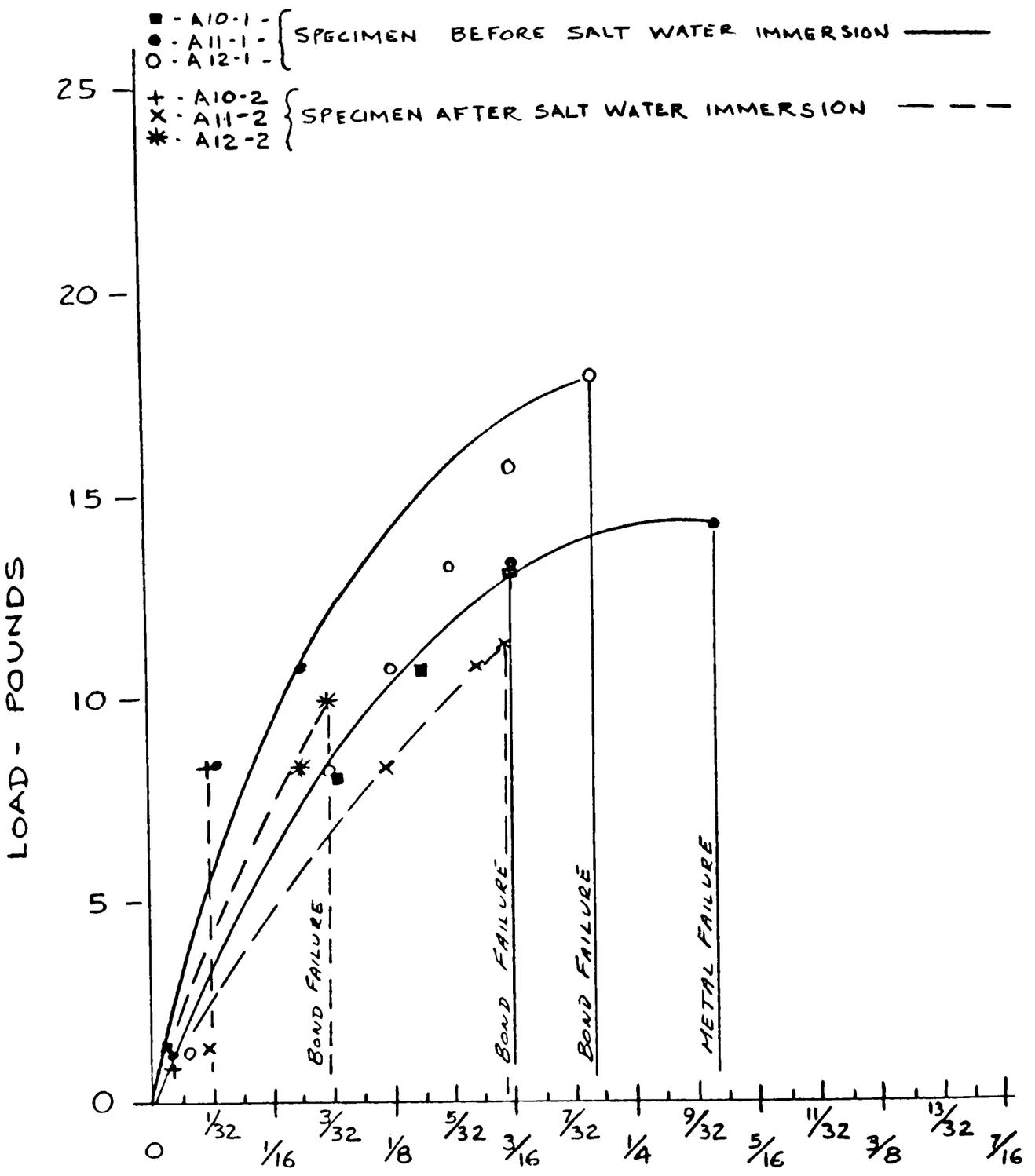

FIG. 35

LOAD DEFLECTION CURVE IV

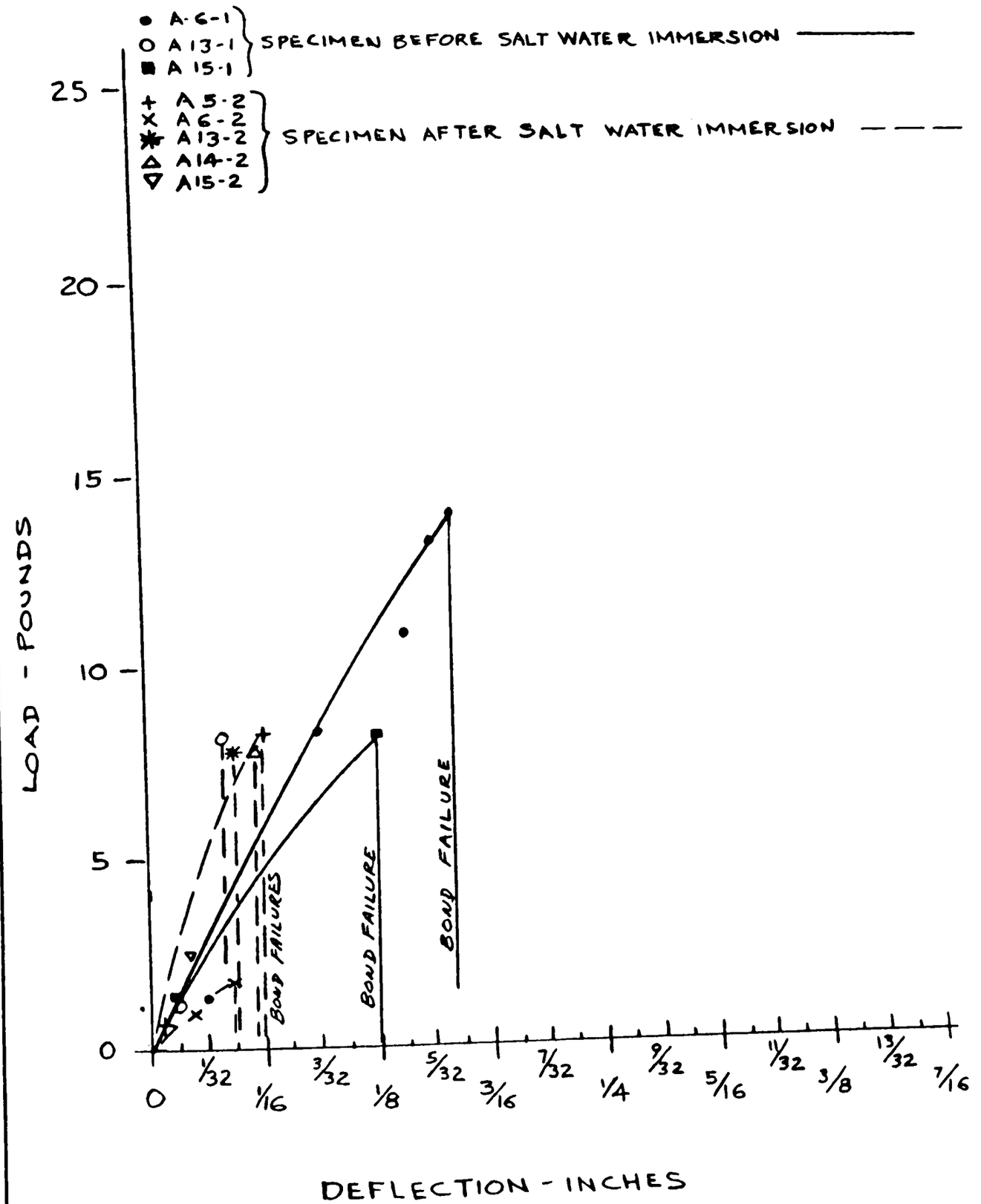

FIG. 36

LOAD DEFLECTION CURVE V

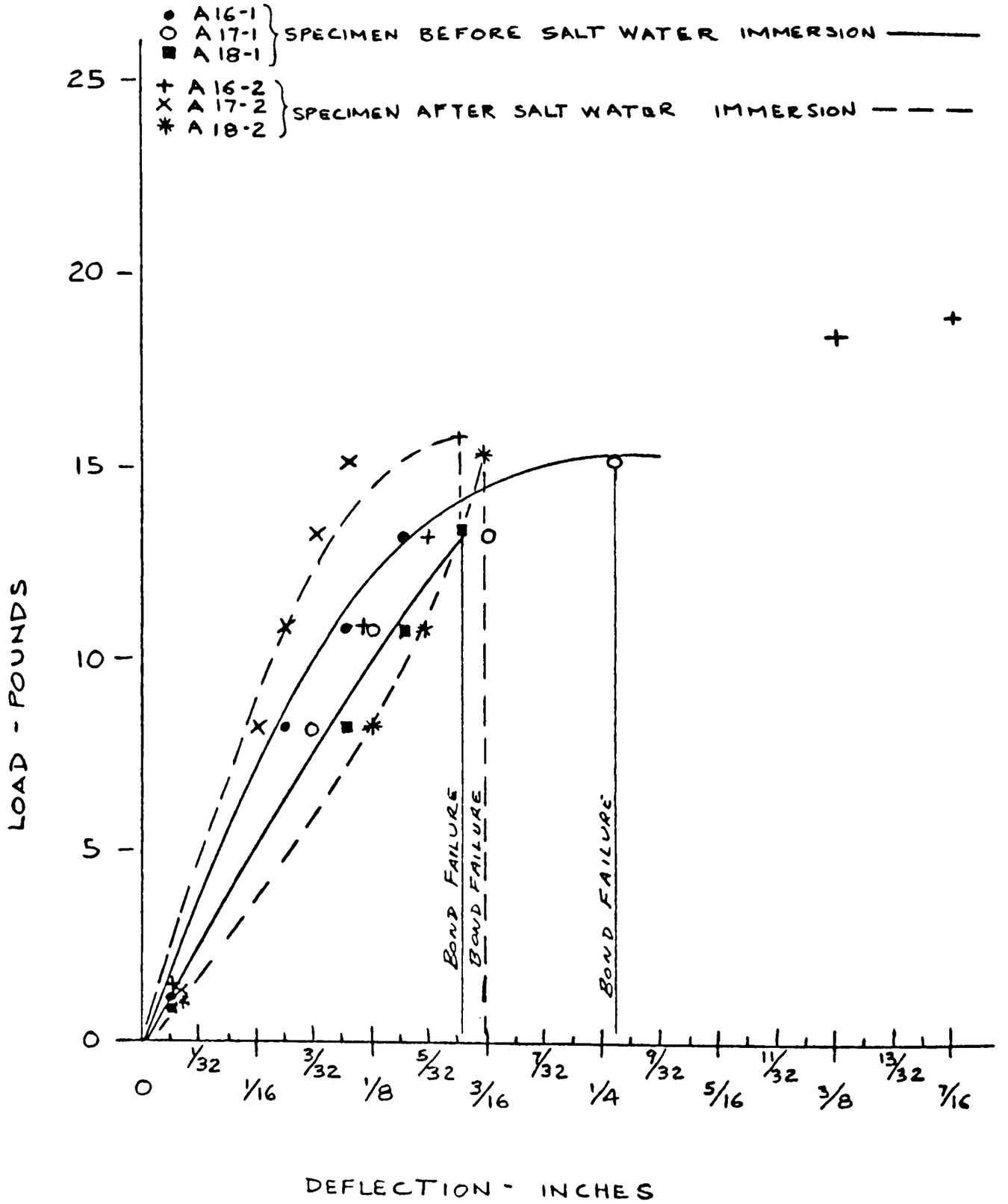

FIG. 37

Results

Comparison of Curves I through V shows that sandblasted surface on low carbon steel gives the strongest bonds. These bonds also are relatively stronger than non-blasted surfaces after salt water immersion. It can also be seen that salt water immersion of the epoxy joints reduces the strength of the joints. These joints were immersed in aerated salt water and these results must be compared to similar results in de-aerated sea-water to note any change. A closed loop system for de-aerating the solution was built for conducting such tests.

DE-AERATING SYSTEM

The expected O_2 content of sea-water in the operating sea water conversion plant is expected to be 0.1 ppm (part per million). Normal O_2 content is around 9 ppm. Considerable difficulty was encountered in attaining the level of 0.1 ppm O_2 content. Changes had to be made from the original design of the system such as the addition of a heating system to the de-aerating column and to the test chamber and the addition of a second vacuum zone at the bottom of the de-aerating column.

Consecutive samples of de-aerated sea-water showed varying oxygen content. A heat exchanger was added to the system to cool the sample before entering the sample bottle. The level of 0.1 ppm was finally reached after the above changes, but it was not able to be maintained consistently. Checks showed the operating range from 0.10 to 0.35 ppm. No reason could be determined for this inconsistency.

Final operating conditions of the de-aerating system were:

- Temperature of sea water in water bath 160°F
- Temperature of sea water at entrance to column 130°F
- Absolute pressure in upper section of column 7-1/2 cm Hg
- Temperature of sump of column 100°F
- Absolute pressure at sump of column 6.3 cm Hg
- Temperature in Test chamber 51-3/4°C (125°F)
- Recirculating water rate 90 c.c./minute
- Second stage heater 350 watt 120 v nominal set at 65 volts.
- Test chamber heater 500 watt 120 v nominal set at 85 volts
- Distilled make up water added to the system at the rate of 4 gallons per 24 hours.
- The leak in the vaccum system with air ejectors off was checked at:

  Upper Manometer 1.2 cm Hg in 2 hours (2.8 cm starting pressure)

  Lower Manometer 2.1 cm Hg in 2 hours (2.4 cm starting pressure)

A schematic of the final de-aerating system is shown in Figure 38 and the actual photograph is shown in Figure 39.

Kaiser Aluminum has run extensive water spray tests on different adhesives and noted the effect of delamination on all adhesives tried with the exception of Epon 422. It was determined to find the effect of de-aeration on delamination. Steel samples were made using E.C. 1386 on sandblasted and sonic cleaned surfaces. The samples were divided into 4 groups. One group tested as joined, one group immersed in normal O_2 content 3% $NaCl$ solution and one group tested after immersion in de-aerated sea water at 125°F at absolute pressure of 6.3 cm Hg.

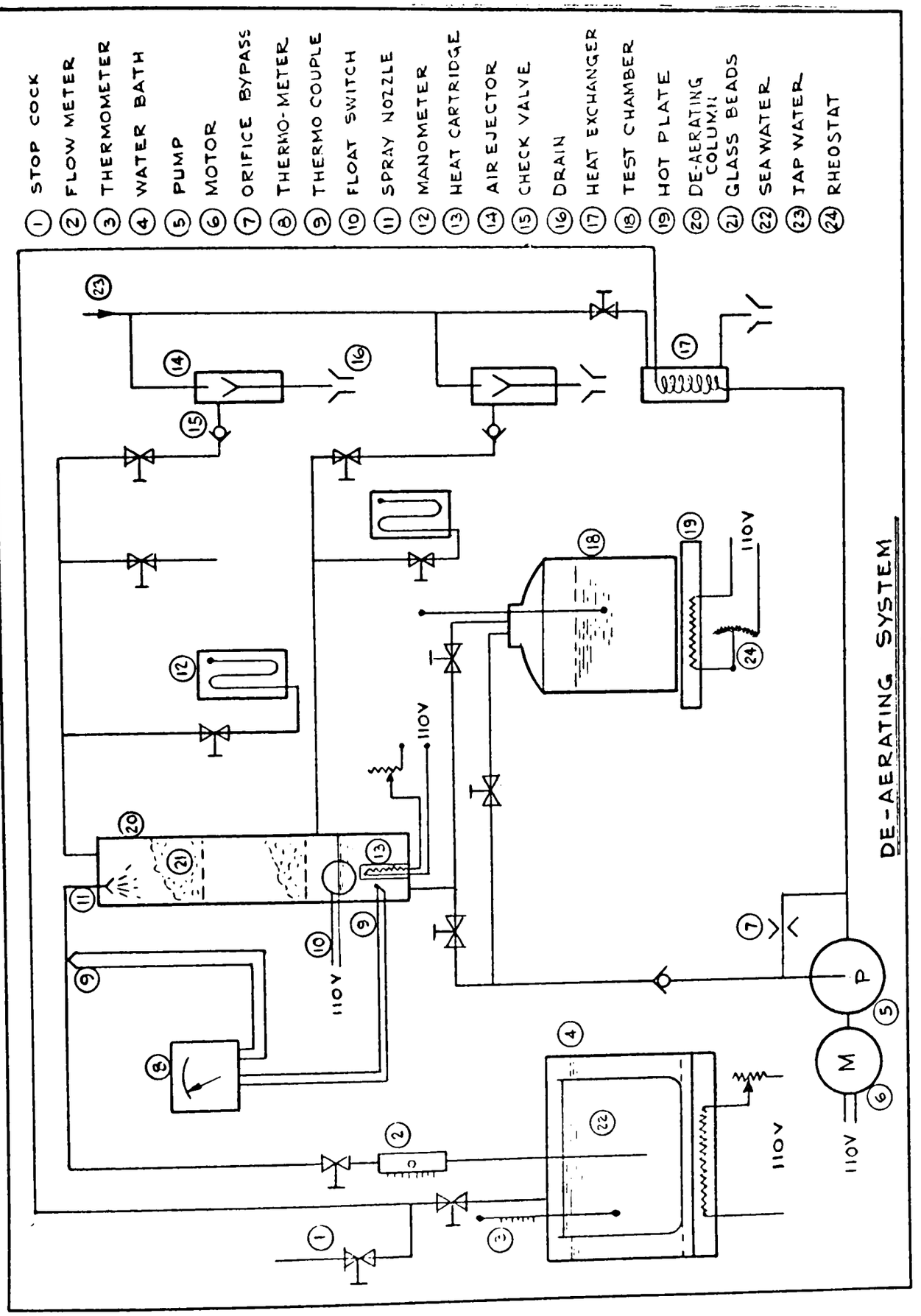
1 STOP COCK
2 FLOW METER
3 THERMOMETER
4 WATER BATH
5 PUMP
6 MOTOR
7 ORIFICE BYPASS
8 THERMO-METER
9 THERMO COUPLE
10 FLOAT SWITCH
11 SPRAY NOZZLE
12 MANOMETER
13 HEAT CARTRIDGE
14 AIR EJECTOR
15 CHECK VALVE
16 DRAIN
17 HEAT EXCHANGER
18 TEST CHAMBER
19 HOT PLATE
20 DE-AERATING COLUMN
21 GLASS BEADS
22 SEA WATER
23 TAP WATER
24 RHEOSTAT
DE-AERATING SYSTEM
110V
110V
110V
110V
P
M

FIG. 38

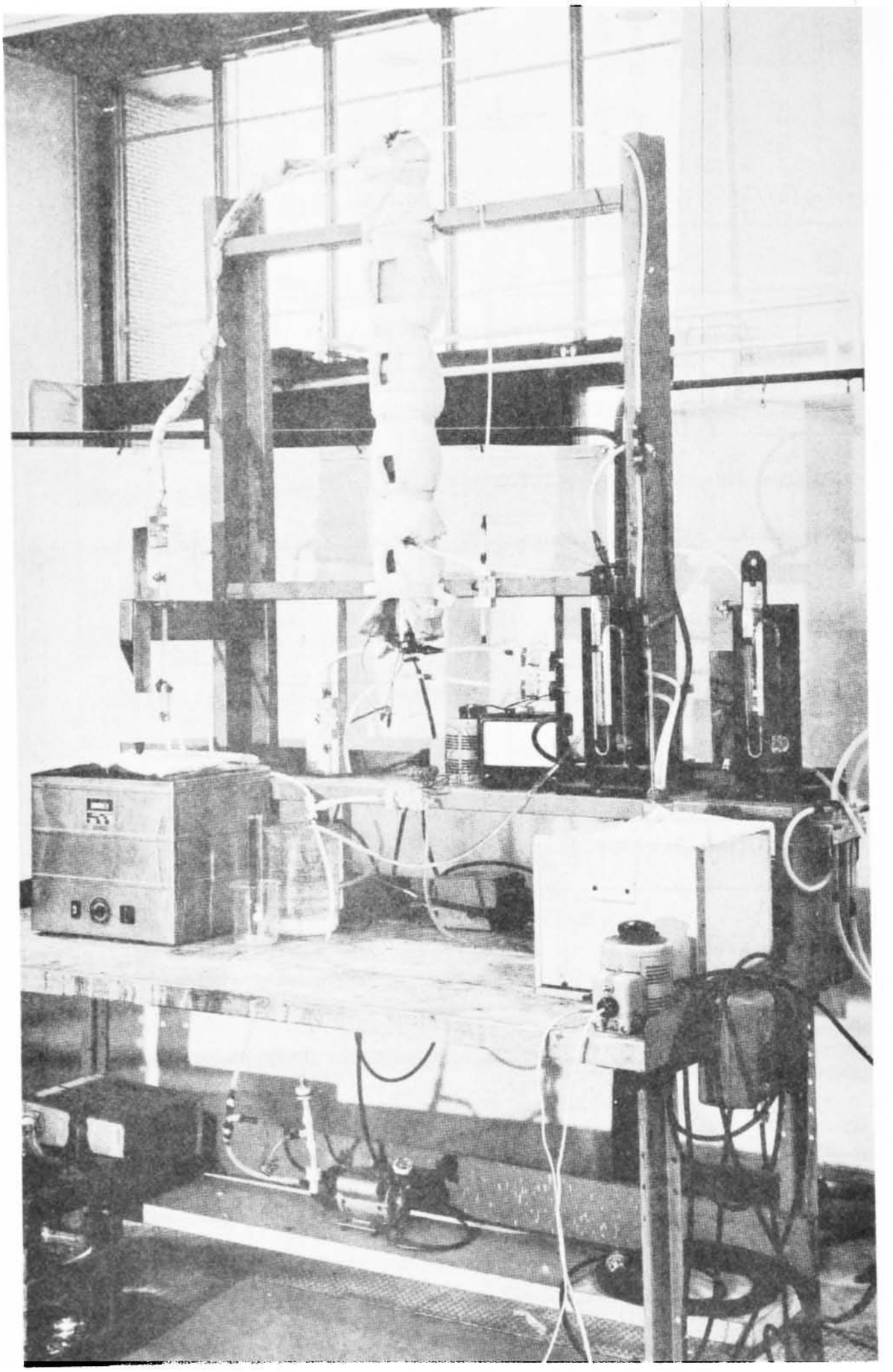

FIG. 39

The results are shown in bar chart Figure 40. It can be seen that the deterioration of the joint is pronounced after 292 hour immersion in N_aCl solution with normal O_2 content. In de-aerated (.352 ppm) sea water, the deterioration is less noticeable and is shown by the 2 instances of adhesive failure compared to metal failure. This shows that de-aeration will improve adhesive life in these particular instances and that there is likelihood of improvement under our operating conditions.

Epon 422

Epon 422 was recommended by Kaiser Aluminum as showing no changes in strength after a 3 year deionized water spray test. With sea water, a 1-1/2 year test also showed no strength change. Their sample pieces were lap joints whereas ours were "T" joints. Shell chemical was contacted for information on Epon 422. It is a phenolic epoxy adhesive available in sheet form as a glass fabric laminate and available to a limited extent in paste form. It was stated to become porous on curing because volatiles or water vapor was given off on curing. Steel samples were made using a plain "T" joint and Epon 422 paste. Porosity of the adhesive was very high and is shown in photo Figure 41. Other steel samples were similarly made using Epon 422 sheet. These showed less porosity because of the thinner amount of 422 used. The samples were sawn into sections in the usual fashion and the joints were found to be extremely fragile so that they could not be subject to the usual test.

Bonded Aluminum samples were made using Epon 422 sheet. Surface treatment was a 15 minute chromic sulphuric etch at 155°F. These were given a 135 minute cure and cut up in the usual fashion. These samples showed surprisingly

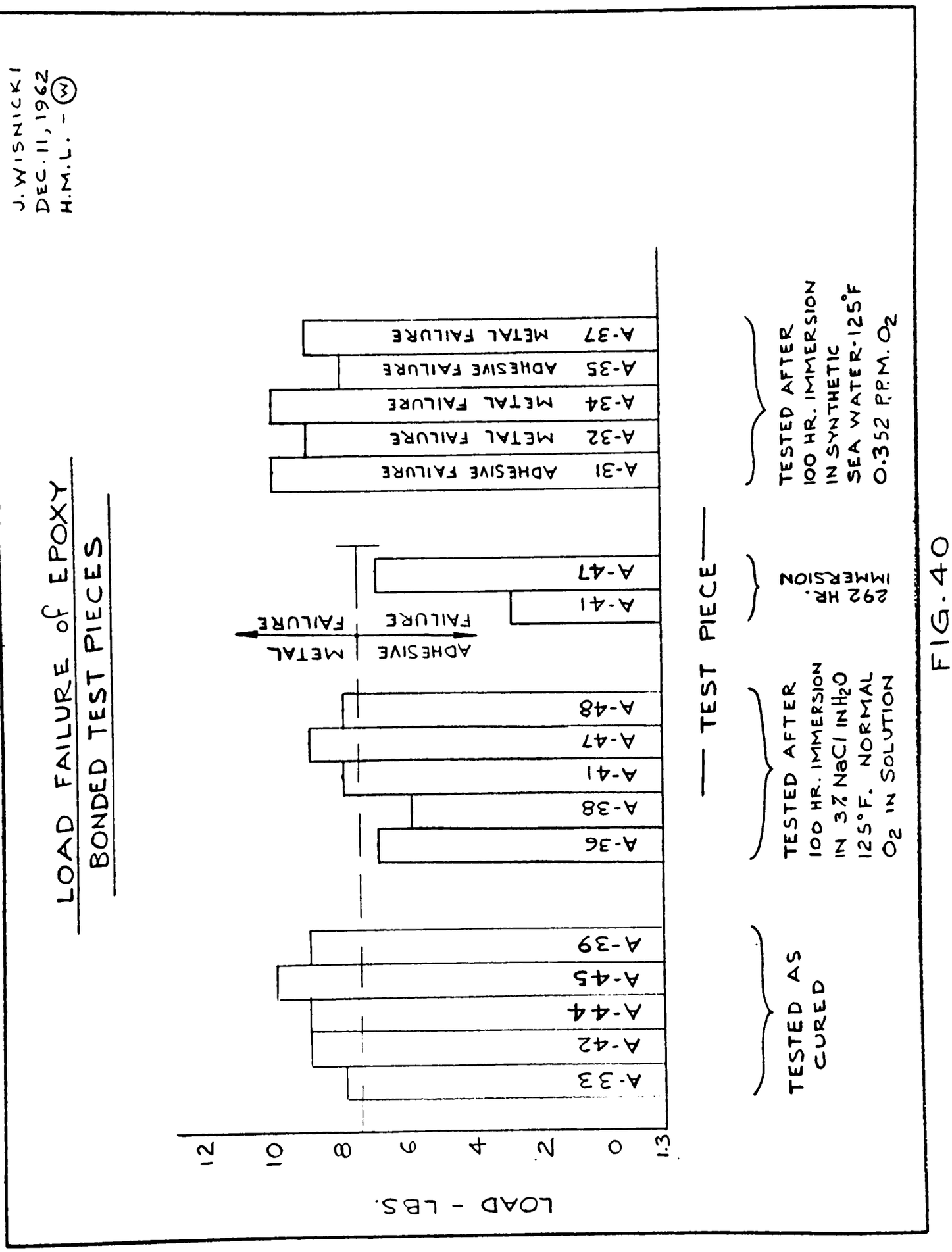
J. WISNICKI
DEC. 11, 1962
H.M.L. - (W)
LOAD FAILURE OF EPOXY
BONDED TEST PIECES
LOAD - LBS.
0
2
4
6
8
10
12
13
A-33
A-42
A-44
A-45
A-39
A-36
A-38
A-41
A-47
A-48
A-41
A-47
ADHESIVE FAILURE
METAL FAILURE
A-31 ADHESIVE FAILURE
A-32 METAL FAILURE
A-34 METAL FAILURE
A-35 ADHESIVE FAILURE
A-37 METAL FAILURE
— TEST PIECE —
TESTED AS CURED
TESTED AFTER 100 HR. IMMERSION IN 3% NaCl IN H2O 125°F. NORMAL O2 IN SOLUTION
TESTED AFTER 192 HR. IMMERSION
TESTED AFTER 100 HR. IMMERSION IN SYNTHETIC SEA WATER-125°F 0.352 P.P.M. O2

FIG. 40

FIG. 41

better strength than the steel samples. Eleven samples were load tested. Four showed cohesive failure i.e. failure within the adhesive, ranging from 2 lbs. to 5-1/2 lbs. Two were not carried to failure. The other 5 showed metal failure in bending. Those that failed in metal were re-straightened and put in the de-aerated salt water test bath for 192 hours along with the two that were not carried to failure. The two that were not loaded to failure showed cohesive failure at 4 and 7-1/2 lbs. load. The 5 that showed metal failure, again showed metal failure indicating that joint strength was still greater than metal strength. No adhesive failure nor delamination was evident. The wide range in joint strength observed by us was also noted by Kaiser Aluminum using plain "T" joints. Their load test was a Tension Test on the vertical member of the "T".

A sample aluminum module 12 inches wide by 18 inches deep (height) by 12 inches long was bonded with Epon 422 sheet using a 2-1/2 hour cure cycle. See photo Figure 42. Fit up error of edges was limited to .020 inch out-of-plane. Silicone rubber pads and weights were used to keep the side sheets in contact with the corrugated sheet edges. No distortion occurred in the aluminum and joints appeared continuous. Maximum cure temperature was 350°F.

In order to minimize tolerance control and accuracies in the side sheet and evaporator sheet, a modified "T" joint using an embossed groove to accept the evaporator sheet is recommended. This would require paste form adhesive and such a joint is shown in photo Figure 43. It can be seen that bubbling occurs to give a porous joint. This porosity is due to gases and/or vapors given off when curing.

Shell Chemical recommends two different cure cycles, one being a 1/2 hour cycle and the other being a 2-1/2 hour cycle. It has been found that the 2-1/2 hour

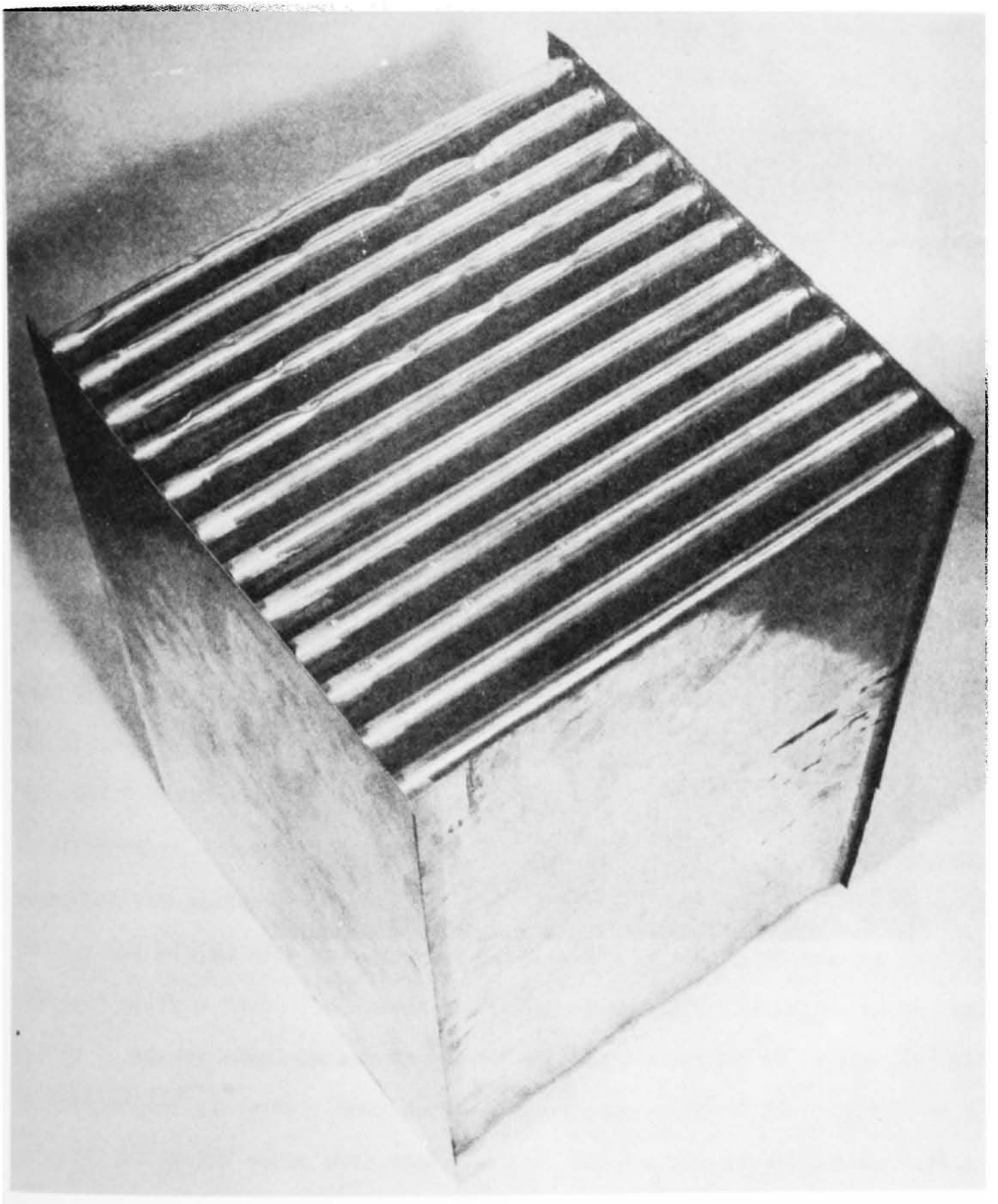

FIG. 42

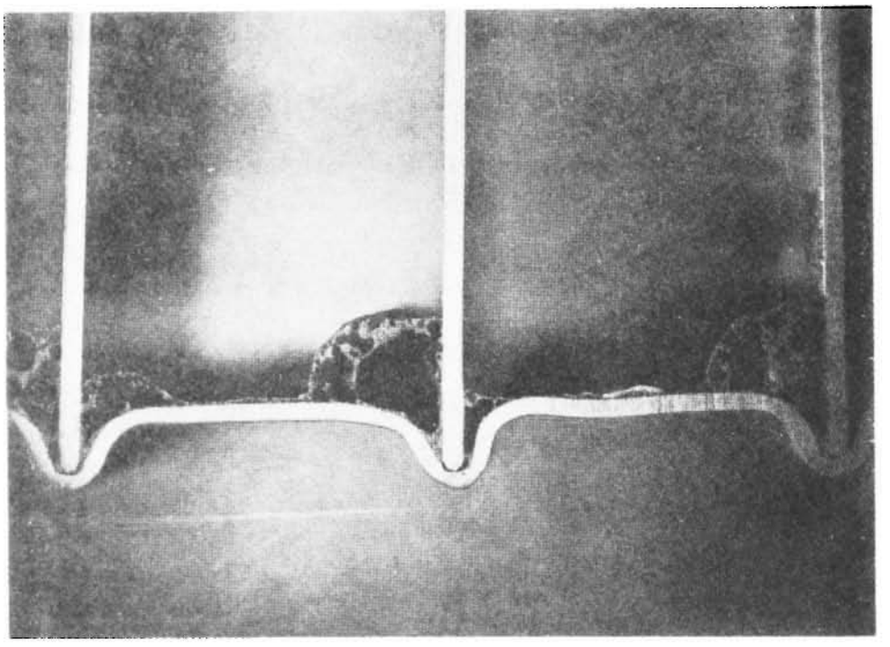

FIG. 43

cycle gives smaller bubbles in the adhesive; also that heating thru the metal will reduce the size of the bubbles, instead of heating metal and adhesive simultaneously as in a circulating heat air oven. Photo Figure 44 shows a joint cured at a 2-1/2 hour cycle heated through a hot plate. It can be seen that bubbles and area of epoxy are reduced 30% as compared to Figure 43.

The porous adhesive joint results in a strong mechanical joint. Whether such a joint will allow minute electrolytic cells to take place at the joint and thus cause rapid corrosion will depend on actual time testing. Leakage of vapor would be from the high pressure condensing side to the low pressure evaporating side. A test chamber was made to determine whether this porosity would allow passage of water or vapors. The test chamber was a 3 inch diameter tube the ends of which were closed with plates. Closing was by bonding with Epon 422 and curing with a 2-1/2 hour cycle. This resulted in a plain "T" joint. The test chamber was pressurized and the rate of air leakage through the joints was established. This was 0.00942 cu. inches free air per hour per inch of joint at 3-1/2 inches water pressure. However, the joint will be operating under vapors and water and therefore the leakage rates will be less than that for air. To prove this the chamber was filled with the proper head (4-1/2") of water and leakage rate was observed after 3 days. No change in level was noted indicating no water leakage.

Kaiser Aluminum has suggested and tried a method of curing Epon 422 to prevent the porosity. This method was to cure at 350°F for 1/2 hour at a pressure above the vapor pressure of water; 200 psi was actually used. This prevented vaporization and porosity. Photo Figure 45 shows a joint cured under pressure to eliminate porosity.

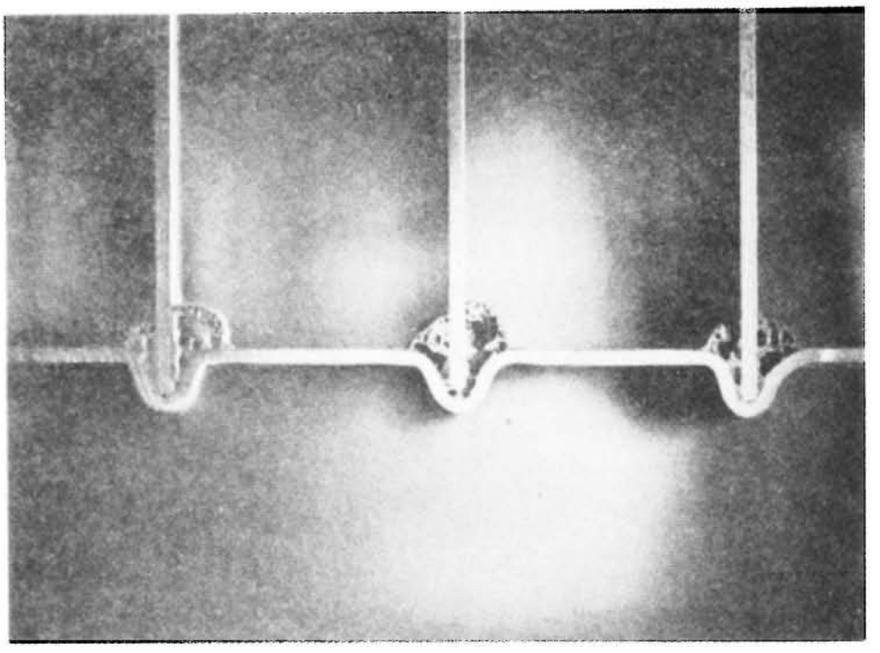

FIG. 44

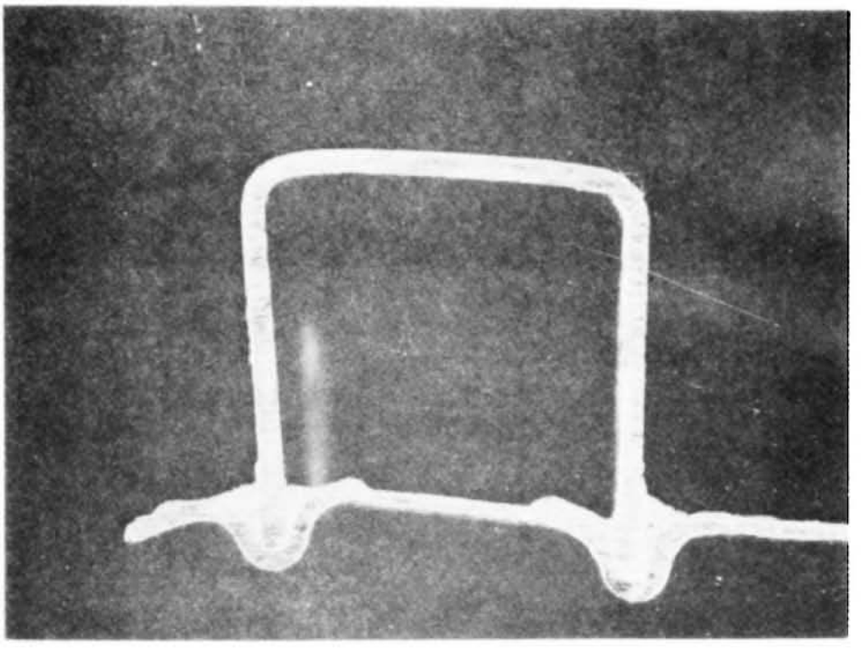

FIG. 45

It is recommended that initial modules such as those for a pilot plant be made by curing Epon 422 without pressure. If the porosity has an adverse effect on joint life, then autoclaves can be purchased and curing done by this method. Two autoclaves approximately 7 ft. O.D. x 18 ft. long would be required for production. Their cost would be about $100,000 for both. J. P. Devine are manufacturers of such equipment, and have sumbitted a quotation for them.

Method of Application

Epon 422 paste is a thick tacky substance at room temperature. It can be troweled on a surface or it can be laid down with a flow gun under air pressure, similar to a caulking gun. The caulking gun application would be ideal for laying the bead down in the embossed groove of the side sheet. Methyl-Ethyl-Ketone should be used to keep the trowel clean. It can also be used to thin down the adhesive for easier application by trowel or caulking gun. Pyles Industries of Los Angeles, California have air powered caulking equipment for adhesives.

Shelf Life

Epon 422 has a short useful life at 75°F, therefore, must be stored at low temperatures. The following listing shows storage life at different temperatures:

STORAGE TEMPERATURE °F	SAFE STORAGE TIME
0	6 months
30	3 months
40	2 weeks
77	2 days
120	30 minutes

The effect of aging on Epon 422 is cumulative and the total time out of refrigeration must be considered. It is recommended that a record of storage conditions be kept and that material be used in the order of shipment.

Curing

Different cure cycles are recommended for Epon 422. The long cure cycle has been found best for our application since it reduces the porosity of the adhesive. The following is recommended:

(1) Heat at a uniformity rate to 210°F ± 10° for a period of 30 - 40 minutes.

(2) Maintain temperature at 210°F ± 10° for 10 - 20 minutes.

(3) Heat at a uniform rate to 340°F ± 10° for a period of 50 - 60 minutes.

(4) Maintain temperature at 340°F ± 10° for a period of 25 - 35 minutes.

RECOMMENDED PROCEDURES FOR SAFE USE OF FORMULATED EPOXY COMPOUNDS

Edited and Published by

EPOXY RESIN FORMULATORS DIVISION
of The Society of the Plastics Industry, Inc.

Introduction

Since their introduction, millions of pounds of formulated epoxy compounds have been used in production in the airframe, automotive, brush setting, electronics, electrical machinery and equipment, industrial metal working, and many other industries in the United States and around the world. The recommendations presented here are based on this long experience; each member of the Epoxy Resin Formulators Division of the SPI will be happy to answer any questions you may have about formulated epoxy compounds.

As with any other industrial material, proper handling is important for optimum performance of your finished product, as well as for maintaining the health and safety of those manufacturing it.

Physiological Reactions

There are many materials used in industry which can cause allergic reactions . . . itching, a rash or other forms of dermatitis in those who work with them. These reactions are similar to those displayed by many people after contact with poison ivy, certain foods, or pharmaceutical compounds. Typical sensitizing materials encountered in industry are: solvents, cleaners, chemicals, plastics, foods, coolants, metals, animals, dust, fumes, inks, dyes, and soaps with a high alkaline or harsh mineral abrasive content. *Experience has shown that the best way to prevent industrial dermatitis reaction is to establish and enforce good housekeeping practices.* The workers themselves must understand the reason for these practices and cooperate in them fully for no supervisor can control all of the action of each employee. Patch testing to see if the individual is sensitive to the compound or to any of its components has proven unsatisfactory since repeated exposure is usually required in order for the individual to develop sensitivity.

Physiological Classification

Material	*Skin Irritating Effect*	*Sensitizing Effect*	*Recommended Protection*
Formulated epoxy liquids	Mild to moderate	Mild to moderate	A, B, C
Formulated epoxy solids	Non-irritating	Non-sensitizing	E
Fully cured compounds	Non-irritating	Non-sensitizing	E
Curing agents or hardeners	Mild to strong	Mild to strong	A, B, C, E
Solvents	Defatting	Non-sensitizing	A, C, D, E

Key to protection: A. Skin protection • B. Goggles or face shield • C. Exhaust ventilation • D. Fire precautions • E. Avoid inhalation of dust or vapor

From field reports, only a small percent of the individuals who handle formulated epoxy compounds develop sensitivity to them.

Precautions

Training, personal cleanliness, ventilation, good housekeeping practices, protective creams and clothing are all essential in preventing dermatitis.

1. Training

Instruct supervisors and workers about the need for care when working with formulated epoxy compounds.

Instruct supervisors and workers as to the need for keeping formulated epoxy compounds off the skin. In addition to smearing or splashing, the workers may get these compounds on the skin through rubbing exposed skin areas with soiled hands; through wearing soiled clothing or gloves; through handling soiled rags, tools, hardware, or through prolonged exposure to vapors.

2. Personal Cleanliness

Wash hands thoroughly before and after work, before rest periods, lunch and other interruptions, before applying skin creams and putting on gloves, and immediately after any hardener or resin has touched the skin. Use a mild soap without abrasive scrubbers or use a waterless cleaner which is low alkaline or neutral and contains minimum quantities of petroleum solvent or defatting agents.

Do not use irritating solvents to wash skin as they tend to remove the skin's natural oils and can alone cause severe irritation. Over a period of years, however, it has been found that denatured alcohol is very effective in the removal of the material from the skin, provided its use is followed by washing with soap and water and then applying lanolin type hand cream.

Keep fingernails short and clean.

Wear only clean clothing and gloves.

3. Ventilation

Forced draft ventilation at the point of work, where vapors are generated, is essential when handling and curing formulated epoxy compounds. *The vapors should be drawn away from the operator* and vented outside the building. Overhead ventilation at work areas should be avoided since it may pull vapors from the bench into the worker's face.

Cured epoxy formulations can be machined readily by conventional wood-working, plastic working, or metal working practice. Fully cured epoxies are quite inert and present no toxicological problem. However, dust from grinding or cutting should be drawn off to prevent inhalation, as with any fine air-borne particles.

4. Good Housekeeping Practices

Do not soil clothing or work areas. Protect floors and benches with disposable plastic film or paper which can be easily replaced as necessary. Use disposable paper wipers instead of rags to avoid contamination from reuse of soiled rags. Use fresh solvent for cleaning.

Mix small quantities of two package formulated epoxy compounds thoroughly in disposable plastic or paper containers using disposable wooden paint stirrers or tongue blades. Stir slowly to avoid entrapping air.

Drums and containers in which epoxy compounds are received should be disposed of and not reused for other purposes.

5. Protection from Contact

Clothing. Change coveralls, shirts, aprons, etc. frequently. If soiled, change at once. Wear coveralls or shirts with long sleeves. Disposable paper sleeves for the wrist and forearm are often used to protect clothing. Plastic or coated fabric sleeves should be discouraged since they cut off air circulation, open skin pores, and cause excessive perspiration.

Gloves. Where contact with the hands presents a constant hazard, wear rubber, plastic coated or disposable plastic gloves over protective cream. Do not soil the inside of the gloves when removing them. Remove gloves by pulling at the fingers. Put gloves on clean hands only.

Eyes. The eyes should be protected against splashes of liquid components by wearing goggles or face shields. *If any component is splashed in the eyes, wash the affected eye immediately and continuously for ten minutes with copious quantities of clean water* such as from a drinking fountain. Bathing the eye further with normal saline solution may be helpful. Referral to a physician is recommended if there is any question about the seriousness of the injury.

Creams. Use a film forming skin cream* on the hands and forearms and on other exposed areas. Emulsified oily or fatty creams are not effective since they dissolve in organic solvents and in the formulated epoxy compounds. Apply the cream at the start of each shift and before each return to work, after relief periods, lunch, wash-ups, etc. Do not forget to wash off the cream at lunch, quitting time, etc. Creams do not protect dirty hands. Wash hands, arms, etc. thoroughly before applying them. After final wash-up of the day, rub in softening cream to counter-act any drying or defatting of the skin. Dispense these creams in individual portions; never use a common jar.

These recommended handling procedures for formulated epoxy adhesives, encapsulating compounds, tooling compounds, can be of great help to engineers, production supervisors and company physicians in establishing efficient and economical procedures for production operations for using these compounds. Additional information can be supplied by any member of the Epoxy Resin Formulators Division of the SPI.

Instruction Sheets and Samples

Before using any formulated epoxy compound, read the manufacturer's Technical Data sheet carefully.

* *Contact your epoxy formulator for recommended product.*

DESIGN OF PRESSURE CONTROL FOR CYCLICAL TRAVERSING SPRAY SYSTEM

Introduction

A design is presented for a pressure control for a cyclical traversing spray system wherein spray bars are located at opposite sides of the area to be covered. This device consists of two variable area orifices which are supplied by a common plenum chamber (see Figure 1).

The variation in orifice area is accomplished by a rotor having a cyclical height variation.

Nomenclature

a - length of sprayed area - ft
A - sprayed area - ft^2
A_j - spray bar total hole area - ft^2
A_o - variable orifice area - ft^2
b - width of sprayed area - ft
C_j - flow coefficient of spray bar holes
C_v - velocity coefficient of jet
g - acceleration of gravity - ft/sec^2
h - length of orifice diameter which is covered in variable orifice - ft
$\triangle h_j$ - pressure drop across spray bar - ft H_2O
$\triangle h_o$ - pressure drop across variable orifice - ft H_2O
$\triangle h_T$ - pressure difference between variable orifice inlet and jet discharge - ft H_2O
K - flow coefficient of orifice
t - time - starting from minimum spray trajectory - sec
W · weight of water - #
W_w · instantaneous flow rate from one spray bar - #/sec
$\overline{W}_w$ - average flow rate from one bar - #/sec
X - horizontal distance from spray bar to point where spray strikes surface - ft
X_o - range of minimum spray trajectory - ft
ω - cyclical rate of spray - cycles/sec
ρ - density - $\#/ft^3$
θ - angle of spray above horizontal - deg

Design Procedure

It is assumed that the flow rate per unit of sprayed area is uniform. If the line losses and the dynamic pressure effects are assumed to be negligible, the pressure differential between the control plenum chamber and the jet discharge is:

$$\Delta h_T = \Delta h_{o1} + \Delta h_{j1} = \Delta h_{o2} + \Delta h_{j2}$$

The expression for the jet pressure drop as a function of control rotor position as developed in Appendix I is:

$$\Delta h_j = \frac{1}{2 \sin 2\Theta \, C_v^2} \left\{ 2\left[(X_o + a)^{\frac{1}{2}} - X_o^{\frac{1}{2}}\right] \omega t + X_o^{\frac{1}{2}} \right\}^2$$

The expressions for Δh_{j1} and Δh_{j2} are identical, apart from their being 180^o out of phase.

Therefore, $$\Delta h_o = \Delta h_T - \frac{1}{2 \sin 2\Theta \, C_v^2} \left\{ 2\left[(X_o + a)^{\frac{1}{2}} - X_o^{\frac{1}{2}}\right] \omega t + X_o^{\frac{1}{2}} \right\}^2$$

The expression for the flow rate through a single spray bar as a function of control rotor position as developed in Appendix II is:

$$W_w = \rho C_j A_j \left[\frac{g C_j A_j a \rho}{\sin 2\Theta \, \overline{W}_w} (\omega t) + \sqrt{g / \sin 2\Theta} \, X_o^{\frac{1}{2}} \right]$$

For a series of ωt values starting at 0 and ending at 0.5, solve for W_w and Δh_o. The orifice area required for each ωt value is then estimated by the following expression:

$$A_o = \frac{W_w}{\rho K \sqrt{2g \ \Delta h_o}}$$

Assume a value of K and calculate the maximum area required. Then select a basic orifice diameter which will give an area slightly greater than this. The diameter for the passage into which the orifice discharges should then be selected so that the diameter ratio is not greater than about 0.3.

The equivalent diameter ratio for each value of ωt can be calculated from the area ratios. Having this equivalent diameter ratio and the corresponding flow rate permits a more precise determination of K from tables or plots for standard orifice installations. The flange top values are the most applicable for this physical situation. If the K values obtained thusly differ significantly from the assumed value, multiply the area values by the following quantity:

$$\text{K Correction} = \frac{\text{assumed K}}{\text{actual K}}$$

Since the pressure drop measured in a flange top orifice installation is not all permanently lost, the orifice area values must be reduced to compensate for this. A correlation of residual pressure loss in percent of measured differential as a function of diameter ratio is given for orifices on page 12 of ASME PTC 19.5; 4-1959. The correction for pressure recovery is $\sqrt{\frac{\% \text{ loss}}{100}}$.

The expression for the area of the variable area orifice is:

$$A_o = \frac{\pi}{4} d_o^2 \left[1 - \frac{\alpha}{360} + \frac{\sin \alpha}{2} \right]$$

where $\cos \frac{\alpha}{2} = 1 - \frac{2h}{d_o}$

Figure 2 gives $A_o / \pi/4\ d_o^2$ as a function of $\frac{h}{d_o}$.

Calculate the h value for each value of ωt and design the rotor and housing accordingly.

If, for some reason, a cyclic rate high enough to introduce measurable dynamic pressure effects must be used, the rotor design will have to be tailored to compensate. This can be done by simulating the system on an analog circuit and/or by trial-and-error experiments on the rotor itself. A satisfactory design is one which gives a uniform flow rate over the sprayed surface.

J. R. Hamm
10-12-61

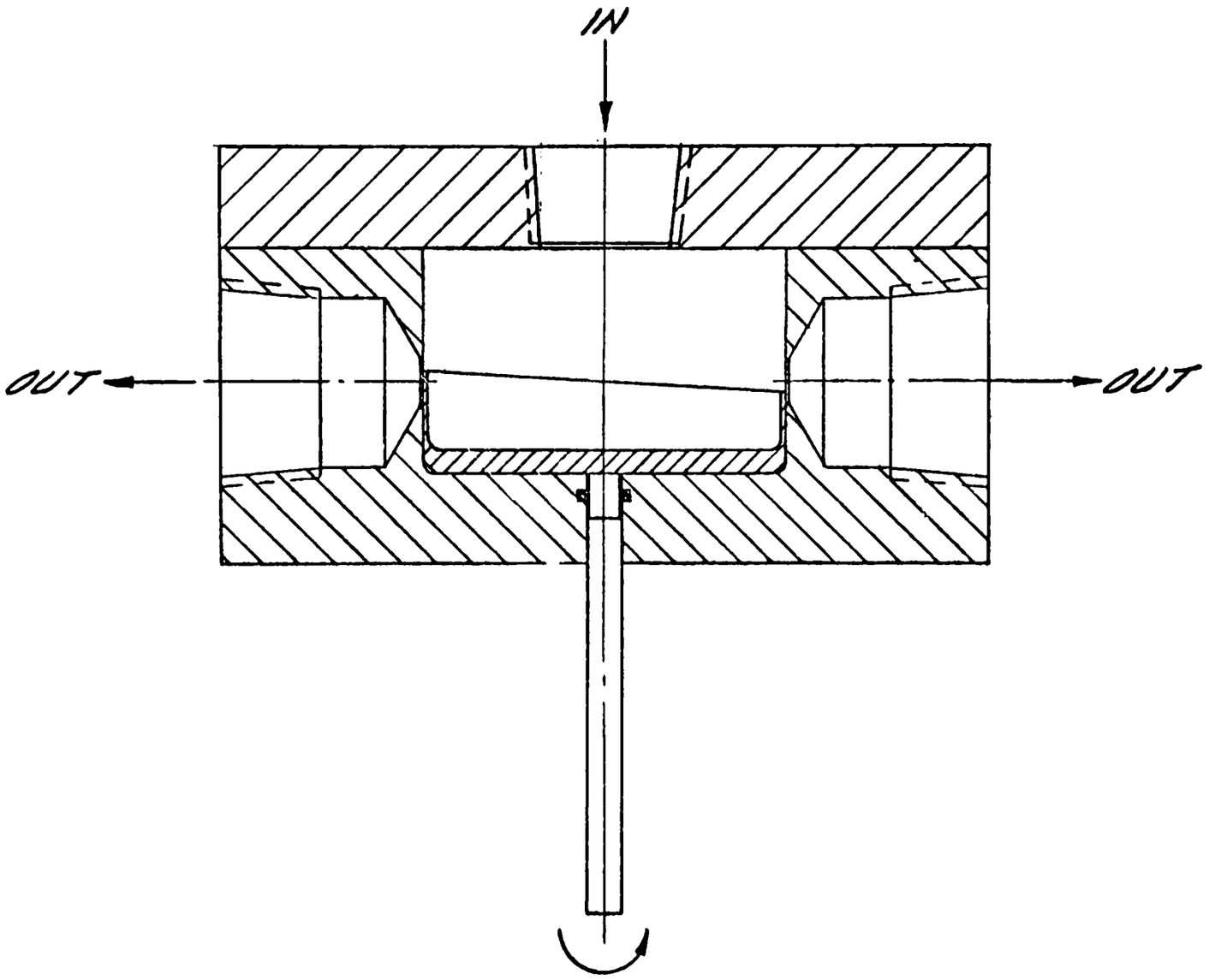
IN
OUT
OUT

WESTINGHOUSE ELECTRIC CORPORATION

CURVE NO._____

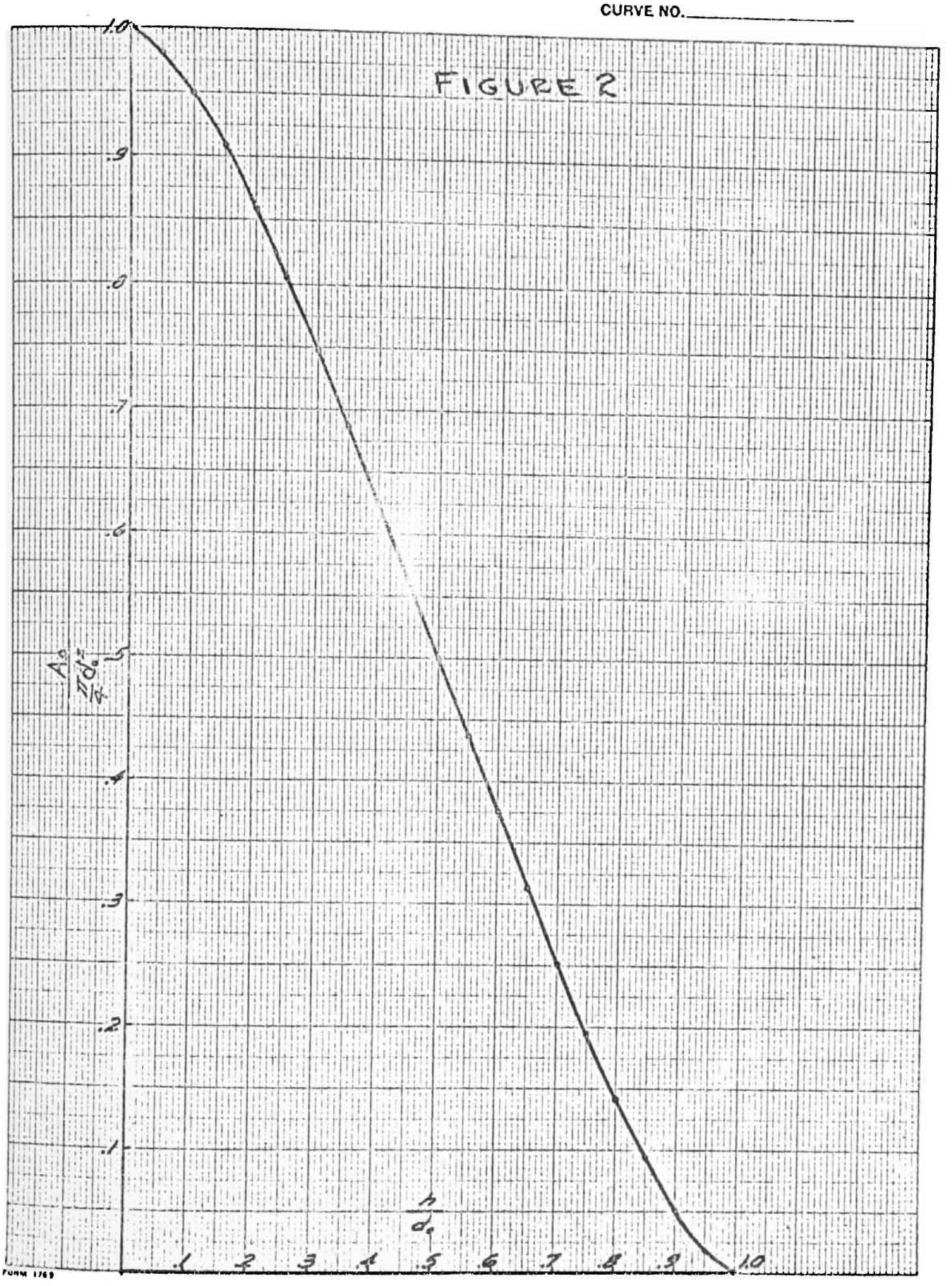

FORM 1769

SIGNATURE_____ DATE_____ CURVE NO.

PRESSURE DROP RELATIONSHIP FOR CYCLICAL SPRAY

The expression for the jet velocity as a function of the spray angle and the horizontal distance of the trajectory is:

$$v_j = \sqrt{\frac{g}{\sin 2\Theta}}\ (X)^{\frac{1}{2}} \tag{1}$$

for the case where the elevation of the spray bar is the same as that of the sprayed surface.

The expression for jet velocity in terms of the pressure drop and velocity coefficient is:

$$v_j = C_v \sqrt{2g \Delta h_j} \tag{2}$$

Combining (1) and (2) gives:

$$\Delta h_j = X/2 \sin 2\Theta\ C_v^2 \tag{3}$$

It is required that the water flow during a cycle be uniformly distributed over the horizontal surface being sprayed, i.e., $\frac{dW}{dA} = C$.

For a half cycle, this becomes:

$$\frac{dW}{dA} = \frac{\bar{W}_w \times \frac{1}{2\omega}}{ab} \tag{4}$$

Dividing both sides by dt gives:

$$\frac{dW/dt}{dA} = \frac{\bar{W}_w \times \frac{1}{2\omega}}{ab} \times \frac{1}{dt} \tag{5}$$

$$\frac{dW}{dt} = W_w = v_j \; C_j \; A_j \; \rho \tag{6}$$

$$dA = b\,dX \tag{7}$$

Substituting gives:

$$\frac{v_j \; C_j \; A_j \; \rho}{b\,dX} = \frac{\bar{W}_w \times \frac{1}{2w}}{ab} \times \frac{1}{dt}$$

$$2wa \; v_j \; C_j \; A_j \; \rho \; dt = \bar{W}_w \; dX \tag{8}$$

Substituting (1) gives:

$$2wa \sqrt{\frac{g}{\sin 2\theta}} \; (X)^{\frac{1}{2}} \; C_j \; A_j \; \rho \; dt = \bar{W}_w \; dX \tag{9}$$

$$2wa \sqrt{\frac{g}{\sin 2\theta}} \; C_j \; A_j \; \rho \; dt = \bar{W}_w \; (X)^{-\frac{1}{2}} \; dX \tag{10}$$

Integrating gives:

$$a \sqrt{\frac{g}{\sin 2\theta}} \; C_j \; A_j \; \rho \; \omega t = \bar{W}_w \; X^{\frac{1}{2}} + C \tag{11}$$

for $\omega t = 0$, $X = X_o$

Therefore, $C = - \bar{W}_w \; X_o^{\frac{1}{2}}$

and

$$a\, C_j\, A_j \rho\, \omega t \sqrt{\frac{g}{\sin 2\Theta}} = \bar{W}_w \left(X^{\frac{1}{2}} - X_o^{\frac{1}{2}}\right) \tag{12}$$

Solving for A_j gives

$$A_j = \frac{\bar{W}_w \left(X^{\frac{1}{2}} - X_o^{\frac{1}{2}}\right)}{a\, C_j \rho\, \omega t \sqrt{\frac{g}{\sin 2\Theta}}} \tag{13}$$

For $\omega t = \frac{1}{2}$

$$X = X_o + a$$

$$A_j = \frac{2\, \bar{W}_w \left[(X_o + a)^{\frac{1}{2}} - X_o^{\frac{1}{2}} \right]}{a\, C_j\, \rho \sqrt{\frac{g}{\sin 2\Theta}}} \tag{14}$$

Substituting (14) in (12) gives:

$$2 \left[(X_o + a)^{\frac{1}{2}} - X_o^{\frac{1}{2}} \right] \omega t = \left(X^{\frac{1}{2}} - X_o^{\frac{1}{2}}\right) \tag{15}$$

Solving for X gives:

$$X = \left\{ 2 \left[(X_o + a)^{\frac{1}{2}} - X_o^{\frac{1}{2}} \right] \omega t + X_o^{\frac{1}{2}} \right\}^2 \tag{16}$$

Substituting (16) in (3) gives:

$$\Delta h_j = \frac{\left\{ 2 \left[(X_o + a)^{\frac{1}{2}} - X_o^{\frac{1}{2}} \right] \omega t + X_o^{\frac{1}{2}} \right\}^2}{2 \sin 2\Theta \;\; C_v^{\,2}} \tag{17}$$

FLOW RELATIONSHIP FOR CYCLICAL SPRAY

$$W_w = \rho C_j A_j v_j \tag{1}$$

From Appendix I

$$v_j = \sqrt{g/\sin 2\theta}\ (X)^{\frac{1}{2}} \qquad \text{I (1)}$$

$$a C_j A_j \rho \omega t \sqrt{g/\sin 2\theta} = \bar{W}_w (X^{\frac{1}{2}} - X_o^{\frac{1}{2}}) \qquad \text{I (12)}$$

Combining I (1) and I (12) gives:

$$a C_j A_j \rho \omega t \sqrt{g/\sin 2\theta} = \bar{W}_w \left(v_j / \sqrt{g/\sin 2\theta} - X_o^{\frac{1}{2}}\right) \tag{2}$$

Solving for v_j gives:

$$v_j = \sqrt{g/\sin 2\theta}\left(\frac{a C_j A_j \rho \sqrt{g/\sin 2\theta}}{\bar{W}} \omega t + X_o^{\frac{1}{2}}\right) \tag{3}$$

Combining (1) and (3) gives:

$$W_w = \rho C_j A_j \sqrt{g/\sin 2\theta}\left[\frac{a \rho C_j A_j \sqrt{g/\sin 2\theta}}{\bar{W}_w} \omega t + X_o^{\frac{1}{2}}\right]$$

BIBLIOGRAPHY

1. R. C. Strauss and W. D. Finnegan
   Dept. of Metallurgical Research
   Kaiser Aluminum and Chemical Corp.
   — The Theory and Practice of Adhesive Bonding

2. E. S. Bober
   Westinghouse Electric Corp.
   — Adhesive Bonding of Metals
   1958 Metals Joining Committee Meeting

3. Henry Lee
   Technical Director
   The Epoxylite Corp.
   — Attainment of Equilibrium in water Absorption Tests of Epoxy Castings Resins

4. Edmund Thelen
   Interscience Publishers
   — Adherend Surface Preparation
   Symposium on Adhesives for Structural Applications

5. Welding Design and Fabrication
   December, 1962
   — Melt Through Welding
   Page 60.

☆ U. S. GOVERNMENT PRINTING OFFICE : 1964 O - 719-026